U.PORTO

DOUTORAMENTO EM QUÍMICA SUSTENTÁVEL

Lab-on-a-chip platforms embedding self-powered electrochemical sensors: a walkthrough approach for bio-analytical applications

Álvaro Miguel Carneiro Torrinha

D

2019

Álvaro Miguel Carneiro Torrinha

Lab-on-a-chip platforms embedding self-powered electrochemical sensors: a walkthrough approach for bio-analytical applications

Tese do 3° Ciclo de Estudos Conducente ao Grau de Doutor em Química Sustentável

Trabalho realizado sob a orientação do Professor Doutor Alberto Nova Araújo e co-orientação da Professora Doutora Maria Conceição Branco Montenegro

Julho 2019

Já fiz uma parte de nada. Agora falta o resto de tudo

Acknowledgements

The accomplishment of the work present herein was possible due to the expertise of my supervisors, Alberto Araújo and Maria Conceição Branco Montenegro. I want to thank all the help provided, friendship and for the integration in the Sensors and Biosensors lab.

I also like to thank Celia, always cheerful and with a smile to give, for her help and encouragement.

I want to thank all my colleagues and friends from FFUP for all the good moments.

I am truly grateful to my former supervisor and Professor Simone Morais for believing in me and make me believe that was possible obtaining a PhD degree.

Thank you Vânia and Eng. Manuela for all the favours done, all the help provided and friendship.

I want to thank Fundação para a Ciência e Tecnologia for the funding through the grant PD/BD/109660/2015.

A special thanks to my parents and my brother Pedro for the support and patience.

For last and not least a very special thought to my wife Isabel Sofia. You have been tireless with all your support and friendship.

About 4 years of my life just flew by really quickly and I am sure that the door will remain always open whenever needed. Thank you.

Abstract

The present dissertation considers the development of enzymatic biofuel cells embedded in lab-on-a-chip platforms, with ability for self-powered biosensing. Since the generated power varies proportionally with the fuel concentration, a biofuel cell can itself be used as a biosensor or instead applied as energy supplier for an external sensor/biosensor. When integrated in a microfluidic platform, other unit operations can be performed and controlled with reduced sample/fuel volumes meeting therefore an ecological and sustainable approach.

The coupling of enzymes to the electrodes allied to their substrate specificity makes possible the operation at mild chemical conditions. At the same time, it simplifies the construction of biofuel cells by avoiding the necessity of separation between anolyte and catholyte, therefore enabling their miniaturization. Nevertheless, the immobilization procedure of enzymes is complex and a challenging process. First, because the catalytic centre of enzymes is buried in an insulating glycoprotein shell which needs proper orientation or cross-linking for direct electron transfer (DET) or requiring the use of diffusional mediators for a successful electronic communication with the electrode. And second, because the use of enzymes outside living organisms lead to stability problems reducing the lifetime of biosensors and biofuel cells.

Almost all experimental work was performed using pencil graphite electrodes (PGEs) as enzymatic conductive supports (transducers). These type of electrodes are a practicable alternative to other traditionally used electrodes due to their comparable electrochemical performance, availability and reduced cost. PGEs were thoroughly characterized by cyclic voltammetry (CV) and modified with carbon based nanostructures in order to enhance the electrochemical signal. Modification with reduced graphene (rGO) gave the best results and was henceforth applied in the construction of PGE bioelectrodes. An alternative approach as biocatalysts support based on conductive transducers produced through vacuum-filtration of a Vulcan carbon black suspension resulting in flexible, paper-like electrodes, was equally assessed and used in one of the developed lab-on-a-chip-platforms.

In biofuel cells, enzymatic oxidation of a fuel occurs at the bioanode with the generated electrons being transferred to the biocathode for the enzymatic reduction of an oxidizer compound, e.g. oxygen. Oxygen reduction bioelectrodes to be used as biocathodes were initially studied. In a first attempt, laccase enzyme from *Rhus vernicifera* was first immobilized in the PGE-rGO surface alongside single-walled carbon nanotubes (SWCNT) by entrapment in a sol-gel matrix. However, a second approach tested with the bilirubin oxidase (BOx) enzyme would reveal a simpler immobilization procedure with much higher

performance regarding biocatalytic reduction of oxygen. This procedure consisted in further modification of PGE-rGO with multi-walled carbon nanotubes (MWCNT) followed by the immobilization of enzyme BOx through a pyrene-based succinimidyl ester compound (PBSE). CV was performed to evaluate the immobilization efficiency whereas amperometric analysis revealed a high sensitivity of 648 μA mM^{-1} cm^{-2} and a low limit of detection value of 1.8 μM for the PGE-rGO-MWCNT-BOx. When employing the bioelectrode as a biocathode, the polarization curves resulted in an open circuit potential (E_{OCP}) of 0.48 V vs Ag/AgCl and generated a maximum current density of about 500 μA cm^{-2} at 0.10 V vs Ag/AgCl.

The glucose oxidase (GOx) bioanode was assembled through an enzyme precipitate coating method. This was accomplished by cross-linking of GOx to MWCNT after a precipitation step with ammonium sulphate and further solubilisation in nafion and deposition in the PGE-rGO surface. The approach enabled high enzyme activity, improved stability of the biofilm coating over PGE surface and its use under flow regimen inside microfluidic platforms. In this last condition, a sensitivity to glucose of 35 μA mM^{-1} cm^{-2} and a LOD of 14.9 μM were achieved in a high analytical range up to 39 mM. The bioelectrode was also successful tested in the detection of cadmium through an inhibitory effect on GOx. As a final work, GOx and BOx paper-like bioelectrodes were conjugated in a biofuel cell, respectively as bioanode and biocathode and finally integrated in a finger pressure-driven microfluidic platform made of poly(methyl methacrylate) - polydimethylsiloxane (PMMA-PDMS). The autonomous, self-powered biosensor device showed a sensitivity of 2.1 μW mM^{-1} cm^{-2} up to 20 mM of glucose at physiological conditions. The maximum power density achieved in 50 mM glucose solution was about 70 μW mM^{-1} cm^{-2} at 0.19 V vs Ag/AgCl.

The work developed in this thesis enabled the fabrication of an autonomous and self-powered biosensors with potential use for *in situ* measurements. This was possible due to the implementation of efficient immobilization procedures of enzymes in miniaturized electrodes and their integration in a platform featuring human propelled fluidics. Meanwhile, the practical use of PGEs in electrochemistry was extensively demonstrated throughout the work.

Keywords: Bioelectrocatalysis, Biofuel cells, Self-powered biosensors, Microfluidics, Enzymes

Resumo

Na presente tese foi equacionado o desenvolvimento de plataformas “lab-on-a-chip” contendo células de biocombustível enzimáticas para serem aplicadas como biossensores autoalimentados. Uma vez que a potência gerada varia proporcionalmente com a concentração de combustível, as células de biocombustível podem ser usadas como biossensores ou serem aplicadas como alimentadores de energia para sensores/biossensores externos. Quando integrados numa plataforma microfluídica, outras operações unitárias podem ser adicionadas e executadas sobre volumes reduzidos de amostra/combustível indo assim ao encontro de uma abordagem ecológica e sustentável.

O acoplamento otimizado de enzimas aos elétrodos, aliado à especificidade daquelas pelos seus substratos torna possível o funcionamento das células de combustível em condições amenas. Por outro lado, simplifica-se a sua construção pois evita-se a necessidade de separar o anólito do católito, tornando assim possível a sua miniaturização. Contudo, o procedimento de imobilização enzimática é um processo complexo e desafiante. Primeiro, porque o centro catalítico das enzimas encontra-se geralmente sob um invólucro glicoproteico isolante. Necessita assim de uma imobilização orientada, ou de uma ligação química que propicie o tunelamento eletrónico direto, ou requer o uso de mediadores difusionais que assegurem a ligação eletrónica com o elétrodo. Em segundo lugar, o uso de enzimas no exterior dos organismos conduz a problemas de estabilidade reduzindo o tempo de operação de biossensores e células de biocombustível.

Quase todo o trabalho experimental foi realizado usando minas de grafite de lapiseira (PGEs) como suporte condutor enzimático (transdutor). Este tipo de elétrodos constitui uma alternativa viável a outros elétrodos tradicionalmente usados pois que, para além de um desempenho eletroquímico comparável, são facilmente disponíveis e apresentam custo muito reduzido. Os PGEs foram completamente caracterizados por voltametria cíclica (CV) e modificados com nanoestruturas à base de carbono, a fim de potencializar o sinal eletroquímico. A modificação com grafeno reduzido (rGO) proporcionou melhores resultados e passou a ser aplicada por rotina na construção dos bioeletrodos. Como abordagem alternativa de suporte dos biocatalisadores, desenvolveram-se transdutores condutivos produzidos por filtração a vácuo de uma suspensão de negro de fumo Vulcan resultando em elétrodos flexíveis semelhantes a papel, igualmente avaliados e usados numa das plataformas de microfluídica desenvolvidas.

Nas células de biocombustível, a oxidação enzimática do combustível ocorre no bioânodo com os eletrões produzidos a serem transferidos para o biocátodo onde se dá a redução enzimática de uma espécie oxidante, por exemplo, oxigénio. Assim, foram estudados

primeiramente biocátodos redutores de oxigénio e bioânodos oxidantes de glicose com elétrodos minas de grafite (PGEs), como suporte condutor. Numa primeira tentativa, a enzima laccase extraída da Rhus vernicifera foi aprisionada numa matriz sol-gel sobre a superfície PGE-rGO juntamente com nanotubos de carbino de superfície simples (SWCNT). Posteriormente, um procedimento de imobilização mais simples baseado na ligação química da bilirrubina oxidase (BOx) revelou um elevado desempenho em relação à redução biocatalítica do oxigénio. Este procedimento consistiu na modificação adicional do PGE-rGO com nanotubos de carbono de superfície múltipla (MWCNT) seguido pela imobilização da enzima BOx através de um composto succinimidil-éster derivado do pireno (PBSE). A análise por voltametria cíclica permitiu averiguar a eficiência da imobilização. Por sua vez, a análise amperométrica evidenciou a elevada sensibilidade do dispositivo ao oxigénio, 648 μA mM^{-1} cm^{-2}, e um valor de limite de deteção reduzido: 1,8 μM para o bioelectrode PGE-rGO-MWCNT-BOx. As curvas de polarização revelaram que, quando aplicado como biocátodo, o dispositivo desenvolvido determinava um potencial de circuito aberto (E_{OCP}) de 0,48 V vs Ag/AgCl e gerava uma densidade máxima de corrente de 500 μA cm^{-2} a 0,10 V vs Ag/AgCl.

O bioânodo de glicose oxidase (GOx) foi construído através de um método de revestimento de enzima precipitada. Depois desse passo de precipitação com sulfato de amónio, propiciava-se a ligação química entre a enzima GOx e os MWCNT, seguida da solubilização em nafion, antes da deposição na superfície do PGE-rGO. Esta abordagem permitiu obter uma atividade enzimática elevada, uma melhoria na estabilidade do biofilme depositado na superfície do PGE e o seu uso nas condições de fluxo usadas em plataformas microfluídicas. Nesta última condição, a sensibilidade à glicose de 35 μA mM^{-1} cm^{-2} num intervalo analítico alargado até 39 mM e um limite de deteção de 14,9 μM. O bioeléctrodo foi também testado com sucesso na deteção de cádmio através do efeito inibitório sobre a GOx.

Como trabalho final, os bioeléctrodos de GOx e BOx foram conjugados em uma célula biocombustível respetivamente como bioânodo e biocátodo e finalmente integrados numa plataforma microfluídica construída em material misto de polimetilmetacrilato - polidimetilsiloxano (PMMA-PDMS), em que a propulsão dos fluidos era assegurada através de pressão com o dedo. O biossensor autónomo e autoalimentado apresentou uma sensibilidade de 2,1 μW mM^{-1} cm^{-2} até 20 mM de glicose em condições fisiológicas. A densidade de potência máxima alcançada em uma solução de glicose de 50 mM foi cerca de 70 μW mM^{-1} cm^{-2} a 0,19 V vs Ag/AgCl.

Como conclusão, o trabalho desenvolvido na presente tese permitiu a fabricação de biossensores autónomos e autoalimentados para potencial uso em medições *in situ*. Isto

foi possível devido à implementação eficiente de procedimentos de imobilização enzimática em elétrodos miniaturizados e a sua integração em plataformas com propulsão de fluidos assegurada pelo operador. Além disso, a praticidade dos PGEs na eletroquímica foi extensivamente demonstrada no decorrer do trabalho.

Palavras-chave: Bioelectrocatálise, células de biocombustível, biossensores autoalimentados, microfluidica, Enzimas

Table of Contents

List of Figures

Chapter 1 – Introduction

Chapter 3 – Experimental section

Chapter 4 – Characterization of an O_2 biosensor with immobilized laccase for implementation as a biocathode

Chapter 5 - Characterization of an O_2 biosensor with immobilized bilirubin oxidase for implementation as a biocathode

Chapter 6 – Characterization of glucose biosensor with immobilized glucose oxidase for implementation as a bioanode

Chapter 7 – Integration of miniaturized Box and GOx bioelectrodes as biofuel cell in a finger pressure-driven microfluidic platform

List of tables

Chapter 1 – Introduction

Chapter 5 - Characterization of an O_2 biosensor with immobilized bilirubin oxidase for implementation as a biocathode

Abbreviations

ABTS	2,2′-Azino-bis(3-ethylbenzothiazoline-6-sulfonic acid) diammonium salt
AchE	Acetylcholinesterase
ADH	Alcohol degydrogenase
AOx	Ascorbate oxidase
Au	Gold
AuFeNPs	Gold-coated iron nanoparticles
AuNPs	Gold nanoparticles
BFC	Biofuel cell
BOx	Bilirubon oxidase
BQ	*p*-benzoquinone
BSA	Bovine serum albumine
CB	Carbon black
Chit	Chitosan
ChOx	Cholesterol oxidase
CNF	Carbon nanfibres
CNP	Carbon nanoparticles
CP	Carbon paste
CV	Cyclic voltammetry
DET	Direct electron transfer
E_{OCP}	Open circuit potential
EGDGE	Ethylene glycol diglycidyl ether
FAD	Flavin adenine dinucleotide
FcAld	Ferrocenecarboxaldehyde
Fc-LPEI	ferrocene polyethyleneimine
GA	Glutaraldehyde
GCE	Glassy carbon electrode
GDH	Glucose dehydrogenase
GluOx	Glutamate oxidase
GOx	Glucose oxidase
H_2O_2	Hydrogen peroxide
HOPG	Highly ordered pyrolytic grapgite
HRP	Horseradish peroxidase
IL	Ionic liquid
ITO	Indium tin oxide
KB	Ketjenblack
LOD	Limit of detection
Lox	Lactate oxidase
LSV	Linear sweep voltammetry
MET	Mediated electron transfer
MWCNT	Multi-walled carbon nanotubes
NAD	*β*-Nicotinamide adenine dinucleotide
ORR	Oxygen reduction reaction
PANI	Polyaniline
PB	Prussian blue
PBS	Phosphate buffer saline

PDMS	Polydimethylsiloxane
PGE	Pencil graphite electrode
PGS	Polyglycerol silicate
PLL	Poly-L-lysine
PMMA	poly(methyl methacrylate)
PPy	Polypyrrole
PQQ	Pyrroloquinoline quinone
PPF	Pyrolyzed photoresist films
Pt	Platinum
PU	Polyurethane
rGO	Reduced graphene oxide
SEM	Scanned electron microscope
SWCNT	Single-walled carbon nanotubes
TBAB	Tetrabutylammonium bromide
VK_3	Vitamin K_3
XOD	Xantine oxidase

Chapter 1

Introduction

1.1 - General introduction

The urge to get analytical information from procedures meeting ecological and environmental sustainability standards can undoubtedly be tackled through different ways. The work reported in this monograph looks to one of those ways, a succeeded combination between biotechnology and analytical chemistry regarding the self-powered sensor device proposal. We were specifically driven by the glimpse of a future where complex determinations can be performed through unit operations and instrumental techniques embedded in miniaturized devices energetically fed in simple way by non-target components in the sample matrix. The major content of this dissertation hence concerns to studies culminating into optimized biofuel cells simultaneously possessing sensory capabilities. Preferences on materials and approaches aimed their integration in microfluidic platforms where some performance features are equally evidenced.

The choice on biofuel cells counts on the observation they comfortably meet the requirements for miniaturization and environmental sustainability. Nonetheless, actual knowledge indicates it would be rather utopian to solve all current mankind demand for energy with processes mediated by microorganisms or, as in this dissertation, with enzymes. Based on the highest power density achieved so far - 2 mW cm^{-2} (1) - a 5 m^2 biofuel cell (2.5 m^2 each electrode) would be required to turn on a simple 50 W television, indeed an impractical solution for generalised use. Still, remarkable applications of biofuel cells are prospected such as conversion of organic waste into electricity, power portable electronic devices, or as energy suppliers for synthetic valves or pacemakers in the regulation of physiological and biological functions. Since early times, NASA evidenced the opportunity to convert into electricity the wastes generated in manned flight missions using microbial fuel cell (2). The multinational Japanese Sony took a first step in the development of a commercial enzymatic biofuel cell to power a music player (3) which will be discussed later. On other hand, the development of an implantable device taking advantage of the physiological fluids to power a cardiac pacemaker would be a landmark of this biotechnology. The specifications regarding power requirements of pacemakers, about 100

μW and 1.4 V (4), are at reach of current enzymatic biofuel cells. Stability issues still hamper prolonged operation times in those examples, which nevertheless made clear that such environmentally clean power sources offer new R&D opportunities for portable applications.

Generally speaking, fuel cells are electrical power sources fed through electrochemical transduction of redox processes. The basic working mechanism of these devices is depicted in Figure 1.1. When the external circuit gets closed, fuel oxidation takes place at the negative anode electrode with the generated electrons flowing towards the positive cathode electrode where an oxidant compound is reduced. The concomitant displacement of positive ions in the electrolyte from the anode to the cathode compartment compensates the charge unbalance (5, 6). The very same definition encompasses the biofuel cells. However, a biological entity in the form of a protein, or whole microorganism is used to enable generation of energy in milder conditions since a physiological environment must be managed in the cell, regardless the electrode material to attain high catalytic or metabolic conversion of substrates (7).

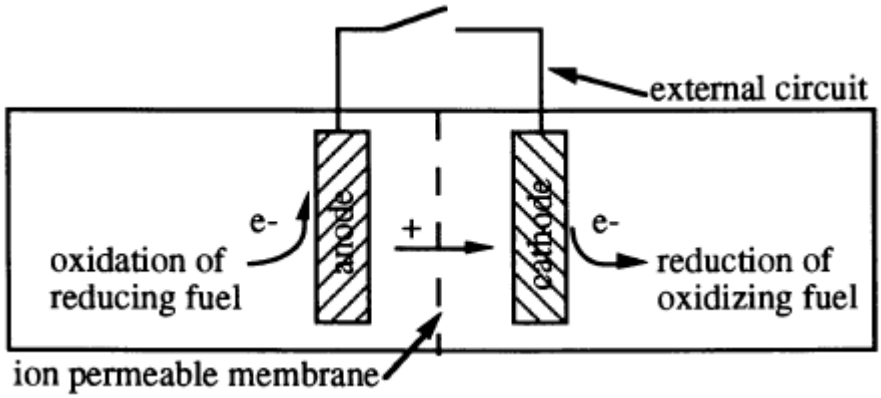

Figure 1.1 - Basic scheme of a fuel cell. If the external circuit is close, generated electrons from oxidation reaction move to the cathode followed by positive ions (5).

Biofuel cells can share some features with biosensors especially if the power being produced is made proportional to fuel concentration bellow the biocatalytic saturation point. Stated simply, a biosensor can be defined as a miniaturized device comprising a biological entity used for real-time analytical purposes. The biological entity serves as selective recognising element of the measurand. The transducer, an electrode in electrochemical biosensors, translates the bio-recognition process into an electrical signal which is then amplified and displayed (8, 9). Thus, in a simplistic way, a biofuel cell can also be thought as the conjunction of up two individual electrochemical biosensors, the bioanode and biocathode, both sharing biocatalysis as recognition processes. Biofuel cells with sensing capability for analytes such as glucose, nitro-based explosive compounds, cyanide,

herbicides, cholesterol, antibiotics, etc, have been in this sense proposed in literature (10-16).

Regardless the device considered, biofuel cell or electrochemical biosensor, whenever the biochemical reaction runs from enzymes, two different mechanisms explain the electrons transfer between enzyme and electrode: mediated electron transfer (MET) or direct electron transfer (DET) (Figure 1.2).

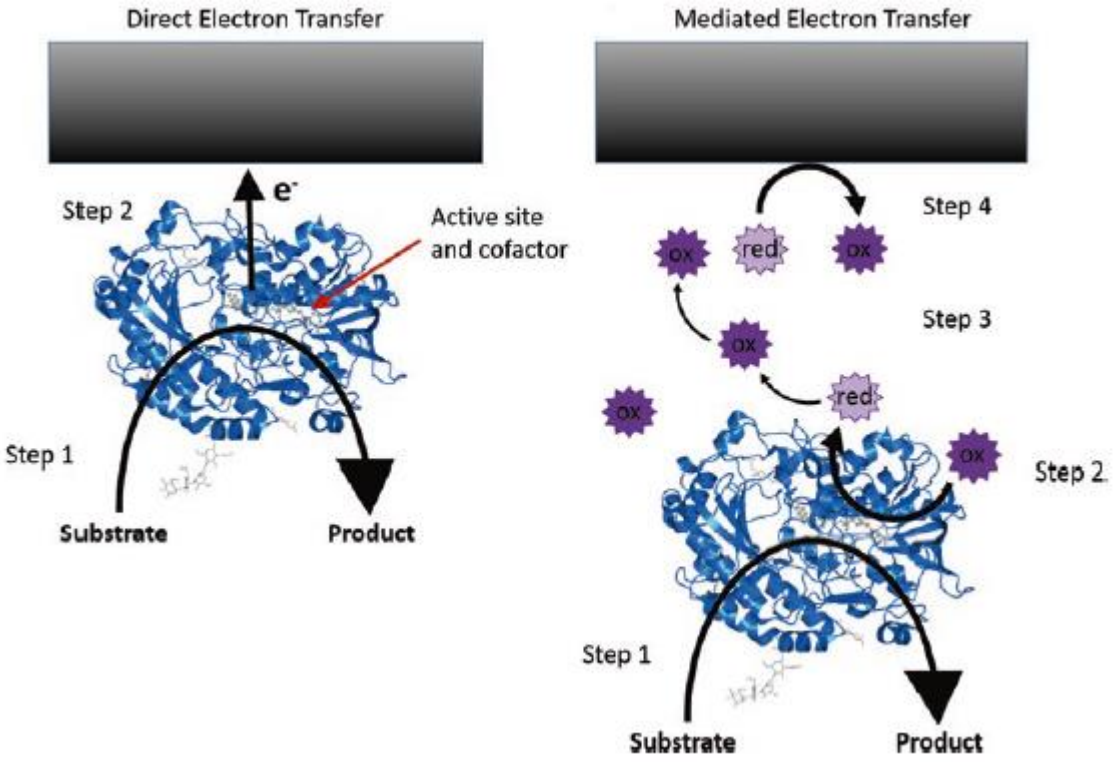

Figure 1.2 - Schemes for the mechanisms of DET (left) and MET (right) for enzymatic oxidation of a fuel/analyte (e.g. glucose) (17).

In MET mechanism, diffusional redox molecules work as shuttles of electrons between the redox active centres and the electrode surface (2, 18, 19). This process lowers the applied potential which favours biosensors regarding possible interferences but compromises biofuel cell efficiency by lowering cell voltage as will be discussed later. In turn, efficient immobilization of an enzyme or microorganisms with conductive pili or expressing plasmalemma cytochrome c proteins may enable DET mechanism. The electrons from the oxidized substrate are transferred directly from the active site to the electrode surface (18, 20). The establishment of DET is always desirable since it simplifies the construction of the biofuel cell, avoids the use of diffusional molecules (mediators) which reduces the cost, allows portability and a higher performance is achieved through gain in cell voltage (21). However, construction of DET biofuel cells is a challenging and difficult process due to the biocatalyst inherent characteristics.

The following subsections will discuss several factors that influence enzyme biofuel cell performance, namely type of electrode, electrode dimensions, electrode pre-treatment, electron enhancer additives, type of enzyme, use of biocompatible films for enzyme stabilization, etc. Moreover, each enzyme is one enzyme which means they interact and respond differently accordingly with the immobilization and the analytical conditions. In the end, fully optimization of the bioelectrode may be extremely complex and cumbersome. The design of miniaturized bioelectrodes herein reported not only allows their use in implantable applications but also allows their integration in microfluidic platforms. This last envisagement is interesting from an environmental point of view since microfluidic self-powered biosensors process small analytical volumes in a lab-on-a-chip approach. In the last subsection of the introduction, a literature overview will be performed concerning the development of microfluidic biofuel cells.

1.2 – History of biofuel cells

Experiments showing possible connection between electricity and biological matter began by the hand of the famous Luigi Galvani in late 18th century with twitching of dissected frog legs after being bridged to the nerve through metal conductors. Galvani recognized the existence of an “animal electricity” as vital force and organic movement as a bioelectric phenomenon. Alessandro Volta would however contest the theory, arguing that electricity had the dissimilar metal nature as source, the very same scientific arguments he explored later to develop the first electric battery (22, 23). The observation of biological activity as possible source of electric energy was demonstrated by the botanist M.C Potter in 1911 (24) and was recognized as the first biofuel cell. In his study, electrical energy was produced from the fermentative process of Saccharomyces cerevisiae yeast cultures. The galvanic cell was implemented by immersion of platinum electrodes in a glucose rich nutritive media. After addition of yeast a gradually increase in voltage was observed, achieving a maximum between 0.3 and 0.5 V. About 20 years later, Cohen (25) managed to obtain over 35 V from half cells of bacterial cultures connected in series. Major advances in the bioelectrochemical energy field have emerged during the 60’s, noting also the interest from the National Aeronautics and Space Administration (NASA) in the subject with a report emphasizing potential application in identification of toxic materials, powering pace makers and as power supplier in remote areas (26). Preliminary experiments employing enzymes (glucose oxidase, GOx) as biocatalysts of biofuel cells were reported in 1962 (27). Enzymatic half fuel cells were studied in more detail by Yahiro et al. in 1964 (28). In their approach, three different types of oxidizing enzymes were tested and added to the anodic compartment

against an O_2 cathode, comprising platinum foil electrodes and separated by an anionic membrane. In these described approaches the biological entity was used dissolved in the electrolyte solution. The prolonged use of enzymes was successfully accomplished in 1962 by Clark (29). The proposed approach comprised the enzyme entrapment between cuprophane layers (dialysis membranes) onto a O_2 sensitive electrode. After glucose oxidase (GOx) entrapment, the substrate glucose was proportionally and indirectly measured through the consumption of O_2 accordingly to the enzymatic reaction. This was a seminal work and a primary step in the research field of portable miniaturized biosensors but also in biofuel cells. Later, Updike and Hicks (1967) (30) simplified the concept of Clark deeming it simply as "enzyme electrode". By following the same line of thought, considerable advances were also achieved by Yaropolov's group when back in 1978/1979 established for the first time direct electron transfer (DET) between the catalytic center of redox proteins and the electrode surface (31, 32). They promoted the electroreduction of O_2 to H_2O_2 without the presence of a mediator compound with electron-shuttling feature in a peroxidase modified electrode but also in a phenol oxidase immobilized onto a carbon based electrode. The achievement opened the possibility for further simplification of biofuel cells construction by eliminating the physical separatoion between anode and cathode compartments.

About 20 years ago, Katz et al. (33) developed the first compartmentless biofuel cell with bioanode and biocathode presenting DET feature, avoiding this way the use of a separator membrane between the anolyte and cayholyte. However, for efficient "wiring", the bioanode and biocathode were engineered by reconstitution from apo-GOx and a pyrroloquinoline quinone (PQQ)-FAD monolayer casted on the Au anode and the transmembrane cytochrome oxidase immobilized in a cytochrome c monolayer at the Au cathode. In a 1 mM glucose air saturated buffer solution, the glucose/O_2 biofuel cell produced 4 μW of power (5 μW cm^{-2}) (33). Since the produced power in the former described DET biofuel cell was low to be used as energy supplier, they applied it as a sensor developing a new concept designated as "self-powered biosensor". They showed that the open-circuit potential of the system varied according to the fuel concentration (glucose) and so a calibration curve could be obtained (10). With all these breakthroughs, experiments on biofuel cell operating *in vivo* started soon after. The first accomplished attempt was done by implanting a tiny biofuel cell in a grape (Figure 1.3). It consisted of 2 cm long and 7 μm diameter carbon fibers modified with glucose oxidase (for the anode) and bilirubin oxidase (for the cathode) enzymes where the direct electron shuttling was performed with the aid of complex redox osmium-based polymers. When inserted near the grape skin the biofuel cell was able to produce about 1.1 μW (240 μW cm^{-2}) at 0.52 V (34).

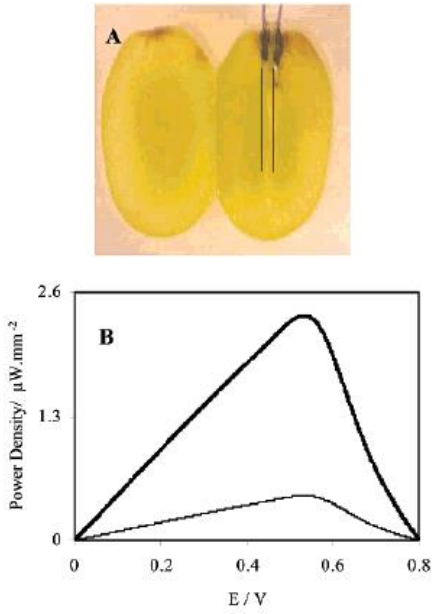

Figure 1.3 - First implantation of a biofuel cell in a living plant showing the carbon fibre electrodes inserted in a grape (above) and the power produced (below) (34).

In 2010, the first tests with biofuel cell implanted in living animals were performed by Cinquin et al. (35) and aimed future medical prosthesis powered through enzymatic biocatalysis. The biofuel cell operated inside a dialysis bag inserted in the abdominal cavity of an anesthetized rat. Briefly, it consisted of a graphite disc combined with freely GOx, catalase and ubiquinone mediator. The cathode was placed in a second dialysis bag, functioning as membrane separator. It also contained a graphite disc with freely polyphenol oxidase and quinone mediator. The whole cell implant was not an impediment to normal activities and movements of the rat, and provided the power of about 24 µW mL^{-1} at 0.13 V, about 8 µW mL^{-1} after stabilization (35). In 2007, the Japanese multinational Sony announced the development of a bio battery to drive up a portable memory-type music player (Figure 1.4). The bio-battery consisted in 4 cubic cells. Each one consisted of porous carbon electrodes afterwards modified with enzymes (glucose dehydrogenase and diaphorase at the anode and bilirubin oxidase at the cathode) and mediators (vitamin K3 and NADH at the anode and potassium ferricyanide at the cathode). A cellophane membrane separated the anode and cathode. Contrary to what seems reasonable in enzyme research, the biofuel cell used high concentrated buffer solution (1.0 M) which showed to maintain maximum enzyme activity on the electrodes. Regarding performance, each cubic cell produced 50 mW (1.5 mW cm^{-2} at 0.3V), the world's highest output at the time (3, 36).

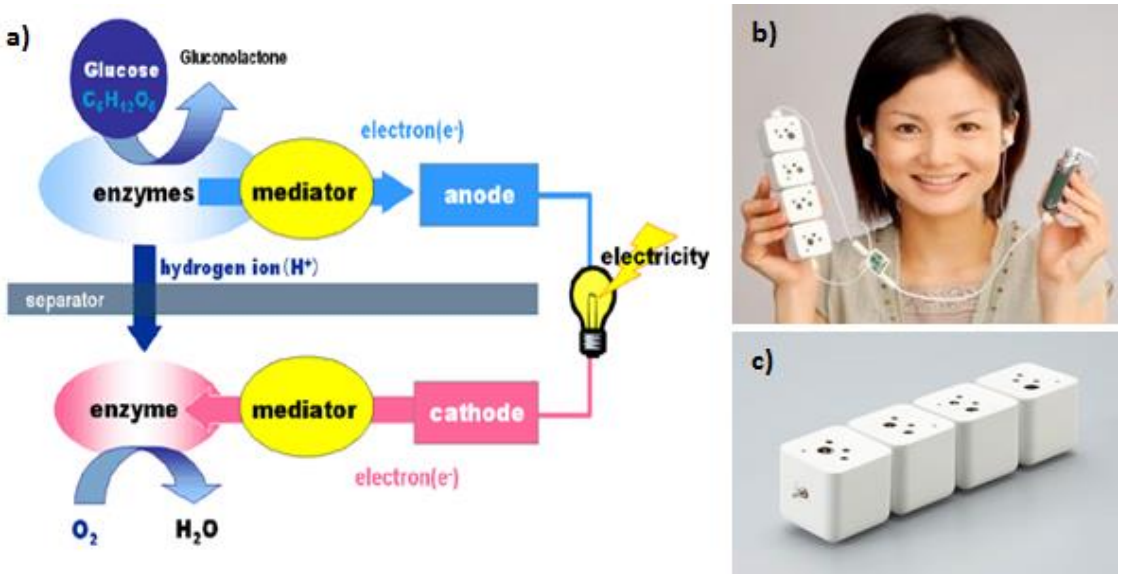

Figure 1.4 - The Sony's bio-battery intended for market commercialization. a) Biofuel cell operation principle. b) and c) images of the final product (3).

A relevant aspect of biofuel cells stems on attention paid to microfabrication of the electrodes. Heller's group developed biofuel cells with reduced dimensions due to the use of carbon fiber electrodes with 0.44 mm^2 active area (37, 38). However, the first prototype biofuel cell integrated in a polydimethylsiloxane (PDMS) microfluidic chip produced by soft lithography was proposed by Moore et al. (39). Micro-molded carbon ink served as anode inside the microchannel. The anode was modified with a methylene green layer and then coated with a mixture of nafion and alcohol dehydrogenase. An external O_2 cathode was connected to the end of the channel and separated by a nafion membrane. The ethanol/O_2 microfluidic half biofuel cell had an efficiency translated by a maximum power density of about 5 μW cm^{-2} and an E_{OCP} (open circuit potential) of 0.34 V in a 1 mM ethanol solution. From this brief historical notes, it becomes clear that biofuel cells, apart from ability to be used as sensors, provide an alternative to traditional fuel cells as energy source with a less harsh environment. The high selectivity of biocatalysis processes, especially in enzymatic fuel cells, turn useless membrane separation between both electrodes, thereby providing opportunity for miniaturization. The maximal power that can be extracted from the biofuel cell is strictly dependent on carefulness dedicated to the selection of enzymes used in cathode and anode as well as to material choice and nanostructuring of each bioelectrode.

1.3 - Biofuel cell mechanics, kinetics and performance

Fuel cells, galvanic cells and supercapacitors share the ability to deliver electric power from processes providing energy at the phase boundary between the electrodes and the

electrolyte. Also in all of them there is separated transport of electrons and ions. However, differently from batteries, energy storage and conversion have different locations in the fuel cell. In turn, energy might not be delivered via redox reactions in supercapacitors (40). Generally speaking, the working principle of fuel cells relies on spontaneous oxidation of the fuel, most of times H_2, at the phase boundary of a solid conductor (anode, reactions 1, 3) with simultaneous reduction of an oxidant, typically O_2, at the cathode (reactions 2, 4):

$H_2 - 2e^- \rightarrow 2 H^+$ (acidic electrolyte) (1)

$O_2 + 4 H^+ + 4e^- \rightarrow 2 H_2O$ (2)

$H_2 + 2 OH^- - 2e^- \rightarrow 2 H_2O$ (alkaline electrolyte) (3)

$O_2 + 2 H_2O + 4e^- \rightarrow 4 OH^-$ (4)

Both electrodes must stand close enough to minimize the internal resistance and at the same time be immersed in a concentrated electrolyte solution capable of conducting ions between the electrodes but also acting as electronic insulator, to prevent self-discharge.
The operational ability of a fuel cell to generate electric power can be measured both by the obtained E_{OCP} and the delivered current density (*j*). The potential difference of both electrodes in the absence of net electronic flow defines the reversible voltage or E_{OCP} (Figure 1.5a). As such, E_{OCP} value can be seen as the electromotive force resulting from the Gibbs free energies enabled through the spontaneous redox chemistries at each electrode (Equation 1.1 - for fuel oxidation) and regarded as an intensity factor of the fuel cell (2, 40):

$$E = E^\circ + \frac{RT}{nF}\ln\frac{A_P}{A_R} \quad (with\ \Delta G = -nFE\ and\ \Delta G^\circ = -nFE^\circ) \qquad (1.1)$$

with *E* and E° being respectively the reversible and standard thermodynamic reversible potential derived from respective Gibbs free energies (ΔG) for the actual activities of reagents A_R and products A_P, *nF* is the number of charges involved in the conversion of one mole of reagent, and *R*,*T* physical constants having their usual meaning.

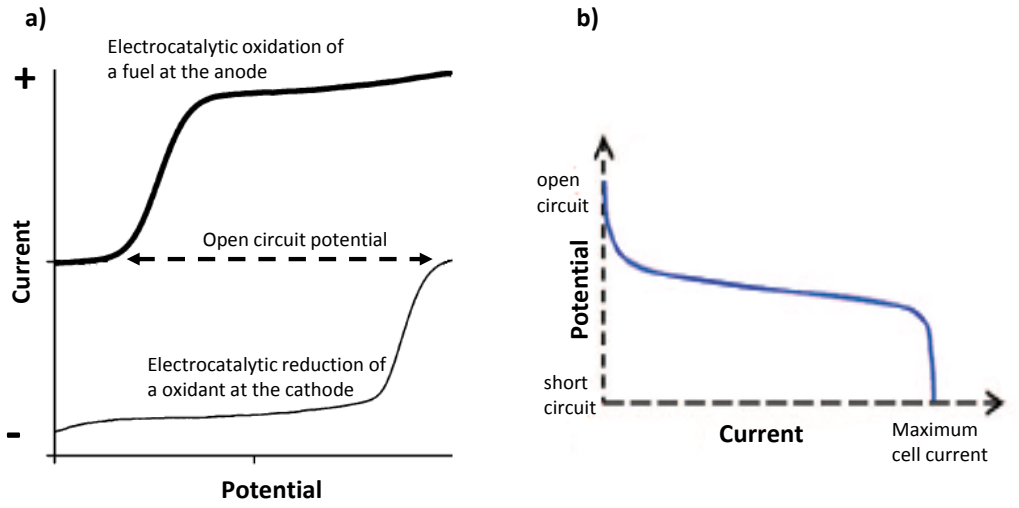

Figure 1.5 – Representation of fuel cell performance. a) Current-potential plot and graph visualization of the theoretical open circuit potential for anode and cathode tested separately; b) potential-current plot generally observed for fuel cells (20).

Though, whenever electronic flow is enabled, unsuspected reactions, kinetic limitations regarding process activation, sluggish charge-transfer and fuel depletion in the vicinity of the electrodes, altogether affect E_{OCP}. Thus, resulting ususlly in overpotential (η) or overvoltage (Equation 1.2):

$$\eta = E_{OCP} - E_{OV} \qquad (1.2)$$

with E_{OV} being the output voltage registered when current flows.

The delivered current density, *i.e.* the electronic current delivered per surface area of the electrode (in A cm^{-2}) is the capacity factor of the fuel cell and is directly connected with the rates of redox processes taking place, internal resistance and limited diffusion of active masses towards the electrode. If the last two polarization causes are minimized, the overpotential due to activation of the main redox process determines current densities described by the Buttler-Volmer equation (Equation 1.3):

$$j = j_0 . \left[e^{\left(\frac{(1-\alpha)nF}{RT}\right).\eta} - e^{-\left(\frac{\alpha nF}{RT}\right).\eta} \right] \qquad (1.3)$$

with j and j_0 representing respectively the current density and the exchange current density, this last being proportional to the overall reaction rate k^0 of the redox process. The transfer coefficients α and $(1-\alpha)$, are the fractions of overpotential determining the change in the oxidation and reduction rates. The occurrence of overpotential phenomena means that the anode potential is less negative and/or the cathode potential is less positive, in practice

always generating less energy than thermodinamically expected. One of most discussed examples, concerns the fuel cell described by the reaction bellow using platinized electrodes:

$$H_2 + ½\ O_2 \rightarrow H_2O \qquad E^o = 1.229\ V,\ \Delta G^o = -235.76\ kJ\ mol^{-1} \qquad (5)$$

Despite being expensive, platinum is an excellent catalyst to be used in both electrodes due to its surface stability in both acidic and alkaline electrolytes. Nevertheless, the oxygen reduction reaction (ORR) taking place at the catholyte imparts overpotential to the cell since the onset of the process occurs consistently 200 mV below the E_{OCP} value at pH = 0 (41, 42) and worsens with increasing pH (43). Besides reaction activation, other causes such as initial electrode poisoning by adsorbed O_2 or OH, underpinned by a multi-step reaction mechanism in which the corroding hydrogen peroxide intermediary is formed have been formulated (44). The use of enzymes as catalysts in biofuel cells also involve overpotential to drive the reaction of substrate catalysis but with similar (45) or even better (43) performance when compared with Pt catalysts. For instance, the onset for oxygen reduction at the active site for laccase from *Trametes versicolor* is about 0.75 V vs SHE (pH = 3) whereas for *Rhus vernicifera* laccase, the onset starts at around 0.4 V vs SHE (pH = 5) (31) and thus a higher overpotential is observed for the later enzyme. So when immobilized in the cathode, *Trametes versicolor* will generate a higher E_{OCP} when compared with *Rhus vernicifera.* Moreover, the activity towards oxygen reduction in Pt surfaces is more negatively affected by the presence of contaminants and interferents such as chloride ions (42) which may not be the case when enzymes are used as catalysts.

In fuel cells, a separation membrane is used to prevent the presence of fuel in the vicinity of the cathode and oxidant in the anode. Since the anode is poised at negative potentials compared to the cathode, the use of platinum metal catalysts would oxidize the fuel more readily at the cathode and the oxidant more readily reduced at the anode (34). The use of enzymes as electrocatalysts may equate a possible elimination of platinum as catalysts and likewise the elimination of the separation membrane in fuel cells. First, enzymes are highly specific to their substrates being less subjected to the interference of other compounds. Secondly, enzymes operate in a wide pH range or even at physiological conditions (46). These factors allied to an efficient electronic coupling between the catalytic centre of the enzyme and electrode open the possibility of construction of compartmentless biofuel cells, thus making possible miniaturization and the foresight of self-powered *in vivo* implants. If direct electron transfer (DET) is not accomplished, then diffusional mediators may be required to allow the biocatalytic reaction. However, a membrane may be essential in this

cases to prevent oxidation of the mediator in the cathode (if anolyte mediator is used) or reduction in the anode (if catholyte mediator is used) (34), which would lead to null or negligible produced current (47). The electric power produced in a fuel cell is derived from a compromise between the limiting cases of open circuit (maximum voltage and no current due to high resistance) and short circuit (maximum current and no voltage due to low resistance), as seen in Figure 1.5b. The representation of cell power and cell voltage gives a curve normally with a shape of a bell.

Despite all advantages offered by enzymes over precious metal catalysts, the power output in biofuel cells is comparably low, in the order of microwatts. Moreover, if soluble mediators are used the cell voltage may decrease further when the redox potential is significantly more positive than the fuel or more negative than the oxidant (more overpotential), compromising therefore the generated power (20, 33).

1.4 - Carbon materials in biosensors and biofuel cells

Carbon based materials have an undeniably importance in the electrochemistry field. Nowadays they stand between, if not the most common used materials in the fabrication of electrochemical sensors, fuel cells and capacitors. Besides the availability and reduced cost, carbon has attractive intrinsic characteristics regarding its conductivity, mechanical properties and biocompatibility. The good electrochemical stability in a wide potential range and especially the slow oxidation kinetics at positive potentials relative to Pt or Hg makes carbon practical for solid electrodes. They can be obtained in various forms such as pyrolytic graphite, glassy carbon, carbon nanofibers and present a surface easily modifiable by reaction or by adsorption, thus providing easily chemically modified electrodes for improved analytical outcomes (48).

Carbon atoms can form different multi-atom structures, resulting in different carbon allotropes, such as diamond, amorphous carbon and graphite, with this last one being widely used in the construction of sensors and fuel cells due to its favourable electronic properties (49). Single-crystal graphite is an anisotropic multilayer structure where each layer is composed by sp^2 carbon atoms disposed in hexagonal configuration resembling a honey comb (50). The interlayer spacing is smaller in the single crystal, but larger for glassy carbon and carbon black, with subsequent different behaviours regarding compounds intercalation. Also the electric resistivity along each layer (basal plane) is twenty-five times superior to the one shown by copper but 10^{-4} inferior to the between layer (edge plane) resistivity. In the high pyrolytic graphite electrode (HOPG), only differing from single-crystal crystal graphite for a slight greater inter-layer rotational disorder, the overall reaction rate k_0

for the common probe $Fe(CN)_6^{3-/4-}$ is also of about 10^{-4} smaller when the basal plane is the electroactive surface, relative to edge plane (48). Table 1.1 describes the dominant structural properties determining the electrodes performance. For instance, polycrystalline graphite electrodes are high porosity electrodes made of several hundred angstroms microcrystallites in random oriented order. Usually some kind of inert binder material fill the pores and provides physical consistence. The background currents in this type of electrodes is small because it is restricted to the islands formed by the conductive microcrystallites on the surface contacting the electrolyte solution. On other hand radial diffusion of electroactive compounds toward this islands adds to perpendicular diffusion observed for homogeneous active surfaces, leading to comparative increased current densities.

Table 1.1 – Solid electrodes based on carbon materials

Carbon electrode type	**Dominant structural property**
Pyrolytic graphite	Long-range order of graphitic layers
Highly ordered pyrolytic graphite	Long-range order of graphitic layers
Polycrystalline graphite: carbon paste spectrographic graphite graphite composite	Porosity
Glassy carbon	Low resistance
Carbon fibres	Reduced dimensions

Apart from the conventional solid electrodes, other carbon nanometre structures such as MWCNT, SWCNT, graphene and carbon black (Figure 1.6), have been used either as electrode support (51-55) or as an additive for modification of the electrode surface.

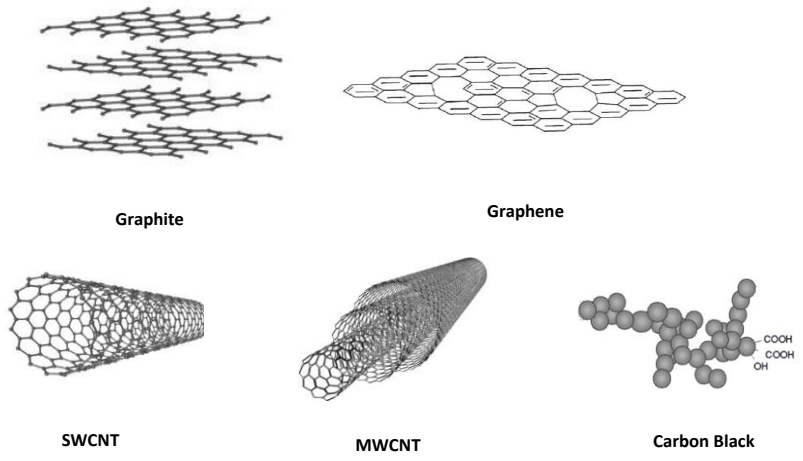

Figure 1.6 – Various graphite based materials commonly used in the construction of biosensors and biofuel cells

Though with the same sp^2 configuration, this new of carbon materials represent three-dimensional variations of graphite layers instead of different arrangements of crystallographic structures (56, 57). Graphene, as example, is obtained from the exfoliation of graphite as single 2D layer of graphite (58) while carbon nanotubes can be seen as a rolled graphene sheet in the form of individual (SWCNT) or multiple concentric arranged tubes (MWCNT) (59). In turn, carbon blacks can be obtained from the combustion of hydrocarbons (56) and are aggregates or agglomerates of spherical particles where each particle owns a turbostratic structure of random packing graphite layers (56, 60, 61), as depicted in Figure 1.7.

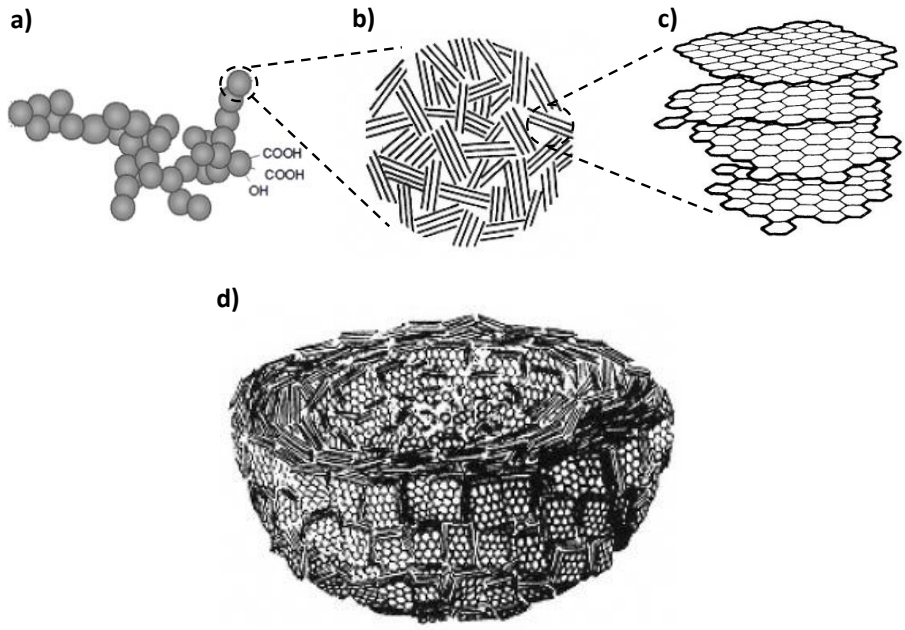

Figure 1.7 - Carbon blacks. a) Carbon black agglomerate (61). b) Scheme of carbon black single particle showing the turbostratic sctructure of graphite layers. c) Graphite layers that compose a single carbon black particle. d) Representation of a half hemisphere of a single carbon black particle (56).

As stated before, the electrochemical properties depend of the anisotropic electrical properties and the chemical activity of the material (57). The edge plane and basal plane, represented in Figure 1.8, of graphitic materials differs in terms of electronic and electrochemical properties. This could be attributed to the surface chemistry, since in the edge plane, broken C – C bonds forms various oxides (57) which may enhance electron transfer kinetics (48). In a different aspect, specific functionalization of the carbon material promote covalent attachment of biomolecules for efficient construction of biosensors and biofuel cells, as is the case of carboxylic groups that form amide bonds with amine containing proteins (62).

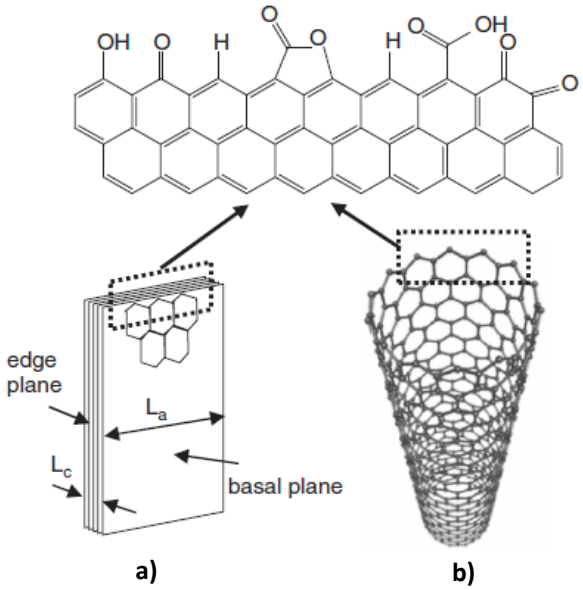

Figure 1.8 - Structure of graphite displaying edge plane and basal plane, showing the surface chemistry on the edge plane. a) HOPG electrode and b) SWCNT (57).

Nanostructuration of the electrode with carbon-based materials enhances the analytical signal by promoting DET between the electrode surface and the enzyme caused by shortening the distance to the enzyme active site. Both MWCNT and SWCNT have been used in the construction of biosensors and biofuel cells featuring DET (63-65). The same is observed for the use of graphene (66-68). As an example, Sehat et al. (68) employed a simple modification method consisting in the simultaneous reduction of graphene oxide and immobilization of GOx by an electrochemical procedure at fixed potential (-1.5 V). The resulting PGE biosensor enabled direct electrochemistry with high sensitivity to glucose, though within a limited concentration range.

Carbon nanofibers have been extensively used by Heller's group as electrode support in highly efficient miniature biofuel cells (34, 37, 38, 46). These tiny electrodes with 7 μm diameter exhibit the same behaviour of ultramicroelectrodes. In ultramicroelectrodes the diameter is usually smaller than the diffusion layer thickness and thus typical non-planar diffusional responses prevail at short times enhancing the signal-to-noise ratio and allowing the use of very fast voltage scan rates (>100 V/s) in voltammetric studies. Although the magnitude of the current decreases, the signal-to-noise ratio can improve a 1000 fold, if the contributions from electronics to noise are negligible (57).

1.4.1 - Pencil mines as reliable and costless solid electrodes

Pencil graphite electrodes (PGE) are a type of solid electrode that consists in carbon pencil mines, commonly used for writing and drawing. Their application have been increasing lately in the electrochemistry field due to the electric properties, ubiquity and negligible cost.

Some studies performed with the $[Fe(CN)_6]^{3-/4-}$ and $[Ru(NH_3)_6]^{2+/3+}$ probes have shown higher stability and analytical reproducibility of PGE when compared with pyrolytic graphite or glassy carbon electrodes and hence looked as a viable alternative in electrochemical studies (69, 70). The pencil mines consist of an extruded mixture of graphite and clay (used as binder) (71). Different starting percentages of graphite and clay allows the fabrication of mines with corresponding hardness. Nowadays, 22 types of pencils can be found in the market scaling from 10H to 10B. The letter B stands for softer pencils which means higher content of graphite and the letter H stands for harder pencils which means a higher content in the binder. The designated HB pencil stands as the middle term of the scale and ~~a~~ typically contains about 68% graphite, 26% clay and 5% of wax (72). So, from a theoretical point of view, since electrical properties of electrodes such as conductivity largely depend on the carbonaceous content, the use softest pencils as electrodes would seem advantageous (73). In fact, this was observed for the determination of phenols, where signal to noise ratios increased together with the pencil softness up to 6B (74). Likewise, the electrodes drawing over cellulosic surfaces with pencils 6B (72, 75) or 8B (73) enhanced the electrochemical performance of the therein reported sensors. Worth of mention, some authors have specifically studied the influence of pencil hardness in the electrochemical performance of PGEs. For instance, Kariuki (76) analysed the surface structure and the electrochemical properties of PGE. The X-ray photoelectron spectroscopy (XPS) results showed higher oxygen to carbon ratio (O/C) in harder pencils (H) compared to softer ones (B) as well as the presence of silica and aluminium, explained by the higher content of clay incorporated on the graphite lead. Resorting to the electrochemical probes $[Fe(CN)_6]^{3-/4-}$ and $[Ru(NH_3)_6]^{2+/3+}$, cyclic voltammograms showed lower peak to peak separation (ΔE_p), which was more evident for HB mines due to faster heterogeneous electron transfer when compared with the H and B varieties. On the contrary, Tavares and Barbeira (77) found that ΔE_p continuously decreased with the increase of PGE hardness when the PGE's were evaluated in a $K_4[Fe(CN)_6]$ solution. Based on a similar conclusion, the PGE type 6H was considered the best choice for the determination of hydrogen peroxide (78) or guanine signal (79). Yet, in caffeic acid detection HB PGEs enabled better signal-to-noise ratio when compared with the 2B, 2H and 5H alternatives (80).

One important factor for the electrochemical performance of all solid electrodes and particularly for carbon-based electrodes is the pre-treatment given to the active surface. In the construction of sensors and biosensors a pre-treatment is usually given, consisting in either mechanical polishing, chemical treatment (using an organic solvent like ethanol or acetone), electrochemical treatment (at fixed or dynamic potentials) or a combination of both these treatments. The electrochemical pre-treatment of carbon electrodes supposedly creates functional groups on the surface of the electrode, serving as electron transfer

mediator between electrode and electroactive species enhancing the electron transfer or adsorption (48, 81). In most works describing PGEs as nucleic acid sensors, the electrode pre-treatment consisted in the application of a fixed positive potential (+1.4 V or higher) for a short period of time (82-86). This anodization seems to be essential to activate the electrode surface, for enhancing the sensitivity performance. It introduces oxygen functionalities as mediators or the formation of a hydrophilic surface which becomes more accessible to electroactive species. Alternatively, the treatment enables the removal of impurities of the electrode from the polishing and preparation process (81, 87). The activation of the PGE allows an effective adsorption of DNA on the graphite surface and improved the analytical signal (88, 89). When comparing a potentiodynamic with the potentiostatic pre-treatment, Özcan´s group found that the first provided even better results in the determination of dopamine (90). Similar conclusions regarding carcinogen Sudan II compound were obtained by Ensafi et al. (89). This higher efficiency of the cyclic voltammetry pre-treatment compared to the anodization pre-treatment alone is explained by the fact that the application of negative potentials (cathodization) after the anodization step reduces the number of oxygen functionalities formed in the anodization process (87). Nonetheless, the absence of pre-treatment may be in some applications favourable to the analytical outcome. In this sense Majidi et al. (91) realized that a rough, unpolished graphite surface can benefit the electrodeposition of copper ions during the nucleation stage.

Pencil graphite electrodes possess structures formed by carbon to carbon bonds with sp^2 configuration, similarly to glassy carbon and pyrolytic graphite. However each carbon electrode may present different physical and electrochemical properties due to variations in the size and in the inter- and intraplanar orientation of graphitic microcrystallites (48, 92). In the study conducted by Kariuki (76), higher voltammetric peaks were obtained for redox probes $Ru(NH_3)_6^{2+/3+}$, $Fe^{2+/3+}$ and dopamine using PGEs when compared to GCE. Also a better performance regarding reproducibility and ΔE_p was achieved in comparison with HOPG. However, the highly disordered edge planes constituting the GC surface provided faster electron transfer kinetics for each probe, translated by the lower ΔE_p. Other works have also confirmed the good performance relatively to GCE for the guanine oxidation signal (82, 93) and the determination of the carcinogen 7,12-Dimethylbenz[a]anthracene (94). When compared with GC, higher background currents are registered for PGE which may advent from the presence of other constituents of pencil mines besides graphite (94). Besides, small differences in carbon structures may be reflected on the background currents affecting the reproducibility of response between electrodes. The porosity of the material and the characteristic surface roughness increases the double-layer capacitance of electrodes as well. Since graphitic materials have void space, solution may be absorbed

resulting in uncontrollable background currents (48). Although there is an absence of general consensus regarding the superiority in analytical performance of PGE over GCE, the former electrode has always the enormous advantage of being inexpensive and commercially available with the possibility of being used as a disposable electrode. In contrast, the perennial GC electrode requires fastidious pre-treatment between usages in order to optimize its electrochemical performance (48). In summary, to achieve the best analytical results, the analyst should take in consideration the several factors described before, especially pre-treatment and hardness, when choosing the ideal PGE. Even different manufactures of pencil mines with respect to the same type will produce different results (77).

Biofuel cells based on PGE have not been reported yet. In turn, several biosensors employing enzymes as catalysts have been described. A diversity of enzymes have been applied in the construction of PGE biosensors namely acetylcholinesterase, alcohol dehydrogenase, ascorbic oxidase, cholesterol oxidase, glucose dehydrogenase, glucose oxidase, glycerol kinase, glycerol-3-phosphate oxidase, L-glutamate oxidase, L-lactate dehydrogenase, L-lactate oxidase, laccase, lipase, peroxidase, uricase and xanthine oxidase. The characteristics and performances of each PGE biosensor is described in Table 1.2. From the comparison between the glucose biosensors tabled is not evident an ideal immobilization process rendering optimal analytical performance. There is a systematic lack of data concerning surface coverage since it influences the diffusion resistance and overall kinetics. Nonetheless, both approaches proposed by Cheng´s group (95, 96) enabled the most sensitive sensors. Such evidence resulted however from the implementation of typical higher active surface of carbon paste electrodes onto pencil conductive supports and from the very high loadings of enzyme used in the electrode preparation. On the other hand, biosensors proposed by Elahi et al. (97) and Sehat et al. (68) where rGO was used for electron transfer enhancement, an improvement in the LOD was obtained underlining faster heterogeneous electron shuttling process, however at the cost of short linear analytical ranges. Surface oxidation to improve wettability plus modification with nanostructures, such as QDs (98), seems to be beneficial since the comparison with similar nanostructured biosensors implemented from HOPG, GC, Au and ITO, revealed better LOD and sensitivity.

Table 1.2 – Enzymatic PGE biosensors characteristics and analytical performance

Analyte	Enzyme	PGE type, diameter (mm)	Pre-treatment	Immobilization	Analytical performance				Ref.
					Linear range (mM)	Sensitivity		LOD (µM)	
						(µA mM^{-1})	(µA mM^{-1} cm^{-2})		
Glucose	Glucose oxidase	HB, 0.5 HB, 0.9	Mechanical (polishing)	PGE-$POs^{+}NH_2$-GOx	0 - 10	-	1	-	(99)
Glucose	Glucose oxidase	0.5	-	PGE-nafion-GOx/BSA/PVA-SbQ-MB-CTA	0.28 – 33.3	0.043	5.5	-	(100)
Glucose	Glucose oxidase	H, 0.3	-	PGE-PB-GOx/GA-nafion-PU	0 – 5.3	0.091	1.9	-	(101)
Glucose	Glucose oxidase	HB, 0.5	-	PGE-CP-AuNPs-cysteine-DCC-GOx	0 – 33.4	5.06	-	22.3	(95)
Glucose	Glucose oxidase	HB, 0.5	-	PGE-CP-AuNPs-cysteine-FcAld-DCC-GOx	0 - 39	2.21	-	7.8	(96)
Glucose	Glucose oxidase	2B, 0.9	Mechanical (polishing) Electrochemical (catodization)	PGE-rGO-GOx	0.04 – 0.6	1.8	278	0.61	(68)
Glucose	Glucose oxidase	2B, 0.5	Electrochemical (catodization)	PGE-CdS-ZnS-Chit/GOx	0.01 – 1	1.83	11.5	3	(98)
Glucose	Glucose oxidase	3	-	PGE-poly(GMA-co-VFc)-APBA-FAD-apoGOx	1 – 17	0.27	3.8	2.7	(102)
Glucose	Glucose oxidase	0.9	Mechanical (polishing)	PGE-rGO-ZnO/Cu_2O-GOx-nafion	0.01 – 2	0.34	54	1.93	(97)
Glucose	Glucose dehydrogenase	2B, 0.5	Electrochemical (catodization)	PGE-CdS-ZnS-BSA/GA/GDH	0.2 – 8	0.118	0.74	90	(103)

Table 1.2 – (Continued)

Analyte	Enzyme	PGE type, diameter (mm)	Pre-treatment	Immobilization	Analytical performance				Ref.
					Linear range (mM)	Sensitivity		LOD (μM)	
						(μA mM^{-1})	(μA mM^{-1} cm^{-2})		
Ascorbic acid	Ascorbate oxidase	2H, 0.3	-	PGE-PEI-BSA/AOx-PU	0 – 0.1	0.196	276	0.26	(104)
Ascorbic acid	Ascorbate oxidase	2H, 0.3	-	PGE-MWCNT-PEI-BSA/AOx-PU	0 – 0.02	0.486	685	0.22	(105)
Cholesterol	Cholesterol oxidase	HB, 1.5	Chemical (acid washing)	PGE-ChOx	1.29 – 10.3	4120	4380	90	(106)
Deferiprone	Horseradish peroxidase	-	-	PGE-AuNPs-GA-HRP	0.1 – 1	375	-	0.005	(107)
Ethanol	Alcohol dehydrogenase	2	Mechanical (polishing) Chemical (orgnc. washing)	PGE-SWCNT-PCV-BSA/GA/ADH	0.0093 – 0.32	0.061	1.94	-	(108)
Hydrogen peroxide	Horseradish peroxidase	6H, 2	Mechanical (polishing) Electrochemical (catodization)	PGE-Chit-AuNPs-HRP	0.01 – 1.5	4.7	149	2	(78)
Hydrogen peroxide	Horseradish peroxidase	2	Chemical (orgnc. washing)	PGE-Poly(GMA-co-VFc)/rGO-HRP	0.000006 – 0.0001	1.83	11.5	0.00002	(109)
L-lactate	L-lactate oxidase	6B, 2	Mechanical (polishing) (Chemical (orgnc. washing)	PGE-PANI-CuNPs/MWCNT-LOx	1 – 17	0.27	3.8	2.7	(110)

Table 1.2 – (Continued)

Analyte	Enzyme	PGE type, diameter (mm)	Pre-treatment	Immobilization	Analytical performance				Ref.
					Linear range (mM)	Sensitivity		LOD (μM)	
						(μA mM^{-1})	(μA mM^{-1} cm^{-2})		
L-glutamate	L-glutamate oxidase	HB, 2	Mechanical (polishing) Chemical (orgnc. washing)	PGE-ZnO/PPy-GluOx	0.00002 – 0.5	1.4	1.1	0.00018	(111)
Organophos. pesticides	Acetylcholinesterase	HB, 0.9	Chemical (orgnc. washing)	PGE-PEI-PB-GA-AchE	0 – 0.9	0.6	6	-	(112)
Oxygen	Laccase (Trametes versicolor)	1.4	Chemical (acid washing)	PGE-PANI-MWCNT-laccase	-	-	-	-	(113)
Oxygen	Laccase (Rhus vernicifera)	HB, 2	Mechanical (polishing)	PGE-rGO-SWCNT/laccase-solgel	0 – 0.45	4.5	132	2.7	(114)
Uric acid	Uricase Horseradis peroxidase	HB, 0.5	Chemical (orgnc. washing)	PGE-GA/uricase/HRP	0 – 0.12	2.6	-	0.6	(115)
Xanthine	Xnathine oxidase	-	Chemical (acid washing) Mechanical (polishing)	PGE-Chit/AuFeNPs-GA-XOD	0.0001 – 0.3	-	1169	0.1	(116)
Xanthine	Xanthine oxidase	2	Chemical (orgnc. washing)	PGE-Poly(GMA-co-VFc)/MWCNT-XOD	0.002 – 0.28	16	24.3	0.12	(117)
Xanthine	Xanthine oxidase	-	Chemical (orgnc. washing)	PGE-Poly(DTP-alkyl-NH_2)-GA-XOD	0.0003 – 0.025	124	-	0.074	(118)

1.5 – Features of Enzymes used as biocatalysts in biosensors and biofuel cells

The biocatalytic processes promoted by the particular class of proteins generically known as enzymes and are important to sustain life in all its aspects. Their function stands on lowering of the activation energy for chemical conversion of metabolites. To this, they are abundantly distributed in living beings in a great variety due to the very specific role each one is needed. Redox enzymes, in particular, enable electron exchange to/from specific compounds along energy chains. They consist of a redox centre assuring bioactivity embedded in a complex polypeptide tertiary structure conferring stable function in surrounding microenvironment and specifying a particular reacting compound, the substrate (119). Guided by the glucose biosensor as ultimate example of its clinical importance and successful commercial application, enzymes turned possible the development of a plethora of useful biosensors in association with the electrochemistry field (120). Most often, enzymes provide direct oxidation and reduction reactions of their substrates where the generated electrons are transduced, hence producing a signal. Yet, in some cases, enzymes enable conversion of non-electroactive substrates into electroactive species which can be then processed by the electrode surface (32). A number of different biosensors and biofuel cells can be implemented given the multiplicity of redox enzymes available. Moreover, isozymes derived from different organisms may present substantial differences regarding catalytic activity and redox potential offering therefore diverse options for optimized use in the intended application as shown later on this chapter. As stated before, the biocatalytic function of redox enzymes is owed to active centres deeply buried in the protein shell. The active site may consist of metal-based centres such as heme, iron-sulphur clusters, copper or copper-zinc held through coordinate-covalent bonds on the amino acid side chains, inorganic ligands or prosthetic groups (e.g. heme) showing particular affinity to different redox reactions with substrates (18). Other enzymes make use of pure organic cofactors, like flavin adenine dinucleotide (FAD) in GOx (121) or pyrroloquinoline quinone (PQQ) in methanol dehydrogenase (MDH) (122) as active centres. The protein shell enclosing the active site protects it from hostile environments. Nevertheless, it has important functions since it defines the substrate selectivity and access, provides an internal electron relay system, proton access and the functional groups at the surface enable reactions for chemical attachment to other molecules or surfaces (20). The catalytic properties of a given catalytic centre can change depending of the proteinaceous environment where it is incorporated. For instance, heme molecule can experience various

formal redox potentials for the couple Fe^{2+}/ Fe^{3+} whether it is incorporated in a HRP enzyme (E^0 = -0.27 V vs SHE) or in a cytochrome c protein (E^0 = +0.26 V vs SHE) (18).
By being non-conductive, the protein shell acts as barrier to the electron shuttling from or towards the electrode surface (123). The achievement of heterogeneous DET enables practical and easier application of enzymes to biosensors and biofuel cells. First because the bioelectrode operates in a potential window close to the enzyme potential avoiding thus possible interferences and second, the use of additional reagents working as mediators is unnecessary (18, 123). Experimental evaluation of DET between enzymes and electrodes can be accomplished through observation of catalytic response current in the presence of substrate and/or observation of a signal corresponding to the active centres of the enzyme in the absence of substrate (32). This subchapter will focus mainly in the most commonly used enzymes in biofuel cells, namely multicopper oxidases at cathodes and the flavin-containing GOx at the anode since these enzymes generally operate at physiological conditions and possess high activity. Their mechanism of action are well described in the literature (18, 32).

1.5.1 - Enzymes for cathodic processes

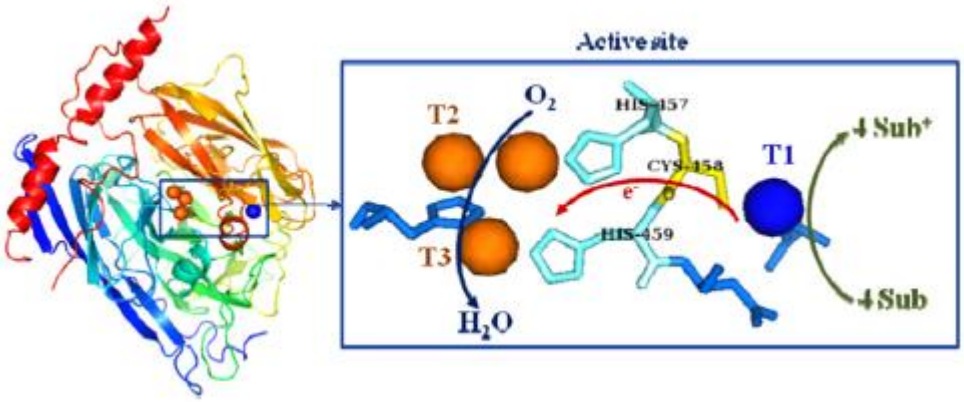

Figure 1.9 - Representation of the structure of BOx (left) and the respective active centres with mechanism of electron transfer (right) (124).

In the majority of fuel cells and biofuel cells, O_2 is chosen as the oxidant since it has a high reduction potential, maximizing the cell voltage and is freely available everywhere (20). As discussed before, enzymes have the ability to reduce oxygen at low overpotentials, being therefore favourably compared to the more expensive platinum electrocatalyst. The so called “blue” multicopper oxidases like tyrosinase, ascorbate oxidase, laccase, bilirubin oxidase (BOx) or ceruloplasmin, are examples of enzymes that notably couple four one-electron oxidations of organic substrates or metal ions to the four-electron reduction of O_2 to H_2O in a two two-electron step process. In all multicopper oxidases the active site is

composed by a minimum of four copper atoms. These are traditionally divided according the spectroscopic features which reflect the geometric and electronic structure of the site: the 600 nm absorbing blue Cu type 1 (T1), one normal copper type 2, binuclear copper centres (type 3) and trinuclear copper clusters (TNC) comprised of one T2 and one T3 centre (Figure 1.9). It is clearly known that the organic substrate binds near the copper T1 site, the primary electron acceptor located about 7 Å under the protein surface. The electrons are then internally transferred, via cysteine-histidine residues to the trinuclear T2/T3 site located about at least 12 Å (125, 126), where dioxygen binding, hydroperoxide reduction and cleavage take place. For example, BOx enzyme becomes active after full reduction of all copper atoms at T1 and TNC from the full oxidized or partial alternate Cu(II) resting forms, usually after binding of bilirruibin at the T1 centre (127). The TNC centre is then able to quickly bind the O_2 molecule thus becoming in the native intermediate form. The redox potential regarding the T1 site of "blue" multicopper oxidases differs greatly from each other, even being suggested that it is correlated to the ligands surrounding the T1 copper site (126, 128). Generally, the tripeptide histidine-cysteine-histidine connects the T1 copper to the lower redox potential trinuclear T2/T3 site along with an axial ligand. Bilirrubin oxidase from *Myrothecium verrucaria* as well as laccase from *Rhus vernicifera* have a methionine residue as axial ligand. Their T1 redox potentials stay close, respectively 490 mV and 430 mV (vs NHE), and both are considered low potential enzymes (31, 126). On the other hand, laccase from *Trametes versicolor* has a phenylalanine coordinating group, with a thereby corresponding T1 redox potential of about 780 mV (vs NHE) and so considered a high potential enzyme. The comparison of redox potentials and the ligands for BOx and laccases from different origins is presented in Table 1.3.

Table 1.3 – Potentials of T1 site and ligands to the T1 site (underlined) of different "blue" multicopper oxidases (32).

"Blue" multicopper oxidases	**Sequence**	**E^0, T1 (mV vs NHE)**
Laccase *Trametes hirsuta*	H...H C H I D F H L E A G F	780
Laccase *Trametes versicolor*	H...H C H I D F H L E A G F	780
BOx *Myrothecium verrucaria*	H...H C H N L I H E D H D M	490
Laccase *Rhus vernicifera*	H...H C H F E R H T T E G M	430

Laccases from different origins, besides catalysing the electroreduction of oxygen at very distinct potentials, can also allow catalytic conversion at different optimal pH regions. Fungal laccases such as *Trametes versicolor* or *Trametes hirsuta* seem to have optimum pH values at acidic regions (31, 129) while tree laccase, *Rhus vernicifera*, operates at more neutral to basic pH's either immobilized and/or in solution (130-132).

At carbon electrodes the DET mechanism of “blue” multicopper oxidases seems to be consistent with the electron transfer mechanism for substrates. So the electrode act as the primary electron donor for the T1 site of the adsorbed enzyme and then through internal electron transfer to the T2/T3 copper cluster where occurs the reduction of molecular oxygen (Figure 1.10).

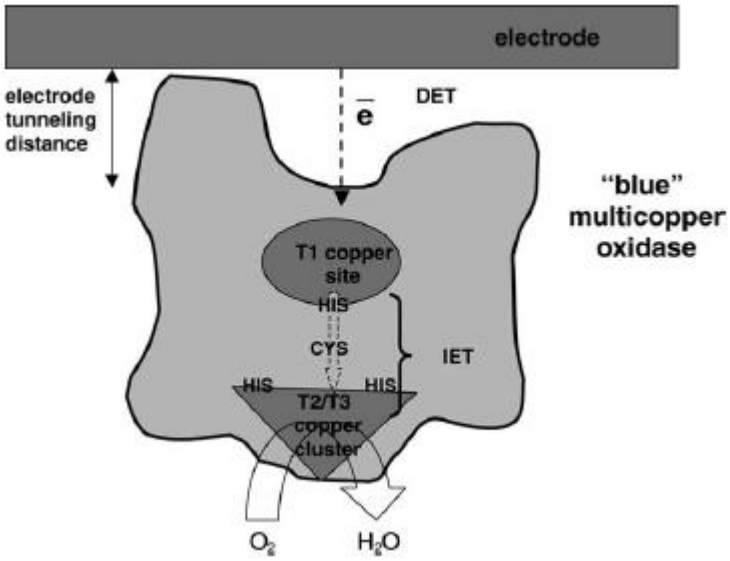

Figure 1.10 - Scheme of DET for a “blue” multicopper oxidase immobilized in a carbon-based electrode (32).

The enzyme cytochrome C oxidase is another example of copper-containing enzymes that has been characterized and applied in the cathode of biofuel cells (33, 133). The high overpotential this enzyme requires for O_2 electrocatalysis (20) lead to poor efficiency of the cell with a generated E_{OCP} of only 120 mV (33, 133).

Another oxidant that can be used in biofuel cells is hydrogen peroxide (15, 134). Pizzariello et al. used horseradish peroxidase (HRP) biocatalyst in the cathode alongside with an immobilized ferrocene mediator to process the reduction of H_2O_2 into H_2O. The glucose / H_2O_2 biofuel cell achieved only a an E_{OCP} of 0.22 V and a power density of 0.15 μW cm^{-2} in 1 mM concentration of fuel and oxidant (134). In the approach from Sekretaryova et al. (15), the enzyme cholesterol oxidase (ChOx) was immobilized both in the anode and cathode. Since H_2O_2 is the by-product of several oxidase enzymes including ChOx, the produced H_2O_2 is then reduced to H_2O in the Prussian blue modified cathode. The onset of H_2O_2 reduction was +0.37 V (vs Ag/AgCl) reaching a current density of 62 μA cm^{-2}. Overall, the biofuel cell generated an E_{OCP} of 0.11 V and a power density of 11.4 μW cm^{-2} for 5 mM of cholesterol.

1.5.2 - Enzymes for anodic processes

Regarding the anode, though gases electrodes allow high oxidation potentials for H_2, the readily available glucose has been the fuel of choice to be oxidized. For this matter, two enzymes have been widely used: glucose oxidase (46, 135-139) and glucose dehydrogenase (140-143).

Glucose oxidase from fungal origins (e.g. *Aspergillus niger*) is a homodimeric glycoprotein where the active site is composed by a FAD cofactor per monomer. The substrate, β-d-glucose binds to the active centre through a series of hydrogen bonds where it is oxidized to d-gluconolactone with concomitant reduction of O_2 to H_2O_2 (144). The cofactor is deeply buried in the carbohydrate shell of the enzyme. When immobilized, the gap between the active site and the electrode surface prevents an efficient electron transfer. To minimize this problem, mediators such as ferrocene are commonly used in the construction of second generation biosensors since ferrocene conjugates well with the enzyme at physiological conditions (121). A much simpler approach consists in the establishment of DET through the use of highly conductive materials such as carbon nanotubes (63-65, 145) or metallic nanoparticles (146). Since the potential of the active site ($FAD/FADH_2$) is negative, this enzyme is well suited as a biocatalyst for anodes (145).

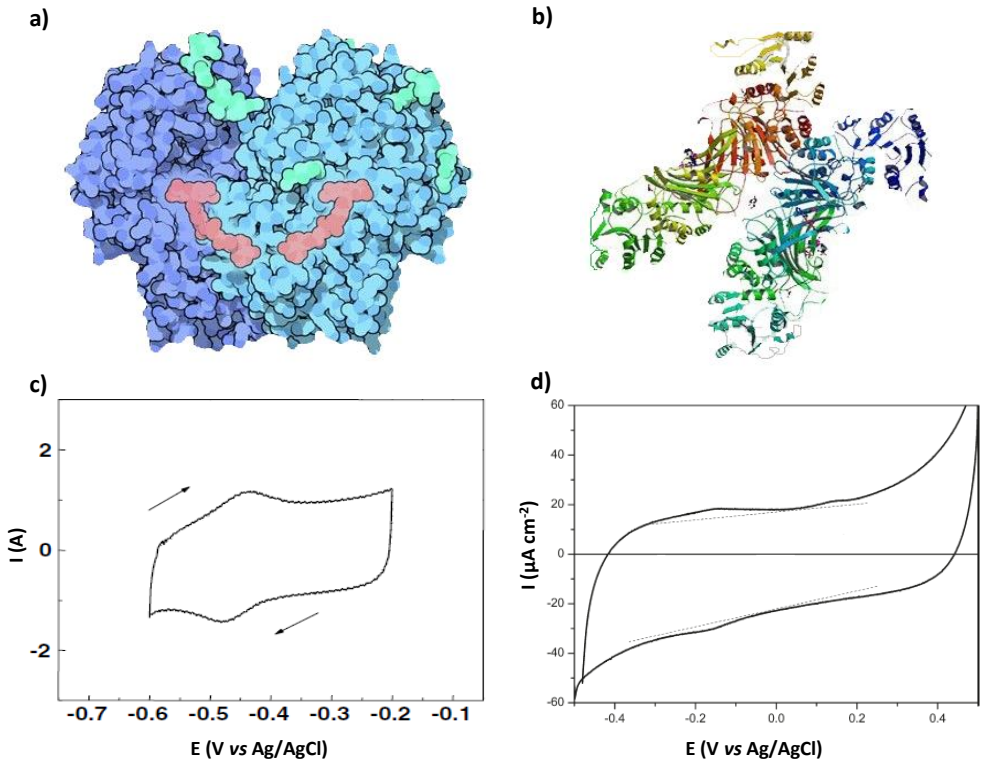

Figure 1.11 - Representation of the structure of GOx (a) and PQQ-GDH (b) and the direct observation of DET through CV, showing the redox peaks of the active centres of GOx (c) and PQQ-GDH (21, 63).

The quinoprotein glucose dehydrogenase is a homodimeric protein containing a pyrroloquinoline quinone (PQQ) prosthetic group together with Ca^{2+} ions in the active site, bounded through electrostatic interactions to amino groups (147). It catalyses the oxidation of D-glucose to D-gluconate with reduction of ubiquinone in a process involving two electrons and two protons (21, 147). It can be found freely soluble in the periplasm of cells (*Acinetobacter calcoaceticus*) or bounded to the membrane of gram-negative bacteria such as *Escherichia coli* (148, 149). The high catalytic activity and the low molecular mass (M_r = 94000) (150) enables DET feature between enzyme active site and electrode surface (21, 147, 151). Both GOx and GDH have maximum catalytic activity at physiological pH being both suitable for the use in biofuel cells (140) however, one important advantage of GDH over GOx is the insensitivity to O_2. When GOx is used at the anode the presence of O_2 may hinder the efficiency of the biofuel cell. Since O_2 is a co-substrate, undesirable electron transfer may occur directly from GOx decreasing the power produced (137). The enzymes GOx and PQQ-GDH are represented in Figure 1.11 with cyclic voltammograms featuring DET of the redox centres of each enzyme.

1.6 - Microfluidic and miniaturized biofuel cells – Theory and literature overview

1.6.1 - Theoretical concepts of microfluidic platforms

The miniaturization of analytical systems took the first steps with the development of the concept “miniaturized total chemical analysis systems” (μTAS) by Manz et al. (152). This analytical approach was later absorbed by the concept of “lab-on-a-chip”, thus designated to encompass the common features and methods used to fabricate generic goal microdevices. These, envisage the integration of diverse laboratory unit operations, in a miniaturized single chip through microfabrication techniques (Figure 1.12). Clear advantages of this approach range from the chemical automation and portability for potential use in point of care diagnostics to the ability of process reduced sample volumes, parallelisation of biochemical assays and mimicking of organ functions. The precise handling of fluids at the microscale as well as the design of systems that enables their manipulation and control defined the science of microfluidics (153). The terms μTAS, Lab-on-a-Chip and microfluidic platforms are commonly used interchangeably, despite existing slight differences between them, and in general describe miniaturized platforms that integrates multiple unit operations such as transportation, mixing, separation, reaction, detection, etc (154).

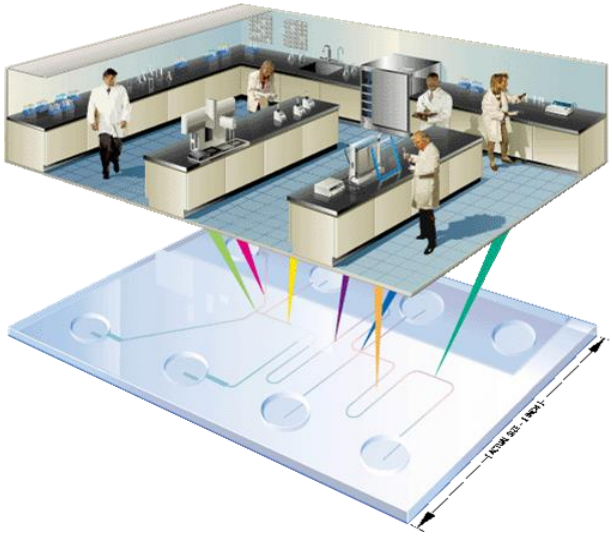

Figure 1.12 - Scheme featuring the Lab-on-a-Chip concept. Diverse laboratorial operations are downsized and integrated in a single chip.

The most striking feature of these miniaturized platforms relies on the use of microfluidics. In fact, different physical forces dominate things at macroscale and microscale. With the object downsizing, the surface to volume ratio increases dramatically (155) to an extent where volume dependent aspects become negligible (Figure 1.13). For a geometrical object with characteristic length dimension *l*, the basic scaling law for surface area to volume ratio is expressed as seen in equation 1.4.

$$\frac{Surface}{Volume} = \frac{l^2}{l^3} = l^{-1} \overset{l \to 0}{\longrightarrow} \infty \qquad (1.4)$$

This means that typically for sub-millimetre sizes, surface forces such as surface tension and viscosity dominate over inertial forces like gravity.

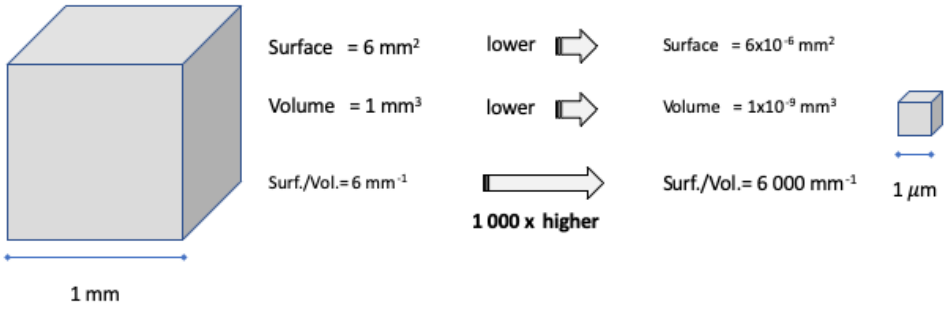

Figure 1.13 - Downsize effects on the characteristic length (l) of objects and their surface-to-volume ratio.

Hence, depending on the size of channels but also on the velocity of the fluid, transportation inside a channel can occur under two different types of flow. At low velocity, a laminar flow regimen is observed. In this type of flow the fluid streamlines are parallel without occurring lateral mixing or cross currents perpendicular to flow direction (Figure 1.14a). Conversely, at high velocities, turbulent flow takes place, which leads to a more chaotic behaviour and intense lateral mixing (Figure 1.14b) (156, 157).

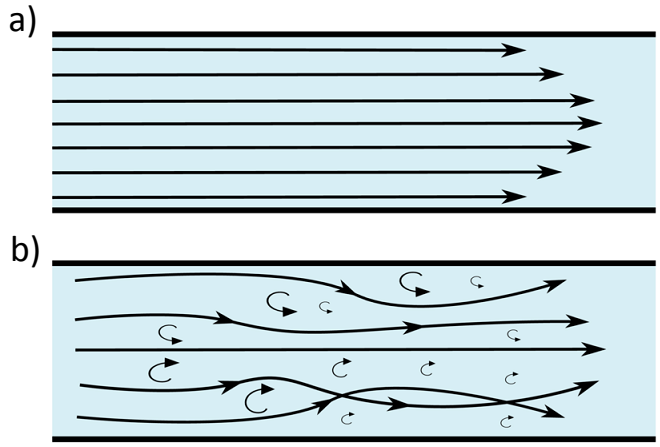

Figure 1.14 – Flow regimen inside a pipe. a) Laminar flow. b) Turbulent flow.

The transition from laminar to turbulent not only depends on the velocity but also is a function of the fluid properties and channel dimensions, as demonstrated in equation 1.5, defining the Reynolds number (156):

$$Re = \frac{Dv\rho}{\mu} \qquad (1.5)$$

where D is the channel diameter, v is the average velocity of the fluid, ρ the fluid density and μ the fluid viscosity. The Reynolds number, Re, is a dimensionless number that, besides defining the type of flow regimen inside a channel, can be looked as the ratio between inertial over viscous forces. A Reynolds number below 2100 defines a laminar flow, whereas a transition region between laminar and turbulent stands between 2100 and about 5000. Higher Reynolds values defines pure turbulent flow (157).

In microfluidic platforms, laminar flow largely predominates even for high fluid velocities, due to the reduced diameter of channels (≤ 1 mm). Hence, two different flow streams can easily run side by side in the same channel without convective mixing. The liquid-liquid interface acts as separation between streams, occurring though some diffusive mixing in the interfacial zone at the center of the channel (158), as exampled in Figure 1.15. Therefore

two different streams flow parallel on the same channel without convective mixing. The liquid-liquid interface acts as separation between streams, occurring only diffusive mixing in an interfacial width at the center of the channel (158). Molecular diffusion occurs at a slower rate compared to convection since molecules moves randomly, following a concentration gradient: from higher concentration regions to lower concentration regions (156). These phenomena eliminates the necessity of using proton exchange membranes separating anolyte and catholyte in fuel cells, thereby enabling easiest miniaturization and integration in microfluidic platforms (159). Protons are exchanged from anode to cathode where the extension of diffusional mixing between fuel and oxidant can be controlled by changing the flow rate or the channel width.

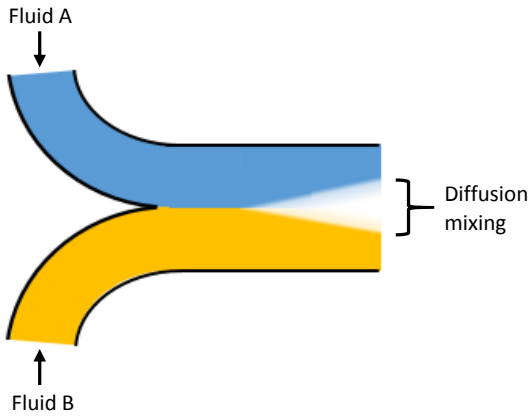

Figure 1.15 – Scheme of diffusive mixing occurring between two different fluids in a channel.

Different types of propulsion, very often determining the complexity and final dimensions of the microfluidic device, can be used to drive the liquids inside the microchannels: capillary, pressure-driven, centrifugal, electrokinetic and acoustic (154). Taken as example, the lateral flow tests are very basic microfluidic devices which are having great success in diagnostic applications (e.g. diabetes testing, abuse drugs, biomarkers, pregnancy testing). In this system, fluid is driven by capillary forces when deposited or immersed in a wettable and porous substrate such as a cellulose-based material, eliminating the need of an external pump. Other unit operations besides sample transportation and detection may be included in the microfluidic device namely metering, filtering and separation which may be important in the analysis of blood samples. Optical detection and quantification, is typically used with this technology. However, several electrochemical paper-based biosensors and biofuel cells have meanwhile been developed (160, 161). Precise fluid handling and flow control stands as the main issue in capillary systems. Other widely used transport mechanism in microfluidics is pressure driven which is based on gradients of positive or negative pressure. The actuator can be integrated inside the device by using pouches and

displacement membranes or resorting to external pressure sources as pumps or syringes. By using external pumps (e.g. peristaltic pump), strictly laminar flow is easily accomplished within the channels and therefore stable phase arrangements between streams and controllable diffusive mixing are achieved. However, some limitations may arise in this type of set. For instance, external pumps are bulky apparatus deserving a contradictory look in lab-on-a-chip applications, since they limit the portability of the device. Moreover, the interface between the external apparatus (pumps and tubes) and the chip should be carefully considered, as the connector must be simple but at the same time robust, preventing any leakages. Considering the specific application of microfluidic fuel cells, the use of two separate streams requires additional design of the device as well as apparatus for inlets and outlets. In turn, the integration of the actuator in the device allows miniaturization of the overall system as well as portability. Though, the fabrication process is still a technological challenge and a cumbersome. Finger-pressure actuation integrated in microfluidic devices can be seen as a good examples (162-164). The working principle consists on the positive and negative pressure created when a finger pushes and sequentially relieves a flexible pouch. Besides the requirement of sample reservoirs and the finger pouch, this system employs flexible membranes or flaps working as check valves to prevent backflow (Figure 1.16) (165). A configuration based on single-stream is used in these type of actuation since there is no precise control of the flow as it may stand in a transition zone between laminar and turbulent flow.

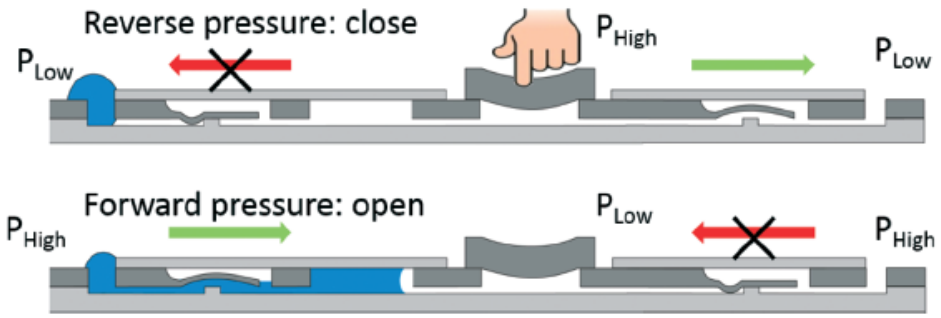

Figure 1.16 – Pressure-driven system for fluid trasnport based on finger pressure actuation (165).

1.6.2 - Literature overview regarding microfluidic biofuel cells

A literature overview of microfluidic biofuel cells is given in this subsection by briefly describing the fabrication of the microfluidic system, enzymes immobilization, and biofuel cell performance. The main characteristics of each microfluidic biofuel cell are shown in Table 1.4.

Several microfluidic biofuel cells were described where enzymes were dissolved in the electrolyte instead of being immobilized in the electrodes (166-171). These approaches seem only appropriate for optimization studies regarding electrode dimensions, channels configuration and flow rates since real usefulness is nevertheless limited due to the large consumption of enzymes. Though not described in detail, the characteristics and performance of these microfluidic biofuel cells are presented in the beginning of Table 1.4. As expected, the majority of developed microfluidic biofuel cell concerns the use of glucose as a fuel given its biological importance for the clinical field, availability in the physiological medium and commercial success of glucose biosensors. Also but in less extent, ethanol, fructose and lactate microfluidic biofuel cells have been studied.

Surprisingly, the first microfluidic biofuel cell, developed by Moore et al. (39), used ethanol to produce power, as pointed out in the introduction subsection 1.2 (History of biofuel cells). The system consisted on a carbon ink track upon a glass substrate, sealed then by a PDMS monolith containing a moulded microchannel and aligned so that the electrode became within the microchannel. The carbon ink electrode was prior modified with methylene green and a mixture of a tetrabutylammonium bromide modified nafion (TBAB-nafion), NAD^+ and the enzyme alcohol dehydrogenase (ADH). The platinum cathode was placed in a reservoir at the end of the channel and separated through a nafion membrane. A 1 mM ethanol solution with 1 mM NAD^+ was pumped at a flow rate of 1 µL min^{-1}, producing a maximum E_{OCP} of 0.34 V and a power density of about 5 µW cm^{-2} (39). Other microfluidic biofuel cells employing ethanol as fuel were developed thereafter by other authors who also have managed to improve the extractable power. For instance, the group of Selloum developed a more efficient biofuel cell comprising the enzyme, ADH, in the bioanode and a laccase in the biocathode. The enzymes were co-immobilized on the surface of Au electrodes with the respective mediators, such as ABTS or the vitamin K_3 (VK_3), for efficient electron shuttling and with carbon nanoparticles (CNPs) for signal enhancement. The bioelectrodes were integrated in an epoxy slide and then sealed with PDMS containing the Y-shaped microchannels with two inlets and two outlets. For an equal flow rate at anolyte and catholyte of 16 µL min^{-1} the device generated an E_{OCP} of 0.8 V and a power density of 90 µW cm^{-2} (172). About two years later, the same research group developed a different immobilization method for the same enzymes. The performance was however inferior in terms of E_{OCP} (0.63 V) and power density (14 µW cm^{-2}) when compared with the previous microfluidic device. In this approach, Toray carbon electrodes were used as catalysts support, modified with methylene green and the enzyme ADH at the anode and with laccase, mediator ABTS, carbon nanoparticles and polypyrrole (PPy) at the cathode (173). The electrode Toray with methylene green was also used by others (174). However, prior to the electropolymerization step, the electrode was modified with nafion. The enzyme ADH

was solubilized and cross-linked in a mixture containing TBAB, nafion, glutaraldehyde (GA) and NAD^+ and then dropwise over the modified surface of the electrode. The bioanode and the inorganic, nafion-covered, platinum-carbon (Pt/CB) cathode were integrated in a silicone elastomer film containing the microfluidic channels and then between to PMMA plates for support. In buffered conditions in both streams the device was highly efficient in energy conversion of ethanol (100 mM) by achieving an E_{OCP} of 1.03 V and a power density of 3150 µW cm^{-2} which is about 35 times higher than the value highest value previously reported for this type of microfluidic device (172). When human blood spiked with 1 g L^{-1} of ethanol is used as anolyte the efficiency lowered as expected resulting in a power density of 371 µW cm^{-2}. However, the use of a double biofuel cell assembled in the device increased the E_{OCP} and power density to respectively 0.74 V and 712 µW cm^{-2} (174).

Regarding the use of glucose as fuel, the research group of Togo et al. (175) employed for the first time immobilized enzymes capable to convert glucose in electrical energy. The device was simply fabricated by patterning the electrodes on a glass slide and covered by PDMS with the moulded microfluidic channel. Prior to the final assembly, the Au disc electrode serving as anode was modified with a mixture of mediator Poly-L-lysine and VK_3 with enzyme diaphorase to convert NADH to NAD^+. The addition of the Ketjenblack (KB) carbon black provided high catalytic activity for the immobilized NAD^+-dependant GDH enzyme. Connected to a PDMS-coated Pt cathode, the single-flow (1000 µL min^{-1}) achieved a power density of 32 µW cm^{-2} and an E_{OCP} of 0.55 V (175). The immobilization of BOx on a KB modified Au electrode, then used as biocathode, enabled the increase in the provided voltage to 0.8 V (176). They also developed a system for time sustained generation of power comprising 3 stacked biofuel cells. The sequence of biofuel cells was designed in order that the connection between each cell was sealed by a dissolvable poly(lactic-co-glycolic acid). After a given time the fuel solution flows through the second cell and later through the third thus boosting the generated power over time. The maximum power was of about 2 µW and maintained for over 40 hours. For each biofuel cell the power decreased quickly and almost linearly with time. Galindo et al. (177) evaluated the electrocatalysis enhancement of GOx by using metal oxides nanoparticles, more specifically, maghemite (γ-Fe_2O_3). The electrocatalyst materials consisting of Vulcan carbon black, maghemite and enzyme GOx were deposited on the side-wall of the Y-shaped microchannel defining the bioanode whereas the cathode was composed of Pt and CB mixture deposited on the opposite side. A moderate E_{OCP} of 0.3 V and a power density of 30 µW cm^{-2} was obtained from separate solutions fed at 60 µL min^{-1}, with the anolyte containing 10 mM glucose (177). In turn, Beneyton et al. (178) immobilized GOx and laccase to patterned SWCNT anode and cathode, respectively, through covalent bonding by using 1-(3-dimethylaminopropyl)-3-

ethylcarbodiimide (EDC) and N-hydroxysuccinimide (NHS). The Y-shaped microfluidic device consisted of a glass slide containing the patterned electrodes sealed with PDMS microchannels. Even using a ferrocene-based mediator in the anolyte and the laccase mediator ABTS in the catholyte, the biofuel cell produced only a maximum power density of 1.7 μW cm^{-2} (178). An inefficient enzyme immobilization in flow conditions or absence of pure laminar flow preventing the adequate separation between anolyte and catholyte could explain the low power density obtained. In a different approach, rapid prototyping of laminated plastic materials were used to attain a microfluidic system comprising a double Y-shaped channel instead the conventional use of PDMS. A silicon layer with integrated pyrolyzed photoresist films (PPF) was shown to possess similar properties to GCE and alternatively used as electrodes. The GOx enzyme was immobilized in the anode alongside with a mediator polymer, ferrocene-based polyethyleneimine (Fc-LPEI) and cross-linker ethylene glycol diglycidyl ether (EGDGE). On the cathode, the suspension of laccase from *Trametes versicolor* was mixed with anthracene-modified MWCNT and TBAB-nafion solution. At an optimum flow rate of 70 μL min^{-1}, the biofuel cell generated an E_{OCP} of 0.54 V and a power density of 64 μW cm^{-2} (179). The same authors developed a paper-based biofuel cell with capillary fluid movement. The configuration of the microfluidic system based on I-shaped (single stream) or Y-shaped (dividing catholyte and anolyte) was compared concerning the performance. The procedure used for the immobilization was similar to a previous work where carbon paper instead PPF electrodes were used. Probably due to the interference of oxygen at the anode, the power available (24 μW cm^{-2}) with the I-shaped configuration biofuel cell was only half regarding to the Y-shaped biofuel cell, while the E_{OCP} remained invariant. In a subsequent study, the I-shaped configuration of the fluidic device was adopted to evaluate the performance of a glucose/O2 biofuel cell where osmium-based polymers were used as mediators either for the FAD-dependant GDH anode and for the BOx cathode. The registered E_{OCP} was 0.65 V but the power density obtained (97 μW cm^{-2}) was approximately four times higher when compared to the previous reported cell (180), because of the FAD dependant GDH indifference to oxygen (181). It is worth noting the biofuel cell performances obtained in the works from Ledesma-Garcia's research group where graphite paper were used as catalysts support (182, 183). In both approaches, GOx was cross-linked with GA to nanostructured carbon materials such as MWCNT and CB and deposited on the surface of graphite adhesive tape. The air-breathing cathode was prepared from Toray paper with Pt/C catalyst exposed directly to air. A silicone film with the microchannel engraved was placed between the electrodes and the set finally held sandwiched between two PMMA slides. In buffered condition containing 5 mM of glucose the E_{OCP} was higher than 0.7 V and equally a high power density of about 600 μW cm^{-2} was attained (182, 183). The device was tested with human blood fed in both anolyte and

catholyte at 8 µL min^{-1} , but lowered the cell voltage to 0.54 V and the produced power to 200 µW cm^{-2} as expected (182). Noh and Shim (184) studied the use of hydrogen peroxide as oxidant, therefore combining different assemblies for reduction of the oxidant. Conductive polymers based on hydrazine and terthiophene were electropolymerized alongside with AuNPs at the anode and cathode. The product of GOx reaction at the anode, H2O2 was catalysed at the cathode either by the HRP enzyme or by the poly 4-(([2,2':5',2''-terthiophen]-3'-yl) phenyl hydrazine (PolyTPHyd-AuNPs) composite as non-enzymatic approach. In buffered glucose solution flowing at 1000 µL min^{-1}, the GOx-HRP arrangement generated the cell voltage of 0.39 V and power density of only 20 µW cm^{-2}. The power density increased to the impressive 580 µW cm^{-2} using solely the polymer PolyTPHyd-AuNPs at the cathode (184).

Some paper-based microfluidic biofuel cells also employed glucose as fuel (185-187), with fluid transport being accomplished through capillary forces. For instance, Zhang et al. (185) applied this technology for power generation from some commercial beverages. Conductive carbon ink applied in the hydrophilic area of the paper substrate served as electrodes which were then modified with ionic liquid functionalized CNTs (CNTs/IL). The anodic response was obtained from a mixture of NAD^+-dependant GDH and chitosan dropcasted upon the ink surface whereas BOx was immobilized on the cathode. The bioelectrodes processed about 30 µL of fuel - phosphate buffer containing 30 mM glucose and 10 mM NAD^+ - enabling the E_{OCP} and power density of respectively 0.56 V and 13.5 µW cm^{-2} (185). In turn, the devices fabricated by (186, 187) consisted on a filter paper presenting the format of a fan and assembled between the bioelectrodes. When the section of the filter paper below the electrodes was immersed, the fuel solution raised up to the electrodes and further to the “fan” type area located at the top, where it was continuously evaporated. A MWCNT buckypaper was used as anode and modified with MG over which NAD^+-dependant GDH and chitosan were spread. The reduction of oxygen at the cathode was driven after immobilizing BOx over a Vulcan CB modified Toray paper. The E_{OCP} generated from a single cell in a 100 mM glucose solution with 50 mM NAD^+ was 0.62 V. A stack of three cells was able to produce 1.67 V which was sufficient to keep working a digital clock for 9h (186). The power extracted with the biofuel cell corresponded to 13 µW, equivalent to the high power density of 1070 µW cm^{-2} (187).

Besides ethanol and glucose, other fuels like fructose and lactate have been proposed for microfluidic biofuel cells (188-190). In 2011, Miyake et al (188) fabricated a miniature biofuel cell operating by immersion in a stirred buffer solution containing 200 mM fructose. Free standing CNT films with immobilized FDH and laccase were used as bioanode and biocathode respectively and assembled in a flexible and gold patterned polyethylene

terephthalate (PET) substrate. The device achieved a power density of 1800 µW cm^{-2} and an E_{OCP} of 0.77 V which was enough to power on a LED in series with a microcapacitor (188). A version of the biofuel cell in paper support was also implemented. For this, anode and cathode were assembled on a filter paper by coating it with a suspension containing cellulose, ionic liquid and MWCNT, and then immersed in the respective enzymatic solutions, FDH and BOx. When fuelled by 2 mL, 200 mM D-fructose solution, a single cell produced 0.6 V voltage and a power of 4.3 µW (34 µW cm^{-2}). A stack of 2 biofuel cells produce almost 2 times higher power (7.9 µW) with similar power density (31 µW cm^{-2}); the E_{OCP} increased to 1.34 V (189). More recently and for the first time, lactate was used as fuel in a microfluidic enzymatic cell using a similar system developed previously by the same group (174). The procedure used for enzyme immobilization was the same of from Gonzalez-Guerrero et al. (180) but employing lactate oxidase (LOx) instead of GOx at the anode. Individual inlets for fuel and oxidant fed the device at the flow rate of 50 µL min^{-1}. The performance was maximum when 10 mM of lactate at pH 7.4 was used as the anolyte solution and catholyte solution at pH 5.6, reaching the E_{OCP} of 0.73 V and power density of 404 µW cm^{-2}.

It seems clear that concerning microfluidic biofuel cell systems, the attainment of maximum power/power density while minimizing as possible components dimensions is generally aimed. The biocatalyst type and the procedure used for its immobilization are probably the most important factors influencing the final cell performance. However, other factors may seem to be important as well. The power output depends on the flow rate adopted in each reported cell since it introduces a mass transport constraint (167). Increasing the flow rate leads to higher generated power as evidenced in some studies (167, 170, 179, 191). Stabilization of the signal with the increase of flow rate may indicate a saturation or limitation in the turnover rate of the enzymes (179). For instance, the power output increased linearly up to about 45 µL min^{-1} in the study conducted by González-Guerrero et al. (179) while in the study performed by Reid et al. (191) the optimum value corresponded to 1000 µL min^{-1}. Similarly, Increasing fuel concentration improve the cell performance up to a certain point where it stabilizes or decreases (180, 181, 190) due to saturation of the bioanode or simply due to limiting rates of O_2 at the biocathode given the low diffusion coefficient and concentration of O_2 present in aqueous electrolytes (192).

Stacking biofuel cells stands as a viable solution to increase power output as demonstrated in some studies (170, 171, 189, 193), rising the power output almost proportionally with the number of cells added to the system though without significant change in the power density value. Nevertheless, du Toit et al. found that a single biofuel cell produced the same power as three biofuel cells aligned sequentially in the same channel (194). This can be explained by the depletion of fuel/oxidant at the passage of the first biofuel cell. If the stack

configuration is connected in series *i.e.*, cathode of the first cell connected to the anode of the second cell and so on, the E_{OCP} increases proportionally (170). When stacked in parallel, the global E_{OCP} remains practically invariable (171). Nonetheless, stacking of biofuel cells has inherent costs: the increase the overall dimensions of the device, and requirement of higher flow rates.

The biofuel cell overall performance is higher when operated in buffered or generally controlled conditions, contrary to the performances achieved with real samples such as human blood given the presence of interfering compounds in the sample matrix (174, 182). As well, microfluidic devices comprising single-stream (mixing fuel with oxidant) instead of separate streams (anolyte and catholyte) produce lesser power output (180) due to the hindrances caused by the O_2 at the anode or operating outside the optimum conditions for one of the enzymes.

From Table 1.4 it is not possible to compare an ideal procedure regarding enzyme immobilization strategy for optimal biofuel cell performance. At least, it seems that biofuel cells with the highest power density employed the commercial Toray carbon paper as electrode support for immobilization of both electrocatalysts and enzymes.

The shape and size of electrodes as well as the distance between anode and cathode should be optimized for maximum performance. Simulation and experimental data from (168) showed that the current density and thus power density decreases with the increase of electrode length. This results from the increase in the depletion zone along the electrode preventing reactant to reach the electrode surface. Moreover, decreased distances between anode and cathode contribute to better performances due minor ohmic losses (168). Shorter and wider electrodes, as demonstrated by Selloum et al., (172) improves power density by creating thinner boundary layers at electrode surfaces.

Table 1.4 – Microfluidic Biofuel cells characteristics and performance

Type	Anode (Anolyte)	Cathode (Catholyte)	Flow rate (µL min^{-1})	E_{OCP} (V)	Current density (µA cm^{-2})	Power density (µW cm^{-2} / µW)	Ref.
ABTS/ABTS	Au (10 mM ABTS, acetate pH 4)	Au (0.5 mg mL^{-1} **laccase**, 5 mM ABTS, O_2 sat., acetate pH 4)	100	0.40	450	26	(166)
Glucose/O_2	Au (0.5 mg mL^{-1} **GOx**, 10 mM gluc., 10 mM $Fe(CN)_6^{3-}$, PBS pH 7)	Au (0.5 mg mL^{-1} **laccase**, 5 mM ABTS, O_2 sat., citrate pH 3)	1000	0.55	690	110	(167)
Glucose/O_2	Au (0.5 mg mL^{-1} **Gox**, 10 mM gluc., 10 mM $Fe(CN)_6^{3-}$, PBS pH 7)	Au (0.5 mg mL^{-1} **laccase**, 10 mM ABTS, O_2 sat., citrate pH 3)	300	0.5	2700	550	(168)
Glucose/$K_3[Fe(CN)_6]$	Au (200 U mL^{-1} **Gox**, 80 mM gluc., 0.5 mM Fc, PBS pH 7.4)	Au (10 mM $K_3[Fe(CN)_6]$, Tris-HCl pH 8.2)	-	-	-	0.85	(169)
Glucose/O_2	Au (1 mg mL^{-1} **Gox**, 100 mM gluc., 10 mM $Fe(CN)_6^{3-}$, PBS pH 7)	Au (1 mg mL^{-1} **laccase**, 10 mM ABTS, O_2 sat., PBS pH 5)	300	0.33	111	12.0 / 4.7 (1 x BFC)	(170)
			300	1.07	40	12.6 / 10.5 (3 x BFC)	
Glucose/O_2	Au (1 mg mL^{-1} **Gox**, 10 mM gluc., 10 mM $Fe(CN)_6^{3-}$, PBS pH 7)	Au (1 mg mL^{-1} **laccase**, 10 mM ABTS, O2 sat., citrate pH 5)	150	0.39	112	14.4 / 3.6 (1 x BFC)	(171)
			150	0.42	340	50 / 12.5 (4 x BFC parall.)	
Glucose/O_2	Au-PLLys/VK3/Diaphorase/KB-**GDH** (5 mM gluc., 1 mM NAD^+, air sat., PBS pH 7.0)	Pt (Same as anolyte)	1000	0.55	130	32	(175)
Glucose/O_2	Au-PLLys/VK3/Diaphorase/KB-**GDH** (10 mM gluc., 1 mM NAD^+, air sat., PBS pH 7.0)	Au-KB/PTFE-**BOx** (same as anolyte)	300	0.8	-	-	(176)

Table 1.4 – (Continued)

Type	Anode (Anolyte)	Cathode (Catholyte)	Flow rate (μL min^{-1})	E_{OCP} (V)	Current density (μA cm^{-2})	Power density (μW cm^{-2} / μW)	Ref.
Glucose/O_2	Au-PLLys/VK3/Diaphorase/KB-**GDH** (50 mM gluc., 1 mM NAD^+, PBS pH 7.0)	Au-PLLysKB/**BOx** (same as anolyte)	800	-	-	55 / 2.2 (1 x BFC)	(193)
				-	-	45 / 5.5 (3 x BFC)	
Glucose/O_2	Carbon_paper-CNT/IL-Chit/**GDH** (30 mM gluc., 10 mM NAD^+, PBS pH 7.0)	Carbon_paper-CNT/IL-**BOx** (same as anolyte)	Batch	0.56	-	13.5	(185)
Glucose/O_2	CB-Fe_2O_3-**GOx** (10 mM gluc., PBS pH 7.4)	Pt-CB (O2 sat., PBS pH 7.4)	60	0.30	260	30	(177)
Glucose/O_2	SWCNT-EDC/NHS-**GOx** (100 mM gluc., 1 mM Fc, PBS pH 7.0)	SWCNT-EDC/NHS-**laccase** (2 mM ABTS, O_2 sat., acet. pH 4.5)	17	0.43	15	1.7	(178)
Glucose/O_2	PPF-FcLPEI/EGDGE/**GOx** (100 mM gluc., PBS pH 7.4)	PPF-MWCNT/Nafion/**laccase** (air sat., citrate pH 4.5)	70	0.54	425	64	(179)
Glucose/O_2	Toray-C8LPEI/ MWCNT/Azine/EGDGE/**GDH** (100 mM gluc., 3 mM NAD^+, PBS pH 7.4)	Pt-CB-Nafion	1000	0.67	705	146	(191)
Glucose/O_2	Pt/Ti-CP-KB/PVDF-Fc/**GOx** (200 mM gluc., air sat., buffer)	Pt/Ti-CP-KB/PVDF-**BOx** (same as anolyte)	1580	0.60	28	7.2 / 1.7	(195)
Glucose/O_2	Buckypaper-MG-Chit/**GDH** (100 mM gluc., 50 mM NAD^+, PBS pH 7.3	Toray-CB-**BOx** (same as anolyte)	batch	0.62	-	- (1 x BFC)	(186)
				1.67	-	- (3 x BFC)	

Table 1.4 – (Continued)

Type	Anode (Anolyte)	Cathode (Catholyte)	Flow rate (μL min^{-1})	E_{OCP} (V)	Current density (μA cm^{-2})	Power density (μW cm^{-2} / μW)	Ref.
Glucose/O_2	Graphite_paper-MWCNT/CB/GA/**GOx** (5 mM gluc., PBS pH 7.0)	Toray-Pt/C/Nafion (PBS pH 7.0)	25	0.86	1930	620	(182)
	(human blood)	(human blood)	8	0.54	1070	200	
Glucose/O_2	Buckypaper-MG-Chit/**GDH** (100 mM gluc., 1mM NAD^+, PBS pH 7.5)	Toray-CB-Buckypaper-**BOx** (same as anolyte)	batch	0.56	6500	1070 / 13	(187)
Glucose/H_2O_2	Carbon_ink-terthiophene-AuNPs-EDC/NHS-**GOx** (10 mM glucose, PBS pH 7.0)	Carbon_ink-terthiophene-AuNPs-EDC/NHS-**HRP** (H_2O_2 from anode reaction, PBS pH 7.0)	1000	0.39	110	20	(184)
Glucose/O_2	Graphite_paper-MWCNT/GA/**GOx** (5 mM gluc., PBS pH 7.0)	Toray-Pt/Vulcan/Nafion (PBS pH 7.0)	8	0.72	2400	610	(183)
Glucose/O_2	Carbon_paper-FcCLPEI/EGDGE/**GOx** (100 mM gluc., PBS pH 7.4)	Carbon_paper-MWCNT/Nafion/**laccase** (PBS pH 4.5)	25	0.60	320	45	(180)
	(100 mM gluc., PBS pH 5.5)	(same as anolyte)		0.55	225	24	
Glucose/O_2	Carbon_paper-Os(dmobpy)PVI/ PEGDGE/MWCNT/**GDH** (50 mM gluc., pBS pH 7.4)	Carbon_paper-Os(bpy)PVI/ PEGDGE/MWCNT/**BOx** (same as anolyte)	batch (capillarity)	0.65	290	97	(181)
Glucose/O_2	Au-**GOx** (27 mM gluc., PBS pH 7.1)	Au-**laccase** (same as anolyte)	350	0.35	-	4.7 / 0.75 (1 x BFC)	(194)
				0.35	-	1.5 / 0.71 (3 x BFC parall.)	
Ethanol/O_2	Carbon_ink-MG-**ADH**/NAD/TBAB_Nafion (1mM ethanol, 1 mM NAD^+, PBS pH7)	Pt (PBS pH 7.15)	1	0.34	53	5	(39)

Table 1.4 – (Continued)

Type	Anode (Anolyte)	Cathode (Catholyte)	Flow rate (µL min^{-1})	E_{OCP} (V)	Current density (µA cm^{-2})	Power density (µW cm^{-2} / µW)	Ref.
Ethanol/O_2	Au-**ADH**/CNP-NAD-diaphorase-VK3/PEI (160 µL ethanol, PBS pH 9.0)	Au-CNP/Nafion/ABTS/**laccase** (O2 sat., PBS pH 5.0)	16	0.8	200	90	(172)
Ethanol/O_2	Toray-MG-NAD/**ADH**	Toray-CNP/**laccase**-ABTS/PPy	50	0.63	42	14	(173)
Ethanol/O_2	Toray-nafion-MG-nafion/GA/NAD/**ADH** (100 mM ethanol, PBS pH 8.9)	Pt/C-nafion (O_2 sat., PBS pH 8.9)	50	1.03	11500	3150 (1 x BFC)	(174)
	1 g L^{-1} ethanol, human blood)	(O_2 sat., PBS pH 8.9)		0.43	-	371 (1 x BFC)	
	(1 g L^{-1} ethanol, human blood)	(O_2 sat., PBS pH 8.9)		0.74	2500	712 (2xBFC ser)	
Fructose/O_2	CNT_film-**FDH** (200 mM fruct., O_2 sat., McIlv. pH 5.0)	CNT_film-**laccase** (same as anolyte)	batch	0.77	4800	1800	(188)
Fructose/O_2	MWCNT/IL/paper-**FDH** (200 mM fructose, buffer pH 5.0)	MWCNT/IL/paper-**BOx** (same as anolyte)	batch	0.61	128	34 / 4.3 (1 x BFC)	(189)
				1.34	134	31 / 7.9 (2 x BFC series)	
Lactate/O_2	Toray-Fc-LPEI/EGDGE/**LOx** (10 mM lactate, PBS pH 7.4)	Toray-MWCNT/Nafion/**laccase** (PBS pH 5.6)	50	0.73	2087	404	(190)

Chapter 2

Objectives

The main objective of the present thesis was the development of lab-on-a-chip platforms comprising biofuel cells for self-powered biosensing. To accomplish this, three partial objectives were equated and performed throughout four years of experimental work developed: i) Implementation and characterization of the bioelectrode used as biocathode; ii) implementation and characterization of the bioelectrode used as bioanode, and iii) assembly of the bioelectrodes in a biofuel cell and further integration in a microfluidic platform:

i) Implementation and characterization of the bioelectrode used as a biocathode in the biofuel cell. In a first stage, a pencil graphite electrode (PGE) used as transducer was characterized through voltammetric, amperometric and impedance spectroscopy techniques and further surface modification with carbon-based materials was assessed by the same techniques. Immobilization strategies for oxygen reduction enzymes such as laccase and bilirubin oxidase were then implemented. These strategies were based on cross-linking and entrapment procedures. The efficiency of the immobilization and further characterization of the bioelectrode for oxygen biosensing and biocathode performance was evaluated through microscopic, voltammetric and amperometric techniques.

ii) Implementation and characterization of the second bioelectrode composed the bioanode of the biofuel cell. Similar to previous immobilization procedures and characterization techniques were employed for the assembly of a glucose oxidase based bioanode. A first attempt for integration of the GOx bioelectrode in microfluidic platform for glucose biosensing was performed.

iii) Assembly of the biocathode and the bioanode in a biofuel cell and its integration in a microfluidic platform. First, prior to miniaturization and integration in the microfluidic platform, the PGE based biocathode and bioanode were assembled in a biofuel cell and

the performance was evaluated. Then, different miniaturization strategies for biocathode and bioanode were pursued, mainly consisting in the fabrication of conductive carbon films on filter paper through vacuum-filtration process. The design and fabrication of platforms with microfluidic core components (microchannels, valves, reaction chamber and reservoirs) were equated. Fully portability of the device was addressed by incorporation of a finger pressure-driven fluidic system. Such microfluidic platforms were fabricated considering materials with low nonspecific adsorption of proteins, low cost and rapid fabrication process by soft-lithography or laser engraving

Other secondary objectives but nevertheless important were also followed whenever possible. They included the simplicity of procedures selected for enzyme immobilization and electrode fabrication processes, the establishment of direct electron transfer (DET) between enzyme and electrode, application of low cost materials but minimizing losses in performance, minimization of waste and use of toxic compounds. All these features were also taken into account, aiming maximum biocatalytic activities of the enzymes, which means that sensitivities of the biosensors towards enzyme substrate were set to be the highest possible, but without compromising the maximum power density achieved by biofuel cells. Since, the use of pencil mines was privileged along the experimental period of the thesis, the state-of-the-art regarding the previous works reporting biosensors based on this transducer was performed and here also addressed as isolated chapter before the general conclusions.

Chapter 3

Experimental section

This section provides a generic overview regarding the analytical techniques, procedures, equipment and apparatus used throughout the experimental work. A more detailed description, including reagents used and purchase sources, prepared stock and working solutions for each individual work is given in the dedicated subsections of the next chapter.

3.1 – Overview of the electrochemical techniques

In the study of electrochemical sensors, biosensors and biofuel cells, probably the most important and used electrochemical techniques are cyclic voltammetry (CV) and Chronoamperometry (or simply amperometry). Hence, mainly these two techniques were applied for the characterization of electrodes and performance evaluation of the developed biosensors and biofuel cells. Other techniques such as linear sweep voltammetry (LSV) was also employed.

3.1.1 Cyclic voltammetry

Cyclic voltammetry is an electrochemical technique that gives insight of electroactive species capable of losing or accepting electrons at the surface of an electrode. It measures the current (i) as a function of the applied potential (E) that sweeps at a constant rate (scan rate) from an initial potential, E_1 to a final potential E_2 and back again to E_1 (scan rate defined as V s^{-1}). In Figure 3.1 is represented a typical voltammogram (Figure 3.1a) for a reversible system e.g. $Fe(CN)_6^{3-}/Fe(CN)_6^{4-}$, at a solid electrode and the concentration profile of oxidized and reduced species with the electrode distance (Figure 3.1b). As the potential is scanned towards negative values, say from A to C, an increasing fraction of $Fe(CN)_6^{4-}$ ions nearby the electrode surface start being oxidized at some specific potential. At the same

time, in the proportion of the concentration unbalance, new compensating reduced ions from bulk solution start diffusing to the electrode vicinity. The current produced from both processes sums-up until a anodic current peak (i_{pa}) is reached at the potential corresponding to the point B. For more positive potentials, from B to C, there is no free reduced species ($Fe(CN)_6^{4-}$) nearby the electrode and eventually the concentration gradient to the solution bulk reaches its maximum. The electrode becomes then polarized by mass transfer being the current proportional to the $Fe(CN)_6^{4-}$ bulk concentration. At this point, C, the potential scan direction is reversed and privilege is now given to the reduction reaction process. The applied potential of the electrode (E) is related with concentration of the oxidized and reduced species at the electrode surface as described by the Nernst equation (Equation 3.1):

$$E = E^0 + \frac{RT}{nF} ln \frac{[Oxidized]}{[reduced]} \quad (3.1)$$

Where E^0 is the standard potential of the oxidized and reduced species, *R* the universal gas constant, *T* the temperature, *n* the number of electrons involved in the reaction, and *F* the Faraday's constant. That way, Nernst equation predicts the response of a system when there is a variation in the species concentration or electrode potential (196-198).

CV is an important technique in the assembly of bioelectrodes for biosensors and biofuel cells in order to assess proper immobilization of the enzyme and to verify the potential where the biocatalytic reactions occur between the enzyme and their substrates (analytes). Normally, a potential value close to the potential where maximum cathodic or anodic current occurs is applied in more sensitive techniques such as amperometry to obtain a calibration curve of enzyme substrate.

Other simple technique widely used for biofuel cell characterization is linear sweep voltammetry (LSV) which is derived from CV. Here the potential is scanned from an initial potential to a final potential without reversing the scan in the opposite direction. This technique is useful in the characterization of biocathodes and bioanodes and is performed at very low scan rates (about 1 mV s^{-1} or lower) between 0 V and the E_{OCP} potential in order to obtain polarization curves.

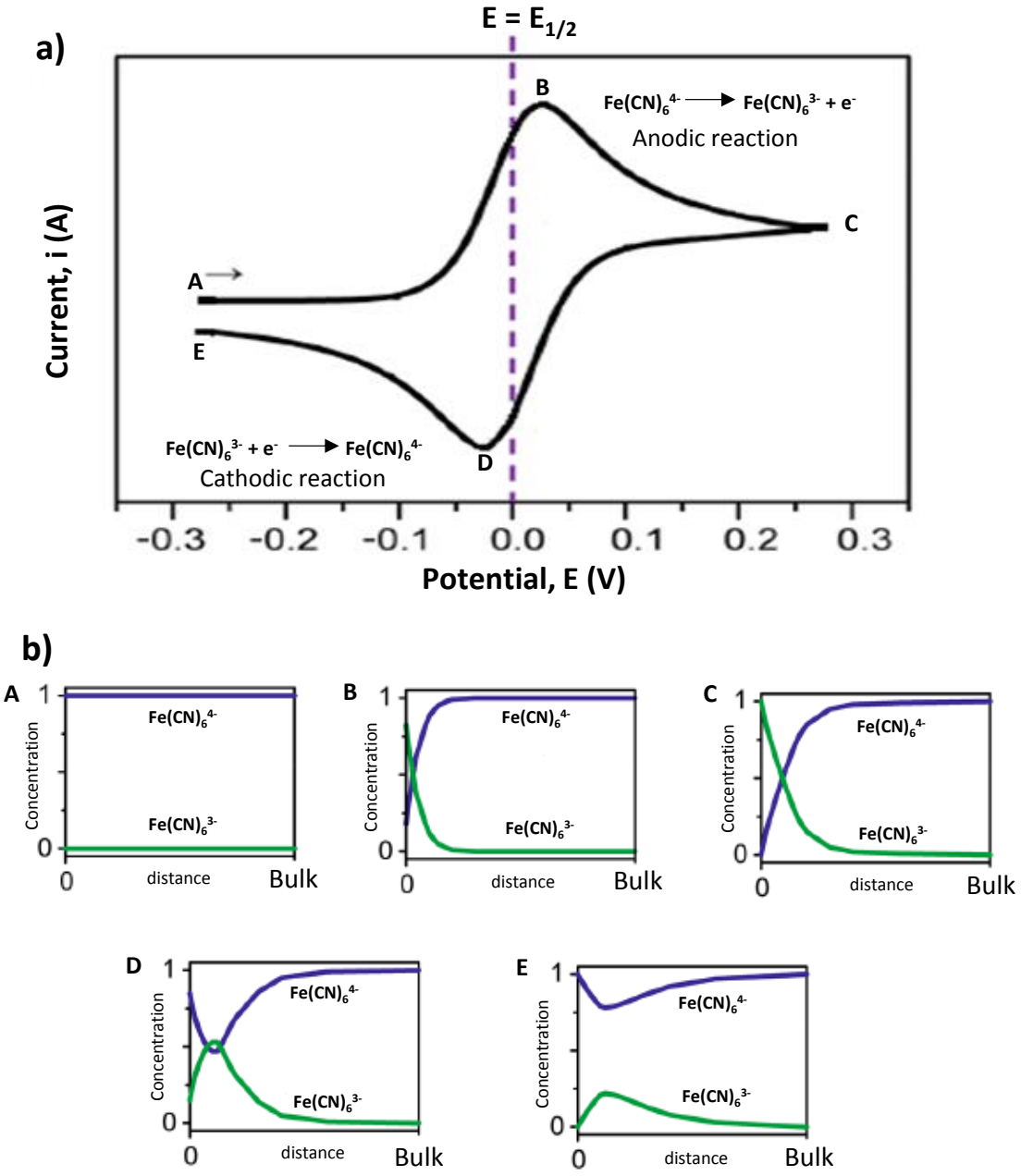

Figure 3.1 – Cyclic voltammetry. a) Typical CV for the species $K_4[Fe(CN)_6]$ / $K_3[Fe(CN)_6]$ in a electrolyte solution. b) Concentration profile from the electrode surface to the bulk of the electrolyte solution.

3.1.2 - Chronoamperometry

In amperometry, the current is measured as function of time. The potential is stepped between an initial potential E_1 where no current flows to a potential E_2 where oxidation or reduction of the electroactive species occurs. In unstirred conditions the faradaic current value from mass-transfer is limited by diffusion and the current decreases with time due to the increase of the concentration gradient. Figure 3.2 shows an example of a double-step amperometric measurement. For instance, when the potential is set negative enough to

ensure proper reduction of the species in solution the current will rise instantaneously and then decrease with time as the concentration of oxidized species at the electrode surface also decrease. An opposite positive potential in the following will cause the reverse redox process.

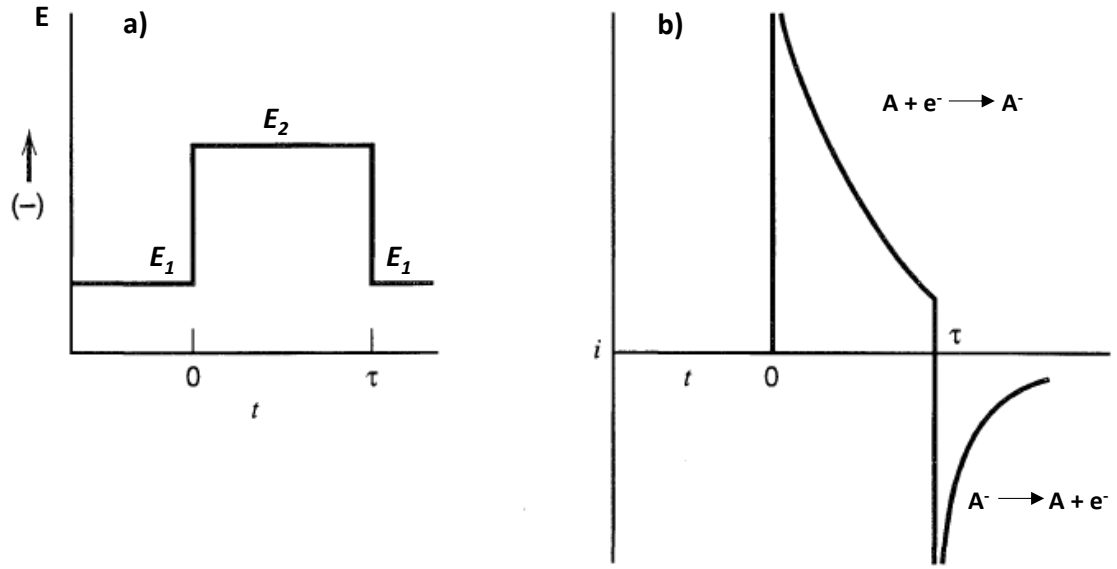

Figure 3.2 – Chronoamperometry. a) Potential step for a given period of time. b) Current profile varying with time for a reduction and a oxidation process.

At planar electrodes under quiescent conditions the current-time (*i-t*) response of a diffusion-controlled process can be represented by the Cottrell equation (Equation 3.2).

$$i = \frac{nFAD^{1/2}C}{(\pi t)^{1/2}} \qquad (3.2)$$

Where *n* is the number of electrons transferred, *F* the Faraday's constant, *A* the electrode surface area, *D* the diffusion coefficient, *C* the concentration of the electroactive species in solution. This is a sensitive technique widely used for analyte calibration studies. The oxidation or reduction potential determined by the CV curve is then applied in single-step amperometric measurements. When the current stabilizes, which means that all the electroactive analyte (or enzyme substrate) is reduced or oxidized at the electrode surface, further addition of analyte will concentrate the initial solution and create a perturbation in the current, stabilizing in another value (196, 199).

A potentiostatic method can be used instead LSV in order to obtain polarization curves for biocathodes, bioanodes and biofuel cells. It consists of applying a series of potentials beginning at the E_{OCP} until reaching 0 V. The current is monitored with respect to time until steady-state value is determined (about 15 min) (200).

3.1.3 – Electrochemical impedance spectroscopy

The electrochemical impedance spectroscopy, EIS, is a technique widely used to study the impedance effects (*i.e.* causes constraining the flow of charges) in electrochemical systems. More commonly, provides information on both the electrode capacitance and heterogeneous charge-transfer kinetics. In alternate-current (AC) systems, both the potential and current change in complex ways with time. To relate each other, the resistance (R) in the Ohm's law is replaced by the impedance (Z), a form of resistance to electron flow that changes with frequency (Equation 3.3).

$$E_{(t)} = I_{(t)}Z \qquad (3.3)$$

where *E* is the potential in Volts, *I* the current in amperes and *Z* the impedance in Ohms. According to the electronic theory, resistors convert the electric energy available to drive electric charges into heat. The net effect is a reduced number of charges flowing across the circuit, and its magnitude is measured as the "resistance" to electron flow. In turn, capacitors and inductors are able to store electrical energy respectively in the form of electrical and magnetic fields. The build-up of this fields produces typical temporary changes to flow of charges easily measured in AC conditions as capacitive or inductive impedances. Analogously, the double layer formed at the electrode surface, the electrode kinetics and the diffusion processes induce measurable changes to flow of charges in an electrochemical cell. EIS measurements are performed by applying small AC potentials or currents at various fixed frequency values. The impedance is then determined at each frequency value (197). More recently, this technique is being used to understand the implications in the electron transfer of electrodes with the surface modified with different layers of conductive materials, bioentities and biofilms (201).

3.2 – Apparatus and equippment

3.2.1 – Electrochemical equippment

All voltammetric and chronoamperometric measurements were performed with a potentiostat/galvanostat Metrohm, model Autolab PGSTAT10, controlled by GPES v3.9

software (Herisau, Switzerland). The equipment was connected to a Penthium II computer with a Windows 98 operating system (Figure 3.3).

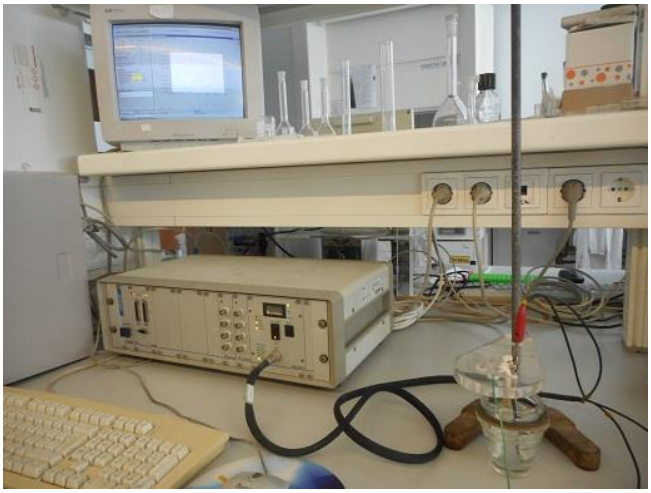

Figure 3.3 – Electrochemical workstation composed by the potentiostat, computer for data processing and electrochemical cell.

For EIS measurements a potentiostat/galvanostat Metrohm, model Autolab FRA32M was used (Figure 3.4). The equipmment was controlled by NOVA software from the same brand.

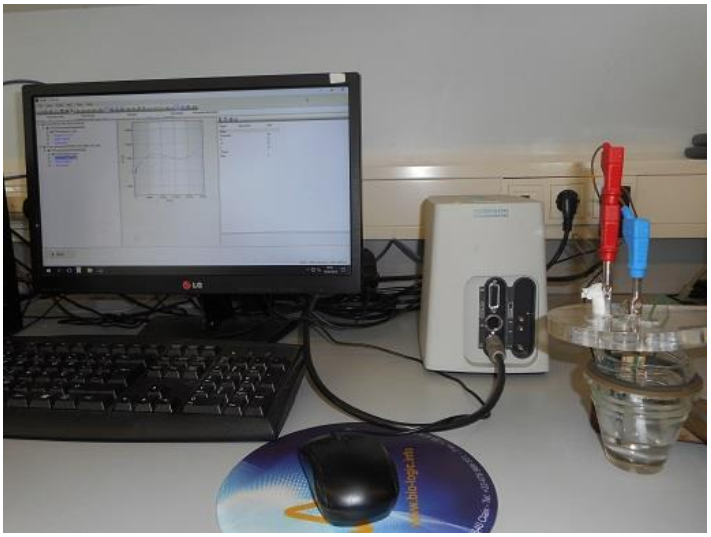

Figure 3.4 – Impedance workstastion composed by potentiostat with impedance module, computer for data processing and electrochemical cell.

3.2.2 - Electrodes

The characteristics of the developed biosensors were evaluated using the usual three-electrode configuration in a conventional electrochemical cell or implemented in a microfluidic platform. In the first case, an Ag/AgCl (KCl, 3M) ref. 6.0727.000 (Figure 3.5a - left) and a platinum rod (Figure 3.5b) were used as reference and counter electrodes

respectively. In the microfluidic platform the measurements were performed using a LF-1, 1 mm diameter leak-free Ag/AgCl reference electrode from Innovative Instruments (Tampa, US), depicted in Figure 3.5a (right) and a thin platinum wire as counter electrode.

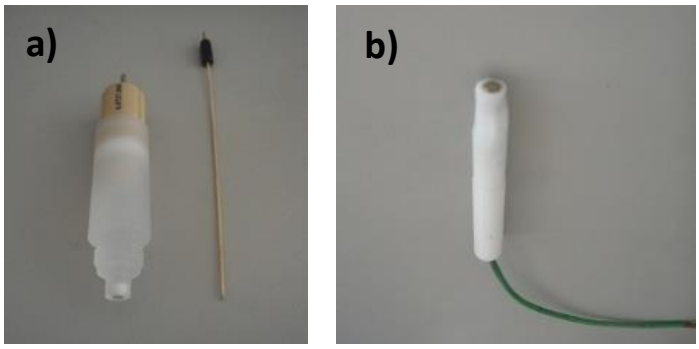

Figure 3.5 – a) Ag/AgCl reference electrodes and b) platinum counter electrode.

As working electrodes, pencil graphite electrodes (Figure 3.6a) were used for sensor and biosensor studies. Pencil leads of 2 mm diameter (type HB, 4H or 4B) were put in contact with the inner copper wire of a coaxial shielded cable and isolated with a flexible polymer sleeve (Tygon) in order that only the tip of the graphite lead was exposed. The PGE were then polished with sandpaper (P1200) and washed with distilled water and in some cases were polished further with alumina slurries (1 µm and 0.05 µm) in a cloth.

Also miniaturized and flexible electrodes (Figure 3.6b) were fabricated for integration as cathodes and anodes in microfluidic biofuel cells. These paper-like electrodes were fabricated similarly as buckypapers by a vacuum filtration process of a carbon-black suspension.

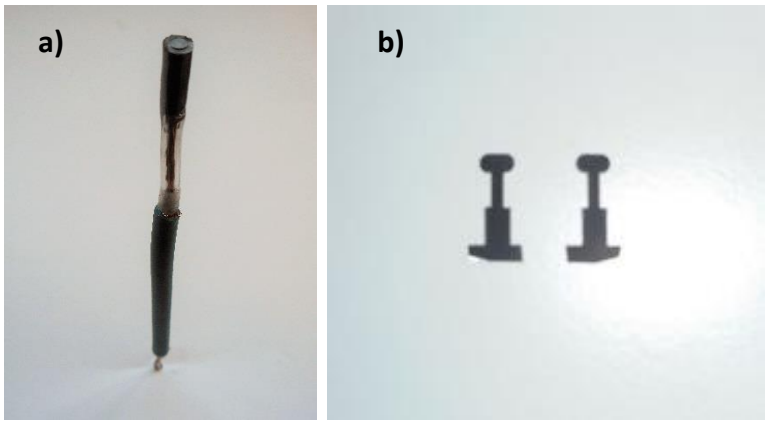

Figure 3.6 – Working electrodes used in biosensors and biofuel cells. a) PGE electrode. b) Pair of miniaturized paper-like electrodes made of carbon black and used in microfluidic platforms.

3.2.3 – Other equipment

For the fabrication of microfluidic devices based on PDMS and PMMA materials, specific equipment were used. For instance, microfluidic devices made of PMMA as well as masks and moulds of the same material were processed using a 2D-laser cutting-engraving machine from Universal Laser Systems Inc. (Scottsdale, US) as depicted in Figure 3.7a. For the assembly of hybrid PDMS-PMMA microfluidic devices, the two parts were joined after plasma treatment using a Diener Zepto plasma system (Diener Electronic GmbH-Co. KG, Ebhausen, Germany) as shown in Figure 3.7b.

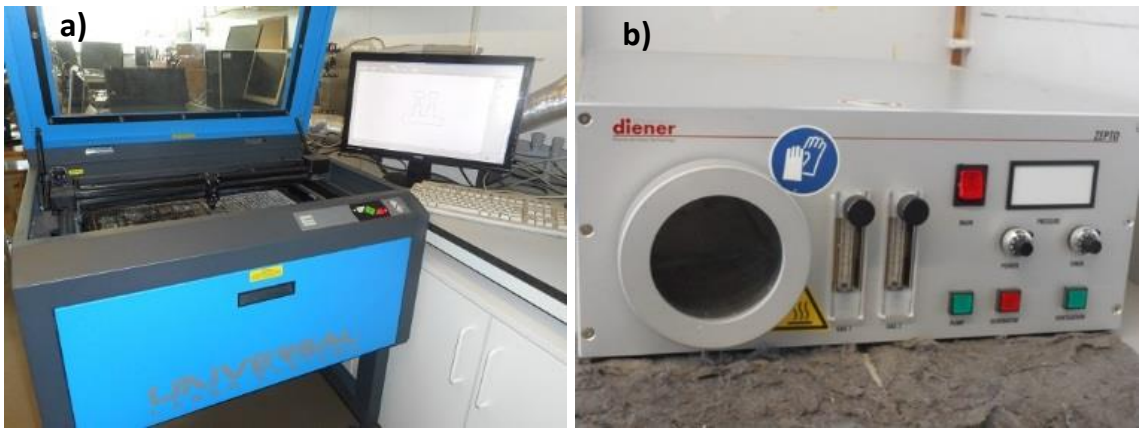

Figure 3.7 – a) 2D laser cutting-engraving machine used for construction of microfluidic platforms.b) Plasma treatment equippment used to bond surfaces.

Other general laboratorial equipment was used in a daily basis for preparation of solution namely pH meter and balances.

3.3 – Strategies used for immobilization of enzymes and construction of biosensors and biofuel cells

Enzyme immobilization on the surface of electrodes can be performed through different approaches such as physical adsorption, entrapment and chemical cross-linking. The last two strategies were followed along the work. Firstly, laccase from *Rhus vernicifera* was immobilized by entrapment in a silane based sol-gel. In the following works the enzymes were immobilized through cross-linking using glutaraldehyde (GA) or a pyrene based compound (PBSE).

The electrodes were always modified in order to provide some level of nanostructuration. To this, carbon based materials providing enhanced electrochemical signals such as

graphene, SWCNT, MWCNT and carbon black were used and whenever possible compared between each other.

3.3.1 - Enzymes

Four different enzymes were used throughout the work. Glucose oxidase from *Aspergillus niger*, type VII (≥ 100000 U g^{-1}) was acquired from Sigma-Aldrich. This enzyme was used for assembly of glucose biosensors and bioanodes of biofuel cells using glucose as fuel. Bilirubin oxidase from *Myrothecium verrucaria* (8.2 U mg^{-1}) and laccases from *Trametes versicolor* (0.53 U mg^{-1}) and from *Rhus vernicifera* (1.05 U mg^{-1}) were also acquired from Sigma-Aldrich and applied for O_2 biosensors and biocathodes.

3.3.2 – Sp^2 carbon additives

About four different types of sp^2 carbon materials were used for nanostructuring the electrodes. Graphene oxide dispersion (4 mg mL^{-1} in water), carboxylic acid functionalized SWCNT (>90% carbon basis, diameter x length 4-5 nm x 0.5-1.5 µm) and carboxylic acid functionalized MWCNT (diameter x length, 9.5 nm x 1.5 µm) were acquired from Sigma-Aldrich. Carbon black type Vulcan XC72 (270 kg m^{-3}) was acquired from Cabot Corporation (Boston, Massachusetts).

All aqueous solutions were prepared with Milli-Q doubly deionized water (conductivity <0.1 µS cm^{-1}) and analytical grade chemicals were used without further purification.
Phosphate buffer solutions in a concentration of 0.1 M with different pH were used for characterization of biosensors and biofuel cells.

Chapter 4

Characterization of an O_2 biosensor with immobilized laccase for implementation as a biocathode

4.1 - Introduction

Several efforts are being made in order to substitute noble metals as catalysts in sensing systems and fuel cells. Using a biocatalyst instead of precious metals in fuel cells enables operation at milder neutral pH and near ambient temperatures and further elimination of physical separation between the anolyte and catholyte. In biosensing applications, they also confer high efficiency and selectivity towards specific substrates. Laccases, alongside with ascorbate oxidase, bilirubin oxidase and ceruloplasmin are multicopper oxidoreductases which catalyze the four-electron reduction of molecular oxygen to water, through the oxidation of a wide number of phenolic compounds. The last feature turned the enzymes attractive for various applications ranging from analytical usages to industrial bleaching processes (202) and wastewater treatment (203). In turn, the ability for ubiquitous dioxygen reduction raised the interest on their use as biocathodes in hence designated biofuel cells (204). The substrate is oxidized at the T1 copper site, the primary electron acceptor, followed by rapid transference of electrons to the triangular T2/T3 copper site where the reduction of molecular oxygen to water occurs (125, 131, 205). Due to proximity of T1 copper center from protein surface (32), the *in vivo* oxidation step of phenols was eventually substituted by the artificial heterogeneous electron transfer to provide further insight on the molecular oxygen reduction step (131). Although tree laccases have the same copper atom configuration as fungal laccases as well as performing the same biological functions, these two types of laccase display different redox potentials. Whereas for fungal laccase *Trametes hirsuta*, the T1 copper site has a redox value of +780 mV (*vs* SHE) (206), tree laccases exhibit low redox potentials of their catalytic centers with *Rhus vernicifera* presenting for each type copper atoms redox values of +420 mV for T1 site, +390 mV for T2 site and +460 mV for T3 site (*vs* SHE) (131). However, a significant advantage is the

higher activity shown at pH nearer physiological conditions instead of acidic mediums needed for optimum activity of the fungal laccases (207).

The direct electron transfer between the surface of an electrode and an enzyme in its vicinity can be efficiently improved by wiring the active site of the biological element using carbon based materials (208). For instance, graphene (and/or reduced graphene) has been used as electrode material to increase the sensitivity and provide excellent detection (209). The high surface area provides higher electron conductivity regarding to graphite and even glassy carbon (210, 211). When compared to carbon nanotubes, another commonly used nanomaterial, reduced graphene also shows better conductivity probably due to the sp2-like planes and various edge defects present on the surface (212) which translates in a much higher electrochemical capacitance (213). To the best of our knowledge the majority of laccases immobilized on carbon material surfaces are from fungal origin (214) namely *Trametes versicolor* (215-217), *Trametes hirsuta* (31, 130, 216) and *Cerrena unicolor* (31, 218, 219). The multicopper blue oxidase *Rhus vernicifera* laccase was first discovered in the Japanese lacquer tree by Yoshida in 1884, and chosen for oxygen reduction in the present work. In contrast the studies regarding the characterization of tree laccase, *Rhus vernicifera*, immobilized on graphite electrodes (130) or other carbon materials based electrodes (132, 206, 220, 221) are until now limited. Thus, the main objective of the present work was the characterization of tree laccase immobilized in costless homemade pencil graphite electrodes for potential application as biocathodes in biofuel cells. Temperature and pH influence in laccase activity is addressed using electrochemical and spectrophotometric methods as well as determination of molecular oxygen in solution. The use of combined nanostructured carbon materials to enhance electron transfer efficiency and their influence on bio-electrode characteristics was also evaluated.

4.2 – Experimental

4.2.1 – Materials and reagents

All aqueous solutions were prepared with Milli-Q doubly deionized water (conductivity <0.1 µS cm^{-1}). Analytical grade chemicals were used throughout without further purification.

Laccase from *Rhus vernicifera* labelled with the activity of 1.07 U mg^{-1} (determined with catechol at pH 5.0 and 25 °C) was acquired from Creative Enzymes (New York, US). Glycerol, graphene oxide (4 mg mL^{-1} dispersion in water), potassium phosphate monobasic, single-walled carbon nanotube functionalized with carboxylic acid (>90%), sodium

carbonate decahydrate, syringaldazine, titanium isopropoxide and tetraethyl orthosilicate were from Sigma-Aldrich (USA). Di-potassium hydrogen phosphate trihydrate, potassium ferrocyanide trihydrate, sodium dodecyl sulfate, SDS, sodium sulfate were obtained from Merck. Potassium chloride was obtained from Pronalab, sodium hydroxide from VWR Prolabo. Functionalized carbon black, Vulcan XC72, was obtained from Cabot Corporation. Pencil mines type HB with 2 mm diameter from BIC (Clichy, France) were used as conductive support electrodes.

Potassium phosphate buffer 0.1 M pH 6.5 was prepared and used as electrolyte solution and in the sol-gel processing. A suspension of single-walled carbon nanotubes (SWCNT) with concentration of 5 mg mL^{-1} was prepared in 2% SDS solution and ultrasonicated for 30 min. A 0.216 mM syringaldazine solution was prepared in absolute methanol. Laccase suspensions were freshly prepared in ultrapure water whenever needed.

4.2.2 - Apparatus

All electrochemical experiments were performed with a potentiostat Metrohm, model Autolab PGSTAT10, controlled by GPES v3.9 software (Herisau, Switzerland). The electrochemical cell was composed of the Ag/AgCl (KCl, 1 M) mini reference electrode Ref. 6.0727.000 from the same brand, the bioelectrode, and a homemade zinc electrode (222) for galvanic cell experiments or a platinum rod for amperometric measurements as auxiliary electrodes. In anaerobic experiments, solutions were purged with N_2 for at least 20 minutes while aerobic experiments were performed by using solutions oxygenated with O_2 (99.999% purity) for 15 minutes.

The spectrophotometric assays regarding determinations of enzymatic activity were conducted in a Citation-3 cell imaging multi-mode reader from Biotek Instruments (Winoosk, US).

4.2.3 – Bioelectrode construction

Graphite pencil mine rods (2 mm) type HB were used for preparing the working electrodes (PGE). The rods were cut with about 1 cm length and the flat end surface was polished first with fine emery paper (P1200) and then with microcloth PSA and alumina 0.05 micron and 1.0 micron (Buehler, USA). Graphene deposition was then proceeded based on the procedure described in Shao et al. (2010) (213). Therefore, a 10 µL aliquot of graphene oxide (1 mg mL^{-1}) was dropped over the electrode surface, left to dry at ambient temperature and finally electroreduced (rGO) in 0.1 M Na_2SO_4 solution. The enzyme immobilization was

performed in polyglycerol silicate (PGS) polymer synthetized accordingly to Harper et al. (2011) (223). Laccase solution (25 mg mL^{-1} in distilled water) was mixed in the same proportion with carbon additive solution and 10 µL were dropcasted over the reduced graphene surface and left to dry for 1 hour at ambient temperature. Afterwards, the surface of the electrode was coated with about 5 µL of PGS sol diluted in phosphate buffer solution and left for gelation for a minimum of 5 hours at room temperature. The bio-electrode final configuration is designated as PGE-rGO/SWCNT-laccase/sol-gel electrode.

4.2.4 – Electrochemical measurements

The electron transfer surface area of the working electrode was determined by chronoamperometry and applied the Cottrell equation (Equation 3.2) in the known hexacyanoferrate redox system (diffusion coefficient, $D_0 = 0.65x10^{-5}$ cm^2 s^{-1} (224)). In accordance, the surface area determined was of 0.034 ± 0.001 cm^2 (n=3).
The laccase activity was routinely determined by spectrophotometry before bioelectrode preparation. For this, the Sigma protocol was followed and consisted firstly in the preparation of a mixture between 30 µL of 0.216 mM syringaldazine, 50 µL of 0.5 mg mL^{-1} laccase and 220 µL of buffer solution 0.1 M. The temperature for the kinetic assays was set to 35 °C and absorbance of the mixture was measured at 530 nm during 10 minutes. Further extension of the protocol was followed by assaying activities at five different pH between 6.0 and 8.0. Temperature experiments were conducted by placing the electrochemical cell in thermostatic water bath. Full immobilization of laccase used to prepare the bioelectrode, 1.28 nmol cm^{-2}, was surmised in calculation of enzymatic activities and turnover numbers.
Amperometric measurements were performed in 10 mL, quiescent, N_2 purged, phosphate buffer solution pH 6.5, with the potential set to -0.2 V. Response to oxygen was recorded by successive additions of 1 mL of buffer solution saturated with oxygen. Polarization curve was determined by linear sweep voltammetry (LSV) at scan rate of 1 mV s^{-1}.

4.3 – Results and discussion

4.3.1 – Characterization of the graphene modified PGE

A driving aspect regarding the implementation of bioelectrodes concerns to the use of cheap and easily accessible raw materials. Therefore, home-made graphite electrodes casted with reduced graphene to promote intimate contact with the high activity tree laccase *Rhus*

vernicifera in direct electron transfer arrangement were envisaged and further characterized through electrochemical and spectrometric techniques. As starting materials either the pencil mine surface or the commercially available graphene have not optimal conductive properties for straight use due to the presence of peroxide, carboxyl, aldehyde and epoxy groups formed in the exfoliation processes (209, 211), so an initial pretreatment aiming to increase the C/O ratio becomes necessary. The reduction of graphene oxide showed to be effective by treatment with strong oxidants or acids such as $KClO_3$, H_2O_2 or HNO_3, by heating above 1000 °C under inert atmosphere or through electrochemical reduction by setting a sufficient negative potential over a period of time. Besides being environmental friendly this last procedure lead to materials with better performance compared with chemical reduced graphene and avoids the energetic costs associated with the thermal treatment (211). Therefore, the electrochemical reduction was selected and performed in 0.1 M Na_2SO_4 salt solution by cyclic voltammetry in a wide potential range (-1.5 V to 0.8 V *vs* Ag/AgCl) to ensure proper reduction that occurs mainly around -0.9 V (213). It was observed a proportional slow increase of the current signals with the number of performed scans (data not shown). At the end of process (1500 scans) the surface of the modified electrodes were easily distinguished from pristine mine surface by their black tone. Infrared analysis of the graphite surface, graphite/graphene oxide and graphite/reduced graphene surfaces allowed to confirm the reduction of oxygen containing groups (225). Strong peaks around 2850 and 2930 cm^{-1} due to CH_2 and CH ligands were observed as main features of all FTIR spectra. Whereas the graphene oxide mid-IR spectrum showed the characteristic bands at 1028 cm^{-1} (C-O), 1620 cm^{-1} (C=C), 1708 cm^{-1} (C=O) and 3200-3350 cm^{-1} (-OH) in the reduced graphene spectrum only the band corresponding to C=C ligand subsisted, indicating high yield removal of the oxygen functional groups.

The redox probe $K_4[Fe(CN)_6]$ was then used to evaluate heterogeneous electron transfer efficiency at the new reduced surface of the graphite-graphene electrode contacting the solution (Figure 4.1a). Significant enhancement of current signals relative to bare graphite electrodes occurred and underlined results referred in previous reports (211, 226) to justify the advantageous use of graphene for sensing applications. The anodic-cathodic peak separation (ΔE_p) was also higher when compared to bare graphite due to a higher specific capacitance of the reduced material. An actual specific capacitance of 195.8 F g^{-1} was determined by chronoamperometry for the implemented graphite-graphene electrode (Figure 4.1b). Shao and colleagues (213) reported the approximately similar value of 150.4 F g^{-1} for electrochemically reduced graphene and compared it with the one obtained for carbon nanotubes (83 F g^{-1}) to justify additional capability to store electrical energy (capacitors).

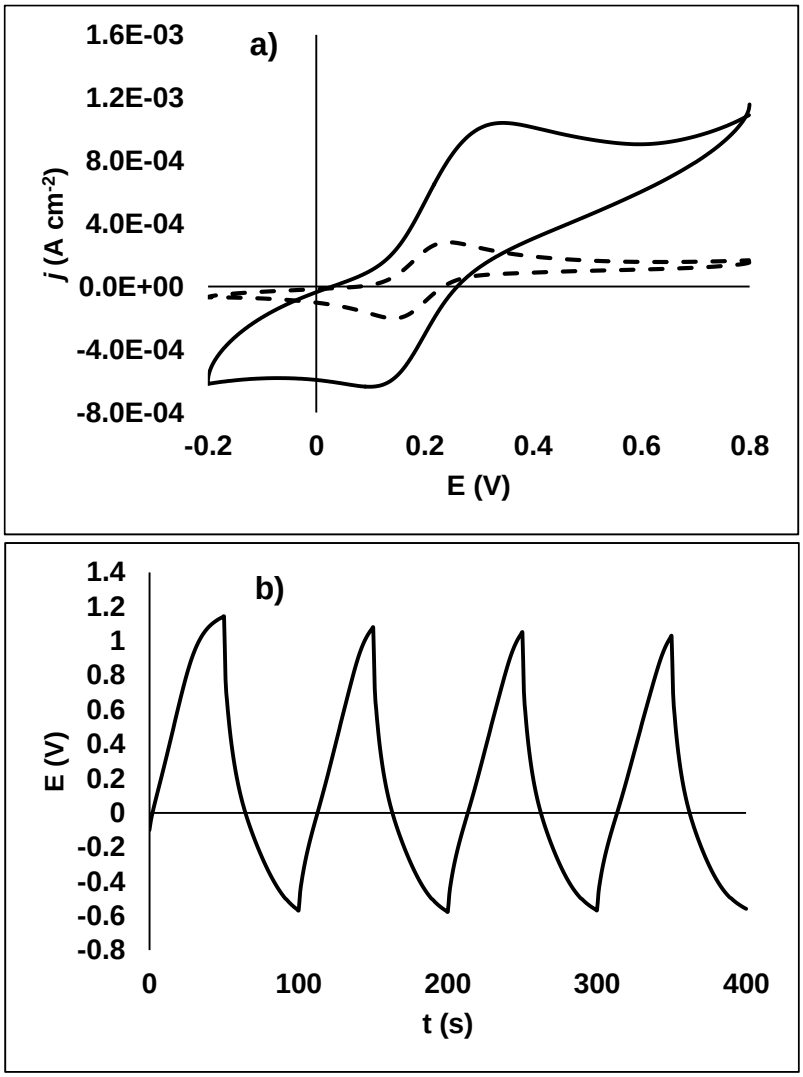

Figure 4.1 - Voltammetric and Amperometric characterization of PGE-rGO electrode. a) Cyclic voltammogram of bare graphite (PGE) (trace line) and graphite modified with reduced graphene (PGE-rGO) (full line) in 5 mM $K_4[Fe(CN)_6]$ with 0.1 M KCl. Scan rate: 10 mV s^{-1}. b) Galvanostatic charge-discharge curves for 6 A g^{-1} of graphene deposited in graphite surface in 0.1 M Na_2SO_4.

4.3.2 – Bioelectrode implementation

The robust immobilization of enzyme over the conductive surface of the electrode by means of a polymeric matrix is a crucial step to ensure a useful operation lifetime. At the same time, it should not impair the electron transfer between the electrode surface and the catalytic T1 center of the enzyme and allow freely diffusion of substrate through the matrix. Previous works refer the succeeded use of inorganic siloxane polymers prepared by the sol-gel technique from simple alcoxyde monomers, mainly tetramethoxysilane (219). Nevertheless, the process requires the addition of mineral acids to promote poly-condensation and gelation steps. In the meantime significant volumes of the protein denaturating ethanol are released and contribute to biocatalytic loss (227). Alternatively,

newly synthesized monomers where the ethoxy groups are substituted by glycerol were proposed to enable friendly enzyme immobilization under milder conditions. Briefly, tetraethoxysilane and titanium isopropoxide are modified with the polyol resulting in a high water miscibility compound (PGS) easily forming the gel backbone structure in saline solutions at near neutral pH condition. The shrinkage observed in the gelation process is minimal when compared to the common alkoxysilane hydrogels and allow conformational preservation of entrapped proteins (228). In this work, the time of about 5 hours was settled to ensure complete immobilization of the mixture of laccase-phosphate buffer (pH 6) in the PGS at room temperature. The laccase activity at different pH conditions determined by spectrophotometric and electrochemical techniques were afterwards compared with the results being depicted in Figure 4.2a. In the spectrophotometric assays the oxidation of syringaldazine in the T1 center acts as the electron source for oxygen reduction at the T2/T3 center while in the electrochemical assay the electron transfer is directly promoted from the structured surface of the electrode. In the presence of syringaldazine as electron-donor substrate, the activity of laccase either free in solution and entrapped in the sol-gel matrix presented a sharp activity decrease starting from pH 6.0 as result from slower kinetics of the charge transfer between the two catalytic centers. The lower activity observed at pH 6.0 for the last can be ascribed to the limited diffusion of the substrate through the silica matrix. After correction for scattering promoted by sol-gel, the activities for the enzyme immobilized were however generally higher and constant in the pH interval from 6.5 to 7.5. This behavior is explained by the rigid structure of silica pores which restrain substantial conformational changes of the enzyme. In turn, the current densities observed with the PGE-rGO/SWCNT-laccase/sol-gel bioelectrode almost follow the same trend thus evidencing effective electron transfer from electrode surface. Nevertheless, in all studies depicted in Figure 4.2b the concentration increase of hydroxyl ion at more alkaline conditions leaded to binding to the T2/T3 copper center site of the enzyme, forming a complex with Cu^{2+} which impairs its oxygen reduction ability (229, 230). In the implementation of the bioelectrode, loadings of enzyme of 0.1 mg mL^{-1}, 1 mg mL^{-1}, 10 mg mL^{-1} and 25 mg mL^{-1} were tried. The catalytic current increased with enzyme loading although for higher concentrations the differences between 10 and 25 mg mL^{-1} were not significant. The temperature effect on the electrodes response was tested between 20 and 40 °C by cyclic voltammetry and evidenced deeper influence on the enzyme turnover values when compared to the pH effect (Figure 4.2b). Electrocatalytic currents for oxygen reduction raised almost linearly with temperature from $5.4x10^{-5}$ A cm^{-2} to a maximum of $1.21x10^{-4}$ A cm^{-2} (E = 0.1 V *vs* Ag/AgCl) at 40 °C, corresponding to almost linear raising in the calculated turnover k_{cat} from 4.7 up to 15.6 min^{-1} regarding oxygen reduction. The Arrhenius semi-ln plot of reaction rates as function of

inverse of temperature (T^{-1}) showed a straight line up to the temperature of 35 °C from which the energy of activation (Ea) of 38 ± 4 kJ mol^{-1} was obtained. This value is in the interval 35–53 kJ mol^{-1} found for reductive cleavage of the O-O bond by different laccases in electrolyte (231, 232) and is inferior to the 52.2 ± 2.5 kJ mol^{-1} reported for laccase from *Cerrena unicolor* immobilized in TMOS sol-gel (232), thus reflecting a kinetic rate determining mechanism. For the highest temperature of 40 °C a slight negative deviation was observed possibly reflecting additional limited diffusion in the membrane. In a broad temperature range study, Wu et al. (132) and Rowiński et al. (233) found a maximum *Rhus vernicifera* activity at 50 °C. For higher temperatures an activity decrease was observed due to denaturation or unfolding of enzymes. The catalytic centers of enzymes are generally buried inside the protein matrix but for copper proteins such as laccase these centers are near the surface which enable more or less efficient direct electron transfer at the interface with the surface of the electrode (32).

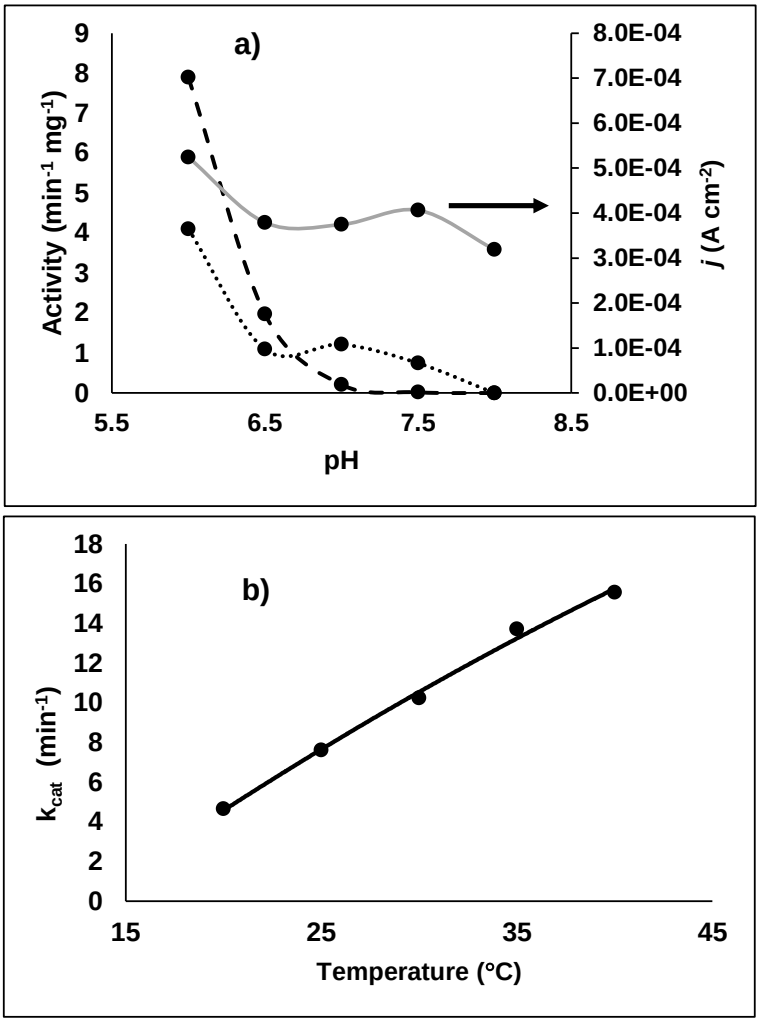

Figure 4.2 - Influence of pH and temperature on laccase activity and bioelectrode (PGE-rGO/SWCNT-laccase/sol-gel) response. a) Spectrophotometric assay of free laccase activity in solution (trace line) and entrapped in PGS sol-gel (dotted line); bioelectrode responses at 0 V vs Ag/AgCl (full line). b) Bioelectrode turnover at raising temperature in oxygen saturated 0.1 M potassium phosphate buffer solution pH 6.5.

To evaluate if the reduced graphene surface, over which the laccase was immobilized, promoted an effective charge transfer further addition of nanoconductors were equated. Cyclic voltammograms were then obtained comparing the additional resort to single-walled nanotubes or functionalized carbon black (Vulcan XC72) (Figure 4.3). Generally higher catalytic responses to oxygen were observed when laccase was entrapped alongside with both the above described nanomaterials. The addition of this nanostructured carbon materials in the preparation of the bioelectrode produced a great enhance in the current densities as result of improved electron transfer from the graphene surface to the T1 center of laccase.

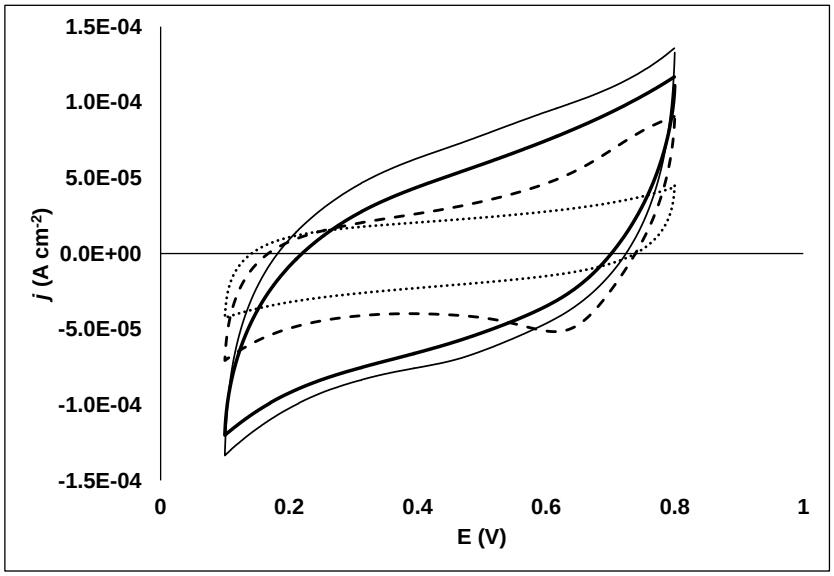

Figure 4.3 - Influence of casting the graphene surface with mixture of carbon additives and laccase in the response enabled by cyclic voltammetry in oxygenated buffer solution. Comparison between functionalized carbon black (bold line), single walled carbon nanotubes (full line), without carbon additives (trace line) and bare graphite electrode (dotted line). Scan rate: 5 mV s^{-1}.

The reduction of molecular oxygen was analyzed by cyclic voltammetry in oxygenated solutions, scanning in the potential range from +0.800 V to -0.200 V *vs* Ag/AgCl. The catalytic response of *Rhus vernicifera* in graphite electrodes occurs from +0.250 V (0.470 V *vs* NHE) to -0.200 V almost matching the redox potential of the T2/T3 center previously reported for *Rhus vernicifera* (131). This potentials window for reduction of oxygen free in solution also agrees with the one described by Yaropolov et al. (130) and differs from fungal laccases where oxygen reduction starts at higher potentials. For instance, in *Trametes hirsuta* the reduction initiates around +800 mV *vs* NHE (31, 32).

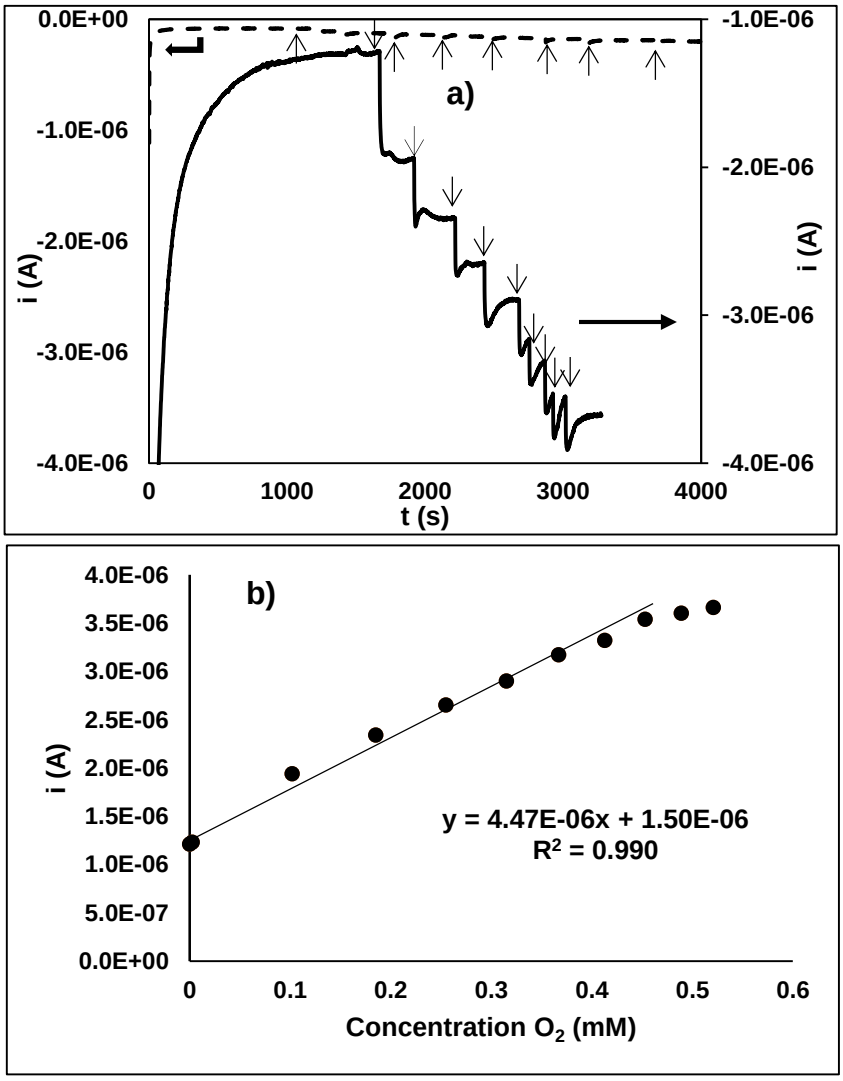

Figure 4.4 - Amperometric detection of O_2 by the PGE-rGO/SWCNT-laccase/sol-gel bioelectrode and compared with the non-structured graphite-laccase (PGE-laccase) electrode. a) Chronoamperometric response to successive 1 mL injections of oxygen saturated buffer solution pH 6.5 into 10 mL, non-stirred, N_2 purged initial solution and applied potential of -0.2 V. b) Calibration curve as function of oxygen concentration for bioelectrode.

The determination of oxygen concentration in solution carried out by amperometry at -0.2 V *vs* Ag/AgCl after successive injections of oxygen saturated buffer solution in a non-stirred, 10 mL of phosphate buffer purged with N_2 is shown in Figure 4.4a where both the bioelectrode and the non-structured graphite-laccase electrode (PGE-laccase) responses are compared. The presence of oxygen produces rapidly the onset of catalytic response. The response shows good linearity up to a concentration of about 0.4 mM with a correlation coefficient (R^2) value of 0.990 (Figure 4.4b). The evaluation of the standard deviation of blank signal enables to obtain the detection limit of 2.7 µM. For the highest oxygen concentrations the current tends to a constant value accordingly to Michaelis-Menten kinetic principles. From the O_2 calibration curve and the electrode surface area, we obtained a sensitivity of 132 ± 15 µA mM^{-1} cm^{-2} (n = 3). This value is comparable with the value of 149 µA mM^{-1} cm^{-2} (calculated from a surface area of 0.07 cm^2) obtained by Wu et al. (132) for

the same laccase adsorbed in a glassy carbon electrode modified with graphene and ABTS. In the presence of a mediator such as ABTS occur an electron-shuttle process between laccase and electrode suitable for the reduction of molecular oxygen, enhancing the sensitivity of detection (234). Higher current densities are achieved in rotating disk experiments where obtained values can be 100 fold higher relative to steady state conditions (235). In the works conducted by Mousty et al. (236) and Gutierrez-Sanchez et al. (237) the O_2 measurement was performed under stirring (with a rotative electrode) and the calculated values were about 474 μA mM^{-1} cm^{-2} and 300 μA mM^{-1} cm^{-2} respectively. The intermedium value of 386 μA mM^{-1} cm^{-2} was obtained by Liu et al. (238) for *Trametes versicolor* immobilized with chitosan and carbon nanotubes in a glassy carbon electrode. This value was probably due to the loss of enzyme activity obtained during chemical immobilization in chitosan as reported by others (239). The working range found for the described bioelectrode almost superimposes the one usually described for the well-known Clark cell (240), but with the advantage of not requiring the overpotential of about 0.8 V *vs* Ag/AgCl. However, the resolution regarding oxygen concentration values is one order of magnitude lower when quiescent conditions of measurement are adopted (240).

4.3.3 – Performance as biocathode

A common method to evaluate a biocathode performance in biofuel cells is by analyzing the polarization curves and consequently power curves. The LSV technique was employed, initializing at high potential with very low scan rate (1 mV s^{-1}) (241, 242). The assembled PGE-rGO/SWCNT-laccase/sol-gel bioelectrode generated a power density of about 4.5 μW cm^{-2} at +0.250 V (Figure 4.5) which is comparable with the power of about 10 μW cm^{-2} obtained by Zheng et al. (243) for *Trametes versicolor* cross-linked to a glassy carbon-MWCNT electrode. The open circuit potential (E_{OCP}) value determined in the present work (+0.45 V *vs* Ag/AgCl) is lower and explained by the different structural characteristics between fungal and tree laccases.

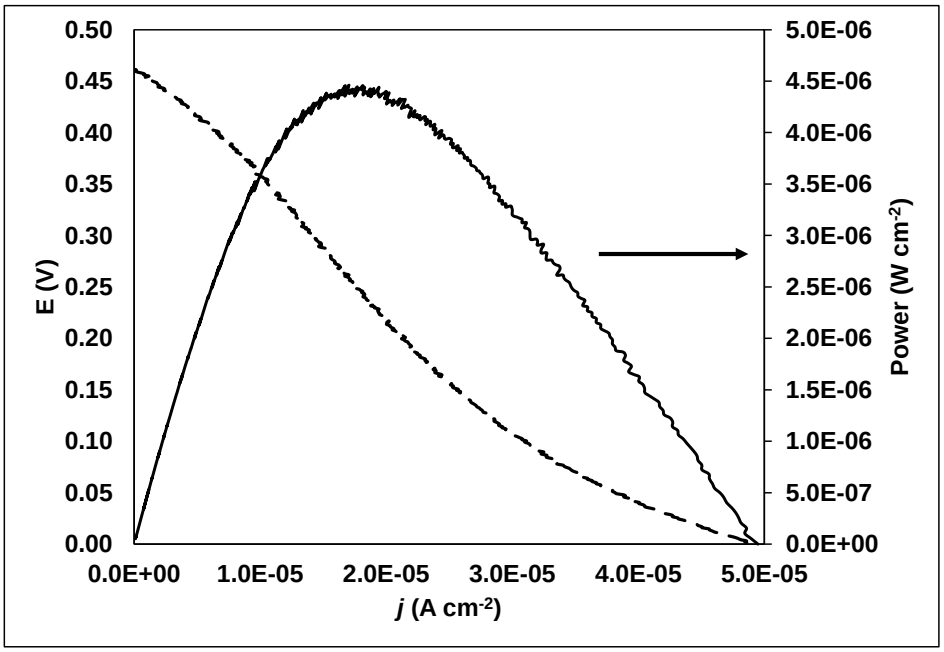

Figure 4.5 - Polarization and power density curves for PGE-rGO/SWCNT-laccase/sol-gel bioelectrode in quiescent 0.1 M phosphate buffer (pH6.5) saturated with oxygen. Polarization curve obtained by linear sweep voltammetry at 1 mV s^{-1}.

4.4 - Conclusions

The performed studies evidenced that laccase from *Rhus vernicifera* is prone to be used in direct electron transfer modified electrodes. In order to improve the process graphene was reduced in mild conditions through electrochemical means. Further use of single walled carbon nanotubes provided maximum activity of the enzyme similar to the one observed in the spectrophotometric assay with the free enzyme in solution at optimal conditions of pH and temperature. Entrapment of laccase in a silica matrix obtained by the sol-gel technique from glycerol modified siloxane monomers rendered constant enzyme activity over an extended range of pH conditions. When evaluated regarding the generated power the electrode described herein showed values similar with the ones previously reported on literature for fungal laccases also evaluated on quiescent solutions, although at lower E_{OCP} potential.

Chapter 5

Characterization of an O_2 biosensor with immobilized bilirubin oxidase for implementation as a biocathode

5.1 - Introduction

Pencil graphite electrodes (PGE) stand as a valuable analytical tool in the electrochemical field considering its negligible cost when compared to more classical electrodes (glassy carbon, platinum, gold, etc.). As suggested by its name, it makes use of commercially available pencil mines as polarizable material in a wide range of different active surface areas. Readily prepared and ubiquitous, this type of electrode is suited for quick proof-of-concept experiments or in daily routine analysis as disposable probes. Although first reported around the 60's (244), PGEs have been used in an increasing number of applications both as sensors and biosensors, since dawn of the new millennium as inferred from recently published reviews (245-248). In terms of electrochemical performance, some studies have obtained similar or better electroanalytical results of PGEs over glassy carbon electrodes (GCE) and highly ordered pyrolitic graphite electrode while others stated worst kinetics compared to GCE (248). Despite these conclusions, an apparent minimal pre-treatment of the active surface area is required to attain optimal analytical conditions whereas for GCE this can be a relatively fastidious procedure (48). Nonetheless, the possibility of modifying the electrode surface can always compensate some lack of performance of the transducer. Nanostructuring with carbon based materials not only enhances the electronic properties of the electrode but also increases the specific surface area. Furthermore, the biocompatibility characteristics and functionalization of the carbon material enables covalent attachment of bioentities (208). An efficient linking allows electron tunnelling between the electrode and the active site of enzymes usually buried in an insulating glycoproteic shell, thus avoiding additional use of diffusional mediators (249). This direct electron transfer feature allied to the enzymes specificity makes the enzymatic biosensor less prone to interferents and turns possible the operation without separation between anolyte and catholyte in biofuel cells. Moreover, certain enzymes perform their

catalysis reaction at physiological conditions. Bilirubin oxidase is a good example, presenting similarities in efficiency (45) or even outperform (43) platinum catalysts regarding the overpotential generated in the oxygen reduction cathodic reaction (ORR).

Hence, the positive features of PGE are in this work assessed through the implementation of a bioelectrode containing immobilized BOx with DET feature, in order to be used as O_2 biosensor or biocathode with high electrocatalytic performance. Prior to enzyme immobilization the PGE transducer was properly characterized and optimized regarding pencil hardness, surface pre-treatment and modification with carbon-based nanomaterials. The immobilization procedure consisted in tethering BOx enzyme to multi-walled carbon nanotubes (MWCNT) via pyrene-based succinimidyl ester compound (PBSE), similarly as performed by others (250).

Study of oxygen biosensing using a PGE as support electrode is not fully described in the literature. Only two studies from the same group assessed the performance of PGEs immobilized with laccase enzyme on the ORR by voltammetric and polarization techniques for potential use as biocathodes (113, 251).

5.2 – Experimental

5.2.1 – Materials and reagents

The enzyme bilirubin oxidase from *Myrothecium verrucaria* (8 U mg^{-1} of solid) was acquired from Sigma-Aldrich. Stock solutions of bilirubin oxidase (1 mg mL^{-1}) were made by dissolving all the solid in 0.01 M phosphate buffer solution pH 7.0, divided in aliquots and stored at -20 ºC until use. The 2,2′-Azino-bis(3-ethylbenzothiazoline-6-sulfonic acid) diammonium salt (ABTS), graphene oxide (4 mg mL^{-1} dispersion in water), hydrochloric acid 37%, MWCNT (carboxylic acid functionalized), potassium hexacyanoferrate (II) trihydrate, potassium hexacyanoferrate (III), potassium phosphate dibasic, potassium phosphate monobasic were also from Sigma-Aldrich. Dimethylformamide (DMF) was acquired from ROMIL Chemicals (Cambridge, UK).

5.2.2 – Electrochemical measurements

Voltammetric and amperimetric experiments were performed with a potentiostat Metrohm, model Autolab PGSTAT10, controlled by GPES v3.9 software (Herisau, Switzerland). Electrochemical impedance spectroscopy (EIS) experiments were performed in an Autolab

PGSTAT204 with model FRA32M controlled by NOVA v1.10.1.9. All experiments were performed in classic three-electrode electrochemical cell composed of an Ag/AgCl (KCl, 3 M) reference electrode (Metrohm, Ref. 6.0727.000), a platinum rod as counter electrode and the PGE sensor/biosensor as working electrode. All potentials presented throughout the test are referenced for Ag/AgCl. An equimolar 5 mM solution of potassium hexacyanoferrate, $Fe(CN)_6^{3-/4-}$ in 0.1 M of KCl (resistance of the solution R_{sol} = 180 Ω) was used for characterization experiments of the PGE sensor (without immobilized enzyme). As for the characterization of the bioelectrode, potassium phosphate buffer 0.1 M pH 7.0 was used as electrolyte solution and was purged with N_2 or oxygenated with O_2 for 15 min.

5.2.3 – Electrode preparation and BOx immobilization procedure

Pencil mines with 2 mm diameter (Staedtler) were put in contact with the inner copper wire of shielded coaxial cables and isolated with flexible polymer sleeves (Tygon). A transversal cut exposed then the pristine PGE surface which was polished mechanically using sandpaper (P1200) and washed with distilled water. The active surface area of the PGE was previously determined by chronoamperometry and corresponds to 0.034 cm^2. Pencil mines with hardness 4H, HB and 4B were additionally pre-treated by polishing with alumina 1.0 µm followed by 0.05 µm in polishing cloth in order to assess the influence of pencil hardness and pre-treatment in the electrochemical performance. A pencil mine HB solely polished using sandpaper was then modified with 10 µL of graphene oxide (1 mg mL^{-1}) and afterward electrochemically reduced in 0.1 M Na_2SO_4 solution at 50 mV s^{-1} along 50 scans performed within -1.2 V and 0.8 V and designated as PGE-rGO. For comparison purposes a PGE modified with 10 µL MWCNT (1 mg mL^{-1} in DMF) and another modified with 10 µL carbon black Vulcan XC72 (1 mg mL^{-1} in water) were similarly prepared and designated as PGE-MWCNT and PGE-CB, respectively. The PGE-rGO was selected for the implementation of the BOx bioelectrode. It was first immersed in a PBSE solution for 1 hour and then washed by immersion in a 0.01 M phosphate buffer solution (pH 7.0) for a few seconds. Next, the electrode was incubated in enzyme BOx solution (0.5 mg L^{-1} in 0.01 M phosphate buffer pH 7.0) for another hour and washed by immersion in a 0.1 M phosphate buffer pH 7.0. This bioelectrode is henceforth designated as PGE-rGO-MWCNT-BOx.

5.3 – Results and discussion

5.3.1 – PGE sensor modification and characterization prior to enzyme immobilization

As mentioned before, different electrochemical signals are expected according the pencil mine hardness used as PGE. The same may be observed when varying the level of pre-treatment applied to its active surface. Thus, PGEs with different clay/carbon ratios (hardness 4B, HB and 4H) and type of pre-treatment were compared regarding their electrochemical performance in a $Fe(CN)_6^{3-/4-}$ solution by cyclic voltammetry (Figure 5.1a) and impedance spectroscopy EIS (Figure 5.1b). At first sight, 4B signals seem better than HB. However anodic voltammetric peaks are higher for HB (i_{pa} = 0.045 mA; i_{pc} = -0.049 mA) with almost unitary i_{pa}/i_{pc} ratio, followed by 4B (i_{pa} = 0.042 mA; i_{pc} = -0.049 mA) and lastly 4H (i_{pa} = 0.035 mA; i_{pc} = -0.040 mA). Also PGE HB have comparative better kinetics by showing lower peak-to-peak separation (ΔE_p = 0.09 V) which is in agreement with the results reported by Kariuki (76). Figure 5.1a also shows that without polishing the surface with alumina the HB have inferior kinetics (ΔE_p = 0.64 V) and lower peak heights (i_{pa} = 0.020 mA; i_{pc} = 0.016 mA). Analysis by EIS also confirmed the higher resistance to electron transfer (R_{ct} = 4000 Ω) in view of the much larger semi-circle in the Nyquist plot (Figure 5.1b). In EIS, semi-circles express induced phase gap relative to the applied AC potential of 0.010V. In the experiment, to the decrease in frequency of the potential signal from 100 kHz to 0.1 Hz, it corresponded to the combined effect of the double capacitive layer at the interface PGE - solution (C_{dl}) in parallel to the resistance to electron transfer in the $Fe(CN)_6^{3-/4-}$ redox process. A straight raising of impedance was also observed for low frequencies, on the right of the semi-circle. Usually referred as Warburg impedance it is ascribed to the diffusion of the electroactive compounds from solution bulk. The proposed equivalent circuit for the response of the assayed electrodes is depicted as inset of Figure 5.1b, and the obtained regression values are referred in Table 5.1. The constant phase element CPE is represented instead of C_{dl}, because it describes better the depressed semi-circles obtained due to surface roughness and varying clay/carbon composition of PGEs. Its inductance value is calculated by $Z_{(\omega)} = q^{-1}(j\,\omega)^{-n}$, where q is a proportionality factor, j=-$1^{1/2}$, ω is the angular frequency and 0.8<n<1 describes distorted capacitance behaviour (252).

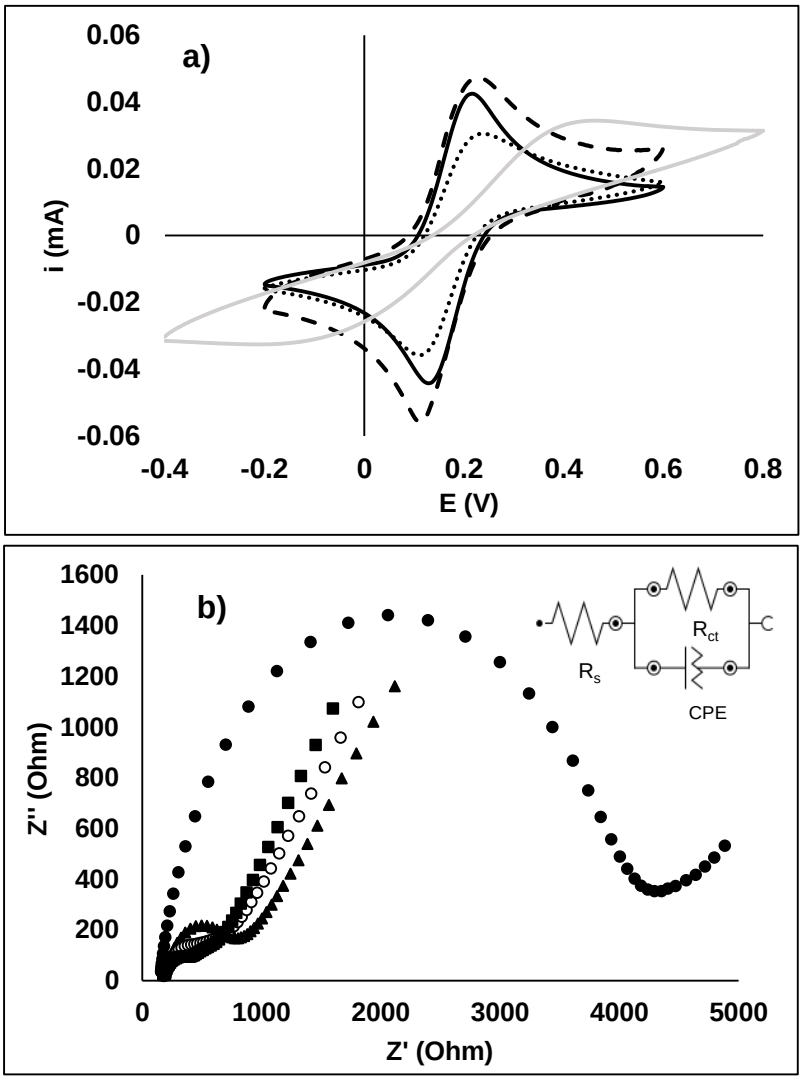

Figure 5.1 - Characterization of PGE regarding influence of pencil hardness and surface pre-treatment. a) Cyclic voltammograms for a PGE type 4B (dashed line), HB (full black line), 4H (dotted line) and for a PGE HB without pre-treatment by polishing with alumina (full grey line). b) Nyquist plots for PGE 4B (squares), HB (open circle), 4H (triangle) and for PGE HB without pre-treatment by polishing with alumina (full circle). Conditions for CV: scan rate 50 mV s^{-1}. Conditions for EIS: frequency 100000 to 0.1 Hz, amplitude 0.01 V, potential set to E_{OCP} value. Electrolyte for both analysis: 5 mM $Fe(CN)_6^{3-/4-}$ with 0.1 M KCl, purged 15 min with N_2.

From the values stated in Table 5.1, it is possible to conclude that additional alumina polishing allowed general improvement of R_{ct} regardless the hardness of pencil mines. Assuming that careful polishing confers similar active surface smoothness, the obtained values of *n* inferior to one corroborate the heterogeneous composition of PGE. In this circumstances the decreasing R_{ct} values from 4H to 4B reflect the progressive lower ratio clay/carbon. Also an increasing deviation regarding Warburg impedance was observed in the same sequence due to non-uniform adsorption processes (252). Polishing procedures with alumina have been stated to improve the kinetics of the electrode in $Fe(CN)_6^{3-/4-}$ (48) by increasing oxygen functionalities at the surface and thus its reactiveness to certain species (253). Others authors have also confirmed an improvement in the electron transfer upon pre-treatment of the PGE surface when compared to bare PGE (90, 254-256),

although in these cases the pre-treatment consisted in a electrochemical procedure at fixed potentials.

Table 5.1 - Equivalent circuit component values for the different PGEs and surface pre-treatment

PGE type	R_{sol} (Ω)	R_{ct} (Ω)	CPE	
			n	Q (Ω^{-1} s^n)
4H (pre-treated with alumina)	180	600	0.76	$4.8x10^{-6}$
HB (pre-treated with alumina)	170	400	0.76	$8.0x10^{-6}$
4B (pre-treated with alumina)	170	300	0.74	$4.8x10^{-6}$
HB (without alumina pre-treatment)	100	4000	0.80	$9.5x10^{-7}$

Nanostructuration of electrodes with carbon-based materials provides higher surface area and enhanced electronic properties. Three different types of sp^2 carbon, commonly used in electrodes modification, were tested and compared by CV using the probe $Fe(CN)_6^{3-/4-}$. The electrode modification was performed both in PGEs with and without alumina pre-treatment. In the first case it was noticed that the layer of carbon material easily detached from the electrode surface after immersion in water resulting in decreased electrochemical due to the increased hydrophilicity of the modified surface. On contrary, the deposited layers of modifying carbon material remained adsorbed in the absence of any previous treatment of the electrode.

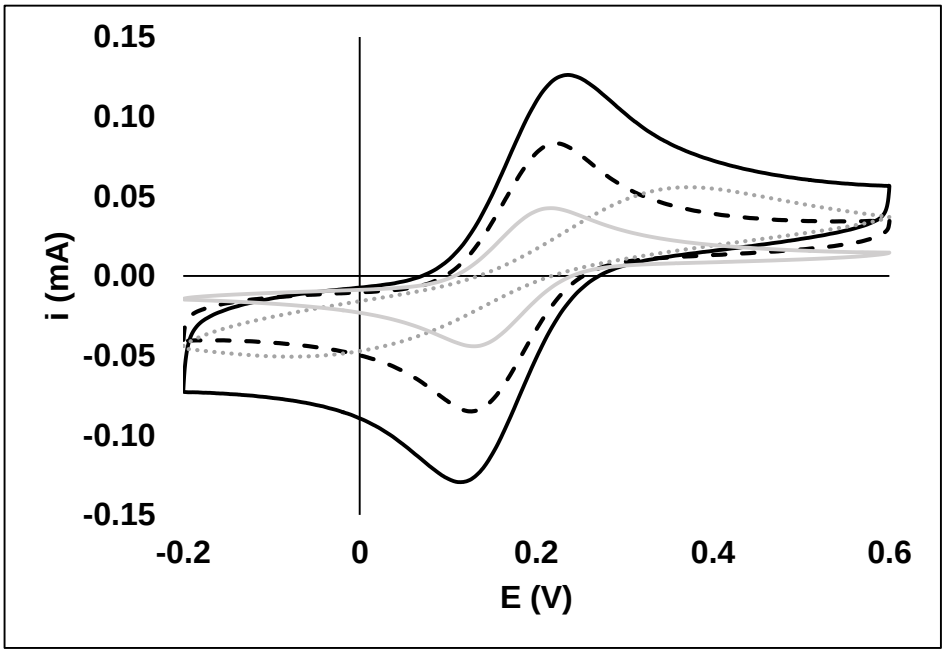

Figure 5.2 - Cyclic voltammograms of PGEs modified with carbon based nanomaterials, namely PGE-rGO (full black line), PGE-MWCNT (dashed line), PGE-CB (dotted line) and bare PGE (full grey line). Conditions: scan rate 50 mV s^{-1}, electrolyte: 5 mM $Fe(CN)_6^{3-/4-}$ with 0.1 M KCl, purged 15 min with N_2.

The results depicted in Figure 5.2 clearly shows that PGE modified with reduced graphene (PGE-rGO) gave higher voltammetric peaks (i_{pa} = 0.115 mA; i_{pc} = -0.122 mA) compared with the other modified PGEs despite the larger background current attributed to the capacitive nature of graphene as previously demonstrated by the obtained specific capacitance of 195 F g^{-1} (114). A good performance was also obtained with the PGE modified with MWCNT (i_{pa} = 0.087 mA; i_{pc} = -0.090 mA) compared with bare PGE and Vulcan carbon black modified PGE (PGE-CB). In fact, the modification with carbon black (PGE-CB) was not efficient, resulting in lower voltammetric peaks (i_{pa} = 0.036 mA; i_{pc} = -0.035 mA) and in higher ΔE_p (0.44 V) as observed in Figure 5.2.

5.3.2 – Bilirubin oxidase immobilized on a PGE and its characterization as an oxygen biosensor

A PGE type HB, without being mechanically pre-treated with alumina was selected for biosensor/biocathode studies. In a First stage a CV analysis was done to assess the proper immobilization of BOx to the PGE surface. Then, the immobilization procedure was optimized accordingly with the sensitivity achieved to oxygen by the biosensor using amperometry. In Figure 5.3 it is observed the catalytic response of the biosensor PGE-MWCNT-BOx to the presence oxygen in the solution, compared to the response in the absence of oxygen (solution purged with N_2). The displacement of the voltammetric curve towards more negative values of current confirms the electroreduction of oxygen by the enzyme through DET mechanism since no redox mediators were used either in solution or immobilized. The onset for oxygen reduction starts at about 0.45 V and the catalytic reduction reaches a maximum current density of -0.83 mA cm^{-2} at 0 V. The biocatalytic behaviour is similar to other BOx based biosensors that employed PBSE as tethering agent (250, 257-259). For instance maximum current achieved was 2.5 times higher when compared to a similar biosensor using the same CV conditions (10 mV s^{-1}) despite a different transducer (Toray carbon paper) and electrolyte pH (5.8) (250). When studying DET of BOx from *Myrothecium verrucaria* adsorbed on GCE and edge-plane pyrolytic graphite (EPPG) electrodes, Li and collaborators (260) identified the enzyme orientation over the electrodes surface according to the difference of redox potential between the catalytic T1 centre (E^0 T1 = 0.70 V vs. NHE) and the complex T2/T3 redox centre (E^0 T2/T3 = 0.49 V vs. NHE). As can be seen in Figure 5.3 for the voltammogram obtained in absence of oxygen, only two small peaks were observed at 0.50 V and 0.38 V ($E_{1/2}$= 0.46 V), which can be ascribed to the catalytic T1 centre for the assayed pH conditions, and indicative of preferential enzyme orientation over the modified electrode surface.

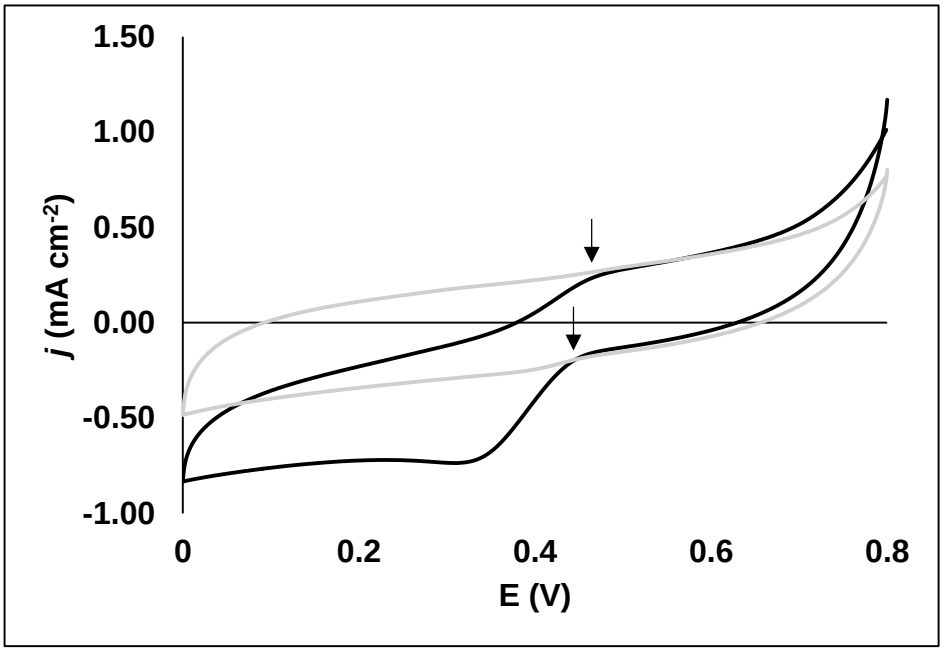

Figure 5.3 - Cyclic voltammograms of a PGE immobilized with BOx (PGE-MWCNT-BOx) in the presence (black line) and absence (grey line) of oxygen. Conditions: scan rate 10 mV s^{-1}. Electrolyte: 10 mL of 0.1 M phosphate buffer pH 7.0.

The optimization of the immobilization procedure was performed through amperometric measurements, more specifically, the importance of reduced graphene and MWCNT in the sensitivity of BOx to oxygen was determined. Thus, different compositions in the biosensor construction were taken in consideration and then compared: PGE-rGO-MWCNT-BOx; PGE-MWCNT-BOx; PGE-rGO-BOx and PGE-BOx. Figure 5.4a shows the amperometric determination of O_2 for biosensor PGE-rGO-MWCNT-BOx at an applied potential of +0.15 V. Constant additions of oxygen saturated solution causes the decrease of current values due to the reduction of oxygen by the enzyme. An unstable response of the biosensor is observed at higher oxygen concentrations (corresponding to about -5 µA) when reaching the saturation threshold of BOx. Calibration curves for the various biosensor configurations were presented in Figure 5.4b and the performance of each one was displayed in Table 5.2.

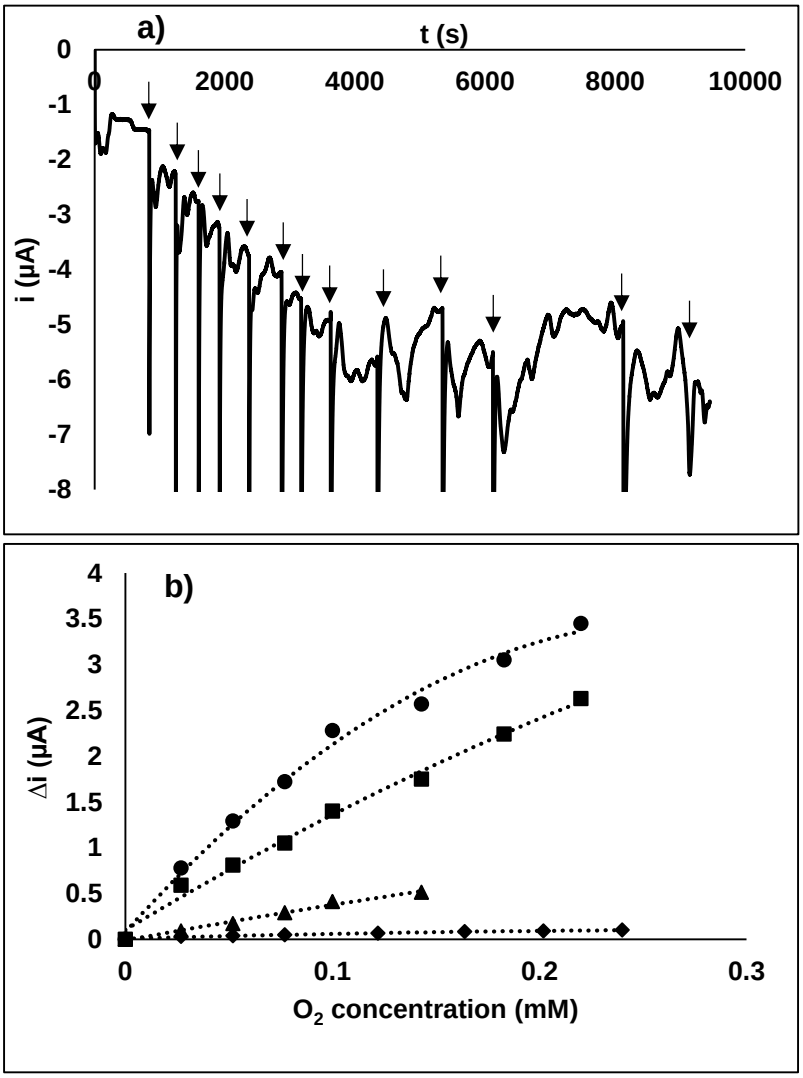

Figure 5.4 - Amperometric determination of oxygen. a) Amperometric response to successive injections of oxygen saturated solution for PGE-rGO-MWCNT-BOx. Arrows indicate the moment of injection. b) Oxygen calibration curves for PGE-rGO-MWCNT-BOx (circles), PGE-MWCNT-BOx (squares), PGE-BOx (triangles) and PGE-rGO-BOx (diamonds). Conditions: Applied potential +0.15 V; electrolyte: 10 mL of 0.1 M phosphate buffer pH 7.0, purged with N_2 15 min. Additions of oxygen saturated electrolyte solution.

The biosensor composed by reduced graphene and MWCNT (PGE-rGO-MWCNT-BOx) achieved the highest sensitivity to oxygen with a value of 648 µA mM^{-1} cm^{-2}, however at a lower linear range (0.10 mM). The limit of detection (LOD) obtained was 2.7 µM and only matched by the LOD of the biosensor PGE-MWCNT-BOx. It seems that the PBSE is a good tethering agent for the carboxylic acid functionalized MWCNT and fairly for graphite given the sensitivities obtained for the biosensors PGE-MWCNT-BOx (332 µA mM^{-1} cm^{-2}) and PGE-BOx (112 µA mM^{-1} cm^{-2}), respectively. However, when linking BOx to rGO via PBSE the biosensor loses its performance (11 µA mM^{-1} cm^{-2}) explained by the reduction process of graphene oxide which eliminates part of the oxygen functionalities of graphene. Thus, rGO was used for electrode modification in order to enhance the electrochemical signal of the biosensor, despite the more fastidious procedure for the biosensor preparation.

Table 5.2 - Optimization of the BOx biosensor. Performance for different biosensor configurations

Biosensor configuration	Linear range (mM)	LOD (µM)	Sensitivity (µA mM^{-1} cm^{-2})
PGE-rGO-MWCNT-BOx	0.10	2.7	648
PGE-MWCNT-BOx	0.31	1.6	332
PGE-BOx	0.15	4.0	112
PGE-rGO-BOx	0.27	71.0	11

The achieved sensitivity of both prepared biosensors (PGE-rGO-MWCNT-BOx and PGE-MWCNT-BOx) was higher when compared with other oxygen biosensors in the literature (132, 236-238, 261). Mousty el al. (236) also obtained high sensitivity value of 470 µA mM^{-1} cm^{-2} although recurring to ABTS and under rotation conditions.

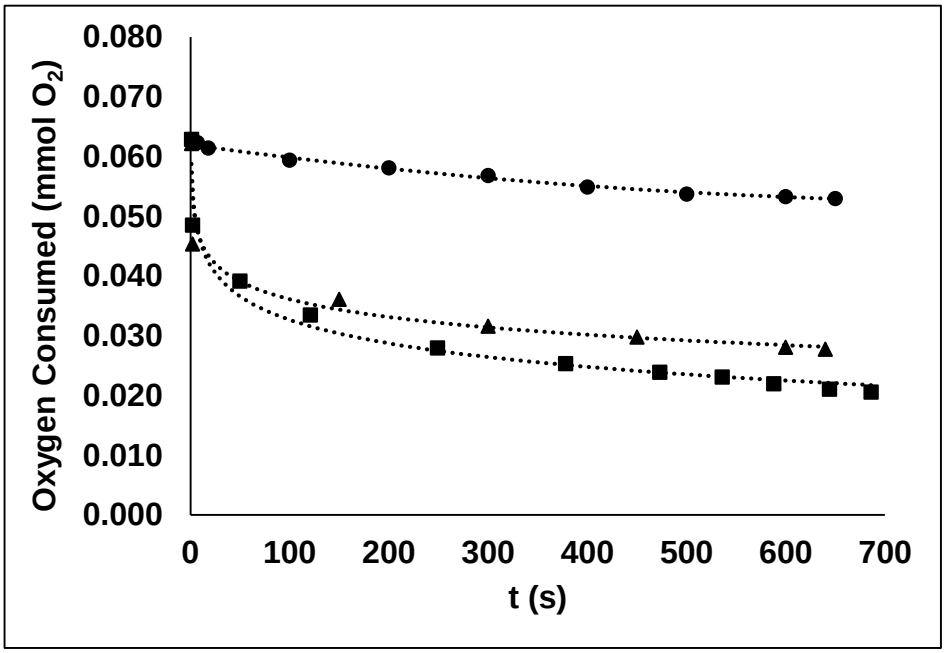

Figure 5.5 - Amperometric oxygen monitoring in yeast fermentation process with biosensor PGE-rGO-MWCNT-BOx in the presence of oxygen and glucose containing 0 mg mL^{-1} (circles), 0.1 mg mL^{-1} (triangles) and 1 mg mL^{-1} (squares) of yeast saccharomyces cerevisiae. Conditions: applied potential + 0.15 V; electrolyte: 10 mL of 0.1 M phosphate buffer pH 7.0 with 100 mM glucose and saturated with O_2.

In the aerobic fermentation process of yeasts, the monitoring of oxygen is important in order to achieve higher productivities since oxygen often governs the metabolic pathways in microbial cells (262). For instance, in breweries the fermentation process of yeast initially requires oxygen to allow cell proliferation and ensure optimal yeast activity. Therefore, the biosensor (PGE-rGO-MWCNT-BOx) was applied in the monitoring the oxygen consumption in the fermentation process of *saccharomyces cerevisiae*. The amperometric response was registered in an oxygen saturated solution containing glucose and different amounts of

yeast (Figure 5.5). A clear tendency on oxygen consumption was observed when increasing the concentration of yeast in solution. At yeast concentration of 10 mg mL^{-1} the response of the biosensor was null due to oxygen depletion at the electrode surface. The biosensor response to oxygen follows a similar tendency of previous reported studies on dissolved oxygen uptake by bacterias (263, 264).

5.3.3 – Characterization of BOx bioelectrode as a biocathode

The establishment of DET between PGE and BOx makes possible the application of the bioelectrode as biocathode in membraneless miniaturized biofuel cells. Therefore the bioelectrode with the highest sensitivity for oxygen (PGE-rGO-MWCNT-BOx) was selected for biocathode experiments. Polarization curves presented in Figure 5.6 were determined from LSV measurements at 1 mV s^{-1}. In an oxygen saturated solution the E_{OCP} of the biocathode corresponded to 0.48 V. A maximum current density of about 500 µA cm^{-2} was achieved at 0.10 V. A control experiment was also performed by using a cathode without enzyme (PGE-rGO-MWCNT) which resulted in negligible catalytic activity towards oxygen (E_{OCP} = 0.08 V; j_{max} = 2.4 µA cm^{-2}).

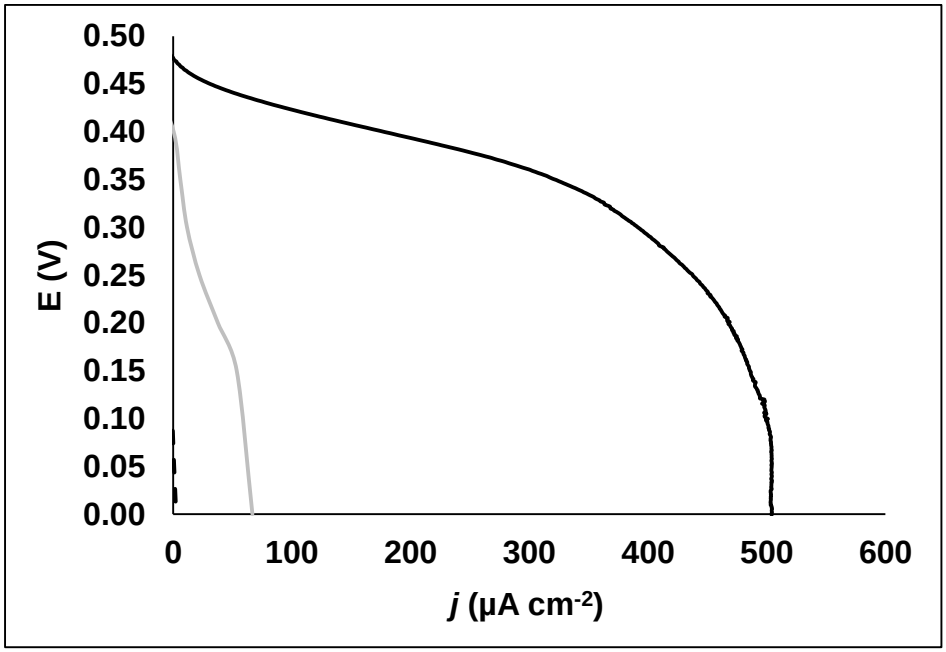

Figure 5.6 - Polarization curves obtained from LSV measurements for biosensor PGE-rGO-MWCNT-BOx in the presence (full black line) and absence (full grey line) of oxygen in solution. Control experiment for cathode PGE-rGO-MWCNT in the presence of oxygen (dashed black line). Conditions: 10 mL of 0.1 M phosphate buffer pH 7.0.

The only PGE-based biocathode found in the literature was developed by Kashyap et al. (113). The biocathode, which employed the mediator ABTS to facilitate the electron transfer

between laccase and the polyaniline-MWCNT modified PGE, achieved a E_{OCP} of 0.58 V and a maximum current density of 296 µA cm^{-2}. Other BOx biocathodes using PBSE as tethering agent have also been studied however using different transducers (250, 257, 258). In the approach from Strack et al. (257), the MWCNT buckypaper biocathode generated an E_{OCP} of 0.48 V and produced about 200 µA cm^{-2} of maximum current density. In turn, Lopez et al. (258) immobilized the enzyme substrate, bilirubin or its artificial analogues, in a MWCNT/nafion modified GCE as a BOx orientating strategy. For either bilirubin or the analogues the E_{OCP} was around 0.5 V however maximum current density corresponded to about 300 µA cm^{-2} in the first case and about 750 µA cm^{-2} for the analogue 2,5-dimethyl-1-phenyl-1H-pyrrole-3-carbaldehyde.

5.4 - Conclusions

In the present work we have prepared a simple and viable O_2 biosensor and biocathode. The availability and easy fabrication of the PGE conjugated with the simplicity of the enzyme immobilization procedure allows its use in practical and disposable applications. The immobilized BOx biosensor presented high sensitivity towards oxygen with a low LOD. A previous PGE modification with reduced graphene increases the sensitivity but also increases the instability of the response near enzyme saturation point and doubles the biosensor preparation time. Therefore, one must choose between fastness or signal enhancement when preparing the bioelectrode. A simple application of the biosensor was demonstrated in the monitoring of oxygen consumption by *Saccharomyces cerevisiae* in this yeast fermentation process. The successful electronic coupling between enzyme and electrode made possible the establishment of DET and therefore suitable for usage as a biocathode in membraneless biofuel cells. Though with significantly lower current densities when compared with cathodes of conventional fuel cells, the design of 3D enzymatic layers or the stacking of cells can be foreseen.

Chapter 6

Characterization of a glucose biosensor with immobilized glucose oxidase for implementation as a bioanode

6.1 - Introduction

The use of pencil graphite electrodes (PGE) as transducer materials have been extensively exploited in (bio)sensor analysis (245, 248). This type of carbon electrode represents a good alternative to others commonly referred in electrochemistry studies. The fact they are commercially available in different gauges and hardness at negligible cost makes them readily viable for disposable applications, advantageously replacing precious metal catalysts such as gold and platinum (43, 45). Several researchers have shown their competitive stability, reproducibility and kinetics (potential peak separation, ΔE_p) regarding the glassy carbon (GCE), pyrolytic graphite and carbon fiber (69, 70, 76). While the irreproducible behavior of GCE can be minimized through extensive surface pre-treatment, simple transversal cut exposes uncontaminated pristine surfaces in PGEs (48). On contrary, PGEs originate higher background currents attributed to the porous, low ordered graphitic structures dispersed between clay regions (48, 94). Such heterogeneous surfaces determine alike microelectrode array responses, hence with corresponding better signal-to-noise ratios as evidenced by the adsorptive stripping analysis of nucleic acids (82, 93, 265). In the last case, the higher relative porosity also improved orientation and coverage by the biopolymer, thus leading to enhanced redox activity.

Different methods regarding the specific immobilization of GOx onto the surface of PGEs were proposed. The first biosensor was introduced in 1990 by the group of Pishko (99) where at its active surface, a readily adsorbed poly-cationic redox polymer provided direct electron transfer from GOx catalytic center. In works that followed, the enzyme was chemically immobilized by double cross-linking with glutaraldehyde (GA) and polyvinyl alcohol containing stilbazolium groups (PVA-SbQ) (100) or simply using GA in a Prussian-Blue modified PGE (101). Bridging between enzyme and gold nanoparticles embedding a

carbon paste cover was established using L-cysteine (95, 96). Graphene, solely (68), as composite with zinc and copper oxides (97), or onto electrochemical precipitated ZnS-CdS (98) were also applied to PGE. In a three step approach, the chemical attachment of FAD cofactor to a conductive polymer modified with ferrocene electron shuttle followed by reconstitution with the stripped GOx apoenzyme was performed (102). Important factors required for commercial establishment of biosensors is their stability and shelf-life period. In most of the glucose PGE biosensors discussed above, it is noticed limitations concerning to stability with decreasing performance when operated or stored for extended periods. A second issue regards the short linear ranges which may limit the biosensor applications outside the clinical scope (e.g. environmental analysis or industrial analysis). In this field, biosensors can be used as an effective analytical tool for heavy metals screening since heavy metals are known inhibitors of enzyme activity (266-268). The monitoring of cadmium plays an environmentally important role and can be seen as preventive measure for human and animal exposure. Cadmium is a toxic metal to higher biological systems and leakage from anthropogenic activities jeopardizes the environment. A series of experimental data on animals and cohorts studies on humans revealed positive associations between cadmium exposure and the development of cancer, especially lung cancer (269, 270). These evidences lead the US Environmental Protection Agency (US EPA) to classify cadmium as probable human carcinogen (B1) (269), while the International Agency on Research on Cancer from the World Health Organization (WHO) are more decisive and places it as carcinogenic agent to humans (group 1) (270). In turn, the problematic of diabetes leads to a continuous development of sensors and biosensors to improve diagnostics and prevention of the disease. Accordingly to a report released in 2016 by the World Health Organization (WHO), estimations pointed that more than 400 million adults (8.5%) lived with diabetes in 2014 which represent an increase of almost 300% since 1980 (271). This is a public health problem with adverse complications varying inversely with measurements frequency and shows growing prevalence in undeveloped countries.

In this work we envisage the fabrication of a PGE biosensor with extended linear range and improved stability by using the enzyme precipitate coatings (EPC) immobilization method (272). The GOx immobilization was performed through the crosslinking of enzyme precipitates onto multi-walled carbon nanotubes (MWCNT) and further deposition on a graphene modified PGE. A microfluidic configuration was also implemented to assess the analytical performance of glucose determination and the inhibitory effect of cadmium. This configuration allows the improvement of analytical signals, and the reduction of sample volume. Moreover, with this set-up it is possible the enlargement of the analytical range, usually required in environmental analysis.

6.2 – Experimental section

6.2.1 – Materials and reagents

All aqueous solutions were prepared with Milli-Q doubly deionized water (conductivity <0.1 μS cm^{-1}). Analytical grade chemicals were used throughout without further purification. Glucose oxidase from *Aspergillus niger*, type VII (≥ 100000 U g^{-1}) was acquired from Sigma-Aldrich and *p*-benzoquinone was acquired from Fluka.

Ammonium sulfate, cadmium chloride, N-(3-dimethylaminopropyl)-N-ethylcarbodiimide hydrochloride (EDC), glutaraldehyde, GA (25% in water), graphene oxide (4 mg mL^{-1} dispersion in water), hydrochloric acid, 2-morpholinoethanesulfonic acid (MES) hydrate, MES sodium salt, MWCNT (carboxylic acid functionalized), nafion (5% wt), N-hydroxysuccinimide (NHS), potassium phosphate dibasic, potassium phosphate monobasic, Trizma base, were also obtained from Sigma-Aldrich and D(+)-glucose monohydrate was obtained from VWR Prolabo.

Potassium phosphate buffer 0.1 M pH 7.0 was used as electrolyte solution. MES buffer solution 0.1 M pH 6.5 was used as electrolyte solution in cadmium determinations and for enzyme dissolution. The glucose solution was prepared near physiological conditions (pH 7.0) and 24 hours before analysis to allow the isomerization of the glucose molecule (121). Solutions were purged with N_2 for at least 15 min in all experiments.

6.2.2 - Apparatus

All electrochemical experiments were performed with a potentiostat Metrohm, model Autolab PGSTAT10, controlled by GPES v3.9 software (Herisau, Switzerland). Electrochemical experiments were performed in a three-electrode cell composed of an Ag/AgCl (KCl, 3 M) mini reference electrode from the same brand Ref. 6.0727.000, the implemented bioelectrode and a platinum rod as counter electrode. Amperometric measurements conducted in the microfluidic platform resorted to a reference electrode leak-free LF-1 (Innovative Instruments, Tampa) instead.

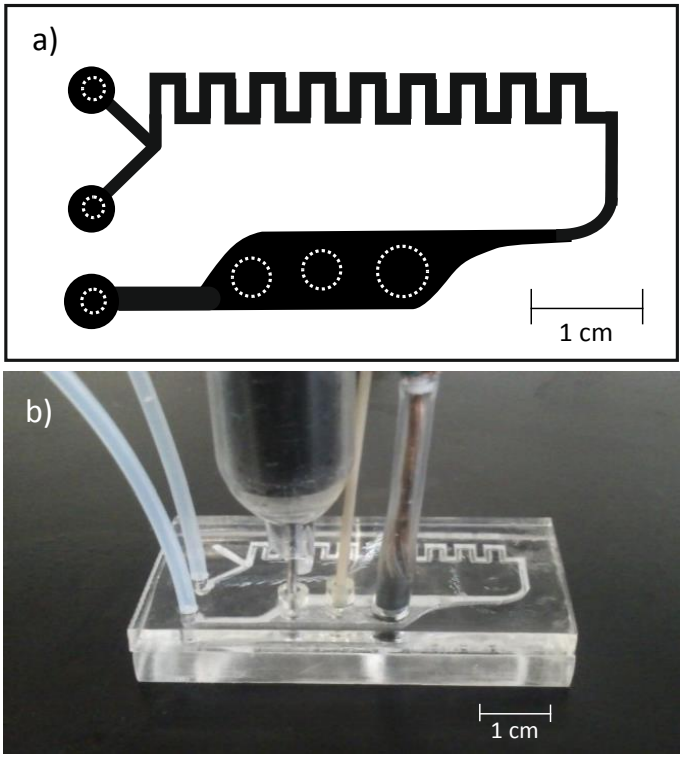

Figure 6.1 - Microfluidic platform. a) Schematics of the platform with channels and detector chamber in black. Insertion holes for tubes and electrodes made in the cover lid in white dashed line; b) Platform with the three-electrode configuration: platinum auxiliary electrode, reference electrode and biosensor.

The microfluidic platform was implemented from 4 mm thick methyl methacrylate cross polymer sheet (PMMA) using a 2D-laser cutting-engraving machine (Universal Laser Systems Inc., Scottsdale). The microfluidic patterning was designed with the scheme depicted in Figure 6.1a using the open source vector graphics software, Inkscape. Two rectangular PMMA pieces were cut (dimensions 0.4 x 3.2 x 6.0 cm) and the microfluidic channels were engraved (width x depth 1.2 x 1.0 mm) in one of the PMMA pieces and the insertion holes for electrodes and inlet/outlet tubes were drilled in the complementary juxtaposed PMMA piece. The sealing of the channels was performed tightening the two pieces with a bench press vise and applying heat (90 ºC) for 90 minutes (273). The final three-electrode configuration of the microfluidic system is depicted in Figure 6.1b.

6.2.3 – Electrode preparation and GOx immobilization procedure

A pencil lead HB 2 mm (Mitsubishi, Japan) was put in contact with the inner copper wire of a coaxial shielded cable and isolated with a flexible polymer sleeve (Tygon). A transversal cut exposed then a pristine PGE surface which was polished mechanically using sandpaper (P1200) and washed with distilled water. The active surface area of the PGE was determined by chronoamperometry (114) and corresponded to about 0.034 cm^2. This surface was modified with 10 µL of graphene oxide (1 mg mL^{-1}) and afterward

electrochemically reduced in 0.1 M Na_2SO_4 solution at 50 mV s^{-1} along 100 scans performed within -1.2 V and 0.8 V (*vs*. Ag/AgCl).

The immobilization of GOx was based on the procedure of Kim et al. (272). First, 20 mg of MWCNT were weighted and suspended in 10 mL of water for 30 minutes at room temperature in an ultrasonic bath. The activation of the nanotubes was performed under stirring for 1h with sequential adding of 4 mL of 0.5 M MES buffer pH 6.5, 4 mL of 0.434 M NHS and 2 mL of 0.053 M EDC. This solution was filtered under vacuum (nylon, 0.22 µm) and the activated nanotubes washed with 0.1 M MES buffer before being re-suspended in water at a concentration of 1 mg mL^{-1}. A 2 mL volume of this suspension was added to 1 mL of GOx solution (about 8 mg to 1 mL of 0.1 M MES buffer pH 6.5), mixed for 1h and left overnight at 4 ºC.

Approximately 1 mL of ammonium sulfate (0.55 g mL^{-1}) was poured over the MWCNT-GOx suspension to promote enzyme precipitation around the nanotubes and stirred for 30 minutes before 80 µL of GA cross-linker were added. The resulting mixture was stirred for further 30 minutes. The precipitate was vacuum-filtered, washed with 0.1 M Tris-HCL buffer pH 7.4, followed by 0.1 M phosphate buffer pH 7.0, and re-suspended in 0.5% w/w nafion solution of the last buffer to a final concentration of 2 mg mL^{-1}. The final step consisted on PGE surface modification through spreading of a 10 µL aliquot of this last suspension then left to dry at room temperature for a minimum of 2 hours. The biosensor is designated as PGE-graphene-MWCNT/GOx/nafion. For performance assessment purposes similarly sensors without GOx and biosensor without graphene were fabricated and henceforth designated as PGE-graphene-MWCNT/nafion and PGE-MWCNT/GOx/nafion, respectively.

6.3 – Results and discussion

6.3.1 – Biosensor preparation and characterization

When the use of PGE in a particular application is equated an important factor influencing the electrochemical response relates to the pencil mine hardness, for the ratio between graphite and clay (76, 77). This work has also departed from previous comparative voltammetric analysis on 3 pencil mines with different hardness (4H, 4B and HB) using the redox probe $Fe(CN)_6^{3-/4-}$ to find out that PGE 4B presented higher redox peaks while the HB showed better signal-to-noise ratio and stability as recently reported (248). Henceforth, a type HB PGE was selected as transducer. The PGE surface was modified with reduced

graphene since we have evidenced that graphene greatly enhances the current signals though increasing also the capacitance of the electrode (114). The procedure implemented for biosensor preparation, known as enzyme precipitate coatings (272) or cross-linked enzyme clusters (274) comprises the covalent attachment of glucose oxidase enzyme onto MWCNT, its precipitation and further cross-linking of protein cluster to achieve optimal enzyme loading and stability. The coupling of nanomaterials to biomolecules can be accomplished using N-ethyl-N'-(3-dimethylaminopropyl) carbodiimide hydrochloride (EDC) and N-hydroxysuccinimide (NHS) (275). The carboxylated MWCNT react firstly with EDC and then with NHS to form an appending active ester. An amide bond is then established through nucleophilic substitution reaction of the ester by amine groups of enzyme (62). Carbon nanotubes provided support for the enzymes and enhanced conducting features regarding the process bioelectrochemistry. A precipitant (ammonium sulfate) is then added forming insoluble enzyme aggregates in the vicinity of nanotubes which is considered a crucial step to maintain maximal enzyme activity. In fact, the precipitant confers to this enzyme a conformation which is "frozen" by cross-linking with glutaraldehyde (276). Glutaraldehyde in acidic or neutral conditions, as in the case of the present work, is a monomer in either its free aldehyde form, hydrate or hemiacetal. These forms can react in different ways with the amino groups of proteins, leading to immobilization (277). Nafion was eventually used for suspension and entrapment of the enzyme precipitate coatings due to its ability to solubilize carbon nanotubes (278), biocompatibility and permeation to protons and neutral molecules such as glucose (272, 279). This immobilization approach yields a bioelectrode with improved enzyme loading, stability, selectivity with reduced leaching (62, 272). As examples, power densities in biofuel cells can be maximized with the nanostructuration of the bioelectrode and a higher stability leads to longer operation time (272, 274, 280). After drying at room temperature, the immobilization process rendered an opaque black film with about 1 μm thickness as demonstrated by SEM results in Figure 6.2a. The nafion matrix with entrapped MWCNTs ribbons and the MWCNTs matrix are shown in Figure 6.2b and 6.2c respectively, presenting similarities with the results obtained by Fischback et al. (280).

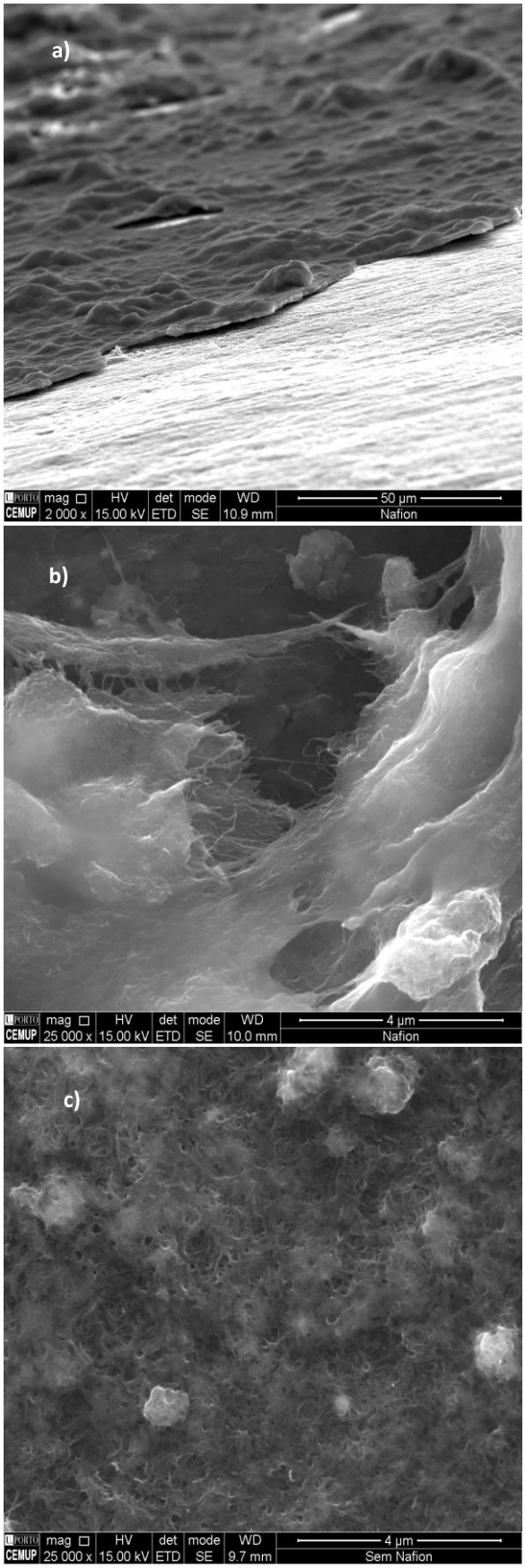

Figure 6.2 - Scanning electron microscope images of biosensor surface. a) Immobilization film over graphite surface. b) Magnified view of the biofilm showing the nafion matrix containing MWCNTs ribbons (MWCNT/GOx/nafion). c) Biofilm without nafion (MWCNT/GOx).

The fabrication cost of a single PGE is estimated to be less than 0.40 euros and further modification with graphene raises the price in about 5%. Considering a properly and efficient use of all compounds, the deposition of the enzyme precipitate coatings (involves the use of GOx, nafion, MWCNT and its respective activation compounds) represent an increment of 60%. This cost is in the same order of magnitude with the one presented by Cheng et al. (96). Taking into account the values indicated, it becomes feasible to use them as low cost replaceable (disposable) sensor.

6.3.2 – PGE performance and mediator kinetics without immobilized GOx

Prior to the characterization of the biosensor, the response to the benzoquinone mediator was performed using the PGE-graphene-MWCNT/nafion as working electrode. In the potential swept window of -0.30 to 0.60 V (*vs* Ag/AgCl), quasi-reversible voltammograms with half wave at $E_{½}$ = +0.131 V were obtained for scan rates up to 100 mV s^{-1}. The influence of pH in the interval of 5 to 8 was then assessed and showed the potential half waves shifting almost 0.122 V in cathodic direction, with both the anodic and cathodic waves slight increasing in intensity and approaching each other. The linear plot of $E_{½}$ vs. the pH of buffer solution showed a slope of about -60 mV/pH. The electrochemistry process of quinones in water is well known, corresponds to the transition of Q to QH_2 in a 2 e^- and 2 H^+ reaction and with a slope of about 59 mV/pH at more acidic conditions. In buffered solution the redox couple of BQ tends to lose its reversibility and the oxidation wave shifts towards more positive potentials indicating that it is thermodynamically favored (281). In fact, increasing the temperature a more pronounced effect is observable in the reduction peak compared to the oxidation one. The application of the Randles–Sevcik response model to the analysis of BQ voltammograms obtained at different scan rates enabled an experimental n= 2.2 electrons, in a diffusion controlled process, thus evidencing that the modified active surface of the electrode had no influence on the mediator electrochemistry.

6.3.3 – Determination of glucose

In order to assess the efficiency of enzyme immobilization and the catalytic response to glucose, a voltammetric analysis was performed (Figure 6.3). The experiments were conducted in the absence of O_2 in the electrolyte since O_2 competes with the mediator as electron acceptor from the reduced state of GOx, impairing the electron transfer to the electrode (282). The Figure shows that in the presence of glucose a voltammogram shift towards more positive values of current and potential are observable. When compared with

the electrode without GOx, the anodic peak shifts to a higher potential values in almost 0.07 V. These results confirm the biocatalytic response to glucose. The oxidation peak of the mediator is maximum at +0.19 V and therefore a potential of +0.25 V was selected for the amperometric measurements to ensure quantitative oxidation of glucose in the vicinity of the biosensor surface. The use of graphene as electron enhancer led to about 4 times higher anodic and cathodic peaks of the catalytic response to glucose when compared with the biosensor without graphene, PGE-MWCNT/GOx/nafion.

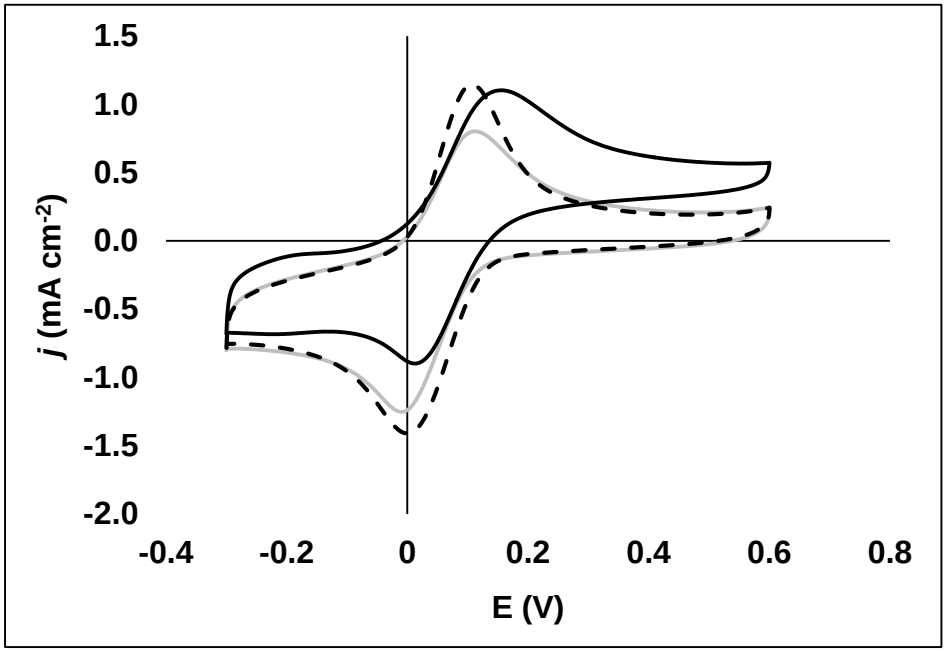

Figure 6.3 - Cyclic voltammograms of the biosensor PGE-graphene-MWCNT/GOx/nafion in the presence (full black line) and absence (full grey line) of glucose and for the electrode without GOx (PGE-graphene-MWCNT/nafion) in the presence of glucose (dashed black line). Working conditions: scan rate 10 mV s^{-1}; electrolyte: 10 mL of 0.1 M phosphate buffer pH 7.0 with 10 mM glucose and 2 mM benzoquinone in electrochemical cell.

The amperometric determination of glucose in solution was carried out after successive additions of known amounts of glucose to the electrochemical cell containing 10 mL of phosphate buffer in stationary state (Figure 6.4a). At high glucose concentration, above 80 mM, the current reaches a plateau, tending to a constant value accordingly to the Michaelis-Menten kinetic principle (non-linear least squares fitting values of V_{max} = 2.0(±0.1)x10^{-4} mmol min^{-1} cm^{-2} glucose, K_M = 42(±5) mM glucose). The biosensor presents a high limit of linearity (up to 39 mM) with an associated sensitivity of 17 µA mM^{-1} cm^{-2} (Figure 6.4b, inset 0.577/0.034 cm^2). Considering a lower linearity range (up to 17 mM), the sensitivity of the biosensor increases to 21 µA mM^{-1} cm^{-2} (Figure 6.4b, 0.727/0.034 cm^2). The limit of detection (LOD) obtained was 12.3 µM and was determined based on the standard deviation of the blank and the slope of the calibration curve. As a comparison, the sensitivity of the biosensor without graphene (PGE-MWCNT/GOx/nafion) was only 11.4 µA mM^{-1} cm^{-}

^{2} (0.387/0.034 cm^2) and for the electrode without GOx (PGE-graphene-MWCNT/nafion) the obtained sensitivity was about 0.2 μA mM^{-1} cm^{-2}.

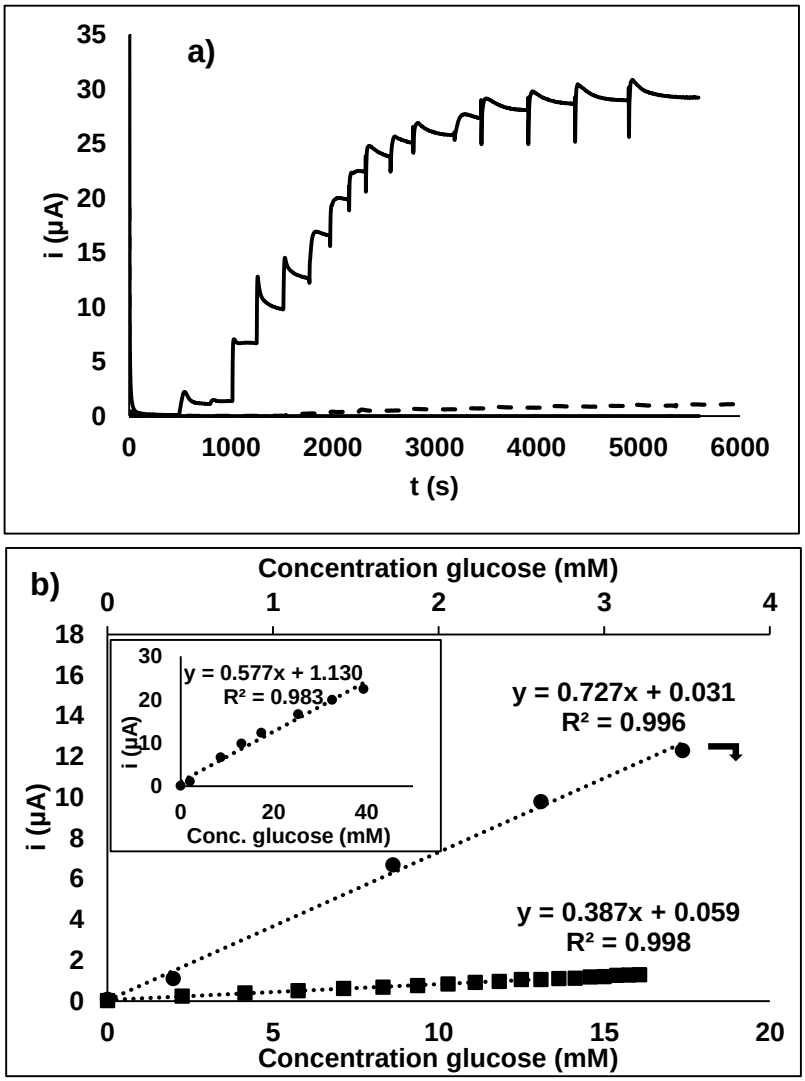

Figure 6.4 - Amperometric measurements of glucose. a) amperometric response to successive glucose injections for biosensor, PGE-graphene-MWCNT/GOx/nafion (full black line) and biosensor without graphene, PGE-MWCNT/GOx/ nafion (dashed black line). b) Glucose calibration curve for biosensor (circles) and biosensor without graphene (squares). Inset: calibration curve with wider linear range for biosensor. Working conditions: applied potential +0.25 V; electrolyte: 10 mL of 0.1 M phosphate buffer pH 7.0 and 2 mM benzoquinone in electrochemical cell. Additions of 100 mM glucose solution.

The amperometric determination of glucose was performed also in continuous flow regimen (Figure 6.5a) at +0.25 V, coupling the biosensor to a microfluidic platform in a three-electrode configuration system as depicted in Figure 6.1b. The system contains two inlets with respect to a blank buffer solution and to a buffer solution with increasing concentrations of glucose. The two streams are mixed in the channels, diluting the glucose concentration by half, before entering the detection chamber. The continuous solution movement at the electrode surface produced a similar effect of a rotating disk electrode by doubling the sensitivity of the method to about 35 μA mM^{-1} cm^{-2} (Figure 6.5b, 1.198/0.034 cm^2). This

arises from the superimposed convective transport of glucose to the sensor interface over the diffusion process due to concentration gradient. The reproducibility of the biosensor was tested for twelve consecutive injections of glucose solution (10 mM) using a three-way low pressure injection valve. A relative standard deviation of 5.4% was obtained. With each injection the current raised and returned to baseline value of the blank solution showing good reversibility.

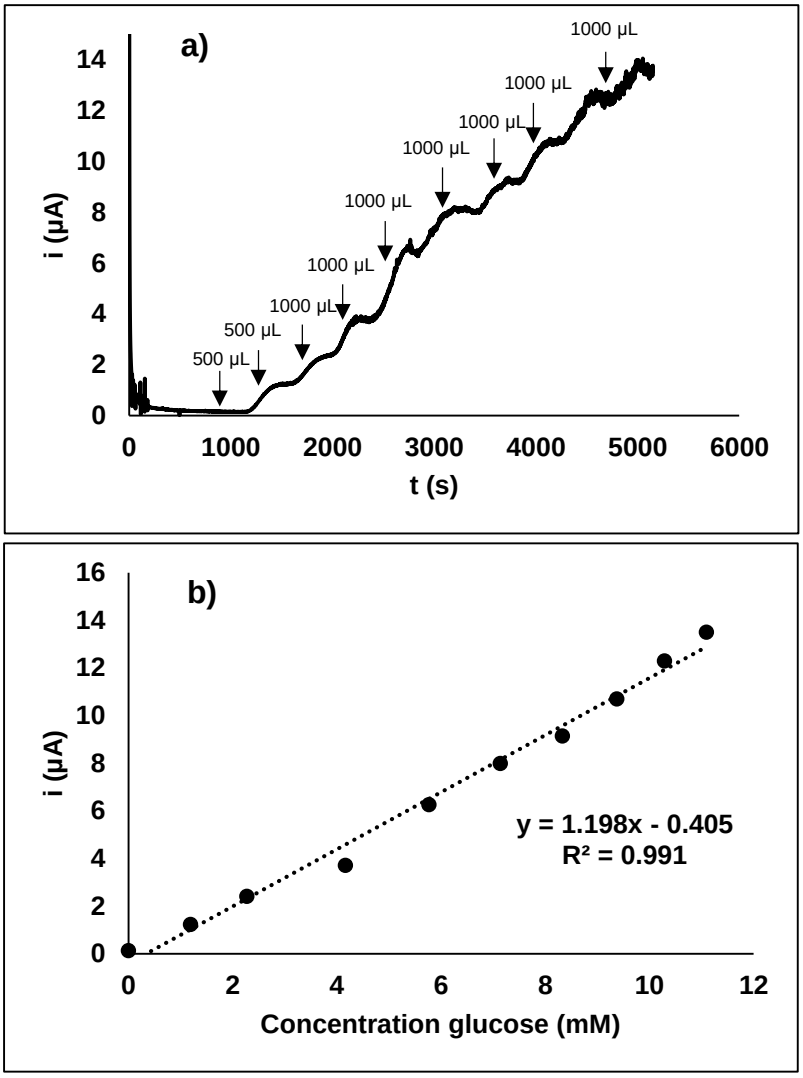

Figure 6.5 - Amperometric measurements of glucose with biosensor PGE-graphene-MWCNT/GOx/nafion in a microfluidic platform. a) Amperometric response to successive injections of glucose. b) Glucose calibration curve. Working conditions: applied potential +0.25 V; electrolyte 1: 0.1 M phosphate buffer pH 7.0 and 2 mM benzoquinone; electrolyte 2: 0.1 M phosphate buffer pH 7.0 and 2 mM benzoquinone with glucose. Flow rate: 0.15 mL min^{-1}.

For comparison purposes, Table 1.2 presents data from literature regarding analytical performance towards glucose detection of biosensors based on GOx immobilized in a PGE. Overall, Table 1.2 shows that the proposed biosensor performs better than most of the reported before. In terms of sensitivity only underperforms when compared with the

biosensor proposed by Cheng et al. (95, 96) and also by Sehat et al. (68). However, this last presented a much more limited linear range (up to 0.6 mM). In fact, the linearity range achieved with our biosensor (up to 39 mM) was only matched by the biosensor from Cheng et al. (96). Regarding LOD, the obtained value (12.3 µM) is similar with the values obtained from the works of Cheng et al. (95, 96) but about 4 to 6 times higher when compared to the works reported by Dervisevic et al. (102), Elahi et al. (97) and Saglam et al. (98) or 20 times higher relatively to the biosensor of Sehat et al. (68).

6.3.4 – Determination of cadmium

The activity of GOx can be inhibited by cadmium in the µM range and in less extent by lead, zinc, copper, mercury and silver (121, 269). Thus, GOx inhibition is at least indicative of possible sample contamination by heavy metals. The high sensitivity achieved with the biosensor enlarged its usefulness to the indirect determination of cadmium, based on the inhibitory effect over glucose oxidase which becomes apparent by decreasing the signal response of the glucose substrate. For the analysis, the same microfluidic system (Figure 6.1) and the same conditions (+0.25 V) were used as in the determination of glucose. The carrier solution consisted in MES buffer at pH 6.5 instead phosphate buffer to avoid complexation and precipitation of cadmium with phosphate ions. Also, both the carrier electrolyte and the stock solution of cadmium (2.5 mM) contained 5 mM of glucose to avoid the decreasing of the signal due to glucose dilution effects. In the beginning of the amperometric analysis, the glucose present in the background electrolyte produced a current of about 5 µA and upon stabilization, cadmium injections were performed leading to a decrease in the catalytic current (Figure 6.6a). The interaction between heavy metal and GOx reaches a steady-state after about 300 s. From the calibration curve presented in Figure 6.6b, the cadmium sensitivity obtained corresponds to 1.04 µA mM^{-1} (30.6 µA mM^{-1} cm^{-2}) which is comparable with the values of 1.1 µA mM^{-1} from Guascito et al. (283) and 1.1 µA mM^{-1} and 5.3 µA mM^{-1} (calculated from electrode dimensions indicated by the authors) from Ghica et al. (284). On the contrary, Chen et al. (285) found no interference of cadmium up to 100 µM in the activity of the enzyme.

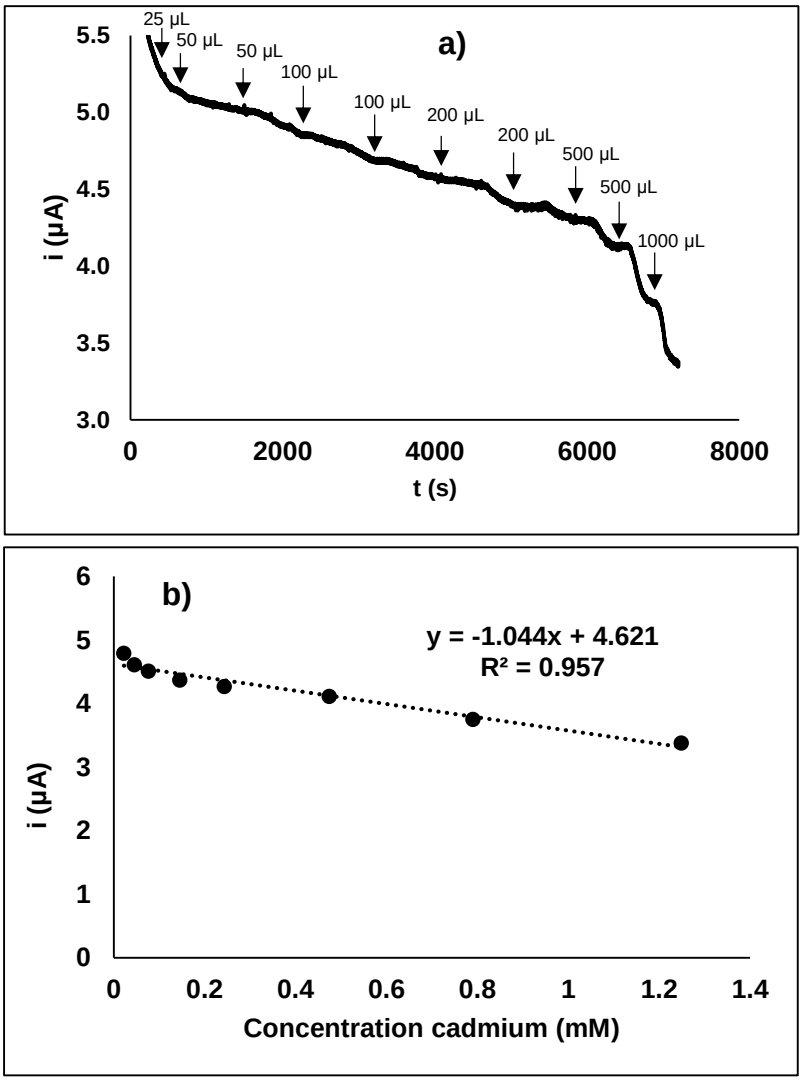

Figure 6.6 - Amperometric measurements of cadmium with biosensor PGE-graphene-MWCNT/GOx/nafion in a microfluidic platform. a) Amperometric response to successive injections of cadmium. b) Cadmium calibration curve. Working conditions: applied potential +0.25 V; electrolyte 1: 0.1 M MES buffer pH 6.5, 2 mM benzoquinone and 5 mM glucose; electrolyte 2: 0.1 M MES buffer pH 6.5, 2 mM benzoquinone, 5 mM glucose with $CdCl_2$. Flow rate: 0.15 mL min^{-1}.

6.3.5 – Stability studies

The immobilization solution composed by the EPC and nafion (MWCNT/GOx/nafion) was stored at 4 ºC after preparation and was continuously used for biosensor preparation during 6 months. This confirms the high stability and activity conservation of GOx with this procedure. Also, the storage stability of prepared biosensors was assessed. The sensitivity performance to glucose was maintained for at least 15 days for biosensors stored in buffer and in dried state at room temperature.

6.4 - Conclusions

The use of a PGE as transducer in electrochemical analysis are a viable alternative to other commonly used and expensive electrodes owing to the comparable performance, negligible cost and simple pre-treatment procedures. The PGE was first modified with electrochemically reduced graphene in order to improve the analytical signals obtained. Further GOx immobilization was achieved through cross-linking enzyme precipitates to MWCNT followed by deposition into PGE, yielding therefore a high enzyme loading, activity and improved stability. The proposed biosensor coupled to a microfluidic platform achieved a high sensitivity and wide linear range concerning glucose detection with a potential use in industrial applications where the glucose levels are generally higher in comparison with the clinical field. Also the reduced sample volume required for each analysis meets with the principles of the sustainable chemistry.

The determination of cadmium through an inhibitory process of GOx also proved the suitability of the biosensor in the quantification of pollutants in environmental samples.

Chapter 7

Integration of miniaturized BOx and GOx bioelectrodes as biofuel cell in a finger pressure-driven microfluidic platform

---

7.1 - Introduction

Microfluidics bring major benefits to microanalysis and in-situ measurements where the analytical system requires to be flexible, portable and with reduced dimensions. This allow prompt results and the replacement of bulky laboratorial instrumentation. Nevertheless, the performance of certain unit operations depends on controllable fluid transport and stable laminar flow profile. Bulky and external energy-consuming apparatus such as peristaltic pumps represent a major drawback and condemn lab-on-a-chip devices to be more like a chip-on-a-lab approach instead. The use of capillary forces as liquid-driving principle in microfluidics may achieve remarkable successful market implementation in point-of-care (POCT) devices. However, these type of devices perform a limited number of unit operations and difficulties arise when precise liquid handling is needed. Human powered fluid driving is a good alternative to energy-consuming pumps allowing portability and controllable transport at negligible cost. Handheld syringes can be used for the purpose (286) but finger-powered microfluidics stands as simpler evolution avoiding the use of additional apparatus by integrating one or more deformable PDMS chambers in the chip. The finger-powered fluid transport have been successfully demonstrated in some works (163, 164, 287-289). An initial proof-of-concept was developed where the pump consisted of a PDMS deformable chamber activated by a human finger for liquid movement into a chip with inclusion of valves (163). Finger-pressing of the PDMS reservoir containing air created the liquid movement. When the reservoir was relieved, the negative pressure lead to back flow, thus being important the inclusion of check or one-way valves in the chip. A simple construction of one-way valve consists of a cross-section membrane placed between two channels of different gauge so that the membrane completely seals the narrower

channel when the liquid flow is reversed from the wider channel (290). Later, Iwai and his colleagues applied the same liquid-driving approach to perform more advanced operations such as microdroplet generation as well as multiple fluid transport and mixing (288). Another valve configuration presented in their study relied on multilayers of PDMS with a thin PDMS membrane staying between upper and lower channels (162, 164, 288). Upon pressure the thin PDMS membrane deforms making a gap for liquid passage between upper and lower channels. Pappa et al. (289) developed a microfluidic biosensor comprising the immobilization of different enzymes for the simultaneously detection of glucose, lactate and cholesterol from saliva samples. By incorporating a finger-powered fluid motion, the device possessed an autonomous and portable configuration thus being the application in point-of-care diagnostics equated.

The design of microfluidic devices intended for electrochemical sensing may require the integration of miniaturized electrodes to achieve portable solutions. Paper-like electrodes stand as excellent choice for miniaturization purposes due to their flexibility and easily controlled dimensions. These type of electrodes, where carbon-based materials are used, can be simply made through a vacuum-filtration process in the same manner as the fabrication of buckypapers. First introduced by Smalley group in 1998 (291-293), buckypapers were obtained through filtration of a SWCNT suspension. The carbon film formed in filter membrane was then peeled off to give a free-standing and entangled carbon nanotubes mat. In order to assure a homogeneous film, filtering of well dispersed suspensions of nanotubes with the aid of a surfactant avoided the aggregation of nanotubes due to strong Van der Waals interactions (54, 294, 295). Besides SWCNT, other carbon-based materials such as MWCNT (296, 297) and graphene (298-300) have been used to fabricate paper-like electrodes for diverse applications such as supercapacitors or electrochemical sensors. The combination between these materials, or even the hybridization with other components, namely polymers and metal particles have been also tried out for the same purposes (301-306). This simple vacuum-filtration method makes viable the production of electrochemical sensors and biosensors with high flexibility and controllable dimensions without disregarding analytical performance. A thin film electrochemical sensor composed of SWCNT over a cellulose ester membrane was produced by vacuum-filtration (52). The flexible sensor exhibited superior sensitivity compared to a glassy carbon electrode and improvements regarding the level of selectivity. In a different approach, BOx enzyme in nafion was deposited in a vacuum-filtered MWCNT film, producing an efficient O_2 electrocatalytic system to be used in biofuel cells (54).

Graphene is a 2D single-layer of sp^2 hybridized carbon atoms disposed in hexagonal configuration while CNTs can be seen as rolled graphene sheets in the form of individual or multiple tubes. These particularities confer outstanding mechanical, thermal and

electrical properties which make them suitable for the construction and modification of electrodes (50). However, the relative high cost may be cumbersome for disposable and cheaper applications. Therefore, carbon blacks might render a viable alternative. The commercially known carbon black, Vulcan XC72 consists of particles with size between 30 and 40 nm with relatively high specific surface area (254 m^2 g^{-1}) (307, 308) and good electrical conductivity, between 0.1 and 100 S cm^{-1} (309, 310). Although these characteristics are inferior when compared with carbon nanotubes (309), the significantly lower cost of Vulcan XC72 and availability lead to the common usage as a conductive support for catalysts in fuel cells (59, 311). Furthermore, electrodes based on Vulcan carbon black have also been developed for applications in sensors (312-315), biosensors (55, 316-319) and biofuel cells (320-323).

In the present work, we aim the evaluation of a simple microfluidic manifold with an incorporated biofuel cell where fluid transport is accomplished by finger-pressure. These features enable a fully portable and energy-consumption free device for envisaged applications in point-of-care diagnostics as disposable self-powered biosensors or as low-cost energy supply component in microfluidic devices. Biofuel cells can be miniaturized because of the high selectivity for the substrate which dispenses the need of a separation membrane between the bioanode and the biocathode (19). Nevertheless, attention must be paid to the pair of selected enzymes regarding optimal pH conditions for catalytic activity and sequent cell efficiency. With this view, Miyake and his collaborators (188) employed fructose dehydrogenase in the anode and laccase from *Trametes versicolor* in the cathode, with both enzymes operating at pH around 5.0, to implement a miniaturized fructose/O_2 biofuel cell. Herein, enzymes GOx and BOx were immobilized in paper-like electrodes based on carbon black catalyst in order to reduce costs and facilitate the integration inside the miniaturized device. For this, the performance features of each immobilized enzyme are firstly characterized as working electrodes in three-classical arrangement electrochemical cells. Then, combined use in the microfluidic device is evaluated regarding the enabled power.

7.2 – Experimental

7.2.1 – Materials and reagents

Analytical grade chemicals were used throughout without further purification. The enzymes, glucose oxidase from *Aspergillus niger*, type VII (≥ 100000 U g^{-1}) and bilirubin oxidase from

Myrothecium verrucaria (8.2 U mg^{-1}) were acquired from Sigma-Aldrich. Stock solutions of bilirubin oxidase (1 mg mL^{-1}) were made by dissolving all the solid in 0.01 M phosphate buffer solution pH 7.0, divided in aliquots and stored at -20 ºC until use.

Ammonium sulfate, 3-(aminopropyl) triethoxysilane (APTES), *p*-benzoquinone, cetyltrimethylammonium chloride in 25% wt. H_2O (cetyl), N-(3-dimethylaminopropyl)-N-ethylcarbodiimide hydrochloride (EDC), D(+)-glucose, 25% glutaraldehyde in water, (GA), graphene oxide (4 mg mL^{-1} dispersion in water), hydrochloric acid, N-hydroxysuccinimide (NHS), indium tin oxide coated PET, MES hydrate, MES sodium salt, MWCNT (carboxylic acid functionalized), nafion (5% wt), potassium phosphate dibasic, potassium phosphate monobasic, 1-pyrenebutyric acid N-hydroxysuccinimide ester (PBSE), sodium dodecyl sulfate (SDS), SWCNT (carboxylic acid functionalized), Triton X100 and Trizma base were obtained from Sigma-Aldrich. Dimethylformamide (DMF) was acquired from ROMIL Chemicals (Cambridge, UK) and Sylgard® 184, silicone elastomer kit (polydimethylsiloxane, PDMS) was obtained from Dow Corning. Carbon black Vulcan XC72 was acquired from Cabot Corporation (Boston, Massachusetts). The *Graphit 33* lacquer for conductive coatings (CRC Industries, Zele, Belgium) was acquired from a local electronic products store.

Potassium phosphate buffer 0.1 M pH 7.0 was used as electrolyte solution. The glucose solution was prepared near physiological conditions (pH 7.0) and 24 hours before analysis to allow the isomerization of the glucose molecule (121).

7.2.2 – Electrochemical measurements

All electrochemical experiments were performed with a potentiostat Metrohm, model Autolab PGSTAT10, controlled by GPES v3.9 software (Herisau, Switzerland). Cyclic voltammetric (CV) and amperometric measurements were performed in a three-electrode cell composed of an Ag/AgCl (KCl, 3 M) mini reference electrode (Metrohm, Ref. 6.0727.000), the working electrode and a platinum rod as counter electrode. Biofuel cell experiments were performed in miniaturized electrochemical cell and in a microfluidic, finger-powered device in a two electrode configuration: biocathode and bioanode. The power density curves were obtained by linear sweep voltammetry (LSV) at 1 mV s^{-1}.

The design and construction of the microfluidic device was performed using the free Inkscape 0.92 vector graphics software and a 2D-laser cutting-engraving platform system VLS4.65 (Universal Laser Systems Inc., Scottsdale), respectively. A Diener Zepto plasma system (Diener Electronic GmbH-Co. KG, Ebhausen, Germany) was used for rugged bonding between PDMS to PMMA.

7.2.3 – Electrodes construction

The paper-like electrodes were made based on the fabrication method of buckypaper without peeling the carbon black film from the filter membrane. Initially, Vulcan XC72 carbon black particles were dispersed ultrasonically in aqueous solution of surfactant SDS (1% wt.) to a final concentration of 0.5 mg mL^{-1} for 90 minutes. The suspension was centrifuged for 15 minutes at 2500 rpm in order to remove larger agglomerates. The stable supernatant was then filtered (total 15 mL divided by 3 aliquots) under vacuum pressure through a 47 mm diameter nylon membrane with a pore size of 0.22 µm (Whatman, UK) using a standard glass microfiltration apparatus. The thin film carbon layer was then washed with 10 mL of water and air dried. Afterwards, a water-proof acrylic varnish was sprayed in the opposite side of the filter membrane, in order to confer more hydrophobic properties and prevent capillarity effect whenever the electrodes were immersed in solution. The paper-like Vulcan XC72 electrodes are henceforth designated as CB electrodes. For comparison purposes, other electrodes were constructed as described next. Paper-like reduced graphene electrode (graphene) and paper-like SWCNT electrode (SWCNT) were made similarly as CB paper-like electrode by vacuum filtration of 0.5 mg mL^{-1} suspension of each material. The reduction of graphene oxide was performed by immersing the filter in a 0.05 g mL^{-1} ascorbic acid aqueous solution at 80 ^{o}C for 30 min. The *Graphit 33* paper-like electrode (*Graphit 33*) was made by spraying the commercial suspension in the filter membrane. The ITO thin-film electrode (ITO) was used as received. The design of the electrodes was accomplished by means of vector graphic software and cut in their final shape in the 2D-laser platform system. Only the tip of the electrodes was used for the electrochemical measurements, considering a geometrical active surface area of about 0.095 cm^2. Finally, a pencil graphite electrode (PGE) was constructed from a 2 mm diameter HB pencil having a geometrical active surface area of about 0.031 cm^2.

7.2.4 – Deposition of enzymes in the miniaturized paper-like electrodes

The methodology used for bioelectrodes assemblage was based on enzyme precipitate coatings procedure for the bioanode and through covalent bonding using a pyrene derivative compound for the biocathode.

In order to develop the GOx bioelectrode/bioanode an amount of carboxylic functionalized MWCNT were first activated with EDC and NHS. The nanotubes were recovered by filtration, re-suspended and mixed with GOx (8 mg mL^{-1}) and left overnight to promote covalent attachment with the enzyme. Ammonium sulfate was then added to precipitate

GOx and form agglomerates in the vicinity of the nanotubes which were then crosslinked with GA for 30 minutes. The precipitate was recovered by vacuum-filtration, washed and re-suspended in a diluted (0.5% wt.) nafion solution to a final concentration of 2 mg mL^{-1}. An aliquot of 10 µL was deposited over the paper-like electrode and dried for at least 2 hours at room temperature. The bioelectrode is henceforth designated as CB-MWCNT/GOx/nafion.

The implementation of the BOx bioelectrode/biocathode started with the CB electrode being immersed in 10 mM PBSE dimethylformamide solution for 1 hour and washed by immersion in 0.01 M phosphate buffer solution (pH 7.0) for a few seconds. Next, the electrode was incubated 0.5 mg mL^{-1} BOx in 0.01 M phosphate buffer (pH 7.0) for another hour and washed by immersion in a 0.1 M phosphate buffer pH 7.0. This bioelectrode is henceforth designated as CB-PBSE-BOx.

7.2.5 – Construction of the finger pressure-driven microfluidic device

The microfluidic finger-powered device with the integrated biocathode and bioanode was implemented from a bottom methyl methacrylate cross polymer sheet (PMMA) and a top PDMS layer bonded together after surface activation by O_2 plasma etching.

Bottom part: A rectangular piece with 50x40x4mm dimension was cut and engraved using a 2D laser cutting platform with 1.0x0.5mm flow paths connecting the sample chamber with the finger squeezing pouch, the detection cell and the waste reservoir (Figure 7.1a).

Valves: Two one-way valves were designed by cutting small 3.0x4.0x0.1 mm pieces of overhead projector acetate film with a “U” cut in the middle and set between lower channel and upper channel to work as a flap that opens or closes the access to the chambers in the PDMS top piece (Figure 7.1C).

Top part: To serve as template, a rectangular PMMA piece with 50x40x2mm dimension was cut and over its surface two cylinders of the same material with 8.0 and 12.0 mm diameter and common height of 4 mm, were glued. Three pieces of overhead projector film, giving 0.3 mm height were cut in elliptical shape to create the valve junctions and detection chamber (Figure 7.1b). This mask was finally inserted in a 7.0 mm height frame. The silicone elastomer was thoroughly mixed with curing agent in a 10:1 proportion and then poured over the template. Air bubbles were removed inside an empty desiccator under vacuum for 1 hour followed by curing in the oven at 90 ºC along 90 minutes. The frame was removed and the PDMS piece released from the PMMA mask with the aid of methanol.

Assembly of the device: The two parts (PMMA and PDMS) were chemically treated with APTES and then bonded after O_2 plasma etching of both surfaces. First the PDMS and PMMA pieces were activated in the plasma for 5 minutes at 50% power. After removing

from the plasma system, the two parts were immersed during 2 minutes in a 2% (v/v) APTES aqueous solution and dried under a N_2 stream. Finally, the PDMS and PMMA were again plasma activated in the same conditions. The electrodes were then integrated in the PMMA bottom part and the activated surfaces were put in contact to seal the device. Punch holes were made in sample and waste reservoirs of the PDMS (at the beginning and end of the circuit) to allow pressure equilibrium and therefore liquid movement. The assembled finger-powered microfluidic biofuel cell is represented in Figure 7.1d.

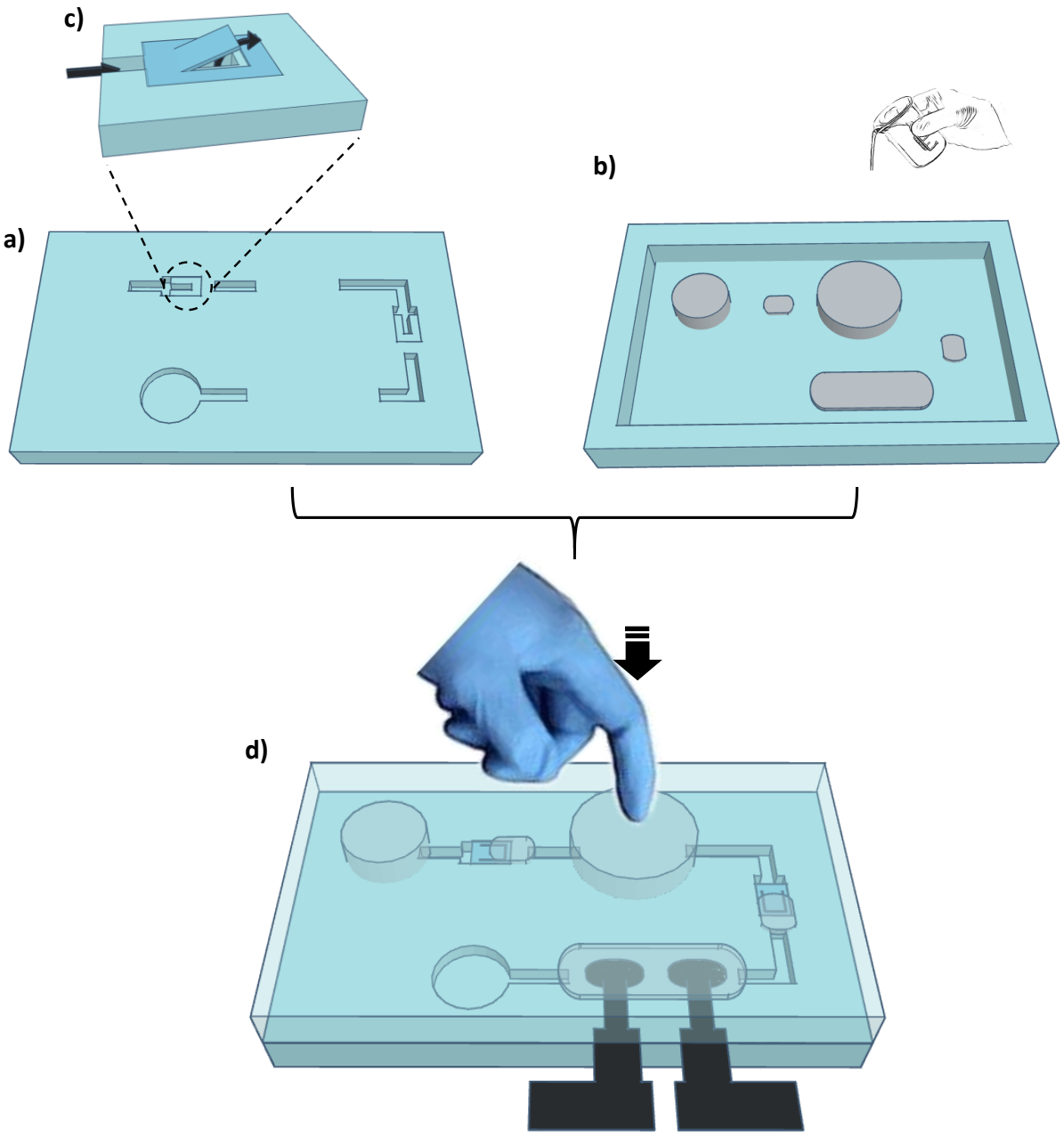

Figure 7.1 - Scheme of the finger-powered microfluidic biofuel cell. a) Bottom part made of PMMA presenting laser engraved channels. b) Soft lithography process for the top part made of PDMS (PDMS poured in a PMMA mask). c) Magnified view of the valve system with arrows showing the movement made by the fluid. d) Final assembly of the device after bonding with APTES and plasma treatment, with integrated electrodes.

7.3 – Results and discussion

7.3.1 – Fabrication and characterization of carbon black paper-like electrodes

The vacuum filtration method allowed a simple and reproducible laboratory scale procedure to obtain thin films of carbon black with smooth and compact appearance and good flexibility to be used as paper type electrodes of any desired size. The homogeneity of electrochemical properties however depend on the level of aggregation between particles (294). Sonication in a surfactant solution contributes to more homogeneous dispersions by inducing electrostatic repulsion and avoiding van der Waals interactions of the carbon particles. This leads to improved conductivity of the carbon film. Three different types of surfactants (anionic, cationic and nonionic) were used in the preparation of CB electrodes and their electrochemical performance assessed by CV in a $Fe(CN)_6^{3-/4-}$ redox system at 10 mV s^{-1}. Higher cathodic and anodic peaks with less separation between them (lower ΔE_p) were obtained for the anionic surfactant, SDS (I_{pc} = 9.4 x 10^{-5} A, I_{pa} = 9.0 x 10^{-5} A, ΔE_p = 0.53 V), followed by cationic Cetyl (I_{pc} = 9.5 x 10^{-5} A, I_{pa} = 8.2 x 10^{-5} A, ΔE_p = 0.59 V) and lastly by the nonionic Triton X100 (I_{pc} = 6.6 x 10^{-5} A, I_{pa} = 4.7 x 10^{-5} A, ΔE_p = 0.84 V). The CB electrode obtained from the anionic surfactant dispersion was afterwards compared through the same CV analysis with other carbon based electrodes namely paper-like graphene, paper-like SWCNT, paper-like *Graphit 33*, pencil graphite electrode and ITO electrode (Figure 7.2). As expected, CB electrodes electrochemically underperformed in relation to SWCNT and reduced graphene electrodes (Figure 7.2a). The anodic and cathodic peak heights were slightly lower and with sluggish kinetics for the CB electrode but better when compared with the remaining electrodes (Figure 7.2b). The electrode seriation for peak height was as follows: reduced graphene > SWCNT > carbon black > *Graphit 33* > ITO > PGE. Despite these results, the Vulcan carbon black showed the best compromise between anodic peak current and overpotential which could be advantageous as anodic material in biofuel cells. Moreover, the availability and reduced cost with easier processability are advantageous features, contrary to graphene which requires a more time-consuming or environmentally hazard reduction step to obtain optimal electrical properties.

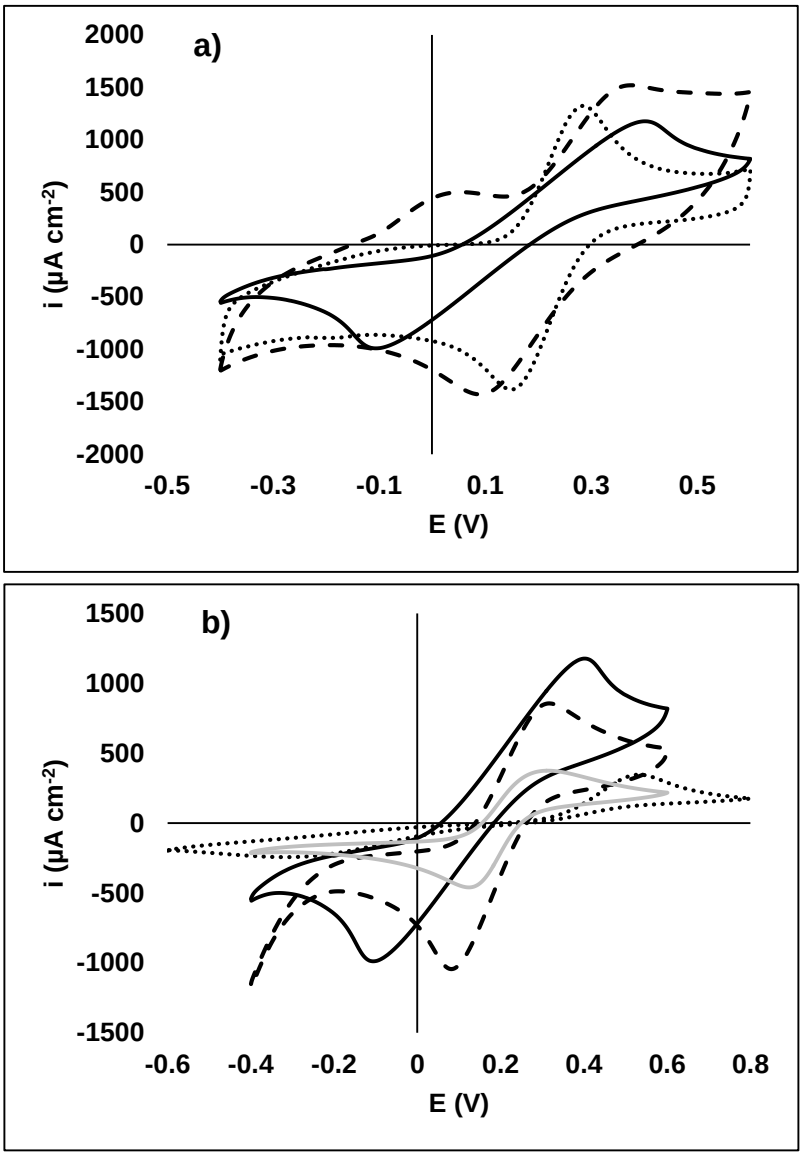

Figure 7.2 - Cyclic voltammograms of equimolar $[Fe(CN)_6]^{3-/4-}$ for Vulcan carbon black paper-like (CB) electrode (full black line). a) Compared with reduced graphene paper-like electrode (dashed line) and SWCNT paper-like electrode (dotted line). b) Compared with Graphit 33 paper-like electrode (dashed line), ITO electrode (dotted line) and PGE (full grey line). Working conditions: 10 mV s^{-1}; electrolyte: 5 mM $K_3[Fe(CN)_6]$ and 5 mM $K_4[Fe(CN)_6]$ in 0.1 M KCl.

7.3.2 – Characterization of the miniaturized glucose oxidase based bioanode

The bioanode CB-MWCNT/GOx/nafion was implemented via the immobilization of enzyme precipitate coatings (EPC) (62, 272). The procedure consisted in the covalent attachment of glucose oxidase enzyme onto MWCNT, precipitation and further cross-linking forming enzyme clusters. To assess proper immobilization of the enzyme the electrode response was first performed by CV from -0.4 to +0.5 V at the sweep rate of 10 mV s^{-1} where faradaic currents are only limited by substrate diffusion (Figure 7.3a).

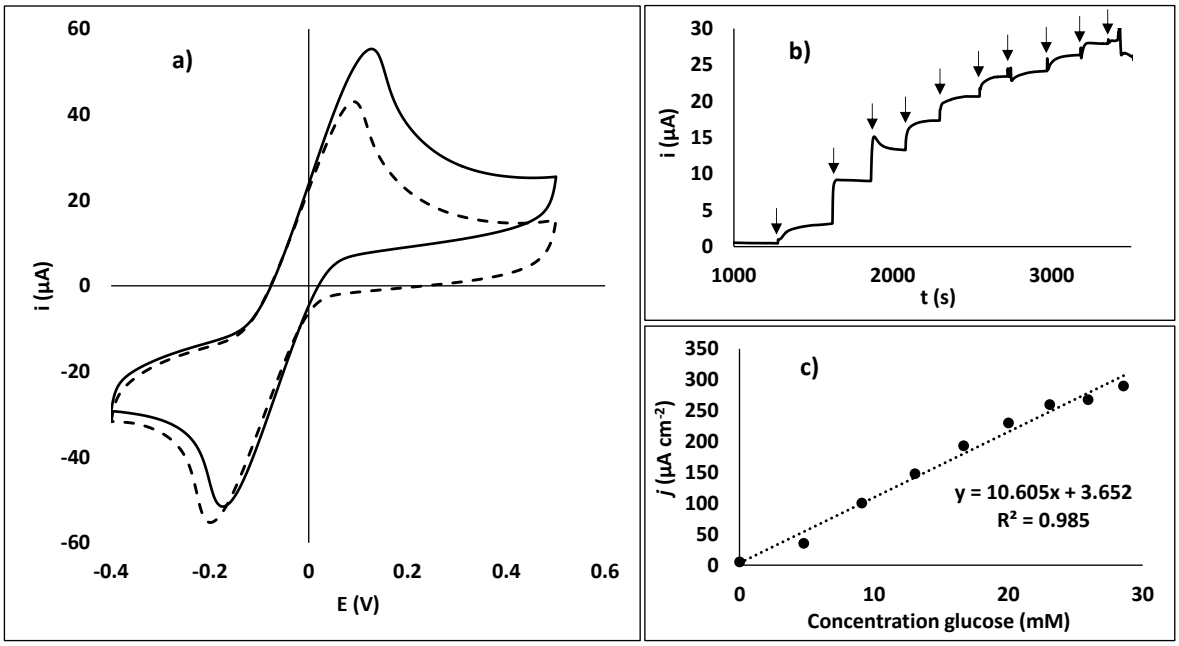

Figure 7.3 - Characterization of paper-like bioelectrode CB-MWCNT/GOx/nafion to be later applied as bioanode. a) Cyclic voltammograms obtained in the presence (full line) and absence (dashed line) of glucose. b) Amperometric response to successive glucose injections. c) Glucose calibration curve. Working conditions: CV scan rate 10 mV s^{-1}; Amperometric applied potential: +0.15 V; electrolyte: 5 mL of 0.1 M phosphate buffer pH 7.0 and 2 mM benzoquinone (10 mM glucose) in electrochemical cell.

In the presence of mediator p-benzoquinone (BQ) two redox peaks are observable, with the oxidation peak at +102 mV and the reduction peak at -197 mV. This electrochemical process becomes however thermodynamically more favorable after adding the glucose substrate since the voltammogram shifts towards more positive potentials, with the oxidation peak increasing in about 34 mV and also with an additional increase in the oxidation current. This confirms the biocatalytic response of the enzyme to glucose with the oxidation of the mediator occurring at +0.13 V. So, for catalytic studies the amperometric measurements were conducted at the potential of +0.15 V to ensure total oxidation at the surface of the electrode. Successive additions of 100 mM glucose solution into 5 mL initial blank electrolyte solution lead to the rapid increase of the oxidation current followed by stabilization (Figure 7.3b). The use of substrate by the enzyme followed a typical Michaelis-Menten profile with maximum rate of 6.39 nmol min^{-1} O_2 and a Michealis constant of 18.3 mM glucose. The bioelectrode presented a sensitivity of 10.6 µA mM^{-1} cm^{-2}. The LOD, which corresponded to 15 µM, was determined by applying the formula LOD = 3.3σ/S, where σ is the standard deviation of the stabilized signal in the absence of glucose and S is the slope of the calibration curve. A wide linear range of up to about 30 mM was obtained (Figure 7.3c), reflecting the improved enzyme loading and stability introduced by the immobilization method and therefore possibly extending the life-time of biofuel cells. The performance of this bioelectrode is comparable to other miniaturized or thin-film biosensors with immobilized GOx described in the literature. The sensitivity is only half when compared with

biosensors based on screen-printed carbon electrodes (SPCE) modified with graphene, polyaniline and gold nanoparticles (324) or Prussian blue (325), and buckypapers with chitosan (326). To the contrary, performed better when compared with those based on carbon ink electrodes modified with Prussian blue (327), ZnO nanowires (328) or chitosan (329), and with SPCE modified with ferrocene mediator (330). Regarding LOD, it showed the best value after comparison with all previous mentioned biosensors except for two biosensors (324, 325). Also achieved a better LOD (5 times lower) when compared with a previous studied biosensor based on the same immobilization procedure but employing a PGE with graphene modified surface (PGE-graphene-MWCNT/GOx/nafion) embedded in a microfluidic platform (331).

7.3.3 – Characterization of the miniaturized bilirubin oxidase based biocathode

The biocathode was assembled through the noncovalent functionalization of Vulcan carbon black using 1-pyrenebutanoic acid, succinimidyl ester. The pirenyl group strongly interacts with graphitic structure of the carbon black aggregates via π-π stacking. On its turn, the free succinimidyl ester group reacts with the amine group of the enzyme through nucleophilic substitution, resulting in the formation of an amide bond (332). This immobilization strategy is simple, fast and efficiently establishes direct electron transfer (DET) between the enzyme and the electrode surface.

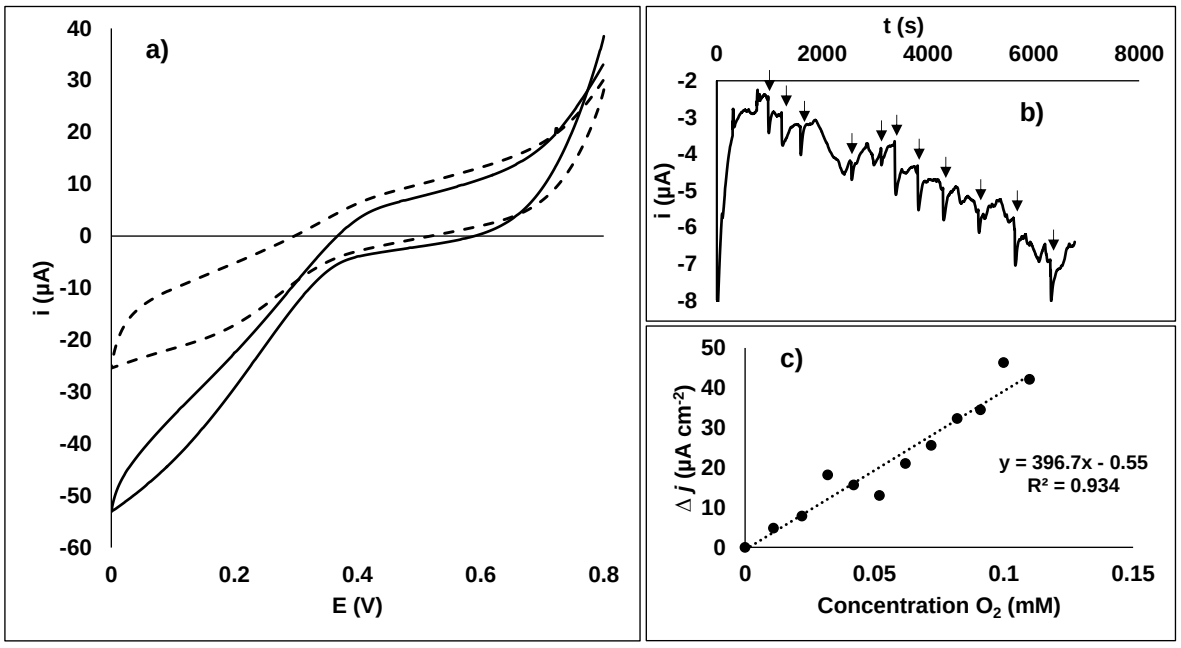

Figure 7.4 - Characterization of paper-like bioelectrode CB-PBSE-BOx to be later applied as biocathode. a) Cyclic voltammograms in the presence (full line) and absence (dashed line) of oxygen. b) Amperometric response to successive injections of oxygen saturated solution. c) Oxygen calibration curve. Working conditions:

CV scan rate 10 mV s^{-1}; Amperometric applied potential: +0.15 V; electrolyte: 5 mL of 0.1 M phosphate buffer pH 7.0 (oxygen) in electrochemical cell.

A voltammetric analysis of the CB-PBSE-BOx was first performed between +0.8 and 0 V at 10 mV s^{-1} in phosphate buffer pH 7.0. As depicted in Figure 7.4a the biocatalytic response of the enzyme in the presence of oxygen displaced the cathodic wave towards more negative current values, with the onset of O2 reduction at about +0.4 V. These results attest the efficient immobilization of BOx onto the carbon black like-paper electrode. The catalytic current achieved at a potential of 0 V (about -500 µA cm^{-2}), was similar to a buckypaper with immobilized BOx via PBSE (257) and 24% greater when compared to a MWCNT modified Toray carbon paper for the same enzyme, immobilization method and scan rate although at more acidic pH (250). The same conclusions are also stated when comparing with anthraquinone modified buckypapers with immobilized laccase (333). Amperometric determinations of O_2 were then performed at +0.15 V. As shown in Figure 7.4b, the increasing concentration of O_2 in solution causes a constant decrease in current values indicating the catalytic response of the enzyme to its substrate, despite the more erratic behavior of the response until stabilization. Results fitting by nonlinear regression to the Michaelis-Menten equation enabled the maximum rate of 1.24 nmol min^{-1} O_2 and a Michaelis constant of 34.2 mM O_2 for the catalytic process. From the calibration curve of Figure 7.4c, the bioelectrode achieves a sensitivity 397 µA mM^{-1} cm^{-2}. The linearity range obtained was up to 0.11 mM and the LOD determined in the same way as the bioanode was of 1.8 µM. The developed bioelectrode presented highest sensitivity towards O_2 when compared with the majority of similar biosensors characterized in the literature (132, 237, 238, 261). Although highest, the sensitivity value reported by Mousty et al. (236), about 470 µA mM^{-1} cm^{-2}, was obtained for rotating electrode conditions.

7.3.4 – Assembly and characterization of the finger pressure-driven microfluidic biofuel cell

One of conceivable applications of biofuel cells is as self-powered biosensors. Theoretically, all biofuel cells can be used as biosensors once the power produced is proportional to the fuel concentration around the Michaelis Menten constant (334, 335). Accordingly, the biofuel cell was evaluated as a self-powered biosensor in quiescent conditions. Figure 7.5a shows the power curves obtained for various concentrations of glucose (1, 5, 10, 20, 50 mM) in air-saturated phosphate buffer solution pH 7.0 at room temperature. The calibration curve, based on the maximum power density obtained for each glucose concentration showed a linear range up to 20 mM and a sensitivity of about 2.1 µW mM^{-1} cm^{-2} (Figure

7.5b). Also we have noticed a decrease in the achieved maximum power density between 15 and 20% when the fuel solution was saturated with O_2. This was expected since O_2 is also a co-substrate of GOx enzyme, occurring undesirable electron transfer and therefore reducing the power output of the biofuel cell as observed by others (137). The results obtained are comparable with similar self-powered glucose biosensors (329, 336). For instance, the calculated sensitivity between 0 and 100 mM glucose was about 0.9 $\mu W\ mM^{-1}\ cm^{-2}$ for the GDH/BOx biofuel cell reported in the work from Milton et al. (336) under continuous stirring conditions. The CB paper-like bioelectrodes representing the bioanode and the biocathode were finally integrated into the microfluidic system.

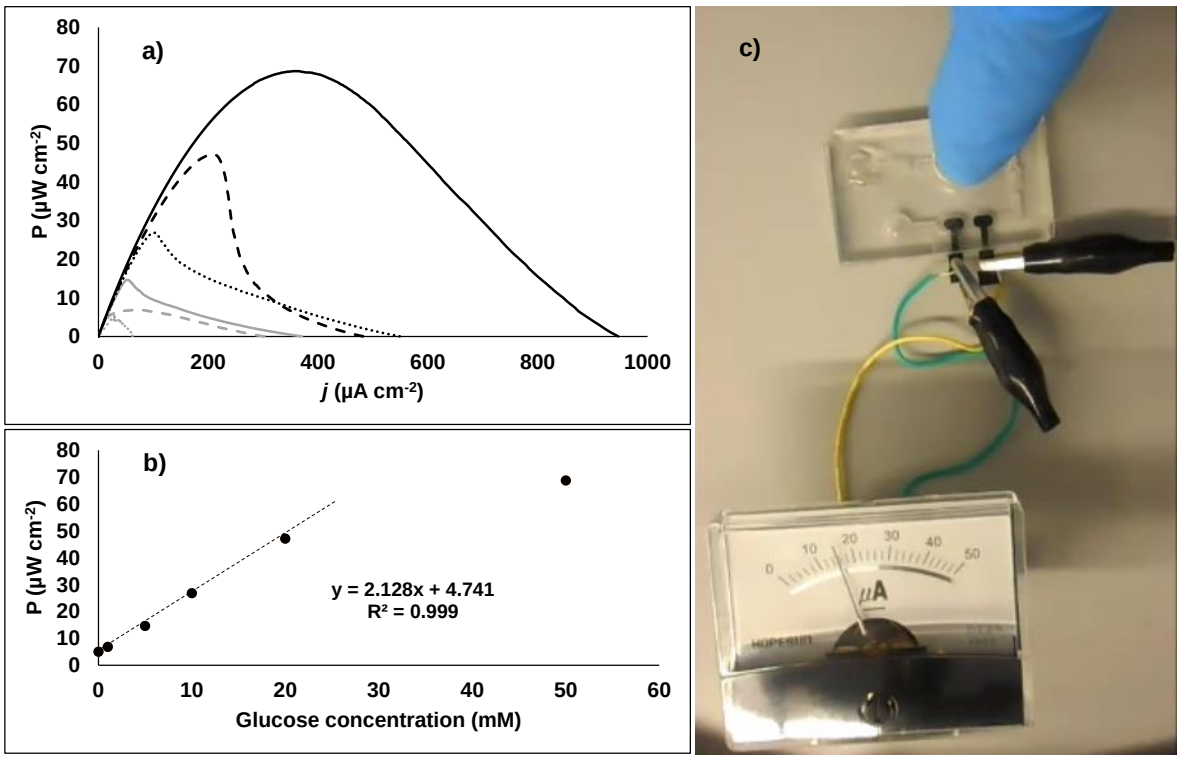

Figure 7.5 - Performance of the biofuel cell as power source. a) Power density curves for various concentrations of glucose, 0 mM (dotted grey line), 1 mM (dashed grey line), 5 mM (full grey line), 10 mM (dotted black line), 20 mM (dashed black line) and 50 mM (full black line). b) Calibration curve for the maximum power density obtained for each glucose concentration. c) Autonomous operation of the finger-powered microfluidic biofuel cell connected to a microammeter in 5 mM glucose solution. Working conditions: 0.1 M phosphate buffer pH 7.0 with 2 mM benzoquinone. Air saturated for a) and O_2 saturated for c).

Finger-powered devices are made of PDMS elastomer due to its flexibility, and squeezing the PDMS thin layer of the reservoir will depress it and causes the fluid motion. In the configuration adopted initial squeeze by finger pressure and relieve drives the liquid between the sample reservoir and the squeezing pouch chamber due to opening the first check valve when its acetate membrane flap upwards. During the following squeeze, positive pressure closes the first check valve, preventing the return of the liquid, and opens the second valve to allow liquid passage to the detection chamber containing the biocathode

and bioanode. Before the final assembly, the surfaces of the PMMA and PDMS pieces were activated by O_2 plasma etching. Besides removing organic residues, plasma radiation breaks down carbon chains and creates reactive oxygen radicals in the surfaces (337, 338). Both surfaces were then treated with amino functionalized silane reagent, APTES, to promote irreversible bonding between thermoplastic PMMA part and the silicon-based PDMS part. The silicon-functionalized surfaces were again plasma activated and joined together after the bioelectrodes insertion, establishing irreversible oxygen-to-silicon bindings between the two parts. Two holes were punched in the PDMS for the inlet and outlet and the electrolyte sample added to the reservoir. A microammeter was connected to the bioanode and biocathode to assess the current produced. Then, successive squeezes with the finger were applied to the pouch creating vacuum-suction. Once the fuel solution, containing 5 mM glucose and saturated O_2, entered the detection chamber and contacted both electrodes the needle of the microammeter moved to a maximum value of about 20 µA and decreased until it stabilized in 6 µA (Figure 7.5c) for about one hour. According to the surface area of the electrodes (0.095 cm^2) the biofuel cell produced a current density of 63 µA cm^{-2}. Some leaks can occur in the interface between the PMMA and PDMS due to bonding imperfections. If the channels of the two parts are not well juxtaposed a homogeneous bonding could not occur and therefore lead to leakages. Moreover, despite the inclusion of two check valves in the device we still observe partial fluid backflow requiring thus sequential squeezing of the PDMS pouch. Since in the present configuration there is no separation between anode and cathode, the use of the mediator benzoquinone for glucose oxidase may hinder the electron transfer as electrooxidation at the biocathode may occur (38). In the same way, the presence of O_2 dissolved in the electrolyte may reduce the external power of the biofuel cell. In this particular case where GOx was used in the anode, O_2 is a co-substrate of the enzyme and therefore hinders the electron transfer to the mediator (137). The implemented device provided consistent and reproducible results along each working day (8 hours) during its assessment.

7.4 - Conclusions

Most of the works described in the literature regarding microfluidic biofuel cells resort to external pumps for fuel feeding. If the energy used by this pumping systems outweighs the energy produced by the biofuel cell, the concept loses purpose.

In the present work we have demonstrated a self-powered microfluidic biofuel cell. The human propelled fluidics feature implemented through finger pressure confers full portability

to the device enabling potential use for autonomous sensing. The use of flexible, paper-like electrodes facilitates the integration in the microfluidic platform. This type of electrodes can be easily fabricated through a controllable vacuum-filtration process. As economically viable alternative and comparable kinetics to commonly used electrodes, Vulcan carbon black was chosen as transducer material. For the implementation of the bioanode, GOx was immobilized through an enzyme precipitate coatings procedure. Although requiring the use of a redox mediator, the procedure enables high analytical signals over an extended range of glucose concentrations. The BOx biocathode was implemented through the functionalization of carbon black electrode using a pyrene derivative enabling direct electron shuttling. Nevertheless, the procedures used revealed enough ruggedness to be compatible with flow conditions adopted in microfluidics. As far as we know, the present work was the first to integrate a biofuel cell in a finger pressure-driven microfluidic system, working as a portable, disposable and self-powered biosensor. In a broader view the succeeded embedding of the biofuel cell might also enlarge power solutions available for development of more complex lab-on-chip devices. In this sense the used microammeter for signal reading is a good example of the autonomy of the device avoiding the use of a potentiostat/galvanostat.

Chapter 8

Final conclusions and future perspectives

The energy production from small biological entities can be summarized to about 100 years, dictating a constant progress and apparent success. Since the first experiment in 1912, biofuel cells systems became sufficiently small and autonomous to allow preliminary tests as bioimplants or power source devices. This was possible due to improvements in the immobilization efficiency together with the specificity of enzymes to their target molecules which permitted the simplification of biosensors and biofuel cells. However, the level of stability that limit biofuel cells utilization and market implementation still are challenges to be addressed. At present, the most promising and practical applications stands as autonomous, self-powered biosensors or as energy supplier to low power-consuming electronics and other sensors/biosensors.

The work conducted in the present thesis sought to contribute for the development of the biofuel cell area, more specifically, portable and self-powered biosensors in order to achieve inexpensive and energetically sustainable analytical solutions. At the end, the overall objectives were successfully met by the design of the first fully autonomous microfluidic biofuel cell. The small sized device incorporated a finger-pressure mechanism for fluid propulsion which enabled portability with potential use in diverse unit operations, accordingly to lab-on-a-chip principles.

Prior to this definitive development each bioelectrode comprising bioanode and biocathode were individually characterized using pencil graphite electrodes (PGEs) as transducer. This type of electrodes have been studied as a valuable electroanalytical tool given the increasing number of publications regarding their use for sensors and biosensors. Commercial pencil mines are used as transducing surface, composed of an extruded mixture of sp^2 carbon graphite and clay. Differences between graphite and clay composition will produce different pencil hardness and therefore influencing the electrochemical response due to variation of the conductive material quantity. Voltammetric and impedance spectroscopic characterization of PGEs revealed a better performance and stability of the middle hardness type PGE, HB, compared to types 4H (lower graphite content) and 4B

(higher graphite content). Also, PGE pre-treatment may affect significantly the response by introducing or removing oxygen functionalities to the surface. Better kinetics were obtained after alumina polishing when the PGE was used directly as a sensor. However, upon surface modification with carbon nanostructured additives, the alumina pre-treatment had minor influence. An improvement of the PGE analytical signal was achieved when overall modified with carbon nanomaterials. Specifically, modifying the surface with reduced graphene revealed higher efficiency when compared to MWCNT and carbon black and therefore applied in the preparation of the bioelectrodes. One major advantage of these electrodes over other conventional carbon-based electrodes are their reduced fabrication cost, estimated to be around 0.40 euros for a single bare PGE. Thus, the ability to offer renewed surface by simple cut or easy replacement provides good reproducibility, implementation efficiency and practicability to use as disposable sensor.

Initially, oxygen reduction bioelectrodes were studied and characterized as O_2 biosensor for potential use as biocathodes. In a first attempt, laccase enzyme was immobilized by entrapment in a sol-gel matrix alongside carbon nanotubes. Although obtaining a good response to oxygen, the generated current density was low which would limit the efficiency of a biofuel cell if implemented as a biocathode. Moreover, this method involved fastidious sol synthesis with the short stability of the biofilm being also a drawback. Another immobilization procedure was therefore implemented which leaded to much higher sensitivity to oxygen. It consisted in the cross-linking of BOx enzyme to carbon-based materials through π-π stacking and amide bond functionalization, resulting in the establishing of DET between enzyme and the electrode. A good performance as biocathode was validated through obtaining high current densities and open circuit potential. Also, the usefulness of this O_2 bioelectrode was demonstrated in the monitoring of O_2 consumption by yeast *Saccharomyces cerevisiae* in a fermentation process.

After characterization of the O_2 reduction process, the fuel oxidation was in turn properly studied. For this purpose, GOx clusters were formed by precipitation and cross-linked to MWCNT with further deposition in the electrode surface. Even though DET was not observed, this method allowed high enzyme loading and activity which resulted in a wide linear range regarding determination of glucose. Also, the improved stability made possible the detection of glucose and cadmium in a microfluidic platform under flow conditions.

With the defined immobilization procedures for biocathode and bioanode, the next step focused in the miniaturization of the bioelectrodes. The concept of the electrodes was an important factor in order to obtain a miniaturized and viable microfluidic device. Therefore, a vacuum filtration method was chosen for production of flexible and cheap, paper-like electrodes to facilitate integration in the microfluidic platform. A Vulcan carbon black

suspension was used as electrocatalyst in the manufacture of these electrodes, standing as a more economical alternative though with lower electrochemical performance when compared directly to carbon nanotubes or graphene. The microfluidic platform, consisting of a PMMA bottom part and a PDMS top part, was designed in order to incorporate a finger squeezing flexible pouch and two membranes working as check valves placed between inlet reservoir and detection chamber. The paper-like bioelectrodes constituting the biofuel cell were then integrated in the microfluidic platform with a fuel driven system based on finger pressure actuation. Although producing a power density below 100 μW cm^{-2} in the presence of glucose and O_2, it varied proportionally with the fuel concentration thereby turning this device suitable for potential applications as a portable, disposable and self-powered biosensor. A biofuel cell that requires energy-consuming pumps for fuel transport seems counterproductive and so the present developed system successfully circumvents this issue.

Specifically regarding the work developed in the present thesis, some adjustments and improvements can still be performed in order to achieve increased performances of the self-powered biosensor. For instance the use of pyrroloquinolinequinone glucose dehydrogenase enzyme (PQQ-GDH) in the bioanode would be more advantageous taking into account the described ability to establish DET with the electrode avoiding the use of mediators and its insensitivity to oxygen as compared to GOx. This measure alone would theoretically increase produced power of the biofuel cell. Other limitation from the microfluidic device was the observation of leakages of fuel from the joints when the device was actuated by constant finger pressure. This was mainly caused by sealing deficiencies due the manual alignment of top and bottom microfluidic channels after plasma etching activation. Also due to the absence of time this activation process (e.g. time of etching) was not thoroughly optimized.

In the near future, a possible trend in biofuel cell research field will be centred on the miniaturization of components and increase of systems stability for applications in the clinical and environmental field. Specifically, development of implantable devices and small, portable and autonomous analytical devices for in-situ measurements are the most promising applications and relatively close to market implementation. On the contrary, scale-up of biofuel cell systems for higher power generation seems to be currently left aside by the scientific community. Efficiency problems related to the heterogeneous conversion of chemical to electrical energy by biological entities still needs to be solved or at least improved for this biotechnology be viably implemented in power generation using residues and waste products as fuel.

One simple solution for increasing power generation is stacking individual biofuel cells, as adopted in various works, but with the counter effect of possible increasing the dimensions of the device and therefore this measure must be carefully weighted depending on the intended application. Other solution involves engineering processes of the enzyme immobilization procedure by creating, for example, enzyme multilayers on the electrode surface, designated as “3D electrode”. If each layer is well oriented, aligned and electrically connected to each other and the electrode surface it will definitely increase the turnover rate and consequently the power produced. New nanomaterials and nanocomposites such as metal oxides particles may also contribute for a performance boost. It is clear that new immobilization strategies leading to more efficient biofuel cells requires joint effort from multidisciplinary areas of science.

References

1. Milton RD, Hickey DP, Abdellaoui S, Lim K, Wu F, Tan BX, et al. Rational design of quinones for high power density biofuel cells. Chem Sci 2015; 6 (8): 4867-75.

2. Slate AJ, Whitehead KA, Brownson DAC, Banks CE. Microbial fuel cells: An overview of current technology. Renew Sust Energ Rev 2019; 101: 60-81.

3. Sony Develops "Bio Battery" Generating Electricity from Sugar: Sony Corporation; 2007 [Available from: https://www.sony.net/SonyInfo/News/Press/200708/07-074E/index.html.

4. MacVittie K, Halamek J, Halamkova L, Southcott M, Jemison WD, Lobeld R, et al. From "cyborg" lobsters to a pacemaker powered by implantable biofuel cells. Energy Environ Sci 2013; 6 (1): 81-6.

5. Palmore GTR, Whitesides GM. Microbial and enzymatic biofuel cells. In: Himmel ME, Baker JO, Overend RP, editors. Enzymatic Conversion of Biomass for Fuels Production. ACS Symposium Series. 566. Washington: Amer Chemical Soc; 1994. p. 271-90.

6. Bullen RA, Arnot TC, Lakeman JB, Walsh FC. Biofuel cells and their development. Biosens Bioelectron 2006; 21 (11): 2015-45.

7. Ikeda T, Kano K. An electrochemical approach to the studies of biological redox reactions and their applications to biosensors, bioreactors, and biofuel cells. J Biosci Bioeng 2001; 92 (1): 9-18.

8. Lowe CR. Biosensors. Trends Biotechnol 1984; 2 (3): 59-65.

9. Owen VM. Biosensors - A Survey of what is truly done and used commercially. AnnNY AcadSci 1987; 501: 233-9.

10. Katz E, Buckmann AF, Willner I. Self-powered enzyme-based biosensors. J Am Chem Soc 2001; 123 (43): 10752-3.

11. Arechederra MN, Fischer CN, Wetzel DJ, Minteer SD. Evaluation of the electron transport chain inhibition and uncoupling of mitochondrial bioelectrocatalysis with antibiotics and nitro-based compounds. Electrochim Acta 2010; 56 (2): 938-44.

12. Deng L, Chen CG, Zhou M, Guo SJ, Wang EK, Dong SJ. Integrated Self-Powered Microchip Biosensor for Endogenous Biological Cyanide. Anal Chem 2010; 82 (10): 4283-7.

13. Rasmussen M, Minteer SD. Self-powered herbicide biosensor utilizing thylakoid membranes. Anal Methods 2013; 5 (5): 1140-4.

14. Cheng HJ, Yu P, Lu XL, Lin YQ, Ohsaka T, Mao LQ. Biofuel cell-based self-powered biogenerators for online continuous monitoring of neurochemicals in rat brain. Analyst 2013; 138 (1): 179-85.

15. Sekretaryova AN, Beni V, Eriksson M, Karyakin AA, Turner APF, Vagin MY. Cholesterol Self-Powered Biosensor. Anal Chem 2014; 86 (19): 9540-7.

16. Conzuelo F, Vivekananthan J, Poller S, Pingarron JM, Schuhmann W. Immunologically Controlled Biofuel Cell as a Self-Powered Biosensor for Antibiotic Residue Determination. ChemElectroChem 2014; 1 (11): 1854-8.

17. VandeZande GR, Olvany JM, Rutherford JL, Rasmussen M. Enzyme Immobilization and Mediation with Osmium Redox Polymers. In: Minteer SD, editor. Enzyme Stabilization and Immobilization: Springer; 2017. p. 165-79.

18. Gorton L, Lindgren A, Larsson T, Munteanu FD, Ruzgas T, Gazaryan I. Direct electron transfer between heme-containing enzymes and electrodes as basis for third generation biosensors. Anal Chim Acta 1999; 400: 91-108.

19. Santoro C, Arbizzani C, Erable B, Ieropoulos I. Microbial fuel cells: From fundamentals to applications. A review. J Power Sources 2017; 356: 225-44.

20. Cracknell JA, Vincent KA, Armstrong FA. Enzymes as working or inspirational electrocatalysts for fuel cells and electrolysis. Chem Rev 2008; 108 (7): 2439-61.

21. Flexer V, Durand F, Tsujimura S, Mano N. Efficient Direct Electron Transfer of PQQ-glucose Dehydrogenase on Carbon Cryogel Electrodes at Neutral pH. Anal Chem 2011; 83 (14): 5721-7.

22. Piccolino M. Luigi Galvani and animal electricity: two centuries after the foundation of electrophysiology. Trends Neurosci 1997; 20 (10): 443-8.

23. Parent A. Giovanni Aldini: From animal electricity to human brain stimulation. Can J Neurol Sci 2004; 31 (4): 576-84.

24. Potter MC. Electrical effects accompanying the decomposition of organic compounds. Proceedings of the Royal Society of London Series B-Containing Papers of a Biological Character 1911; 84 (571): 260-76.

25. Cohen B. The bacterial cell as an electrical half cell. Journal of Bacteriology 1935; 21: 18-9.

26. Del Duca MG, Fuscoe JM. Thermodynamics and applications of bioelectrochemical energy conversion systems. Washinton D. C.: National Aeronautics and Space Administration; 1967.

27. Davis JB, Yarbrough HF. Preliminary Experiments on a Microbial Fuel Cell. Science 1962; 137 (3530): 615-&.

28. Yahiro AT, Lee SM, Kimble DO. Bioelectrochemistry I. Enzyme Uutilizing Bio-Fuel Cel Studies. Biochimica Et Biophysica Acta 1964; 88 (2): 375-&.

29. Clark LC, Lyons C. Electrode Systems For Continuous Monitoring In Cardiovascular Surgery. AnnNY AcadSci 1962; 102 (1): 29-&.

30. Updike SJ, Hicks GP. The Enzyme Electrode. Nature 1967; 214: 986.

31. Shleev S, Jarosz-Wilkolazka A, Khalunina A, Morozova O, Yaropolov A, Ruzgas T, et al. Direct electron transfer reactions of laccases from different origins on carbon electrodes. Bioelectrochemistry 2005; 67 (1): 115-24.

32. Shleev S, Tkac J, Christenson A, Ruzgas T, Yaropolov AI, Whittaker JW, et al. Direct electron transfer between copper-containing proteins and electrodes. Biosens Bioelectron 2005; 20 (12): 2517-54.

33. Katz E, Willner I, Kotlyar AB. A non-compartmentalized glucose vertical bar O-2 biofuel cell by bioengineered electrode surfaces. J Electroanal Chem 1999; 479 (1): 64-8.

34. Mano N, Mao F, Heller A. Characteristics of a miniature compartment-less glucose-O-2 biofuel cell and its operation in a living plant. J Am Chem Soc 2003; 125 (21): 6588-94.

35. Cinquin P, Gondran C, Giroud F, Mazabrard S, Pellissier A, Boucher F, et al. A Glucose BioFuel Cell Implanted in Rats. PLoS One 2010; 5 (5): 7.

36. Tokita Y, Nakagawa T, Sakai H, Sugiyama T, Matsumoto R, Hatazawa T. Sony's biofuel cell. ECS Transactions 2008; 13 (21): 89-97.

37. Chen T, Barton SC, Binyamin G, Gao ZQ, Zhang YC, Kim HH, et al. A miniature biofuel cell. J Am Chem Soc 2001; 123 (35): 8630-1.

38. Mano N, Mao F, Shin W, Chen T, Heller A. A miniature biofuel cell operating at 0.78 V. Chem Commun 2003; (4): 518-9.

39. Moore CM, Minteer SD, Martin RS. Microchip-based ethanol/oxygen biofuel cell. Lab Chip 2005; 5 (2): 218-25.

40. Winter M, Brodd RJ. What are batteries, fuel cells, and supercapacitors? Chem Rev 2004; 104 (10): 4245-69.

41. Ramaswamy N, Mukerjee S. Fundamental mechanistic understanding of electrocatalysis of oxygen reduction on Pt and non-Pt surfaces: acid versus alkaline media. Advances in Physical Chemistry 2012; 2012.

42. Shinozaki K, Zack JW, Richards RM, Pivovar BS, Kocha SS. Oxygen Reduction Reaction Measurements on Platinum Electrocatalysts Utilizing Rotating Disk Electrode Technique I. Impact of Impurities, Measurement Protocols and Applied Corrections. J Electrochem Soc 2015; 162 (10): F1144-F58.

43. Mano N, Fernandez JL, Kim Y, Shin W, Bard AJ, Heller A. Oxygen is electroreduced to water on a "wired" enzyme electrode at a lesser overpotential than on platinum. J Am Chem Soc 2003; 125 (50): 15290-1.

44. Gomez-Marin AM, Ticianelli EA. A reviewed vision of the oxygen reduction reaction mechanism on Pt-based catalysts. Curr Opin Electrochem 2018; 9: 129-36.

45. dos Santos L, Climent V, Blanford CF, Armstrong FA. Mechanistic studies of the 'blue' Cu enzyme, bilirubin oxidase, as a highly efficient electrocatalyst for the oxygen reduction reaction. Phys Chem Chem Phys 2010; 12 (42): 13962-74.

46. Mano N, Mao F, Heller A. A miniature biofuel cell operating in a physiological buffer. J Am Chem Soc 2002; 124 (44): 12962-3.

47. Heller A, Feldman B. Electrochemical glucose sensors and their applications in diabetes management. Chem Rev 2008; 108 (7): 2482-505.

48. McCreery RL, Cline KK. Carbon Electrodes. In: Kissinger P, Heineman WR, editors. Laboratory Techniques in Electroanalytical Chemistry. New York: Marcel Dekker Inc.; 1996. p. 293-332.

49. Kinoshita K. Carbon: Electrochemical and Physicochemical Properties. New York: John Wiley & Sons; 1988.

50. Thostenson ET, Ren ZF, Chou TW. Advances in the science and technology of carbon nanotubes and their composites: a review. Compos Sci Technol 2001; 61 (13): 1899-912.

51. Barisci JN, Wallace GG, MacFarlane DR, Baughman RH. Investigation of ionic liquids as electrolytes for carbon nanotube electrodes. Electrochem Commun 2004; 6 (1): 22-7.

52. Hu CH, Ding Y, Ji YP, Xu JH, Hu SS. Fabrication of thin-film electrochemical sensors from single-walled carbon nanotubes by vacuum filtration. Carbon 2010; 48 (5): 1345-52.

53. Gwon H, Kim HS, Lee KU, Seo DH, Park YC, Lee YS, et al. Flexible energy storage devices based on graphene paper. Energy Environ Sci 2011; 4 (4): 1277-83.

54. Hussein L, Urban G, Kruger M. Fabrication and characterization of buckypaper-based nanostructured electrodes as a novel material for biofuel cell applications. Phys Chem Chem Phys 2011; 13 (13): 5831-9.

55. Ciniciato GPMK, Lau C, Cochrane A, Sibbett SS, Gonzalez ER, Atanassov P. Development of paper based electrodes: From air-breathing to paintable enzymatic cathodes. Electrochim Acta 2012; 82: 208-13.

56. Donnet J-B. Carbon black: science and technology. New York: Marcel Dekker, Inc.; 1993.

57. Li J. Carbon-Based Sensors. In: Serp P, Figueiredo JL, editors. Carbon Materials For Catalysis. New Jersey: John Wiley & Sons, Inc.; 2009. p. 507-34.

58. Novoselov KS, Geim AK, Morozov SV, Jiang D, Zhang Y, Dubonos SV, et al. Electric field effect in atomically thin carbon films. Science 2004; 306 (5696): 666-9.

59. Antolini E. Carbon supports for low-temperature fuel cell catalysts. Appl Catal B-Environ 2009; 88 (1-2): 1-24.

60. Goritz D, Raab H, Frohlich J, Maier PG. Surface structure of carbon black and reinforcement. Rubber Chem Technol 1999; 72 (5): 929-45.

61. Three main properties of carbon black Japan: Mitsubishi Chemical Corporation; 2006 [Available from: http://www.carbonblack.jp/en/cb/tokusei.html.

62. Jiang KY, Schadler LS, Siegel RW, Zhang XJ, Zhang HF, Terrones M. Protein immobilization on carbon nanotubes via a two-step process of diimide-activated amidation. J Mater Chem 2004; 14 (1): 37-9.

63. Guiseppi-Elie A, Lei CH, Baughman RH. Direct electron transfer of glucose oxidase on carbon nanotubes. Nanotechnology 2002; 13 (5): 559-64.

64. Liu Y, Wang MK, Zhao F, Xu ZA, Dong SJ. The direct electron transfer of glucose oxidase and glucose biosensor based on carbon nanotubes/chitosan matrix. Biosens Bioelectron 2005; 21 (6): 984-8.

65. Ivnitski D, Branch B, Atanassov P, Apblett C. Glucose oxidase anode for biofuel cell based on direct electron transfer. Electrochem Commun 2006; 8 (8): 1204-10.

66. Devadas B, Mani V, Chen SM. A Glucose/O-2 Biofuel Cell Based on Graphene and Multiwalled Carbon Nanotube Composite Modified Electrode. Int J Electrochem Sci 2012; 7 (9): 8064-75.

67. Jiang YY, Zhang QX, Li FH, Niu L. Glucose oxidase and graphene bionanocomposite bridged by ionic liquid unit for glucose biosensing application. Sens Actuator B-Chem 2012; 161 (1): 728-33.

68. Sehat AA, Khodadadi AA, Shemirani F, Mortazavi Y. Fast Immobilization of Glucose Oxidase on Graphene Oxide for Highly Sensitive Glucose Biosensor Fabrication. Int J Electrochem Sci 2015; 10 (1): 272-86.

69. Aoki K, Okamoto T, Kaneko H, Nozaki K, Negishi A. Applicability Of Graphite Reinforcement Carbon Used As The Lead Of A Mechanical Pencil To Voltammetric Electrodes. J Electroanal Chem 1989; 263 (2): 323-31.

70. Sujaritvanichpong S, Aoki K. Electrode Reactions Of 3,4-Dihydroxyphenylacetic Acid (DOPAC) At Glassy Carbon, Graphite Reinforcement Carbon, And Carbon Fiber Electrodes. Electroanalysis 1989; 1 (5): 397-403.

71. Ishida N, Saito K, inventorsPencil lead and manufacturing method of the same1977.

72. Down MP, Foster CW, Ji XB, Banks CE. Pencil drawn paper based supercapacitors. RSC Adv 2016; 6 (84): 81130-41.

73. Lee SH, Ban JY, Oh CH, Park HK, Choi S. A solvent-free microbial-activated air cathode battery paper platform made with pencil-traced graphite electrodes. Sci Rep 2016; 6: 10.

74. Vishnu N, Kumar AS. A preanodized 6B-pencil graphite as an efficient electrochemical sensor for mono-phenolic preservatives (phenol and meta-cresol) in insulin formulations. Anal Methods 2015; 7 (5): 1943-50.

75. Foster CW, Brownson DAC, de Souza APR, Bernalte E, Iniesta J, Bertotti M, et al. Pencil it in: pencil drawn electrochemical sensing platforms. Analyst 2016; 141 (13): 4055-64.

76. Kariuki JK. An Electrochemical and Spectroscopic Characterization of Pencil Graphite Electrodes. J Electrochem Soc 2012; 159 (9): H747-H51.

77. Tavares PHCP, Barbeira PJS. Influence of pencil lead hardness on voltammetric response of graphite reinforcement carbon electrodes. J Appl Electrochem 2008; 38 (6): 827-32.

78. Teepoo S, Chumsaeng P, Nethan P, Prueprang W, Tumsae P. Highly Sensitive Pencil-Based Renewable Biosensor for Hydrogen Peroxide Detection With a Novel Bionanomultilayer. Int J Electrochem Sci 2012; 7 (5): 4645-56.

79. Wang J, Kawde AN. Pencil-based renewable biosensor for label-free electrochemical detection of DNA hybridization. Anal Chim Acta 2001; 431 (2): 219-24.

80. Buratti S, Scampicchio M, Giovanelli G, Mannino S. A low-cost and low-tech electrochemical flow system for the evaluation of total phenolic content and antioxidant power of tea infusions. Talanta 2008; 75 (1): 312-6.

81. Engstrom RC, Strasser VA. Characterization Of Electrochemically Pretreated Glassy Carbon Electrodes. Anal Chem 1984; 56 (2): 136-41.

82. Wang J, Kawde AN, Sahlin E. Renewable pencil electrodes for highly sensitive stripping potentiometric measurements of DNA and RNA. Analyst 2000; 125 (1): 5-7.

83. Karadeniz H, Erdem A, Caliskan A, Pereira CM, Pereira EM, Ribeiro JA. Electrochemical sensing of silver tags labelled DNA immobilized onto disposable graphite electrodes. Electrochem Commun 2007; 9 (9): 2167-73.

84. Palaska P, Aritzoglou E, Girousi S. Sensitive detection of cyclophosphamide using DNA-modified carbon paste, pencil graphite and hanging mercury drop electrodes. Talanta 2007; 72 (3): 1199-206.

85. Mathur S, Erdem A, Cavelius C, Barth S, Altmayer J. Amplified electrochemical DNA-sensing of nanostructured metal oxide films deposited on disposable graphite electrodes functionalized by chemical vapor deposition. Sens Actuator B-Chem 2009; 136 (2): 432-7.

86. Pournaghi-Azar MH, Ahour F, Hejazi MS. Differential Pulse Voltammetric Detection of Hepatitis C Virus 1a Oligonucleotide Chain by a Label-Free Electrochemical DNA

Hybridization Biosensor Using Consensus Sequence of Hepatitis C Virus 1a Probe on the Pencil Graphite Electrode. Electroanalysis 2009; 21 (16): 1822-8.

87. Engstrom RC. Electrochemical Pretreatment Of Glassy Carbon Electrodes. Anal Chem 1982; 54 (13): 2310-4.

88. Sabzi RE, Sehatnia B, Pournaghi-Azar MH, Hejazi MS. Electrochemical detection of human papilloma virus (HPV) target DNA using MB on pencil graphite electrode. J Iran Chem Soc 2008; 5 (3): 476-83.

89. Ensafi AA, Heydari-Bafrooei E, Amini M. DNA-functionalized biosensor for riboflavin based electrochemical interaction on pretreated pencil graphite electrode. Biosens Bioelectron 2012; 31 (1): 376-81.

90. Ozcan A, Ilkbas S, Ozcan AA. Development of a disposable and low-cost electrochemical sensor for dopamine detection based on poly(pyrrole-3-carboxylic acid)-modified electrochemically over-oxidized pencil graphite electrode. Talanta 2017; 165: 489-95.

91. Majidi MR, Asadpour-Zeynali K, Hafezi B. Reaction and nucleation mechanisms of copper electrodeposition on disposable pencil graphite electrode. Electrochim Acta 2009; 54 (3): 1119-26.

92. McCreery RL. In: Bard AJ, editor. Electroanalytical Chemistry. New York: Marcel Dekker, Inc.; 1991. p. 221-374.

93. Erdem A, Papakonstantinou P, Murphy H. Direct DNA hybridization at disposable graphite electrodes modified with carbon nanotubes. Anal Chem 2006; 78 (18): 6656-9.

94. Yardim Y, Keskin E, Levent A, Ozsoz M, Senturk Z. Voltammetric studies on the potent carcinogen, 7,12-dimethylbenz a anthracene: Adsorptive stripping voltammetric determination in bulk aqueous forms and human urine samples and detection of DNA interaction on pencil graphite electrode. Talanta 2010; 80 (3): 1347-55.

95. Cheng C, Chang KC, Chen CS, Pijanowska DG. Biosensor with Nano-gold Particle Modified Pencil Lead Carbon Electrode for Long-term Glucose Monitoring of Waste Tree Branch Hydrolysis. J Chin Chem Soc 2011; 58 (6): 739-48.

96. Cheng CY, Chang KC, Pijanowska DG. On-line flow injection analysis using gold particle modified carbon electrode amperometric detection for real-time determination of glucose in immobilized enzyme hydrolysate of waste bamboo chopsticks. J Electroanal Chem 2012; 666: 32-41.

97. Elahi MY, Khodadadi AA, Mortazavi Y. A Glucose Biosensor Based on Glucose Oxidase Immobilized on ZnO/Cu2O Graphene Oxide. Nanocomposite Electrode. J Electrochem Soc 2014; 161 (5): B81-B7.

98. Saglam O, Kizilkaya B, Uysal H, Dilgin Y. Biosensing of glucose in flow injection analysis system based on glucose oxidase-quantum dot modified pencil graphite electrode. Talanta 2016; 147: 315-21.

99. Pishko MV, Katakis I, Lindquist SE, Heller A, Degani Y. Electrical communication between graphite electrodes and glucose oxidase/redox polymer complexes. Molecular Crystals and Liquid Crystals 1990; 190: 221-49.

100. Chen CY, Tamiya E, Ishihara K, Kosugi Y, Su YC, Nakabayashi N, et al. A Biocompatible Needle-Type Glucose Sensor Based On Platinum-Electroplated Carbon Electrode. Appl Biochem Biotechnol 1992; 36 (3): 211-26.

101. Jaffari SA, Pickup JC. Novel hexacyanoferrate (III)-modified carbon electrodes: Application in miniaturized biosensors with potential for in vivo glucose sensing. Biosens Bioelectron 1996; 11 (11): 1167-75.

102. Dervisevic M, Cevik E, Senel M. Development of glucose biosensor based on reconstitution of glucose oxidase onto polymeric redox mediator coated pencil graphite electrodes. Enzyme Microb Technol 2015; 68: 69-76.

103. Ertek B, Akgul C, Dilgin Y. Photoelectrochemical glucose biosensor based on a dehydrogenase enzyme and NAD(+)/NADH redox couple using a quantum dot modified pencil graphite electrode. RSC Adv 2016; 6 (24): 20058-66.

104. Barberis A, Spissu Y, Bazzu G, Fadda A, Azara E, Sanna D, et al. Development and Characterization of an Ascorbate Oxidase-based Sensor-Biosensor System for Telemetric Detection of AA and Antioxidant Capacity in Fresh Orange Juice. Anal Chem 2014; 86 (17): 8727-34.

105. Barberis A, Spissu Y, Fadda A, Azara E, Bazzu G, Marceddu S, et al. Simultaneous amperometric detection of ascorbic acid and antioxidant capacity in orange, blueberry and kiwi juice, by a telemetric system coupled with a fullerene- or nanotubes-modified ascorbate subtractive biosensor. Biosens Bioelectron 2015; 67: 214-23.

106. Chauhan N, Narang J, Pundir CS. Amperometric determination of serum cholesterol with pencil graphite rod. American Journal of Analytical Chemistry 2010; 1 (02): 41.

107. Narang J, Malhotra N, Singh G, Pundir CS. Electrochemical impediometric detection of anti-HIV drug taking gold nanorods as a sensing interface. Biosens Bioelectron 2015; 66: 332-7.

108. Zhu J, Wu XY, Shan D, Yuan PX, Zhang XJ. Sensitive electrochemical detection of NADH and ethanol at low potential based on pyrocatechol violet electrodeposited on single walled carbon nanotubes-modified pencil graphite electrode. Talanta 2014; 130: 96-102.

109. Dervisevic M, Cevik E, Durmus Z, Senel M. Electrochemical sensing platforms based on the different carbon derivative incorporated interface. Materials science & engineering C, Materials for biological applications 2016; 58: 790-8.

110. Dagar K, Pundir CS. An improved amperometric L-lactate biosensor based on covalent immobilization of microbial lactate oxidase onto carboxylated multiwalled carbon nanotubes/copper nanoparticles/polyaniline modified pencil graphite electrode. Enzyme Microb Technol 2017; 96: 177-86.

111. Batra B, Yadav M, Pundir CS. L-Glutamate biosensor based on L-glutamate oxidase immobilized onto ZnO nanorods/polypyrrole modified pencil graphite electrode. Biochem Eng J 2016; 105: 428-36.

112. Wilkins E, Carter M, Voss J, Ivnitski D. A quantitative determination of organophosphate pesticides in organic solvents. Electrochem Commun 2000; 2 (11): 786-90.

113. Kashyap D, Kim C, Kim SY, Kim YH, Kim GM, Dwivedi PK, et al. Multi walled carbon nanotube and polyaniline coated pencil graphite based bio-cathode for enzymatic biofuel cell. Int J Hydrog Energy 2015; 40 (30): 9515-22.

114. Torrinha A, Montenegro MCBSM, Araujo AN. Implementation of a Simple Nanostructured Bio-electrode with Immobilized Rhus Vernicifera Laccase for Oxygen Sensing Applications. Electroanalysis 2017; 29 (6): 1566-72.

115. Tsai WC, Wen ST. Determination of uric acid in serum by a mediated amperometric biosensor. Anal Lett 2006; 39 (5): 891-901.

116. Devi R, Yadav S, Nehra R, Yadav S, Pundir CS. Electrochemical biosensor based on gold coated iron nanoparticles/chitosan composite bound xanthine oxidase for detection of xanthine in fish meat. J Food Eng 2013; 115 (2): 207-14.

117. Dervisevic M, Custiuc E, Cevik E, Senel M. Construction of novel xanthine biosensor by using polymeric mediator/MWCNT nanocomposite layer for fish freshness detection. Food Chem 2015; 181: 277-83.

118. Dervisevic M, Dervisevic E, Azak H, Cevik E, Senel M, Yildiz HB. Novel amperometric xanthine biosensor based on xanthine oxidase immobilized on electrochemically polymerized 10 4H-dithieno(3,2-b:2 ',3 '-d)pyrrole-4-yl decane-1-amine film. Sens Actuator B-Chem 2016; 225: 181-7.

119. Hitaishi VP, Clement R, Bourassin N, Baaden M, De Poulpiquet A, Sacquin-Mora S, et al. Controlling Redox Enzyme Orientation at Planar Electrodes. Catalysts 2018; 8 (5): 192.

120. Wang J. Glucose biosensors: 40 years of advances and challenges. Electroanalysis 2001; 13 (12): 983-8.

121. Wilson R, Turner APF. Glucose-Oxidase - an Ideal Enzyme. Biosens Bioelectron 1992; 7 (3): 165-85.

122. Anthony C, Williams P. The structure and mechanism of methanol dehydrogenase. BBA-Proteins Proteomics 2003; 1647 (1-2): 18-23.

123. Gorton L. Carbon Paste Electrodes Modified Withe Enzymes, Tissues, And Cells. Electroanalysis 1995; 7 (1): 23-45.

124. Mano N, Edembe L. Bilirubin oxidases in bioelectrochemistry: Features and recent findings. Biosens Bioelectron 2013; 50: 478-85.

125. Solomon EI, Sundaram UM, Machonkin TE. Multicopper oxidases and oxygenases. Chem Rev 1996; 96 (7): 2563-605.

126. Piontek K, Antorini M, Choinowski T. Crystal structure of a laccase from the fungus Trametes versicolor at 1.90-angstrom resolution containing a full complement of coppers. J Biol Chem 2002; 277 (40): 37663-9.

127. Solomon EI, Augustine AJ, Yoon J. O2Reduction to H2O by the multicopper oxidases. Dalton Transactions 2008; (30): 3921-32.

128. Farver O, Skov LK, Pascher T, Karlsson BG, Nordling M, Lundberg LG, et al. Intramolecular Electron Transfer In Single Site Mutated Azurins. Biochemistry 1993; 32 (28): 7317-22.

129. Lee CW, Gray HB, Anson FC, Malmstrom BG. Catalysis of the reduction of dioxygen at graphite electrodes coated with fungal laccase. J Electroanal Chem 1984; 172 (1-2): 289-300.

130. Yaropolov AI, Kharybin AN, Emneus J, MarkoVarga G, Gorton L. Electrochemical properties of some copper-containing oxidases. Bioelectrochem Bioenerg 1996; 40 (1): 49-57.

131. Johnson DL, Thompson JL, Brinkmann SM, Schuller KA, Martin LL. Electrochemical characterization of purified Rhus vernicifera laccase: Voltammetric evidence for a sequential four-electron transfer. Biochemistry 2003; 42 (34): 10229-37.

132. Wu XM, Hu YJ, Jin J, Zhou NL, Wu P, Zhang H, et al. Electrochemical Approach for Detection of Extracellular Oxygen Released from Erythrocytes Based on Graphene Film

Integrated with Laccase and 2,2-Azino-bis(3-ethylbenzothiazoline-6-sulfonic acid). Anal Chem 2010; 82 (9): 3588-96.

133. Katz E, Lioubashevski O, Willner I. Magnetic field effects on bioelectrocatalytic reactions of surface-confined enzyme systems: Enhanced performance of biofuel cells. J Am Chem Soc 2005; 127 (11): 3979-88.

134. Pizzariello A, Stred'ansky M, Miertus S. A glucose/hydrogen peroxide biofuel cell that uses oxidase and peroxidase as catalysts by composite bulk-modified bioelectrodes based on a solid binding matrix. Bioelectrochemistry 2002; 56 (1-2): 99-105.

135. Kim HH, Mano N, Zhang XC, Heller A. A miniature membrane-less biofuel cell operating under physiological conditions at 0.5 V. J Electrochem Soc 2003; 150 (2): A209-A13.

136. Barriere F, Kavanagh P, Leech D. A laccase-glucose oxidase biofuel cell prototype operating in a physiological buffer. Electrochim Acta 2006; 51 (24): 5187-92.

137. Habrioux A, Merle G, Servat K, Kokoh KB, Innocent C, Cretin M, et al. Concentric glucose/O-2 biofuel cell. J Electroanal Chem 2008; 622 (1): 97-102.

138. Hansen BJ, Liu Y, Yang RS, Wang ZL. Hybrid Nanogenerator for Concurrently Harvesting Biomechanical and Biochemical Energy. ACS Nano 2010; 4 (7): 3647-52.

139. Zhao M, Gao Y, Sun JY, Gao F. Mediator less Glucose Biosensor and Direct Electron Transfer Type Glucose/Air Biofuel Cell Enabled with Carbon Nanodots. Anal Chem 2015; 87 (5): 2615-22.

140. Tsujimura S, Kano K, Ikeda T. Glucose/O-2 biofuel cell operating at physiological conditions. Electrochemistry 2002; 70 (12): 940-2.

141. Okuda J, Yamazaki T, Fukasawa M, Kakehi N, Sode K. The application of engineered glucose dehydrogenase to a direct electron-transfer-type continuous glucose monitoring system and a compartmentless biofuel cell. Anal Lett 2007; 40 (3): 431-40.

142. Pinyou P, Conzuelo F, Sliozberg K, Vivekananthan J, Contin A, Poller S, et al. Coupling of an enzymatic biofuel cell to an electrochemical cell for self-powered glucose sensing with optical readout. Bioelectrochemistry 2015; 106: 22-7.

143. Cadet M, Gounel S, Stines-Chaumeil C, Brilland X, Rouhana J, Louerat F, et al. An enzymatic glucose/O-2 biofuel cell operating in human blood. Biosens Bioelectron 2016; 83: 60-7.

144. Witt S, Wohlfahrt G, Schomburg D, Hecht HJ, Kalisz HM. Conserved arginine-516 of Penicillium amagasakiense glucose oxidase is essential for the efficient binding of beta-D-glucose. Biochem J 2000; 347: 553-9.

145. Ivnitski D, Artyushkova K, Rincon RA, Atanassov P, Luckarift HR, Johnson GR. Entrapment of enzymes and carbon nanotubes in biologically synthesized silica: Glucose oxidase-catalyzed direct electron transfer. Small 2008; 4 (3): 357-64.

146. Zhao S, Zhang K, Bai Y, Yang WW, Sun CQ. Glucose oxidase/colloidal gold nanoparticles immobilized in Nafion film on glassy carbon electrode: Direct electron transfer and electrocatalysis. Bioelectrochemistry 2006; 69 (2): 158-63.

147. Ivnitski D, Atanassov P, Apblett C. Direct bioelectrocatalysis of PQQ-dependent glucose dehydrogenase. Electroanalysis 2007; 19 (15): 1562-8.

148. Yamada M, Sumi K, Matsushita K, Adachi O, Yamada Y. Topological Analysis Of Quinoprotein Glucose Dehydrogenase In Escherichia Coli And Its Ubiquinone Binding Site. J Biol Chem 1993; 268 (17): 12812-7.

149. Olsthoorn AJJ, Duine JA. Production, characterization, and reconstitution of recombinant quinoprotein glucose dehydrogenase (soluble type; EC 1.1.99.17) apoenzyme of Acinetobacter calcoaceticus. Arch Biochem Biophys 1996; 336 (1): 42-8.

150. Dokter P, Frank J, Duine JA. Purification And Characterization Of Quinoprotein Glucose Dehydrogenase From Acinetobacter-calcoaceticus LMD-79.41. Biochem J 1986; 239 (1): 163-7.

151. Gobel G, Schubart IW, Scherbahn V, Lisdat F. Direct electron transfer of PQQ-glucose dehydrogenase at modified carbon nanotubes electrodes. Electrochem Commun 2011; 13 (11): 1240-3.

152. Manz A, Graber N, Widmer HM. Miniaturized total chemical analysis systems - a novel concept for chemical sensing. Sens Actuator B-Chem 1990; 1 (1-6): 244-8.

153. Figeys D, Pinto D. Lab-on-a-chip: A revolution in biological and medical sciences. Anal Chem 2000; 72 (9): 330A-5A.

154. Mark D, Haeberle S, Roth G, von Stetten F, Zengerle R. Microfluidic lab-on-a-chip platforms: requirements, characteristics and applications. Chem Soc Rev 2010; 39 (3): 1153-82.

155. Beebe DJ, Mensing GA, Walker GM. Physics and applications of microfluidics in biology. Annual review of biomedical engineering 2002; 4: 261-86.

156. Geankoplis C. Transport processes and unit operations. third edition ed. New Jersey, USA: Prentice-Hall International, Inc.; 1993.

157. Perry RH, Green DW, Maloney JO. Perry's chemical engineer's handbook. seventh edition ed. USA: McGraw-Hill; 1997.

158. Choban ER, Markoski LJ, Wieckowski A, Kenis PJA. Microfluidic fuel cell based on laminar flow. J Power Sources 2004; 128 (1): 54-60.

159. Kjeang E, Djilali N, Sinton D. Microfluidic fuel cells: A review. J Power Sources 2009; 186 (2): 353-69.

160. Liana DD, Raguse B, Gooding JJ, Chow E. Recent Advances in Paper-Based Sensors. Sensors 2012; 12 (9): 11505-26.

161. Yang Y, Liu TY, Tao K, Chang HL. Generating Electricity on Chips: Microfluidic Biofuel Cells in Perspective. Ind Eng Chem Res 2018; 57 (8): 2746-58.

162. Grover WH, Skelley AM, Liu CN, Lagally ET, Mathies RA. Monolithic membrane valves and diaphragm pumps for practical large-scale integration into glass microfluidic devices. Sens Actuator B-Chem 2003; 89 (3): 315-23.

163. Iwai K, Sochol RD, Lin L, Ieee. Finger-powered, pressure-driven microfluidic pump. 2011 Ieee 24th International Conference on Micro Electro Mechanical Systems. Proceedings: Ieee Micro Electro Mechanical Systems. New York: Ieee; 2011. p. 1131-4.

164. Li W, Chen T, Chen Z, Fei P, Yu Z, Pang Y, et al. Squeeze-chip: a finger-controlled microfluidic flow network device and its application to biochemical assays. Lab Chip 2012; 12 (9): 1587-90.

165. Xu KR, Begley MR, Landers JP. Simultaneous metering and dispensing of multiple reagents on a passively controlled microdevice solely by finger pressing. Lab Chip 2015; 15 (3): 867-76.

166. Lim KG, Palmore GTR. Microfluidic biofuel cells: The influence of electrode diffusion layer on performance. Biosens Bioelectron 2007; 22 (6): 941-7.

167. Zebda A, Renaud J, Cretin M, Pichot F, Innocent C, Ferrigno R, et al. A microfluidic glucose biofuel cell to generate micropower from enzymes at ambient temperature. Electrochem Commun 2009; 11 (3): 592-5.

168. Zebda A, Renaud L, Cretin M, Innocent C, Ferrigno R, Tingry S. Membrane less microchannel glucose biofuel cell with improved electrical performances. Sens Actuator B-Chem 2010; 149 (1): 44-50.

169. Zhou M, Chen CG, Du Y, Li BL, Wen D, Dong SJ, et al. An IMP-Reset gate-based reusable and self-powered "smart" logic aptasensor on a microfluidic biofuel cell. Lab Chip 2010; 10 (21): 2932-6.

170. Renaud L, Selloum D, Tingry S. Xurography for 2D and multi-level glucose/O-2 microfluidic biofuel cell. Microfluid Nanofluid 2015; 18 (5-6): 1407-16.

171. Desmaele D, Renaud L, Tingry S. A wireless sensor powered by a flexible stack of membraneless enzymatic biofuel cells. Sens Actuator B-Chem 2015; 220: 583-9.

172. Selloum D, Tingry S, Lecher V, Renaud L, Innocent C, Zouaoui A. Optimized electrode arrangement and activation of bioelectrodes activity by carbon nanoparticles for efficient ethanol microfluidic biofuel cells. J Power Sources 2014; 269: 834-40.

173. Desmaele D, Nguyen-Boisse TT, Renaud L, Tingry S. Integration of cantilevered porous electrodes into microfluidic co-laminar enzymatic biofuel cells: Toward higher enzyme loadings for enhanced performance. Microelectron Eng 2016; 165: 23-6.

174. Galindo-de-la-Rosa J, Arjona N, Moreno-Zuria A, Ortiz-Ortega E, Guerra-Balcazar M, Ledesma-Garcia J, et al. Evaluation of single and stack membraneless enzymatic fuel cells based on ethanol in simulated body fluids. Biosens Bioelectron 2017; 92: 117-24.

175. Togo M, Takamura A, Asai T, Kaji H, Nishizawa M. An enzyme-based microfluidic biofuel cell using vitamin K-3-mediated glucose oxidation. Electrochim Acta 2007; 52 (14): 4669-74.

176. Togo M, Takamura A, Asai T, Kaji H, Nishizawa M. Structural studies of enzyme-based microfluidic biofuel cells. J Power Sources 2008; 178 (1): 53-8.

177. Galindo R, Dector A, Arriaga LG, Gutierrez S, Herrasti P. Maghemite as a catalyst for glucose oxidation in a microfluidic fuel cell. J Electroanal Chem 2012; 671: 38-43.

178. Beneyton T, Wijaya IPM, Ben Salem C, Griffiths AD, Taly V. Membraneless glucose/O-2 microfluidic biofuel cells using covalently bound enzymes. Chem Commun 2013; 49 (11): 1094-6.

179. Gonzalez-Guerrero MJ, Esquivel JP, Sanchez-Molas D, Godignon P, Munoz FX, del Campo FJ, et al. Membraneless glucose/O-2 microfluidic enzymatic biofuel cell using pyrolyzed photoresist film electrodes. Lab Chip 2013; 13 (15): 2972-9.

180. Gonzalez-Guerrero MJ, del Campo FJ, Esquivel JP, Giroud F, Minteer SD, Sabate N. Paper-based enzymatic microfluidic fuel cell: From a two-stream flow device to a single-stream lateral flow strip. J Power Sources 2016; 326: 410-6.

181. Gonzalez-Guerrero MJ, del Campo FJ, Esquivel JP, Leech D, Sabate N. Paper-based microfluidic biofuel cell operating under glucose concentrations within physiological range. Biosens Bioelectron 2017; 90: 475-80.

182. Dector A, Escalona-Villalpando RA, Dector D, Vallejo-Becerra V, Chavez-Ramirez AU, Arriaga LG, et al. Perspective use of direct human blood as an energy source in air-breathing hybrid microfluidic fuel cells. J Power Sources 2015; 288: 70-5.

183. Escalona-Villalpando RA, Dector A, Dector D, Moreno-Zuria A, Duron-Torres SM, Galvan-Valencia M, et al. Glucose microfluidic fuel cell using air as oxidant. Int J Hydrog Energy 2016; 41 (48): 23394-400.

184. Noh HB, Shim YB. Catalytic activity of polymerized self-assembled artificial enzyme nanoparticles: applications to microfluidic channel-glucose biofuel cells and sensors. J Mater Chem A 2016; 4 (7): 2720-8.

185. Zhang LL, Zhou M, Wen D, Bai L, Lou BH, Dong SJ. Small-size biofuel cell on paper. Biosens Bioelectron 2012; 35 (1): 155-9.

186. Villarrubia CWN, Lau C, Ciniciato G, Garcia SO, Sibbett SS, Petsev DN, et al. Practical electricity generation from a paper based biofuel cell powered by glucose in ubiquitous liquids. Electrochem Commun 2014; 45: 44-7.

187. Villarrubia CWN, Soavi F, Santoro C, Arbizzani C, Serov A, Rojas-Carbonell S, et al. Self-feeding paper based biofuel cell/self-powered hybrid mu-supercapacitor integrated system. Biosens Bioelectron 2016; 86: 459-65.

188. Miyake T, Yoshino S, Yamada T, Hata K, Nishizawa M. Self-Regulating Enzyme-Nanotube Ensemble Films and Their Application as Flexible Electrodes for Biofuel Cells. J Am Chem Soc 2011; 133 (13): 5129-34.

189. Wu XE, Guo YZ, Chen MY, Chen XD. Fabrication of flexible and disposable enzymatic biofuel cells. Electrochim Acta 2013; 98: 20-4.

190. Escalona-Villalpando RA, Reid RC, Milton RD, Arriaga LG, Minteer SD, Ledesma-Garcia J. Improving the performance of lactate/oxygen biofuel cells using a microfluidic design. J Power Sources 2017; 342: 546-52.

191. Reid RC, Giroud F, Minteer SD, Gale BK. Enzymatic Biofuel Cell with a Flow-through Toray Paper Bioanode for Improved Fuel Utilization. J Electrochem Soc 2013; 160 (9): H612-H9.

192. Bedekar AS, Feng JJ, Krishnamoorthy S, Lim KG, Palmore GTR, Sundaram S. Oxygen limitation in microfluidic biofuel cells. Chem Eng Commun 2008; 195 (3): 256-66.

193. Miyake T, Oike M, Yoshino S, Yatagawa Y, Haneda K, Nishizawa M. Automatic, sequential power generation for prolonging the net lifetime of a miniature biofuel cell stack. Lab Chip 2010; 10 (19): 2574-8.

194. du Toit H, Rashidi R, Ferdani DW, Delgado-Charro MB, Sangan CM, Di Lorenzo M. Generating power from transdermal extracts using a multi-electrode miniature enzymatic fuel cell. Biosens Bioelectron 2016; 78: 411-7.

195. Koide S, Sasaki T, Sano R, Mogi H, Fukushi Y, Nishioka Y. Flexible biofuel cell with electrodes modified by glucose oxidase-ferrocene and bilirubin oxidase fabricated using microfabrication processes. Journal of the Chinese Advanced Materials Society 2014; 2 (3): 159-70.

196. Kissinger PT, Preddy CR, Shoup RE, Heineman WR. Fundamental Concepts of Analytical Electrochemistry. In: Kissinger PT, Heineman WR, editors. Laboratory Techniques in Electroanalytical Chemistry. New York: Marcel Dekker, Inc.; 1996. p. 11-50.

197. Bard AJ, Faulkner LR. Electrochemical methods: Fundamentals and applications. Second edition ed. USA: John Wiley & Sons, Inc.; 2001.

198. Elgrishi N, Rountree KJ, McCarthy BD, Rountree ES, Eisenhart TT, Dempsey JL. A Practical Beginner's Guide to Cyclic Voltammetry. J Chem Educ 2018; 95 (2): 197-206.

199. Inzelt G. Chronoamperometry, Chronocoulometry, and Chronopotentiometry. In: Kreysa G, Ota K-i, Savinell RF, editors. Encyclopedia of applied electrochemistry. New York: Springer Science & Business Media; 2014. p. 207-14.

200. Strack G, Nichols RK, Atanassov P, Luckarift HR, Johnson GR. Modification of Carbon Nanotube Electrodes with 1-Pyrenebutanoic Acid, Succinimidyl Ester for Enhanced Bioelectrocatalysis. In: Guisan JM, editor. Immobilization of Enzymes and Cells. Methods in Molecular Biology. 1051. Third edition ed. New York: Springer Science & Business Media; 2013.

201. Lvovich VF. Electrochemical Impedance Spectroscopy (EIS) Applications to Sensors and Diagnostics. In: Kreysa G, Ota K-i, Savinell RF, editors. Encyclopedia of applied electrochemistry. New York: Springer Science & Business Media; 2014. p. 485-507.

202. Gamelas JAF, Pontes ASN, Evtuguin DV, Xavier A, Esculcas AP. New polyoxometalate-laccase integrated system for kraft pulp delignification. Biochem Eng J 2007; 33 (2): 141-7.

203. Arica MY, Altintas B, Bayramoglu G. Immobilization of laccase onto spacer-arm attached non-porous poly(GMA/EGDMA) beads: Application for textile dye degradation. Bioresour Technol 2009; 100 (2): 665-9.

204. Kamitaka Y, Tsujimura S, Setoyama N, Kajino T, Kano K. Fructose/dioxygen biofuel cell based on direct electron transfer-type bioelectrocatalysis. Phys Chem Chem Phys 2007; 9 (15): 1793-801.

205. Lee SK, George SD, Antholine WE, Hedman B, Hodgson KO, Solomon EI. Nature of the intermediate formed in the reduction of O-2 to H2O at the trinuclear copper cluster active site in native laccase. J Am Chem Soc 2002; 124 (21): 6180-93.

206. Pankratov DV, Zeifman YS, Morozova OV, Shumakovich GP, Vasil'eva IS, Shleev S, et al. A Comparative Study of Biocathodes Based on Multiwall Carbon Nanotube Buckypapers Modified with Three Different Multicopper Oxidases. Electroanalysis 2013; 25 (5): 1143-9.

207. Gupta G, Rajendran V, Atanassov P. Bioelectrocatalysis of oxygen reduction reaction by laccase on gold electrodes. Electroanalysis 2004; 16 (13-14): 1182-5.

208. Wang J. Carbon-nanotube based electrochemical biosensors: A review. Electroanalysis 2005; 17 (1): 7-14.

209. Vashist SK, Luong JHT. Recent advances in electrochemical biosensing schemes using graphene and graphene-based nanocomposites. Carbon 2015; 84: 519-50.

210. Zhou M, Zhai YM, Dong SJ. Electrochemical Sensing and Biosensing Platform Based on Chemically Reduced Graphene Oxide. Anal Chem 2009; 81 (14): 5603-13.

211. Ambrosi A, Bonanni A, Sofer Z, Cross JS, Pumera M. Electrochemistry at Chemically Modified Graphenes. Chem-Eur J 2011; 17 (38): 10763-70.

212. Alwarappan S, Erdem A, Liu C, Li CZ. Probing the Electrochemical Properties of Graphene Nanosheets for Biosensing Applications. J Phys Chem C 2009; 113 (20): 8853-7.

213. Shao YY, Wang J, Engelhard M, Wang CM, Lin YH. Facile and controllable electrochemical reduction of graphene oxide and its applications. J Mater Chem 2010; 20 (4): 743-8.

214. Fernandez-Fernandez M, Sanroman MA, Moldes D. Recent developments and applications of immobilized laccase. Biotechnol Adv 2013; 31 (8): 1808-25.

215. Liu Y, Huang L, Dong S. Electrochemical catalysis and thermal stability characterization of laccase-carbon nanotubes-ionic liquid nanocomposite modified graphite electrode. Biosens Bioelectron 2007; 23 (1): 35-41.

216. Blanford CF, Heath RS, Armstrong FA. A stable electrode for high-potential, electrocatalytic O-2 reduction based on rational attachment of a blue copper oxidase to a graphite surface. Chem Commun 2007; (17): 1710-2.

217. Shrier A, Giroud F, Rasmussen M, Minteer SD. Operational Stability Assays for Bioelectrodes for Biofuel Cells: Effect of Immobilization Matrix on Laccase Biocathode Stability. J Electrochem Soc 2014; 161 (4): H244-H8.

218. Jarosz-Wilkolazka A, Ruzgas T, Gorton L. Amperometric detection of mono- and diphenols at Cerrena unicolor laccase-modified graphite electrode: correlation between sensitivity and substrate structure. Talanta 2005; 66 (5): 1219-24.

219. Szot K, Nogala W, Niedziolka-Jonsson J, Jonsson-Niedziolka M, Marken F, Rogalski J, et al. Hydrophilic carbon nanoparticle-laccase thin film electrode for mediatorless dioxygen reduction SECM activity mapping and application in zinc-dioxygen battery. Electrochim Acta 2009; 54 (20): 4620-5.

220. Sun DM, Cai CX, Xing W, Lu TH. Immobilization and direct electrochemistry of copper-containing enzymes on active carbon. Chin Sci Bull 2004; 49 (23): 2452-4.

221. Wang KQ, Tang J, Zhang ZM, Gao Y, Chen G. Laccase on Black Pearl 2000 modified glassy carbon electrode: Characterization of direct electron transfer and biological sensing properties for pyrocatechol. Electrochim Acta 2012; 70: 112-7.

222. Shin W, Lee J, Kim Y, Steinfink H, Heller A. Ionic conduction in Zn-3(PO4)(2)(.)4H(2)O enables efficient discharge of the zinc anode in serum. J Am Chem Soc 2005; 127 (42): 14590-1.

223. Harper JC, Lopez DM, Larkin EC, Economides MK, McIntyre SK, Alam TM, et al. Encapsulation of S. cerevisiae in Poly(glycerol) Silicate Derived Matrices: Effect of Matrix Additives and Cell Metabolic Phase on Long-Term Viability and Rate of Gene Expression. Chem Mat 2011; 23 (10): 2555-64.

224. Konopka SJ, McDuffie B. Diffusion coefficients of ferricyanide and ferrocyanidde ions in aqueous media using twin electrode thin-layer electrochemistry. Anal Chem 1970; 42 (14): 1741-&.

225. Mani V, Devadas B, Chen SM. Direct electrochemistry of glucose oxidase at electrochemically reduced graphene oxide-multiwalled carbon nanotubes hybrid material modified electrode for glucose biosensor. Biosens Bioelectron 2013; 41: 309-15.

226. Chen LY, Tang YH, Wang K, Liu CB, Luo SL. Direct electrodeposition of reduced graphene oxide on glassy carbon electrode and its electrochemical application. Electrochem Commun 2011; 13 (2): 133-7.

227. Gill I, Ballesteros A. Bioencapsulation within synthetic polymers (Part 1): sol-gel encapsulated biologicals. Trends Biotechnol 2000; 18 (7): 282-96.

228. Khonina TG, Safronov AP, Shadrina EV, Ivanenko MV, Suvorova AI, Chupakhin ON. Mechanism of structural networking in hydrogels based on silicon and titanium glycerolates. J Colloid Interface Sci 2012; 365 (1): 81-9.

229. Andreasson LE, Reinhammar B. The mechanism of electron transfer in laccase-catalysed reactions. Biochimica Et Biophysica Acta 1979; 568: 145-56.

230. Jones SM, Solomon EI. Electron transfer and reaction mechanism of laccases. Cell Mol Life Sci 2015; 72 (5): 869-83.

231. Solomon EI, Chen P, Metz M, Lee SK, Palmer AE. Oxygen binding, activation, and reduction to water by copper proteins. Angew Chem-Int Edit 2001; 40 (24): 4570-90.

232. Zawisza I, Rogalski J, Opallo M. Electrocatalytic reduction of dioxygen by redox mediator and laccase immobilized in silicate thin film. J Electroanal Chem 2006; 588 (2): 244-52.

233. Rowinski P, Bilewicz R, Stebe MJ, Rogalska E. Electrodes modified with monoolein cubic phases hosting laccases for the catalytic reduction of dioxygen. Anal Chem 2004; 76 (2): 283-91.

234. Haghighi B, Gorton L, Ruzgas T, Jonsson LJ. Characterization of graphite electrodes modified with laccase from Trametes versicolor and their use for bioelectrochemical monitoring of phenolic compounds in flow injection analysis. Anal Chim Acta 2003; 487 (1): 3-14.

235. Barton SC, Kim HH, Binyamin G, Zhang YC, Heller A. Electroreduction of O-2 to water on the "Wired" laccase cathode. J Phys Chem B 2001; 105 (47): 11917-21.

236. Mousty C, Vieille L, Cosnier S. Laccase immobilization in redox active layered double hydroxides: A reagentless amperometric biosensor. Biosens Bioelectron 2007; 22 (8): 1733-8.

237. Gutierrez-Sanchez C, Shleev S, De Lacey AL, Pita M. Third-generation oxygen amperometric biosensor based on Trametes hirsuta laccase covalently bound to graphite electrode. Chem Pap 2015; 69 (1): 237-40.

238. Liu Y, Qu XH, Guo HW, Chen HJ, Liu BF, Dong SJ. Facile preparation of amperometric laccase biosensor with multifunction based on the matrix of carbon nanotubes-chitosan composite. Biosens Bioelectron 2006; 21 (12): 2195-201.

239. Delanoy G, Li Q, Yu J. Activity and stability of laccase in conjugation with chitosan. Int J Biol Macromol 2005; 35 (1-2): 89-95.

240. The Dissolved Oxygen Handbook. YSI Incorporated; 2009.

241. Gallaway J, Wheeldon I, Rincon R, Atanassov P, Banta S, Barton SC. Oxygen-reducing enzyme cathodes produced from SLAC, a small laccase from Streptomyces coelicolor. Biosens Bioelectron 2008; 23 (8): 1229-35.

242. Moehlenbrock MJ, Arechederra RL, Sjoholm KH, Minteer SD. Analytical Techniques for Characterizing Enzymatic Biofuel Cells. Anal Chem 2009; 81 (23): 9538-45.

243. Zheng W, Li QF, Su L, Yan YM, Zhang J, Mao LQ. Direct electrochemistry of multi-copper oxidases at carbon nanotubes noncovalently functionalized with cellulose derivatives. Electroanalysis 2006; 18 (6): 587-94.

244. Mašek J. A simple microcoulometric arrangement for polarographic purposes using the three-electrode system. Journal of Electroanalytical Chemistry (1959) 1960; 1 (5): 416-21.

245. Akanda MR, Sohail M, Aziz MA, Kawde AN. Recent Advances in Nanomaterial-Modified Pencil Graphite Electrodes for Electroanalysis. Electroanalysis 2016; 28 (3): 408-24.

246. David IG, Popa DE, Buleandra M. Pencil Graphite Electrodes: A Versatile Tool in Electroanalysis. J Anal Methods Chem 2017: 22.

247. Kawde AN, Baig N, Sajid M. Graphite pencil electrodes as electrochemical sensors for environmental analysis: a review of features, developments, and applications. RSC Adv 2016; 6 (94): 91325-40.

248. Torrinha A, Amorim CG, Montenegro MCBSM, Araujo AN. Biosensing based on pencil graphite electrodes. Talanta 2018; 190: 235-47.

249. Heller A. Electrical wiring of redox enzymes. Accounts Chem Res 1990; 23 (5): 128-34.

250. Ramasamy RP, Luckarift HR, Ivnitski DM, Atanassov PB, Johnson GR. High electrocatalytic activity of tethered multicopper oxidase-carbon nanotube conjugates. Chem Commun 2010; 46 (33): 6045-7.

251. Bandapati M, Dwivedi PK, Krishnamurthy B, Kim YH, Kim GM, Goel S. Screening various pencil leads coated with MWCNT and PANI as enzymatic biofuel cell biocathode. Int J Hydrog Energy 2017; 42 (44): 27220-9.

252. Yuan X-ZR, Song C, Wang H, Zhang J. Electrochemical impedance spectroscopy in PEM fuel cells: fundamentals and applications: Springer Science & Business Media; 2009.

253. Kamau GN. Surface preparation of glassy carbon electrodes. Anal Chim Acta 1988; 207 (1-2): 1-16.

254. Rezaei B, Esfahani MH, Ensafi AA. Modified Au Nanoparticles/Imprinted Sol-Gel/Multiwall Carbon Nanotubes Pencil Graphite Electrode as a Selective Electrochemical Sensor for Papaverine Determination. IEEE Sens J 2016; 16 (19): 7037-44.

255. Karakaya S, Dilgin Y. Flow Injection Amperometric Analysis of H2O2 at Platinum Nanoparticles Modified Pencil Graphite Electrode. Electroanalysis 2017; 29 (6): 1626-34.

256. Vishnu N, Gandhi M, Rajagopal D, Kumar AS. Pencil graphite as an elegant electrochemical sensor for separation-free and simultaneous sensing of hypoxanthine, xanthine and uric acid in fish samples. Anal Methods 2017; 9 (15): 2265-74.

257. Strack G, Luckarift HR, Sizemore SR, Nichols RK, Farrington KE, Wu PK, et al. Power generation from a hybrid biological fuel cell in seawater. Bioresour Technol 2013; 128: 222-8.

258. Lopez RJ, Babanova S, Ulyanova Y, Singhal S, Atanassov P. Improved Interfacial Electron Transfer in Modified Bilirubin Oxidase Biocathodes. ChemElectroChem 2014; 1 (1): 241-8.

259. Chakraborty S, Babanova S, Rocha RC, Desireddy A, Artyushkova K, Boncella AE, et al. A Hybrid DNA-Templated Gold Nanocluster For Enhanced Enzymatic Reduction of Oxygen. J Am Chem Soc 2015; 137 (36): 11678-87.

260. Li DA, Okajima T, Mao LQ, Ohsaka T. Bioelectrocatalytic Oxygen Reduction Reaction by Bilirubin Oxidase Adsorbed on Glassy Carbon and Edge-Plane Pyrolytic Graphite Electrodes: Effect of Redox Mediators. Int J Electrochem Sci 2014; 9 (3): 1390-8.

261. Palys B, Bokun A, Rogalski J. Poly-o-phenylenediamine as redox mediator for laccase. Electrochim Acta 2007; 52 (24): 7075-82.

262. Garcia-Ochoa F, Gomez E, Santos VE, Merchuk JC. Oxygen uptake rate in microbial processes: an overview. Biochem Eng J 2010; 49 (3): 289-307.

263. García-Ochoa F, Castro EG, Santos V. Oxygen transfer and uptake rates during xanthan gum production. Enzyme Microb Technol 2000; 27 (9): 680-90.

264. Gomez E, Santos VE, Alcon A, Martin AB, Garcia-Ochoa F. Oxygen-uptake and mass-transfer rates on the growth of pseudomonas p utida cect5279: Influence on biodesulfurization (BDS) capability. Energy & fuels 2006; 20 (4): 1565-71.

265. Cai XH, Rivas G, Farias PAM, Shiraishi H, Wang J, Palecek E. Evaluation of different carbon electrodes for adsorptive stripping analysis of nucleic acids. Electroanalysis 1996; 8 (8-9): 753-8.

266. Van Assche F, Clijsters H. Effects of metals on enzyme activity in plants. Plant, Cell & Environment 1990; 13 (3): 195-206.

267. Louie AY, Meade TJ. Metal complexes as enzyme inhibitors. Chem Rev 1999; 99 (9): 2711-34.

268. Ghica ME, Brett CMA. Glucose oxidase inhibition in poly(neutral red) mediated enzyme biosensors for heavy metal determination. Microchim Acta 2008; 163 (3-4): 185-93.

269. U.S. Environmental Protection Agency, Cadmium; CASRN 7440-43-9, Integrated Risk Information System, USA. 1989.

270. Cadmium and cadmium compounds. France: International Agency for Research on Cancer; 2012.

271. Global Report on Diabetes. France: World Health Organization (WHO); 2016.

272. Kim BC, Zhao XY, Ahn HK, Kim JH, Lee HJ, Kim KW, et al. Highly stable enzyme precipitate coatings and their electrochemical applications. Biosens Bioelectron 2011; 26 (5): 1980-6.

273. Klank H, Kutter JP, Geschke O. CO2-laser micromachining and back-end processing for rapid production of PMMA-based microfluidic systems. Lab Chip 2002; 2 (4): 242-6.

274. Dudzik J, Chang WC, Kannan AM, Filipek S, Viswanathan S, Li PZ, et al. Cross-linked glucose oxidase clusters for biofuel cell anode catalysts. Biofabrication 2013; 5 (3): 9.

275. Goldstein L, Manecke G. The Chemistry of Enzyme Immobilization. In: Goldstein L, Katchalski-Katzir E, Wingard LB, editors. Applied Biochemistry and Bioengineering: Immobilized Enzyme Principles. New York: Academic Press; 1976. p. 34-110.

276. Cao LQ, van Langen L, Sheldon RA. Immobilised enzymes: carrier-bound or carrier-free? Curr Opin Biotechnol 2003; 14 (4): 387-94.

277. Walt DR, Agayn VI. The chemistry of enzyme and protein immobilization with glutaraldehyde. TrAC Trends in Analytical Chemistry 1994; 13 (10): 425-30.

278. Wang J, Musameh M, Lin Y. Solubilization of carbon nanotubes by Nafion toward the preparation of amperometric biosensors. J Am Chem Soc 2003; 125 (9): 2408-9.

279. Fan ZH, Harrison DJ. Permeability of glucose and other neutral species through recast perfluorosulfonated ionomer films. Anal Chem 1992; 64 (11): 1304-11.

280. Fischback MB, Youn JK, Zhao XY, Wang P, Park HG, Chang HN, et al. Miniature biofuel cells with improved stability under continuous operation. Electroanalysis 2006; 18 (19-20): 2016-22.

281. Quan M, Sanchez D, Wasylkiw MF, Smith DK. Voltammetry of quinones in unbuffered aqueous solution: Reassessing the roles of proton transfer and hydrogen bonding in the aqueous Electrochemistry of Quinones. J Am Chem Soc 2007; 129 (42): 12847-56.

282. Tsujimura S, Kojima S, Kano K, Ikeda T, Sato M, Sanada H, et al. Novel FAD-Dependent Glucose Dehydrogenase for a Dioxygen-Insensitive Glucose Biosensor. Bioscience, Biotechnology, and Biochemistry 2006; 70 (3): 654-9.

283. Guascito MR, Malitesta C, Mazzotta E, Turco A. Inhibitive determination of metal ions by an amperometric glucose oxidase biosensor - Study of the effect of hydrogen peroxide decomposition. Sens Actuator B-Chem 2008; 131 (2): 394-402.

284. Ghica ME, Carvalho RC, Amine A, Brett CMA. Glucose oxidase enzyme inhibition sensors for heavy metals at carbon film electrodes modified with cobalt or copper hexacyanoferrate. Sens Actuator B-Chem 2013; 178: 270-8.

285. Chen C, Xie QJ, Wang LH, Qin C, Xie FY, Yao SZ, et al. Experimental Platform to Study Heavy Metal Ion-Enzyme Interactions and Amperometric Inhibitive Assay of Ag+ Based on Solution State and Immobilized Glucose Oxidase. Anal Chem 2011; 83 (7): 2660-6.

286. Gong MM, Macdonald BD, Vu Nguyen T, Sinton D. Hand-powered microfluidics: A membrane pump with a patient-to-chip syringe interface. Biomicrofluidics 2012; 6 (4): 44102.

287. Iwai K, Sochol R, Lee L, Lin L, editors. Finger-powered bead-in-droplet microfluidic system for point-of-care diagnostics. Micro Electro Mechanical Systems (MEMS), 2012 IEEE 25th International Conference on; 2012: IEEE.

288. Iwai K, Shih KC, Lin X, Brubaker TA, Sochol RD, Lin LW. Finger-powered microfluidic systems using multilayer soft lithography and injection molding processes. Lab Chip 2014; 14 (19): 3790-9.

289. Pappa AM, Curto VF, Braendlein M, Strakosas X, Donahue MJ, Fiocchi M, et al. Organic Transistor Arrays Integrated with Finger-Powered Microfluidics for Multianalyte Saliva Testing. Adv Healthc Mater 2016; 5 (17): 2295-302.

290. Adams ML, Johnston ML, Scherer A, Quake SR. Polydimethylsiloxane based microfluidic diode. J Micromech Microeng 2005; 15 (8): 1517-21.

291. Liu J, Rinzler AG, Dai H, Hafner JH, Bradley RK, Boul PJ, et al. Fullerene pipes. Science 1998; 280 (5367): 1253-6.

292. Rinzler AG, Liu J, Dai H, Nikolaev P, Huffman CB, Rodriguez-Macias FJ, et al. Large-scale purification of single-wall carbon nanotubes: process, product, and characterization. Appl Phys a-Mater 1998; 67 (1): 29-37.

293. Mickelson ET, Huffman CB, Rinzler AG, Smalley RE, Hauge RH, Margrave JL. Fluorination of single-wall carbon nanotubes. Chem Phys Lett 1998; 296 (1-2): 188-94.

294. Vigolo B, Penicaud A, Coulon C, Sauder C, Pailler R, Journet C, et al. Macroscopic fibers and ribbons of oriented carbon nanotubes. Science 2000; 290 (5495): 1331-4.

295. Islam MF, Rojas E, Bergey DM, Johnson AT, Yodh AG. High weight fraction surfactant solubilization of single-wall carbon nanotubes in water. Nano Lett 2003; 3 (2): 269-73.

296. Arif MF, Kumar S, Shah T. Tunable morphology and its influence on electrical, thermal and mechanical properties of carbon nanostructure-buckypaper. Mater Design 2016; 101: 236-44.

297. Mustafa I, Lopez I, Younes H, Susantyoko RA, Abu Al-Rub R, Almheiri S. Fabrication of Freestanding Sheets of Multiwalled Carbon Nanotubes (Buckypapers) for Vanadium Redox Flow Batteries and Effects of Fabrication Variables on Electrochemical Performance. Electrochim Acta 2017; 230: 222-35.

298. Li D, Muller MB, Gilje S, Kaner RB, Wallace GG. Processable aqueous dispersions of graphene nanosheets. Nat Nanotechnol 2008; 3 (2): 101-5.

299. Abouimrane A, Compton OC, Amine K, Nguyen ST. Non-Annealed Graphene Paper as a Binder-Free Anode for Lithium-Ion Batteries. J Phys Chem C 2010; 114 (29): 12800-4.

300. Valles C, Nunez JD, Benito AM, Maser WK. Flexible conductive graphene paper obtained by direct and gentle annealing of graphene oxide paper. Carbon 2012; 50 (3): 835-44.

301. Wang SR, Liang ZY, Pham G, Park YB, Wang B, Zhang C, et al. Controlled nanostructure and high loading of single-walled carbon nanotubes reinforced polycarbonate composite. Nanotechnology 2007; 18 (9): 095708.

302. Wang DW, Li F, Zhao J, Ren W, Chen ZG, Tan J, et al. Fabrication of Graphene/Polyaniline Composite Paper via In Situ Anodic Electropolymerization for High-Performance Flexible Electrode. ACS Nano 2009; 3 (7): 1745-52.

303. Cheng Q, Tang J, Ma J, Zhang H, Shinya N, Qin LC. Graphene and carbon nanotube composite electrodes for supercapacitors with ultra-high energy density. Phys Chem Chem Phys 2011; 13 (39): 17615-24.

304. Cheng Q, Tang J, Ma J, Zhang H, Shinya N, Qin LC. Graphene and nanostructured MnO2 composite electrodes for supercapacitors. Carbon 2011; 49 (9): 2917-25.

305. Huang JQ, Xu ZL, Abouali S, Garakani MA, Kim JK. Porous graphene oxide/carbon nanotube hybrid films as interlayer for lithium-sulfur batteries. Carbon 2016; 99: 624-32.

306. Zhang MW, Haider A, Hou CY, Ulstrup J, Chi QJ. Free-standing and flexible graphene papers as disposable non-enzymatic electrochemical sensors. Bioelectrochemistry 2016; 109: 87-94.

307. Uchida M, Aoyama Y, Tanabe M, Yanagihara N, Eda N, Ohta A. Influences of both carbon supports and heat-treatment of supported catalyst on electrochemical oxidation of methanol. J Electrochem Soc 1995; 142 (8): 2572-6.

308. Proch S, Kodama K, Inaba M, Oishi K, Takahashi N, Morimoto Y. The “particle proximity effect” in three dimensions: a case study on Vulcan XC 72R. Electrocatalysis 2016; 7 (3): 249-61.

309. Che AF, Germain V, Cretin M, Cornu D, Innocent C, Tingry S. Fabrication of free-standing electrospun carbon nanofibers as efficient electrode materials for bioelectrocatalysis. New J Chem 2011; 35 (12): 2848-53.

310. Zhang K, Hu Z, Chen J. Functional porous carbon-based composite electrode materials for lithium secondary batteries. J Energy Chem 2013; 22 (2): 214-25.

311. Sharma S, Pollet BG. Support materials for PEMFC and DMFC electrocatalysts—a review. J Power Sources 2012; 208: 96-119.

312. Yu JJ, Du W, Zhao FQ, Zeng BZ. High sensitive simultaneous determination of catechol and hydroquinone at mesoporous carbon CMK-3 electrode in comparison with multi-walled carbon nanotubes and Vulcan XC-72 carbon electrodes. Electrochim Acta 2009; 54 (3): 984-8.

313. El Khatib K, Hameed RA. Development of Cu2O/Carbon Vulcan XC-72 as non-enzymatic sensor for glucose determination. Biosensors and Bioelectronics 2011; 26 (8): 3542-8.

314. Abdel Hameed RM. Amperometric glucose sensor based on nickel nanoparticles/carbon Vulcan XC-72R. Biosens Bioelectron 2013; 47: 248-57.

315. Chang SH, Yeh MH, Rick J, Su WN, Liu DG, Lee JF, et al. Bimetallic catalyst of PtIr nanoparticles with high electrocatalytic ability for hydrogen peroxide oxidation. Sens Actuator B-Chem 2014; 190: 55-60.

316. Cardosi MF, Birch SW. Screen Printed Glucose Electrodes Based on Platinized Carbon Particles and Glucose-Oxidase. Anal Chim Acta 1993; 276 (1): 69-74.

317. Cao ZX, Zou YJ, Xiang CL, Sun LX, Xu F. Amperometric glucose biosensor based on ultrafine platinum nanoparticles. Anal Lett 2007; 40 (11): 2116-27.

318. Ammam M, Easton EB. High-performance glucose sensor based on glucose oxidase encapsulated in new synthesized platinum nanoparticles supported on carbon Vulcan/Nafion composite deposited on glassy carbon. Sens Actuator B-Chem 2011; 155 (1): 340-6.

319. Mutyala S, Mathiyarasu J. Direct electron transfer at a glucose oxidase–chitosan-modified vulcan carbon paste electrode for electrochemical biosensing of glucose. Appl Biochem Biotechnol 2014; 172 (3): 1517-29.

320. Martinez-Ortiz J, Flores R, Vazquez-Duhalt R. Molecular design of laccase cathode for direct electron transfer in a biofuel cell. Biosens Bioelectron 2011; 26 (5): 2626-31.

321. Yuan Y, Ahmed J, Zhou LH, Zhao B, Kim S. Carbon nanoparticles-assisted mediator-less microbial fuel cells using Proteus vulgaris. Biosens Bioelectron 2011; 27 (1): 106-12.

322. Lopez-Gonzalez B, Dector A, Cuevas-Muniz FM, Arjona N, Cruz-Madrid C, Arana-Cuenca A, et al. Hybrid microfluidic fuel cell based on Laccase/C and AuAg/C electrodes. Biosens Bioelectron 2014; 62: 221-6.

323. Najafabadi AT, Ng N, Gyenge E. Electrochemically exfoliated graphene anodes with enhanced biocurrent production in single-chamber air-breathing microbial fuel cells. Biosens Bioelectron 2016; 81: 103-10.

324. Kong FY, Gu SX, Li WW, Chen TT, Xu Q, Wang W. A paper disk equipped with graphene/polyaniline/Au nanoparticles/glucose oxidase biocomposite modified screen-printed electrode: Toward whole blood glucose determination. Biosens Bioelectron 2014; 56: 77-82.

325. Sekar NC, Shaegh SAM, Ng SH, Ge L, Tan SN. A paper-based amperometric glucose biosensor developed with Prussian Blue-modified screen-printed electrodes. Sens Actuator B-Chem 2014; 204: 414-20.

326. Ahmadalinezhad A, Wu GS, Chen AC. Mediator-free electrochemical biosensor based on buckypaper with enhanced stability and sensitivity for glucose detection. Biosens Bioelectron 2011; 30 (1): 287-93.

327. Dungchai W, Chailapakul O, Henry CS. Electrochemical Detection for Paper-Based Microfluidics. Anal Chem 2009; 81 (14): 5821-6.

328. Li X, Zhao C, Liu XY. A paper-based microfluidic biosensor integrating zinc oxide nanowires for electrochemical glucose detection. Microsyst Nanoeng 2015; 1: 7.

329. Fischer C, Fraiwan A, Choi S. A 3D paper-based enzymatic fuel cell for self-powered, low-cost glucose monitoring. Biosens Bioelectron 2016; 79: 193-7.

330. Lawrence CSK, Tan SN, Floresca CZ. A "green" cellulose paper based glucose amperometric biosensor. Sens Actuator B-Chem 2014; 193: 536-41.

331. Torrinha Á, Montenegro MCBSM, Araújo AN. Microfluidic Platform with an Embedded Pencil Graphite Electrode Biosensor for the Detection of Glucose and Cadmium. J Electrochem Soc 2019; 166 (2): B155-B60.

332. Chen RJ, Zhang Y, Wang D, Dai H. Noncovalent sidewall functionalization of single-walled carbon nanotubes for protein immobilization. J Am Chem Soc 2001; 123 (16): 3838-9.

333. Gross AJ, Robin MP, Nedellec Y, O'Reilly RK, Shan D, Cosnier S. Robust bifunctional buckypapers from carbon nanotubes and polynorbornene copolymers for flexible engineering of enzymatic bioelectrodes. Carbon 2016; 107: 542-7.

334. Zhou M. Recent Progress on the Development of Biofuel Cells for Self-Powered Electrochemical Biosensing and Logic Biosensing: A Review. Electroanalysis 2015; 27 (8): 1786-810.

335. Grattieri M, Minteer SD. Self-Powered Biosensors. ACS Sens 2018; 3 (1): 44-53.

336. Milton RD, Lim K, Hickey DP, Minteer SD. Employing FAD-dependent glucose dehydrogenase within a glucose/oxygen enzymatic fuel cell operating in human serum. Bioelectrochemistry 2015; 106: 56-63.

337. Sunkara V, Park DK, Hwang H, Chantiwas R, Soper SA, Cho YK. Simple room temperature bonding of thermoplastics and poly(dimethylsiloxane). Lab Chip 2011; 11 (5): 962-5.

338. Wu W, Wu J, Kim JH, Lee NY. Instantaneous room temperature bonding of a wide range of non-silicon substrates with poly(dimethylsiloxane) (PDMS) elastomer mediated by a mercaptosilane. Lab Chip 2015; 15 (13): 2819-25.

APPENDIX

Appendix A – Review article

Talanta 190 (2018) 235–247

Contents lists available at ScienceDirect

Talanta

journal homepage: www.elsevier.com/locate/talanta

Biosensing based on pencil graphite electrodes

Álvaro Torrinha, Célia G. Amorim, Maria C.B.S.M. Montenegro, Alberto N. Araújo*

LAQV-REQUIMTE, Laboratório Química Aplicada, Faculdade Farmácia da Universidade do Porto, Porto, Portugal

ARTICLE INFO

Keywords:
Pencil graphite electrodes
Biosensors
Electrochemical transduction
Enzymes

ABSTRACT

Pencil leads have been increasingly used as electrode material in electrochemical applications. Commonly denominated as pencil graphite electrodes (PGE), they represent a viable alternative to other standard electrodes due to their comparable electrical properties but mainly for their low cost and availability, enabling disposable applications. In order to achieve the best analytical performance literature evidences the type of lead (hardness level) and electrode surface pre-treatment are critical to the envisaged application. The present review describes the use of PGE in biosensing analysis, more specifically those sensors comprising immobilized enzymes but also briefly referring nucleic acids and other biological entities. It lays an emphasis in the immobilization process of the biological entities while focusing in the analytical performance of each biosensor, mainly sensitivity, linear range and limit of detection as comparative criteria. This review also addresses the main characteristics and properties of PGEs as transducer material in the electrochemical field.

1. Introduction

Writing and drawing with ever sharp utensils based on carbonaceous threads of Ø ≤ 2 mm encased in mechanical devices, have been a common alternative to standard pencils since the beginning of last century. Also in the continuous search for easily polarizable electrodes electrochemists were attracted by their electrical conductance properties, tiny dimensions, low cost and ubiquity. Commonly referred as pencil graphite electrodes (PGE), first reports dated back to the 50's/60's. At the time, a pencil lead served as anode against the classic dropping mercury electrode into a microcoulometric arrangement for the numbering of electron charges involved in irreversible electrolysis processes [1]. In the 80's, surface covering with a thin layer of polyvinyl chloride plasticized with dioctylphthalate enabled successful use in titrations performed at null current [2]. Independent results obtained from voltammetric studies with well-known redox probes $[Fe(CN)_6]^{3-/4-}$ and $[Ru(NH_3)_6]^{2+/3+}$, highlighted the higher stability and analytical reproducibility regarding the much more expensive glassy carbon (GC), pyrolytic graphite and carbon fiber electrodes [3,4]. Sustained development of electrochemical applications and patent request referring different usages began in the nineties mainly by Asiatic research groups [5–12]. Meanwhile, the first biosensor implemented with a PGE was described in 1990 by Pishko group [13] and transduced the interaction between substrate and the glucose oxidase enzyme wrapped in polycation redox polymer formed from osmium complexes with poly(vinylpyridine) and immobilized on its surface. The opposite charges between the reduced form of the enzyme and the polymer enabled a simplified electron transfer feature, direct "wiring" to the active catalytic centre, and obviated use of additional redox mediators.

Pencil mines are produced by extrusion of a mixture composed of graphite powder and clay (used as binder material) in water, afterwards heated up to 1000 °C in order to gain rigidity. Immersion in a wax bath enables pores filling and confers smooth appearance to the end product [14]. An approximate composition of around 68% (w/w) graphite, 26% (w/w) clay and 5% (w/w) wax was recently stated as example of medium hardness Staedtler HB [15]. The thinnest leads tend to easily break due to the brittle nature of clay and require additional use of a polymer to provide resilient bonding after thermal treatment [16,17]. Besides differing in gauge, pencil mines come in diverse hardness varieties depending on the graphite/clay proportion in the extruded mixture, which can also differ between manufacturers. The ones labelled as H have lower graphite/clay ratios and give harder writing sensation, while B mines are produced with higher carbonaceous content to enable softer and darker writing. Thus, PGEs can be implemented from mines with different graphite/clay ratios corresponding to the scale from 10H to 10B (22 Types) (Japanese Mitsubishi Pencil Co. (Uni)). From pure theoretical point of view, since electrical properties of electrodes such as conductivity largely depend on the carbonaceous content, generic use of softest pencils would seem obvious [18]. In fact, softer leads were advantageously used to draw miniaturized electrodes over cellulosic flat surfaces. For that purpose, pencils like 6B [15,19] or 8B [18] were the best due to the enhanced

* Corresponding author.
E-mail address: anaraujo@ff.up.pt (A.N. Araújo).

https://doi.org/10.1016/j.talanta.2018.07.086
Received 20 April 2018; Received in revised form 24 July 2018; Accepted 27 July 2018
Available online 27 July 2018

electrochemical performance obtained. In other applications, variation in hardness (clay content) as well as in a particular pencil brand have shown marked influence on the achieved performance [16,17,20]. For instance, 5H pencils provided higher oxidation peaks in the determination of analgesic drug acetaminophen when compared with 2B mines [21]. In the determination of caffeic acid, better signal-to-noise ratio was observed for HB mines when compared to the 2B, 2H and 5H counterparts [22]. To unveil the influence of hardness, PGEs from three different manufacturers, labelled from 4B to 4H were evaluated by cyclic voltammetry (CV) [17]. The anodic peak currents clearly raised from softest to medium type leads (HB) and stabilized for those with increased hardness while potential peak separation (ΔE_p) consistently decreased. The authors of the study also observed that similarly labelled pencil mines could have significant differences concerning to reproducibility and redox peak ratios according the manufacturer. Kariuki [20] studied the surface structure and electrochemical properties of PGEs. Higher oxygen/carbon ratio, as well as higher silica and aluminium content with increasing in hardness was observed by means of X-ray photoelectron spectra (XPS). Resorting to the redox probes $Fe(CN)_6^{3-/4-}$ and $Ru(NH_3)_6^{3+/2+}$, a lower peak separation ΔE_p was more evident for HB mines due to faster heterogeneous electron transfer rate. The surface reactivity of chemical species at HB mine exhibited improved kinetics regarding to H and B varieties though without a clear tendency between these last. As it happens with other carbon electrodes, namely glassy carbon, pyrolytic graphite, spectroscopic graphite and carbon fibres, the prevalent structure of the carbonaceous component was carbon to carbon bonds in the sp^2 configuration. Differences in electrochemical properties were thus ascribed to variations in size and orientation of graphitic inter- and intraplanar microcrystallites [23,24]. On other hand, the electrochemical response of a PGE of suited hardness might change dramatically after pre-treatment. To accomplish determination of phenols, best results were obtained after anodization treatment and responses improved for soft mines up to the 6B. Phenol adsorption at unacceptable levels was observed for softer varieties with consequent fouling and signals loss. Without pre-treatment however, the HB variety presented the best results with responses worsening with increasing in softness [25]. Also importantly, the choice between PGEs for biosensing applications revealed specific chemical interactions between the analyte and the clay/graphite composite regardless to any pre-treatment given to the electrode prior the analysis (under detailed discussion below). In this context, best results for hydrogen peroxide (H_2O_2) biosensing [26] or in the detection of DNA hybridization [27] were consistently achieved with 6H labelled PGE.

The use of modified or non-modified PGEs for the determination of organic and inorganic compounds were reviewed by other authors [28–30]. However, the results discussed above highlight several features of PGEs which also affect the immobilization of different biological entities during implementation of biosensors as well their final analytical performance. A systematic literature review is carried-out concerning use of this electrodic material for biosensors comprising enzymes, nucleic acids and whole organisms, in order to guide the researchers in future works. As far as we know, this is the first review regarding the application of this type of material in transducing schemes with biological entities. Here we give insight of (i) pencil lead characteristics and features; (ii) immobilization processes of the biological entities while (iii) addressing the achieved analytical performance as comparative criteria between the described biosensors.

1.1. Differences between PGE and other carbon electrodes

In order to highlight the surface composition of different PGEs we have analysed 3 types of pencil leads (4B, HB and 4H) by energy-dispersive X-ray spectroscopy and scanning electron microscopy. The results obtained are illustrated in Fig. 1 (unpublished). The spectra reveal silicon, aluminium and oxygen as main components of clay besides the carbon microcrystallites in chunks of juxtaposed thin platelets with approximately 2–10 μm length (Fig. 1a).

Traditional hand-polishing (0.05 μm alumina) revealed entangled filament structure (Fig. 1.b) with darker but less defined regions in the less disordered 4B lead. In the study conducted by Kariuki [20], Raman spectra showed that HOPG electrode had the lowest ratio between the two 1370 cm^{-1}/1583 cm^{-1} bands (D/E_{2g} ratio) reflecting ordered basal plane surface structure. The disorder rises for PGE followed by GC and is in direct relation with the clay content. In turn, redox peaks obtained with different probes, $Ru(NH_3)_6^{3+/2+}$, $Fe^{2+/3+}$, dopamine and $Fe(CN)_6^{3-/4-}$, showed this last as the more appropriate to test for surface characteristics namely disorder and oxygen to carbon ratio. The highly disordered edge plane in GC electrode presented faster electron transfer kinetics translated in bit smaller peak separation for each redox probe, ΔE_p, when compared to PGEs labelled as HB. Basal plane HOPG electrode showed higher values of ΔE_p and also lower reproducibility. On the contrary, specific analysis regarding guanine oxidation signal [31,32] or the determination of the carcinogen 7,12-dimethylbenz[a] anthracene [33] revealed better electrochemical results of PGEs over GC. While the stated conclusions can be looked as guiding criteria to select a particular electrode for an intended application, other studies demonstrated equivalent performance between both electrodes [5,16,34]. An important aspect to be taken into account considers the differences on carbon electrode surface structures leading to apparent high double layer specific capacitances in the implemented electrochemical method which may affect the quality of the electrode response. A first cause is related to the presence of other constituents besides graphite [33]. As can be seen from Fig. 2 (data not published), PGEs generally show potential limits *vs* Ag/AgCl between −1.2 V and + 1 V in 0.1 M KCl, being pristine B mines characterized by larger capacitance but also poor signal-to-noise ratio. Other factors influencing the performance of the PGEs are related to surface roughness as well as to porosity of the material. In the presence of void space, unsuspected compounds in solution might be adsorbed thus imparting uncontrollable background currents [24]. A particular feature of PGEs is that the surface contacting the sample is a mix of insulating clay regions and conductive graphite regions unlike GCE and carbon fiber electrodes. This aspect determines an akin of "microelectrode array" behavior with corresponding better signal-to-noise ratios as noticed in few studies regarding adsorptive stripping analysis involving nucleic acids [31,32,35]. A second aspect relates with the higher relative porosity which in the case of the same biopolymer can improve orientation, coverage and redox activity. In the absence of a general consensus about their comparative performance with the more traditional carbon electrodes, PGEs have the enormous advantage of being inexpensive and commercially available in different diameters and hardness suited to encompass a larger number of applications as disposable electrodes. Moreover, if specific pre-treatment to improve the general outcome of the electrode is intended, experience shows that achievement of adequate performance with GC can be rather fastidious [24]. On contrary, pencil lead electrodes can be cut each time offering renewable and reproducible individual surfaces for simpler and faster polishing procedures [32]. They are also better materials for miniaturization and portability purposes, though the considerable dimensions for in vivo applications when compared to carbon fibres electrodes [36–38].

During biosensors construction process, different pre-treatments of electrodes are usually referred, namely mechanical (polishing process), chemical (using an organic solvent like ethanol or acetone), electrochemical (potentiostatic/potentiodynamic) or a combination of the three. There is not a preferred protocol since it depends on factors such as the diameter of leads used, target analyte or immobilized compound. Nevertheless, whatever the procedure used it decisively influences the final performance in specific applications. If creation of functional groups, mediation of the heterogeneous electronic transfer to electroactive species or adsorption enhancement of these last is envisaged, electrochemical pre-treatments should be adopted [24,39]. Most works describing nucleic acid sensors with PGEs employed high fixed positive

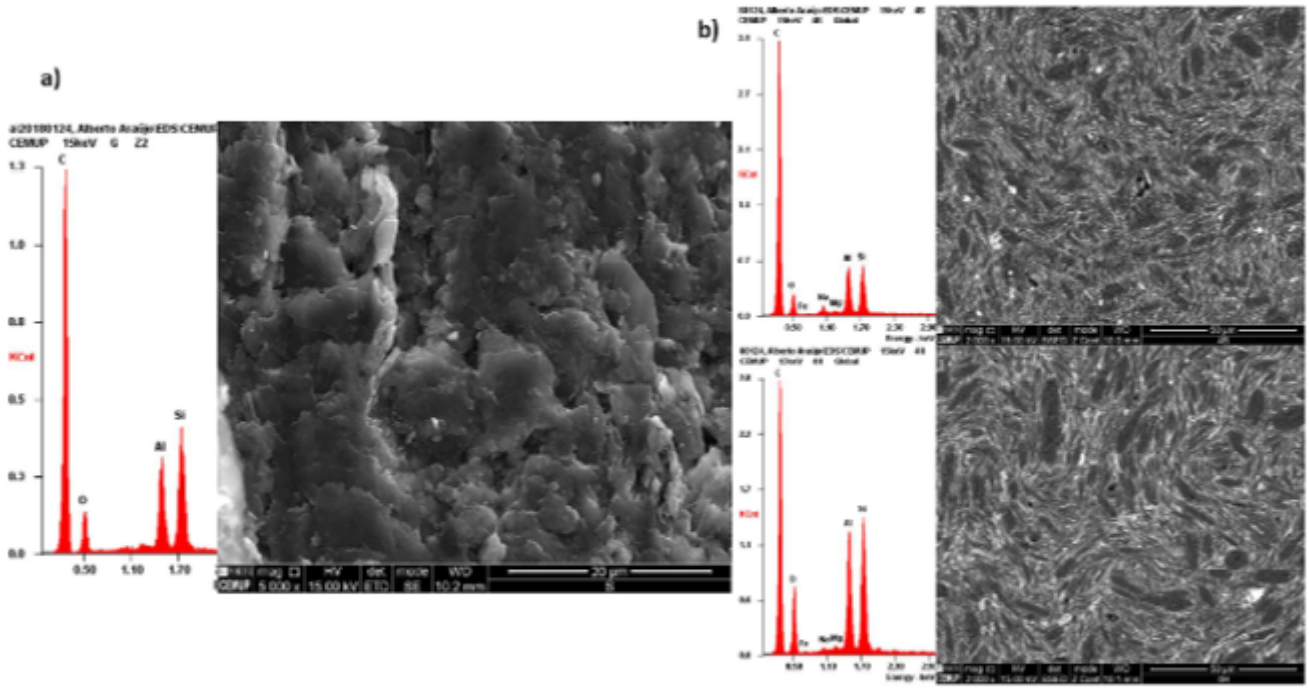

Fig. 1. SEM-EDS micrographs of carbonaceous spot in a) Staedtler HB mine and of b) 4B and 4H transverse surfaces after mechanical polishing with 0.05 μm alumina aqueous slurry onto a polishing cloth followed by profuse washing with purified water.

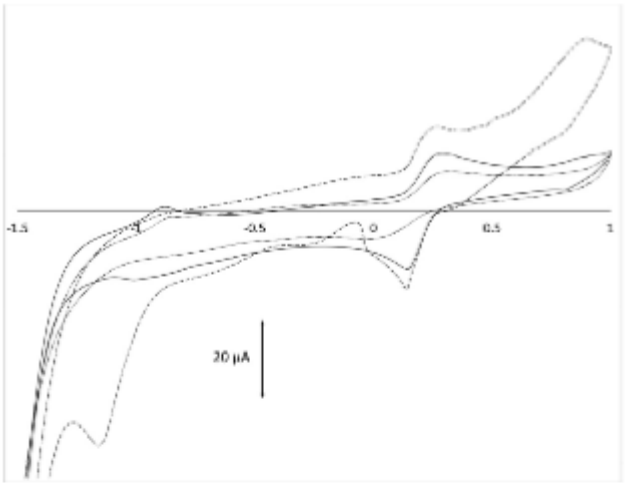

Fig. 2. First cyclic voltammograms obtained for Staedtler HB (plain), 4B (trace) and 4 H (dotted) versus Ag/AgCl reference electrode, using a platinum wire as counter electrode. The scans were obtained sweeping potentials first in the reverse direction at 10 mV s^{-1} for a 5 mM potassium $Fe(CN)_6^{2-/4-}$ in 0.1 M KCl electrolyte solution.

potential for a short period of time [32,40–44]. This anodization step seems to be essential to activate the surface and improve the analytical sensitivity. It introduces mediating oxygen functionalities and the formation of a hydrophilic surface readily accessible to the electroactive compounds. Otherwise, treatment provides simple removal of impurities from the polishing and preparation process [39,45]. Özcan group [46] compared the determination of dopamine in blood by using PGEs previously conditioned by two different electrochemical pretreatments (potentiostatic or potentiodynamic). They found that potentiodynamic provided best results by achievement of dopamine signals three times higher. The same conclusions regarding to the effectiveness of the PGE pre-treatment were reached when carcinogen sudan II compound was determined by adsorptive stripping differential pulse voltammetry [47]. The higher efficiency of potentiodynamic over the potentiostatic pre-treatment is explained by the fact that application of negative potentials (cathodization) after the anodization step contributes to the reduction of oxygen passivation, overcoming the inhibitory layer formed during anodization [45]. By means of electrochemical impedance spectroscopy (EIS), some authors evidenced the decrease in the charge transfer resistance (R_{ct}) occurring after the electrochemical pretreatment of PGEs [48–51]. The electrolyte used in the electrochemical pre-treatment can also influence transfer process as shown by Özcan [52] who obtained lower R_{ct} and consequently, better oxidation signals for bisphenol A with PGE pre-treated in an electrolyte composed of $LiClO_4$ and NaOH compared to other electrolytes. However, some works omitted any type of treatment performed prior to analysis or modification of the electrode [20,53–55]. Whereas a rough, unpolished graphite surface showed to be beneficial for electrodeposition of copper ions in the nucleation stage [56], a PGE electrochemically pre-treated at + 1.4 V, provided lower signal and lower reproducibility during homocysteine determination [57].

2. PGE biosensors

An electrochemical biosensor is defined as an analytical device comprising a recognition surface with a biological entity immobilized over the transducing system. The biological entity may it be an enzyme, whole microorganism, protein or tissue is used with the purpose of detecting specific analytes by converting biochemical energy into a quantifiable electrical signal. The transducer, i.e. the electrode, monitors the biological element in action or processes the product of the biocatalytic reaction and relays it to the amplifier after which the data is displayed [58,59]. An example refers to the immobilization of DNA molecules onto PGE surface to query its interaction with different drugs acting as potential carcinogens. The response is mainly indicated through the variation of the electrochemical signal provided by guanine residues [40,44,60,61]. Main commercially available biosensors are

Table 1
Enzymatic PGE biosensors characteristics and analytical performance.

Analyte	Enzyme (source)	PGE type and diameter	Pre-treatment	Immobilization	Analytical performance				Stability (days)	Reference
					Linear range (mM)	Sensitivity		LOD (μM)		
						(μA mM^{-1})	(μA mM^{-1} cm^{-2})			
Glucose	Glucose Oxidase	HB 0.5 mm HB 0.9 mm	mechanical (polishing)	PGE-$POs^{+}NH_2$-GOx	0 - 10	-	1	-	-	[13]
		0.5 mm	-	PGE-Nafion-GOx/BSA/PVA-SbQ-MB-CTA	0.28 - 33.3	0.043	5.5	-	2	[7]
		H 0.3 mm	-	PGE-PB-GOx/GA-Nafion-PU	0 - 5.3	0.091	1.9	-	7	[67]
		HB 0.5 mm	-	PGE-CP-AuNPs-cysteine-DCC-GOx	0 - 33.4	5.06	-	22.3	45	[68]
		HB 0.5 mm	-	PGE-CP-AuNPs-cysteine-FcAld-DCC-GOx	0 - 39	2.21	-	7.8	50	[69]
		2B 0.9 mm	mechanical (polishing) Electrochemical (catodization)	PGE-rGO-GOx	0.04 - 0.6	1.8	278	0.61	21	[72]
		2B 0.5 mm	Electrochemical (catodization)	PGE-CdS-ZnS-Chit/GOx	0.01 - 1	1.83	11.5	3	-	[75]
		3 mm	-	PGE-poly(GMA-co-VFc)-APBA-FAD-apoGOx	1 - 17	0.27	3.8	2.7	6	[70]
		0.9 mm	mechanical (polishing)	PGE-rGO-ZnO/Cu_2O-GOx-Nafion	0.01 − 2	0.34	54	1.93	20	[71]
		B 0.5 mm	Electrochemical (anodization)	PGE-rGO/GOx	0.01 - 1	0.62	9.6	5.8	10	[73]
		HB 0.5 mm	Electrochemical	PGE-GOx	0.1 - 8	0.03	0.9	50	1	[74]
	Glucose dehydrogenase	2B 0.5 mm	Electrochemical (catodization)	PGE-CdS-ZnS-BSA/GA/GDH	0.2 - 8	0.118	0.74	90	-	[76]
		2B 0.5 mm	-	PGE-PAMAM-MB-BSA/GA/GDH	0.01 - 1	0.79	5	4	10	[78]
Hypoxanthine	Xanthine oxidase	-	Chemical (acid washing)	PGE-AuFeNPs-XOD	0.00005 - 0.15	-	-	0.05	100	[83]
Xanthine		-	Chemical (acid washing) mechanical (polishing)	PGE-Chit/AuFeNPs-GA-XOD	0.0001 - 0.3	-	1169	0.1	100	[82]
		2 mm	Chemical (organic washing)	PGE-Poly(GMA-co-VFc)/MWCNT-XOD	0.002 - 0.028	16	24.3	0.12	25	[84]
		-	Chemical (organic washing)	PGE-poly(DTP-alkyl-NH_2)-GA-XOD	0.0003 - 0.025	124	-	0.074	16	[85]
Hydrogen peroxide	Horseradish peroxidase	6 H 2 mm	Mechanical (polishing) Electrochemical (catodization)	PGE-Chit-AuNPs-HRP	0.01 - 1.5	4.7	149	2	30	[26]
		2 mm	Chemical (organic washing)	PGE-Poly(GMA-co-VFc)/rGO-HRP	0.000006 - 0.0001	0.027	0.041	0.00002	-	[94]
Deferiprone		-	-	PGE-AuNPs-GA-HRP	0.1 - 1	375	-	0.005	70	[96]
Oxygen	Laccase (*Trametes versicolor*)	1.4 mm	Chemical (acid washing)	PGE-Pani-MWCNT-laccase	-	-	-	-	-	[98]
		5 H 2 mm	Chemical (acid washing)	PGE-Pani-MWCNT-laccase	-	-	-	-	-	[99]
	Laccase (*Rhus vernicifera*)	HB, 2 mm	Mechanical (polishing)	PGE-rGO-SWCNT/laccase-solgel	0 - 0.45	4.5	132	2.7	-	[100]
Ascorbic acid	Ascorbate oxidase (*Cucurbita sp.*)	2 H, 0.3 mm	-	PGE-PEI-BSA/AOx-PU	0 - 0.1	0.196	276	0.26	-	[102]
	Ascorbate oxidase (*Cucurbita sp.*)	2 H, 0.3 mm	-	PGE-SWCNT-PEI-BSA/AOx-PU	0 - 0.02	0.32	451	0.2	11	[103]
				PGE-MWCNT-PEI-BSA/AOx-PU	0 - 0.02	0.486	685	0.22	12	
Cholesterol	Cholesterol oxidase (*Streptomycin sp.*)	HB, 1.5 mm	Chemical (acid washing)	PGE-ChOx	1.29 - 10.3	4120	4380	90	25	[105]
	Cholesterol oxidase (*Brevibacterium sp.*)	-	Chemical (organic washing)	PGE-PTBA-FAD-apoChOx	0.0008 – 0.0048	210	-	0.22	17	[106]
Triglyceride	Lipase (*candida rugosa*) Glycerol kinase (*Cellulomonas sp.*) Glycerol-3-phosphate oxidase (*Aerococcus viridans*)	6B 2 mm	Electrochemical (catodization)	PGE-GA/cysteamine/Lipase/GK/GPO	0.1 - 45	185	116	0.0001	240	[107]

(*continued on next page*)

Table 1 (*continued*)

Analyte	Enzyme (source)	PGE type and diameter	Pre-treatment	Immobilization	Analytical performance				Stability (days)	Reference
					Linear range (mM)	Sensitivity ($\mu A\ mM^{-1}$)	Sensitivity ($\mu A\ mM^{-1}\ cm^{-2}$)	LOD (μM)		
Ethanol	Alcohol dehydrogenase (*Saccharomyces cerevisiae*)	2 mm	Mechanical (polishing) Chemical (organic washing)	PGE-SWCNT-PCV-BSA/GA/ADH	0.0093 - 0.32	0.061	1.94	-	52	[108]
L-lactate	L-lactate dehydrogenase	6B 2 mm	Mechanical (polishing) Chemical (organic washing)	PGE-GONPs-LDH	5 - 50	3	1.6	0.1	60	[111]
	L-lactate oxidase (*Pediococcus sp.*)	6B, 2 mm	Mechanical (polishing) Chemical (organic washing)	PGE-PANI-CuNPs/MWCNT-LOx	0.001 – 2.5	1300	1009	0.25	140	[112]
L-glutamate	L-Glutamate oxidase	HB, 2 mm	Mechanical (polishing) Chemical (organic washing)	PGE-ZnO/PPy-Glu-Ox	0.00002 - 0.5	1.4	1.1	0.00018	90	[114]
Uric acid	Uricase (*Arthrobacter globiformis*) Horseradish peroxidase (horseradish)	HB, 0.5 mm	Chemical (organic washing)	PGE-GA/Uricase/HRP	0 – 0.12	2.6	-	0.6	16	[115]
organophosphate pesticides	Acetylcholinesterase (Electric eel)	HB, 0.9 mm	Chemical (organic washing)	PGE-PEI-PB-GA-AChE	0 – 0.9	0.6	6	-	60	[116]

however typically enzymatic being the most prominent example the glucose sensor. Enzyme biosensors are highly selective for respective substrates and are distinguishable from other types of biosensors by their biological function as catalysers. Nevertheless, responses obtained with the catalyser in solution and upon immobilization are most of times different [62]. The charged nature and hydrophilic/hydrophobic character of the immobilization support determines a new micro-environment. Therefore concentrations of electroactive compounds, ionic strength or pH can differ significantly from those found in bulk solution [63]. Both adsorption and covalent immobilization can impart conformation and steric hindrances to response as well, especially when high loads and crosslinking between the bio-element determines the formation of multiple layers. Unfortunately, most of these aspects are not conveniently addressed in reviewed works, thus limiting envisagement of the most suited protocol for each particular bio-element considered. Thus, literature overview concerning to enzymatic, nucleic acid and whole microorganism PGE-based biosensors will be limited and with emphasis on the pre-treatment used before immobilization and corresponding final analytical performance. The main features are additionally summarized in Table 1.

2.1. Glucose oxidase

The fabrication of electrochemical biosensors for point-of-care testing devices used by diabetic patients stands as the most relevant use of glucose oxidase (GOx) in analytical applications. GOx from fungal origin are homodimeric glycoproteins with one FAD cofactor per monomer and shows high selectivity towards β-D-glucose substrate. It is certainly the most used enzyme in research given the high catalytic activity, low cost and availability. The deeply buried cofactor/ active site additionally challenges electrochemists in the search of more effective mediated or direct electron transfer schemes. As molecular oxygen acts as co-substrate by reoxidizing GOx and producing H_2O_2 several works resort to such more traditional measuring approach [64,65].

As mentioned earlier, Pishko group [13] was the first to immobilize a biological entity on PGE surface. In low ionic strength medium, the negatively charged GOx was folded by a polycationic redox polymer readily adsorbed onto graphite. The polymer referred as $POs^{+}NH_2$ was synthesised from poly(4-vinylpyridine-*co*-4-aminostyrene) and Os(2,2′-bipyridine)$_2$Cl$_2$. Thin polished HB leads were encased on heat-shrinkable polypropylene sleeve, and immersed firstly in the polymer suspension which adsorbed strongly (10^{-8} mol cm^{-2}) and further coated with glucose oxidase solution (> 100 U mL^{-1}, 4 μL). The polymer folding onto glucose oxidase in low ionic strength medium enabled the direct electron shuttle between the buried active catalytic centre of enzyme and the electrode surface. Amperometric measurements of substrate were then performed with a sensitivity value of about 1 μA mM^{-1} cm^{-2}. The sensitivity was low but the principle simplicity and ruggedness paved the way for the use of osmium-based redox polymers in latter applications such as in biofuel cells [36]. Two years after a new type of configuration was implemented [7]. The working PGE and an Ag/AgCl reference electrode were inserted inside a hypodermic needle, the latter functioning as counter electrode. The pencil lead was previously electroplated with platinum to allow detection of H_2O_2 formed during the GOx catalytic reaction and coated with nafion in order to prevent interferences from ascorbate and urate. The immobilization process consisted in dropcasting the mixture of bovine serum albumin (BSA), stilbazolium polyvinyl alcohol adduct (PVA-SbQ) and the enzyme. In order to avoid a minimal disturbance on enzymatic activity and protein configuration a double crosslinking with glutaraldehyde (GA) vapour followed by photo activation of PVA-SbQ under a fluorescent light was performed according to a previous validated procedure [66]. The setup provided sensitive measurements of glucose with a linear response of 0.06–2 mM, though unfitted with physiological levels. An increase in the analytical range (0.3–33.3 mM) but with

10 times reduced sensitivity trade-off (5.5 μA mM^{-1} cm^{-2}) was obtained when a triacetate cellulosic membrane (MB-CTA) was interposed between the sample and the cell. The wide working range of the sensor and its small configuration enabled to hypothesize future application to undiluted blood samples as well as in vivo studies [7].

In 1996 another configuration based on PGE was proposed as implantable biosensor [67]. After electrochemical modification with Prussian blue (PB), an H pencil (0.3 mm ϕ) was placed inside a plastic pipette tip and sealed with epoxy resin. The emergent tip was cross-linked with GOx (12,000 U mL^{-1}, 2 μL) using glutaraldehyde, GA (25%), in four repeated cycles. Nafion was then deposited followed by polyurethane (15% w/v). The H_2O_2 produced was detected by amperometry conducted at + 0.75 V (*vs* Ag/AgCl) in PBS (pH 7.4). The obtained responses showed a constant sensitivity of 0.091 μA mM^{-1} (1.9 μA mM^{-1} cm^{-2}) and a linearity up to 5.3 mM glucose. The electrode sensitivity decreased in plasma samples due to membrane fouling by unspecific components of blood. Its sensitivity was lower when compared with the one described before [7] and was less stable for low analyte concentrations, turning it impeditive for in vivo applications. About two decades later, an HB pencil was covered with carbon paste incorporating gold nanoparticles (AuNPs) to provide chemical anchorage to GOx protein [68]. The biosensor exhibited very good electrochemical performance concerning to stability and durability (reusable after 228 days) though after a fastidious implementation procedure. PGE surface was firstly isolated through coating with carbon paste to avoid interference from native impurities from clay component. The modified surface was sequentially immersed in L-cysteine and *N,N′*-dicyclohexylcarbodiimide (DCC) solution and finally in GOx (865 U mL^{-1}). An analytical range up to 33.4 mM glucose, a sensitivity of 5.06 μA mM^{-1} and a limit of detection (LOD) lower than 22.3 μM were obtained. However, the biosensor was this time used in the analysis of hydrolysed extracts of waste tree brunch being the results validated by using HPLC method. A similar approach was performed with ferrocenecarboxaldehyde (FcAld) immobilized onto PGE surface to accomplish the glucose produced in cellulase hydrolysis of waste bamboo chopsticks [69]. Ferrocene derivatives are widely used as diffusional or immobilized electron relays due to their capacity for fast heterogeneous electron transfer at low potentials. So, additional incorporation of FcAld widened the working range up to 39 mM and improved LOD to 7.8 μM when compared to their previous biosensor [68]. However, the sensitivity obtained decreased by half (2.2 μA mM^{-1}) showing that mediator immobilization was not entirely beneficial for the analytical performance of the biosensor [69]. In another proposal [70], GOx enzyme was stripped from its native FAD redox centre to yield the apo-enzyme (apoGOx). The PGE was first modified by dropcasting with poly (glycidyl methacrylate-*co*-vinylferrocene), and then immersed in 0.1 M 3-aminophenylboronic acid (APBA) to establish covalent link between the stripped FAD and the polymer. The modified PGE was then soaked in the apo-enzyme solution for effective enzyme reconstitution. A linear range of about 1–17 mM, a sensitivity of 0.27 μA mM^{-1} (3.8 μA mM^{-1} cm^{-2}) and a LOD of 2.7 μM were obtained.

The works referred before show that pencil mines provided miniaturized biosensors with good sensitivities owed to enhanced electron transfer at the surface. This aspect is even more evident when metal oxide particles and graphene were used to provide high surface area and enhanced electrochemical properties [71]. Here, the pencil lead was first physically polished with alumina slurry and washed with water. Afterwards, graphene oxide suspension (10 mg mL^{-1}) was casted and further electrochemically reduced (rGO). The electrode was then respectively immersed in Zn and Cu solutions and an applied fixed potential modified it with ZnO and Cu_2O nanoparticles. The enzyme was dropcast on the modified surface and left to dry (surface coverage of 3.87×10^{-12} mol cm^{-2}) before being stabilized with nafion. According the authors, electrostatic forces between the negatively charged enzyme and the positively charged ZnO/Cu_2O particles accelerate the heterogeneous charge transfer process. Given the small electroactive area only a sensitivity of 0.34 μA mM^{-1} was reported but corresponding to a value 54 μA mM^{-1} cm^{-2}. Although with a LOD of 1.93 μM, the short linear range (0.01–2 mM) achieved imposed additional sample dilution when human blood serum samples were tested.

Pure electrochemical methods allowing simultaneous reduction of graphene oxide and immobilization of GOx were also described [72]. The pencil lead (type 2B) was first pre-treated by polishing and then applying an oxidizing potential. A solution of graphene oxide (0.5 mg mL^{-1}) was applied onto the PGE surface followed by GOx suspension (650 U mL^{-1}, 2 μL). Both reduction and immobilization occurred when a potential of −1.5 V for 30 s was applied. This way, a covalent bond between the carboxylic groups of graphene and the side-chain amine groups in the protein were formed. The amperometric biosensor showed a linear response between 0.040 and 0.600 mM, a LOD of 0.61 μM and a sensitivity of 1.8 μA mM^{-1} (278 μA mM^{-1} cm^{-2}), for measurements performed at the optimized reduction potential of −0.6 V. Despite the simpler construction process, better general biosensor characteristics were obtained regarding the previously described work [71]. The improvement was due to the increase of specific surface enabled by graphene and its better conductive response in the reduced form (heterogeneous electron transfer of $k = 5.84\ s^{-1}$). However, the linear range upper limit was only 0.6 mM, further away from physiological levels which stand above 4 mM. A very similar procedure as the one described above was adopted, however with the immobilization of enzyme and the GO reduction steps being performed through potentiodynamic means, between −1.3 V and 0.2 V. The sensitivity of 0.62 μA mM^{-1} and LOD of 5.8 μM indicated that the achieved performance was nevertheless poorest [73].

An amperometric biosensor with an automated set up was developed for sequential analyses of 24-well microplates and therefore, perform repetitive analyses without manual operation for several hours [74]. The electrochemical pre-treated PGE (HB, 0.5 mm), containing carboxyl groups was first immersed in EDC and NHS solution followed by immersion in GOx (136 U mg^{-1}, 2 mg mL^{-1}) solution. In PBS the automated biosensor responded linearly to glucose from 0.1 to 8 mM but only achieving a sensitivity of 0.03 μA mM^{-1} (0.9 μA mM^{-1} cm^{-2}) and a one higher order of magnitude LOD of 50 μM.

The combined use of quantum dots (QDs) with GOx have also been proposed showing that electronic and optical properties of the former enhanced the direct electron transfer feature [75]. A 2B pencil mine was first pre-treated by electrochemical anodization followed by two-step electrosynthesis of QDs on electrode surface. First, CdS deposition was performed by immersing in a mixture of $CdCl_2$, $Na_2S_2O_3$, EDTA and mercapto acetic acid solutions and applying −1 V for 1000 s. At last, ZnS was deposited in similar conditions but using a $ZnCl_2$ solution. The modified PGE was incubated in 0.5% chitosan (Chit) and GOx (200 mg mL^{-1}) solution for 1 h, dried and rinsed with water before analysis. Accurate detection of substrate concentrations was accomplished in a FIA system. After optimization of hydrodynamic conditions an analytical linear range of 0.01–1 mM was obtained with a LOD of 3 μM and sensitivity of 11.5 μA mM^{-1} cm^{-2} (1.83 μA mM^{-1}).

The above described works did not allow identification of a best fitted immobilization process. There is a lack of data to enable comparison of enzyme surface coverage since this influences the diffusion resistance and overall kinetics. As can be seen from Table 1, both approaches proposed by Cheng group [68,69] enabled the most sensitive sensors. Such evidence resulted however from the implementation of typical higher active surface of carbon paste electrodes onto pencil conductive supports and from the very high loadings of enzyme used in the electrode preparation. On the other hand, biosensors proposed by Elahi et al. [71] and Sehat et al. [72] where rGO was used for electron transfer enhancement, an improvement in the LOD was obtained underlining faster heterogeneous electron shuttling process. Surface oxidation to improve wettability plus modification with nanostructures, such as QDs [75], seems to be beneficial since the comparison with similar nanostructured biosensors implemented from HOPG, GC, Au

and ITO, revealed better LOD and sensitivity. This last feature was corroborated after comparison with the works where coverage data is available [13,71].

2.2. Glucose dehydrogenase

The glucose dehydrogenase (GDH) is another enzyme seldom used in glucose biosensors. It has similar specificity for β-D-glucose substrate but requires the soluble NAD^+ cofactor for catalysis [64] which represents a major drawback to implement third generation biosensors. Recently, a photoelectrochemical biosensor coupled to a FIA system was developed [76]. The anodization pre-treatment of the PGE and modification with CdS-ZnS QDs was performed accordingly to the previous work [75]. The modified PGE was finally immersed in a mixture of GDH (27 kU mL^{-1}) and BSA using GA as crosslinking agent. The evaluation of glucose detection was performed by CV with and without QDs irradiation. When the surface was previously irradiated, the peak significantly increased due to facilitated promotion of charges between the valence to the conduction band in the dots. The FIA method under optimized flow conditions and without previous irradiation gave rise to an analytical range of 0.2–8 mM and the obtained LOD and sensitivity was respectively 90 μM and 0.118 μA mM^{-1} (0.74 μA mM^{-1} cm^{-2}). When the biosensor was irradiated the sensitivity increased about 2 fold to 0.245 μA mM^{-1} (1.54 μA mM^{-1} cm^{-2}) and the obtained LOD decreased to 50 μM [76]. Direct comparison between works where quantum dots were used [75,76] shows that chitosan provided more efficient enzyme immobilization, since both GDH and GOx have similar glucose specificity [77]. The use of QDs was advantageous in terms of biosensor sensitivity although deleterious from the environmental point of view owed to heavy metals used during synthesis. The same research group, in a different immobilization procedure, obtained better results regarding sensitivity (0.79 μA mM^{-1}) and LOD (4 μM) using the same enzyme (GDH) and PGE characteristics [78]. The surface was initially modified with polyamidoamine (PAMAM), a dendrimer capable of assisting in enzyme immobilization and electron transfer followed by an electropolymerizable redox mediator, methylene blue (MB). The GDH (338.7 U mg^{-1}, 80 mg mL^{-1}) was immobilized through cross-linking procedure with GA in the presence of 1% BSA.

2.3. Xanthine oxidase

The determination of xanthine and/or hypoxanthine is of great importance in the food industry since it is indicative of freshness especially regarding fish meat. With time of storage, the levels of xanthine increase along degradation. Also in the clinical field the control of xanthine levels in body fluids may be useful for the diagnosis of certain xanthine related diseases such as hypo- and hyperuricemia [79], xanthinuria [80], gout and renal failure [81]. The use of electrochemical biosensors for the detection of xanthine and hypoxanthine may present some advantages over the conventional enzymatic spectrometric and chromatographic techniques since they are less time consuming, cheaper and do not require high-skilled personnel to operate [82].

To the best of our knowledge only Pundir˙s [82,83] and Şenel˙s [84,85] research groups, have developed PGEs based biosensors where the enzyme xanthine oxidase (XOD) was immobilized. Xanthine oxidase is present in a wide variety of organisms, including humans but is often isolated and purified from bovine milk for scientific purposes. The enzyme is a metalloflavoprotein containing a molybdopterin cofactor, two iron sulphur centres (2Fe-2S) and one FAD cofactor, which catalyses the conversion of hypoxanthine into xanthine and xanthine into uric acid in the presence of molecular oxygen as co-substrate. The substrate is oxidized at the molybdenum active centre and electrons transferred intramolecularly to the co-substrate at flavin site [86,87].

In the initial proposal of these biosensors [82], a mixture of Chit and gold-coated iron nanoparticles (AuFeNPs) was electrochemically immobilized by CV in the surface of a PGE previously treated in acidic solution and mechanically polished. The enzyme XOD (0.15 U, 100 μL) was then covalently bonded via GA reaction. As expected, the nanoparticles decreased the electron transfer resistance through Chit but not compensated the increased upon enzyme immobilization since most biological molecules are poor conductors leading to electrical hindrance. The biosensor presented a LOD of 0.1 μM, linear range from 0.1 to 300 μM and achieved a xanthine sensitivity of 1169 μA mM^{-1} cm^{-2} in phosphate buffer at pH 7.4. The biosensor applicability was tested with fish meat samples and recoveries better than 95% were obtained at two different concentration levels. The functionalization of AuFeNPs with boronic acid improved the covalent immobilization of XOD in a subsequent work [83]. A maximum response for hypoxanthine was obtained at pH 7.2 and 30 °C. In this case a slightly better LOD of 0.05 μM and a shorter linear range (0.05–150 μM) was registered when compared with the previously study [82]. Hypoxanthine levels were successfully determined in fish, chicken, beef and pork samples and corroborated the substrate concentration increase with the storage time [83].

The approach based on the modification of PGE with Poly(GMA-co-VFc) reported before for the glucose biosensor [70] was extended to produce a xanthine biosensor [84]. The referred polymer was mixed with MWCNT and dropcasted over the PGE surface after cleaning with acetone and deionized water. After this modification the electrode was oven dried and soaked in a XOD solution of 9 mg mL^{-1} (source and activity not stated but higher that 3.6 U) for 48 h. The addition of MWCNT to the redox polymer led to an increase in peak height and the electrochemical kinetics of the biosensor was proven to be diffusional controlled through CV measurements at different scan rates. The best amperometric results at oxidation potential of + 0.35 V were linear in the range of 2–28 μM, resulting in a sensitivity of 16 μA mM^{-1} (24.3 μA mM^{-1} cm^{-2}) and a LOD of 0.12 μM. The sensitivity of the present biosensor is about 48 times lower (1169 μA mM^{-1} cm^{-2}) than the one proposed by Devi et al. [82], and reflected in achievement of a shorter linear working range. The biosensor was applied to the determination of xanthine in fish meat stored from 5 to 20 days where a linear increase of xanthine concentration up to 32 μM was found [84]. One year later a biosensor with the enzyme conjugated with an dithieno (3,2-b:2′,3′-d)pyrrole derivative polymer was proposed [85]. The planar structure of the polymer and the electron releasing groups makes it suitable for electron transfer enhancement and overcome the difficulty of enzyme direct electron transfer. Prior to modification, the PGE was cleaned with water and acetone and then modified with poly 10-[4H-dithieno(3,2-b:2′,3′-d)pyrrole-4-yl]decane-1-amine (poly(DTP-alkyl-NH_2)) through electropolymerization. The covalent immobilization was obtained by immersing firstly in a GA solution followed by XOD solution in ammonium sulphate for 48 h at 4 °C. Amperometric xanthine measurements in chicken samples were performed at the oxidation potential of + 0.5 V in pH 7.0 buffered medium. The electroactive polymer allowed better response characteristics related to LOD (0.074 μM) and sensitivity (124 μA mM^{-1}) when compared with the previously described [84].

2.4. Peroxidase

As known, hydrogen peroxide plays important roles in industrial processes where it is used as oxidizing agent in paper bleaching, wastewater treatment and disinfection. Biologically, as reactive oxygen species (ROS), promotes oxidative stress and ageing [88] being also a signalling molecule of ischemia/hypoxia events [89]. Partial reduction of molecular oxygen as by several redox enzymes such as GOx and XOD which utilize O_2 as co-substrate in catalysis processes leads to hydrogen peroxide production [90,91]. In turn, H_2O_2 is the main substrate of a number of enzymes being horseradish peroxidase (HRP) the best known in the analytical field. As oxidizing agent, it reacts with the heme iron (III) state of the enzyme in a two-electron oxidation process to form an

intermediate compound comprising the Fe(IV) oxoferryl centre and a porphyrin radical cation with concomitant formation of a water molecule [92,93].

A PGE biosensor with immobilized HRP to accomplish H_2O_2 determinations was initially proposed by Teepoo group [26]. The pencil mine (6H) was cleaned by mechanical polishing with alumina followed by electrochemical treatment in acetate buffer and then coated with Chit (0.5%). A layer by layer method was implemented for subsequent immobilization of AuNPs along 6 h followed by adsorption of HRP (5 mg mL^{-1}) for 12 h. These last two steps were repeated once more to attain best amperometric response. As stated before, AuNPs used together with redox proteins enabled to increase the specific area, conductivity and promote direct electron transfer between the redox centres and the electrode. The performance of the biosensor was evaluated at the optimized potential of −0.2 V with pH of solutions adjusted to 6.0, hence evidencing linear response range from 0.01 to 1.5 mM with a LOD of 2 μM. The biosensor showed a good response to H_2O_2 with a specific sensitivity of 149 μA mM^{-1} cm^{-2} (4.7 μA mM^{-1}), six times better when compared with a similar biosensor without AuNPs modification. Good reproducibility (± 5%) and recoveries between 80% and 104% were achieved in the determination of H_2O_2 in hair dye and disinfectant samples.

Other studies evaluated the efficiency of a PGE modified with various carbon additives [94]. The mediator polymer (poly(GMA-*co*-VFc) used in GOx and XOD biosensors [70,84] was this time mixed with carbon additives (carbon black, carbon nanofibers, extended graphite, MWCNT and rGO). Each mixture was dropcasted on a PGE surface, previously cleaned with acetone. After dried it was soaked in 5 mg mL^{-1} HRP solution (pH 7.0) for 48 h at 4 °C under agitation. The best amperometric performance was obtained for the modified PGE doped with rGO and resulted from lower electron transfer resistance as evidenced by electrochemical impedance spectroscopy (EIS). Sensitivity values of 27.4 nA mM^{-1} (0.041 μA mM^{-1} cm^{-2}) were however significantly lower than the one determined by Teepoo et al. [26].

Since HRP catalyses the oxidation of a wide spectrum of substrates [93] including pyridine-based compounds [95], direct detection of 3-Hydroxy-1,2-dimethyl-4(1 *H*)-pyridone (deferiprone), an anti-HIV drug, justified the proposal of a new HRP biosensor based on PGE [96]. The pencil mine was first modified with Chit followed by gold nanorods particles. The PGE was then dipped in a 2.5% GA solution to promote crosslinking and finally in a HRP solution (40 mg mL^{-1}) for 24 h at 4 °C. EIS studies showed that the two-electron oxidation of the drug catalysed by HRP enhanced the charge transfer rate leading to decreased R_{ct}. The response was linear from a concentration of deferiprone of 0.1–1 mM with a LOD of 0.005 μM. These results were also observable by square wave voltammetry where a sensitivity of 375 μA mM^{-1} was obtained. Results validated against a conventional procedure enabled recovery values of about 99% after analyte determination in urine and serum samples thus stressing the usefulness of the described biosensor [96].

2.5. Laccase

Some important advantages are pointed out to the ability of enzymes to generate power in fuel cell applications relatively to traditional batteries. In fact, enzymatic biofuel cells do not require use of precious metal catalysts and drive multi-electron redox reactions in less harsh pH conditions. However, produced powers are in the order of microwatts and long-term reduced stability of the biological element are still major issues fostering research. Laccases are blue multicopper oxidases which catalyse the oxidation of several phenolic compounds with concomitant four-electron reduction of O_2 to H_2O. This last feature attracted researchers on their use as biocathode in fuel cells. Laccases are widely obtained from fungal and plant origins being respectively *Trametes versicolor* and *Rhus vernicifera* the most representative sources. Laccases from fungi are nevertheless mostly referred since they are able to drive reduction of O_2 at higher potentials when compared with plant laccases. This way, higher open circuit potential (OCP) and consequently higher power generation is allowed. On the other hand, plant laccases present optimal activity at more neutral pH compared to the more acidic pH of fungal laccases [97]. In this context, an electrode with immobilized laccase from *T. versicolor* was evaluated concerning its efficiency in oxygen reduction [98]. The modification procedure started by ultrasonic assisted cleaning of bare PGE with HCl and finally dried before use. Aniline was electropolymerized (Pani) on the surface of PGE and then immersed in a suspension containing MWCNT (1 mg mL^{-1}) and N-ethyl-N′-(3-dimethylaminopropyl) carbodiimide hydrochloride / N-hydroxysuccinimide (EDC/NHS) (1 mg mL^{-1}) in order to provide covalent anchorage between the activated carboxyl group of MWCNT and side-chain amine functionalities of laccase in 3 mg mL^{-1} concentrated solution. For comparison purposes, another PGE was prepared in a similar way but without the polymer. In experiments with N_2 saturated buffer the OCP measured was low and the generated current density negligible. In the presence of oxygen and ABTS mediator the maximum OCP and current density achieved was respectively + 0.6 V and 296 μA cm^{-2} for the modified PGE, against 229 μA cm^{-2} for PGE without Pani. The higher current density observed for the PGE with Pani was attributed to the highly porous three dimensional nanofibrous structure of the polymer which provided large surface area for enzyme immobilization. Two years later, the same research group repeated the work above but optimizing the type of lead used in the PGE (H, 3 H, 5 H and B) with type 5 H achieving the highest current density, followed by type B [99].

In our group, it was developed and characterized a biocathode comprising the tree laccase *Rhus vernicifera* immobilized in a nanostructured PGE. The electrode was implemented on a HB type PGE casted with a graphene oxide that was further electrochemically reduced. A mixture containing 25 mg mL^{-1} laccase (1.07 U mg^{-1}) suspension and 5 mg mL^{-1} single-walled carbon nanotubes (SWCNT) was dropped over the surface followed by the addition of tetrakis(2,3-dihydroxypropyl)-silane monomer sol to provide enzyme physical entrapment. By setting the potential of −0.2 V, the modified PGE enabled a proportional response to molecular oxygen up to 0.45 mM and a sensitivity of 132 μA mM^{-1} cm^{-2} with a LOD of 2.7 μM. Assembled as a biofuel cell, the biocathode was capable to generate the maximum power of 4.5 μW cm^{-2} at + 0.25 V in quiescent oxygen saturated solution [100].

2.6. Ascorbic oxidase

Fruits and vegetables are naturally rich in vitamin C compound, further used as natural additive to preserve colour, prevent bacterial growth and extend freshness of other foodstuffs [101]. Thus, analytical strategies based on use of biosensors to this compound usually fit important applications in both industrial and clinical contexts. As indicator of antioxidant capacity and biologically powerful reducing agent, ascorbic acid has firstly captured the attention of Barberis group in a proposal based on PGE biosensing [102,103]. Therefore, a telemetric online system to assess levels in orange juice was devised, which included a biosensor based on ascorbate oxidase (AOx). The system, highlighting all versatility of PGE in electrochemical applications, consisted of four pencil leads (type 2H): biosensor, sensor, auxiliary electrode and a pseudo-reference electrode. The pencil lead used as biosensor had its surface modified with polyethylenimine (PEI) for enzyme stabilization, and was simply immersed in a solution containing 10% BSA and AOx (1 U $μL^{-1}$) and dried. Soaking in a 0.2% polyurethane (PU) solution enabled final enzyme immobilization. The PGE sensor was implemented in the same way but without enzyme. Biosensor response differed in about 30% of that recorded for PGE without enzyme and reflected the selectivity for the substrate oxidized by AOx. In buffered medium, the linear response to ascorbic acid extended from 0 to 0.1 mM with sensitivities of 0.668 μA mM^{-1} (941 μA mM^{-1} cm^{-2})

and 0.196 μA mM^{-1} (276 μA mM^{-1} cm^{-2}) for the sensor and biosensor, respectively. However, during analysis of orange juice samples, such sensitivities decreased probably as result of interfering species [102]. Later, the same authors studied the influence of different fullerenes (C_{60} and C_{70}) and nanotubes (SWCNT and MWCNT) for electron transfer enhancement in nanostructured sensors. Significant increase in sensitivity towards ascorbic acid in phenols mixture was observed for PGE modified with SWCNT and MWCNT (5.1 times) compared with fullerene C_{60} and C_{70} (1.2 and 1.5 times respectively). Biosensors with both types of nanotubes achieved the same linear range (0–0.02 mM) and LOD (0.2 μM). However, with MWCNT the sensitivity was 0.486 μA mM^{-1} (685 μA mM^{-1} cm^{-2}) while for SWCNT was only 0.32 μA mM^{-1} (451 μA mM^{-1} cm^{-2}). This biosensor was applied in the determinations of ascorbate and total antioxidant capacity of fruit juices [103].

2.7. Cholesterol oxidase

Cholesterol is a sterol molecule essential to structural integrity and fluidity of cell membranes and a major precursor in biosynthetic pathways leading to vitamin D and steroid hormones [104]. As important nutritional parameter directly related with health disorders, cholesterol was quantitatively determined by means of a cholesterol oxidase (ChOx) modified PGE [105]. In this biosensor development, the pencil lead (type HB) was chemically pre-treated with HCl solution followed with HNO_3. The treatment aimed either the removal of surface impurities and improvement in the adsorption of ChOx by creating oxygen functionalities that might interact with negatively charged enzyme. After treatment, the PGE was immersed in a ChOx solution and then washed with buffer. The amperometric response was linear for cholesterol in the range of 1.29–10.3 mM and with a LOD of 90 μM. The sensitivity of the biosensor was about 4120 μA mM^{-1} (4380 μA mM^{-1} cm^{-2}). The results obtained in serum samples were in good agreement with the standard method.

An apoChOx biosensor have been also proposed for cholesterol determination [106]. The best analytical results were obtained for a PGE modified with poly(thiophen-3-boronic acid) (PTBA) with 10 times higher sensitivity (210 μA mM^{-1}) when compared with the other polymer tested, poly(3-aminophenyl boronic acid). The LOD obtained was low (0.22 μM) and the electrode responded to cholesterol in a very short linear range (0.8–4.8 μM) which required a high dilution factor if the biosensor was to be used in blood samples. The reconstitution procedure of the enzyme and immobilization on the PTBA modified PGE was based on previously published work from the same authors [70].

2.8. Lipase, glycerol kinase and glycerol-3-phosphate oxidase

The monitoring of triglycerides levels present similar importance as cholesterol in terms of cardiovascular disorders and therefore was the target of an amperometric biosensor comprising co-immobilization of three enzymes [107]. In the proposed biosensor, the co-immobilization of lipase, glycerol kinase (GK) and glycerol-3-phosphate oxidase (GPO) allow the breakdown of the triglyceride molecule, triolein and consequently the detection of the H_2O_2 produced. The attachment of the enzymes on electrochemically pre-treated PGE (type 6B) was performed through GA and cysteamine linking. Triolein was detected in a wide linear range (0.1–45 mM) with a sensitivity of 185 μA mM^{-1} (116 μA mM^{-1} cm^{-2}) and LOD of 0.1 nM.

2.9. Alcohol dehydrogenase

Albeit biosensors may be considered an important instrument accomplishing the evolution of ethanol levels in fermentation processes in beverage industries, as far as known only one report aimed the use of a PGE based on alcohol dehydrogenase (ADH) [108]. In the biosensor construction, pencil leads were mechanically treated with alumina, followed by sonication in water and then ethanol for removal of adsorbed particles. The clean surface was further casted with SWCNT (0.1 mg mL^{-1}) and then the pyrocatechol violet (PCV) used as an electron transfer mediator was electrodeposited by CV.The immobilization of the enzyme was performed by dipping the PGE in a solution of ADH (30 mg mL^{-1}) containing BSA and GA. The biosensor was applied in amperometric measurements of ethanol, obtaining a range of 0.0093–0.32 mM with a sensitivity of 1.94 μA mM^{-1} cm^{-2} (0.061 μA mM^{-1}). Ethanol levels were determined in different alcoholic beverages and the results compared with a gas chromatographic method where the relative errors stayed between 2.7% and 4.4%.

2.10. L-Lactate dehydrogenase

The production of L-lactate may have an important role in the study of some clinical pathologies such as diabetes [109]. Beyond the presence of L-lactate in plasma, this compound may also play interest in the food industry since it is used as additive due to its preservative properties. Produced by lactic acid bacteria, it is present in milk products being responsible for the sour taste [110].

Two types of L-lactate enzymes (dehydrogenase and oxidase) have been used in two different PGE biosensors by Pundir group [111,112]. In the L-lactate dehydrogenase (LDH) biosensor, a PGE (6B, 2 mm) was mechanically polished and washed with ethanol. Graphene particles were electrodeposited by CV in the treated PGE surface and the carboxylic groups were activated with EDC and NHS for 6 h to further immobilize LDH through the amine bonds by incubating the PGE in the enzyme solution (1 mg mL^{-1}, 25 U mg^{-1}) overnight. The PGE biosensor achieved a linear range from 5 to 50 mM and a sensitivity of 3 μA mM^{-1} (1.6 μA mM^{-1} cm^{-2}) with LOD of 0.1 μM [111].

2.11. L-lactate oxidase

The L-lactate oxidase (LOx) biosensor comprised a different immobilization procedure in comparison with the LDH. Here, a similar treated PGE was modified by electropolymerization of aniline to polyaniline (Pani) followed by electrodeposition of a mixture of copper nanoparticles (CuNPs) with EDC/NHS treated MWCNT in the same conditions as Pani. Finally, the modified PGE was immersed in the LOx solution and kept overnight at room temperature. The amperometric response increased linearly with lactate concentration up to 2.5 mM, with a LOD of 0.25 μM and sensitivity of 1300 μA mM^{-1} (1009 μA mM^{-1} cm^{-2}). Successful determinations of L-lactate were performed in samples taken from healthy persons and lactoacidosis patients as well as in milk, wine and beer products [112].

2.12. L-glutamate oxidase

By being a neurotransmitter, quantitative analysis of glutamate can be relevant to study the neural mechanisms involved in cognition, memory and learning functions [113]. An L-glutamate PGE biosensor was developed as an alternative to chromatographic, spectrophotometric and titration methods [114]. First, the surface of the electrode (type HB) was polished with alumina, rinsed and sonicated in ethanol to remove slurry particles. A mixture of zinc oxide nanorods (ZnO) and pyrrole was electropolymerized (PPy) on the PGE surface. Glutamate oxidase (GluOx) was fixed by immersion in a 5 U mL^{-1} enzyme solution and kept overnight at room temperature. Amperometric studies showed that oxidation current increased linearly with L-glutamate concentration from 0.02 to 500 μM. The calculated sensitivity was 1.4 μA mM^{-1} (1.1 μA mM^{-1} cm^{-2}) and the LOD was 0.18 nM. The biosensor was applied lastly in food samples (Chinese soup) where glutamate is responsible for the umami taste, achieving a good correlation with the standard colorimetric method.

2.13. Uricase

Uric acid is the final product from purine metabolic breakdown and it is frequently tested in blood to diagnose gout or kidney disorders. Tsai and Wen [115] proposed a biosensor where two enzymes, uricase and HRP, were co-immobilized together with a mediator for detection of uric acid at low potential. Here, uricase enzyme catalyses first uric acid into H_2O_2 which is further used by HRP. The electrons generated were then mediated to the electrode by ferrocenemonocarboxylic acid. Before the co-immobilization, the PGE (type HB) was cleaned in methanol and rinsed with water. Then it was incubated in a mixture of uricase (20 U mL^{-1}) and HRP (350 U mL^{-1}) containing GA as cross-linker. The amperometric current increased linearly with uric acid concentration up to 0.12 mM and the LOD was 0.6 μM. The calculated sensitivity was about 2.6 μA mM^{-1}. The results obtained in the analysis of blood serum were accurate when compared with the standard spectrometric method.

2.14. Acetylcholinesterase

The detection of compounds at trace levels are generally accomplished by at least one extraction/pre-concentration step in organic medium. Wilkins group [116] evidenced the possibility of dipping high sensitive PGE sensors directly in the organic medium in order to screen organophosphate compounds. Regarding portability, the analysis of environmental samples performed in situ and in a faster way was further hypothesized. The immobilized acetylcholinesterase (AChE), hydrolyses the acetylthiocholine substrate to thiocoline which in turn reacts with the haxacyanoferrate (III) electron shuttle. First, PGE (type HB) was cleaned in methanol and distilled water. The AChE (950 U mL^{-1}) was covalently immobilized via GA in the PGE previously modified with PEI and subsequently electro-polymerized with PB. The use of the positive charged PEI polymer created a microenvironment, favouring partition effects regarding the analyte (organophosphate inhibitors). The linear range of the calibration plot was between 0 and 0.9 mM and the sensitivity was about 0.6 μA mM^{-1} (6 μA mM^{-1} cm^{-2}) which was about 10 times higher than the sensitivity obtained for biosensor without PEI-PB film. The percentage of the enzyme inhibition increased with the increase in concentration of dichlorvos, diazinon and fenthion pesticides and the LOD for the three pesticides were 0.5×10^{-6} M, 0.8×10^{-6} M and 1.0×10^{-6} M respectively.

2.15. Antibodies

Ivnitski and Rishpon research group [117–119] resorted to disposable PGEs to implement the so-called enzyme channelling immunosensor. The viewpoint was that through heterogeneous sandwich immunoreaction at the electrode surface was possible to bring together complementary enzymes regarding a common electroactive substrate thus providing amplified detection in one-step procedure. The enzymes GOx and peroxidase were typically chosen to label the PGE bound and free conjugate antibodies. To further improve distinction between conjugate bound antibody and the one remaining free in the sample medium additional dipping of the PGE in spinning mode was used. The typical procedure for preparation of PGE (HB, 0.5 mm diameter) included wet cleaning with methanol and water prior to dipping in methanol solution containing 2–5% polyethylenimine (PEI). Then 5 mm long PGE surface was immersed in 2.5% glutaraldehyde (GA) for 2 h. GOx or HRP labelled antibody were immobilized on PGE by dipping it in a 1 mg mL^{-1} or 0.5 mg mL^{-1} PBS solution for 4 h at 4 °C. Finally, the PGE was immersed by 1 h in a glycine (0.1 M) solution to block unreacted aldehyde groups. In the presence of glucose GOx produced H_2O_2 in turn used as substrate of peroxidase to oxidize iodide ions (mediator) to iodine. The iodine formed is then monitored at a constant reduction potential of −0.07 V (vs SCE) and hence regenerated again to iodide. For practical purposes, human luteinizing hormone (hLH) was determined in blood serum in a 'sandwich' immunoassay by modifying a PGE with avidin. The hLH determination principle was based sandwich formed between the analyte to be detected and two specific monoclonal antibodies, each directed against a different epitope on the hLH molecule. The captured antibodies were conjugated with biotin (αhLH-b), while the other antibodies (used to reveal the reaction) were labelled with HRP (αhLH-HRP). The catalytic current was observed at −0.07 V and the produced calibration curve for hLH showed linearity from 0 to 10 ng mL^{-1} with detection limit of 1 ng mL^{-1} [117].

A similar configuration was implemented in order to study the location of binding site of immobilized calmodulin with target proteins through its immunochemical response [118]. On the other work conducted by Rishpon and Ivnitski [119] the enzyme-channelling immunoassay was tested in different model systems including biotin-advin, HIV viral antigens (CD4-gpl20) and detection of bacteria *Staphylococcus aureus*. For the determination of biotin, PGE immobilized with avidin/GOx was performed in a competitive assay at −0.1 V (vs Ag/AgCl) in a solution containing mediator (KI), glucose and biotin-HRP. A sigmoidal shape response was obtained with increasing concentrations of biotin with current stabilizing with a concentration of 200 ng mL^{-1}. The immunosensor was then applied to quantitative determination of HIV glycoprotein gpl20 due to the specific interaction with the immobilized antigen CD4 in the presence of glucose and gpl20-HRP. The current was maximum in the absence of gpl20 and decreased with the increasing concentration. In the last model system, RbIgG was co-immobilized with GOx on the PGE surface promoting the binding of S. aureus cells to the antibody enabling its detection. With increasing concentration of cells in solution more will be attached to the RbIgG in the electrode which in turn will create the binding of RblgG-HRP in a "sandwich" format, generating an increased amperometric signal. S. aureus cells were detected at concentrations as low as 1000 cells mL^{-1}.

2.16. Living cells

The activity of nitrate reductase in viable bacteria involved in denitrification was assessed in a comparative fashion by using the same mechanical polishing on the surfaces of a PGE (0.79 mm2), one GC electrode (3.14 mm2) and one basal plane HOPG electrode (15 mm^2). The same volume of the bacteria strain suspension was dropped over respective surfaces and enclosed with a dialysis membrane fixed to the electrode body with a nylon net. When both the tetramethyl-p-benzoquinone mediator and KNO3 substrate were present in phosphate buffer solution a reduction peak was observed at −0.5 V (vs Ag/AgCl) on forward scans performed at 500 mV s^{-1}. The signals obtained were similar for PGE and basal plane HOPG electrodes, 20 μA cm^{-2} but only half of the value reported for GC electrode. After exposure of bacteria modified electrodes to magnetic field (10 mT, 50 Hz) for 24 min peaks similarly decreased by about 20%, due to bacterial death [120]. The specific detection of the virulent K12 strain of Escherichia coli in concentrations above 10^3 CFU mL^{-1}, also showed the ability of PGE in analysis involving whole cells. The terminal 10 mm length of pristine Tombow HB 0.5 mm leads were immersed for one hour in nanoemulsion of CTAB capped gold nanorods in PBS [121]. Before assay the PGEs were incubated for one hour with 10^6 PFU mL^{-1} bacteriophage T4 dilutions from 1:2 up to 1:10. The equilibration with 100 μL of suspicious suspensions of bacteria for 10 min, followed by rinsing with PBS (pH 7.4), and impedance measurement for further 25–30 min in the presence of 2.5 mM equimolar ferricyanide/ferrocyanide $[Fe(CN)_6]^{4-/3-}$ redox system completed the assay. Phage specificity for the K12 strain was evidenced by the decrease of registered impedance due to lytic action on the bacteria layer adsorbed on the PGE surface. Also, a passive adsorption protocol was adopted to provide immobilization onto PGE surface of 450 nm nanoparticles of diphenylalaninamide grown in aqueous medium by crosslinking with glutaraldehyde [122]. Before assay, the modified PGE sensor was allowed to dry for 15 min and within the biological suspension showed selectivity towards DLD-1

colorectal cancer cells translated by increasing interfacial electron transfer impedance with the same above cited redox probe.

2.17. Nucleic acids

Mature microRNAs are 20–30 nucleotides-long, non-coding nucleic acids transcribed from genetic material in cells of living beings. They are able to pair in different extent molecules of messenger RNA in order to silence protein production and regulate gene expression [123]. Profiling of microRNAs in biological samples revealed typical patterns associated with inherited or acquired pathological conditions including tumorigenesis, degenerative, development and addictive diseases. This recent observation has challenged analytical research community to find new selective and expeditious diagnostic tools as alternative to the tedious Northern blot procedure in use [124,125]. In this context, Kilic group [41] exploited the use of disposable PGEs for the direct detection of upregulated microRNA 21 (miR-21) in cell lysates of human breast adenocarcinoma. The PGEs (Tombo HB, 0.5 mm diameter) were initially anodized by applying a potential of + 1.4 V (*vs* Ag/AgCl) in acetate buffer (pH 4.8). Formed carboxylates were then modified to succinimidyl ester groups through dipping in EDC (5 mM) and NHS (8 mM) mixture for 1 h (step deemed as surface covalent activation). The -COOSuc groups on the surface of pencil leads were now able to attach nucleic acids via amide linkage with guanines (N7 position) after 20 min of contact in solution. To ensure specificity and sensitivity the method comprised respectively further hybridization with complementary antimiR21 labelled with biotin, and incubation in solution containing streptavidin labelled with alkaline phosphatase. If hybridization occurred, also the complex biotin-labelled streptavidin remained after a step of surface washing to finally allow the enzymatic conversion of alpha naphtyl phosphate, into the electroactive alpha naphtol easily oxidized and detected by differential pulse voltammetry at + 0.23 V *vs* Ag/AgCl electrode. The procedure was able to detect miR-21 at concentrations 6 pmol in total RNA cell lysates. A biosensor also aimed for the same target was recently proposed, where the PGE surface was initially coated with gold nanoparticles in order to provide higher immobilization yield regarding the probe [126]. Unfortunately, the limit of detection achieved was one order of magnitude higher, 100 pM. The same group proposed a simpler biosensor for detection of miRNA-34a in breast cancer cell lysates [127], which up-regulation promotes both inhibition in cells growth and enhanced sensitivity to drug therapy. The tip of a Tombow HB pencil (1 cm) was initially cleaned and activated at + 1.4 V *vs* Ag/AgCl for 60 s in acetate buffer solution (pH 4.8). Then, it is was soaked in a solution containing the antimiRNA-34a (5 μg mL^{-1}) probe and pyrrole added under stirring for 1 min (0.1 M prepared in 0.3 M KCl). Finally, the entrapment of the probe into a polypyrrole film covering the surface of PGE was enabled just by electrochemical scanning from − 0.6 V to + 0.8 V *vs* Ag/AgCl at the scan rate of 25 mV s^{-1}. The impedance of the biosensor changed after the hybridization process corresponding to the detection, whenever miRNA-34a exceeded 0.2 μg mL^{-1} in the sample. A similar approach for miR-21 showed the reliability of both the entrapment scheme and transduction principle [128]. DNA molecule also is effectively adsorbed onto PGE surface and provides amplified signal compared to pristine PGE [47,129]. Pividori and Alegret [130] showed that adsorption of DNA on the pre-treated electrodes depends more on the DNA bases than on the phosphate–sugar backbone. In order to achieve the best adsorption of the biological material and/or highest analytic signal optimum anodization potential should be nevertheless optimized. Pournaghi-Azar group [44], found a suitable PGE pre-anodization potential of + 1.7 V in acetate buffer pH 4.8 for the analysis of hepatitis C virus DNA from a range of studied potentials within the − 2 V to + 2.5 V window. They noticed that potentials above + 2 V and more negative than − 1.5 V could lead to the formation of gaseous products from the background electrolyte.

Not only RNA but also single-stranded oligonucleotide DNA sequences can be folded in diverse tertiary structures and then rival monoclonal antibodies regarding the cognate targets or even mimic enzyme catalysis in a wide variety of reactions. At least for compounds ideally bearing positive charge, proton acceptor-donor groups and having planarity features this new wave bio-ligands, known as aptamers, show affinities in the nM to pM range and astonishing selectivity even for simple stereoisomer molecules as is the case between L- and D-aminoacids [131]. Because the synthesis dispenses biological living machinery and can be tailored to the target using a combinatorial chemistry approach on libraries of initial randomized oligonucleotides, several hundreds of reliable aptamers are nowadays available at reasonable costs for heavy metals, antibiotics, toxins, hormones and proteins [132]. Their use in biosensor schemes with electrochemical transduction, may it be of the sandwich type, impedance or structure switching-based assays, showed that immobilization with higher surface densities is potentially enabled due to smaller size of aptamers. Through application of denaturing-renaturing chemical or temperature cycles, the reversibility of the recognition process is also possible [133,134]. Four years ago, a modified PGE for the detection of lysozyme based on the use of an amino-linked anti-lysozyme single-stranded DNA aptamer was proposed [135]. The tip of the pencil lead, 10 mm length, was electrochemically activated as already described above for Kilic group paper [41] and sequentially immersed for 15 min in 110 μL of optimized mixture of graphene oxide in the chitosan polycationic polymer, and for 30 min in equal volume of the aptamer. The high impedance for electron charge transfer due to charge repulsion between the anionic $Fe(CN)_6^{3-/4-}$ redox probe and the negative charged phosphate backbone of the aptamer decreased proportionally in the presence of lysozyme in concentrations above 28.53 nM, being the transduction facilitated by the presence of graphene. Rotring HB pencil leads with 0.5 mm were modified as described above [41] to exhibit -COOSuc groups on the surface and immersed in 40 μL of 15 μg mL^{-1} amino-linked ss-DNA anti-thrombin in Tris-HCL buffer. This biosensor provided at the + 0.23 V *vs* Ag/AgCl electrode for sinusoidal 10 mV signals in the frequencies interval between 1 mHz to 100 kHz, increasing impedances for charge transfer to the probe with the thrombin-aptamer complex concentration [136]. More recently, Ensafi group resorted to a 30 base long ss-DNA with high affinity to insulin, after acquiring a G-quadruplex conformation in the presence of Mg^{2+}, to propose a disposable impedance biosensor almost exclusively constructed along successive optimized electrochemical steps [137]. The surface tip of a Pentel HB 0.7 mm lead was in the first step immersed in 0.1 M of sodium carbonate, lithium perchlorate solution and activated through 5 run cycles, 50 mV s^{-1}, within the potential limits of − 0.40 and 2.00 V. The active surface was then coated with an electro polymerized film of conductive poly-orthophenylene diamine which in turn served as substrate for gold nanoparticles obtained along more run cycles within − 0.50 to 1.50 V at a scan rate of 2 mV s^{-1}. Final dipping in the thiolated aptamer resulted in self-assemblage of the bio-ligand due to the affinity of SH groups for the gold surface of nanoparticles. The biosensor was responsive to insulin in the 1–1000 nM range, using urine or plasma 1:1 diluted with PBS as samples. The assemblage of thiolated anti-dopamine over gold nanostars showed the possibility of having impedance biosensors with sensitivity comparable with the elctrochemiluminescence method for this neurotransmitter molecule. The biosensor was however reusable after immersion for 15 min in aptamer denaturizing solution containing 7 M urea [138]. The gold nanostars were synthesised according to the seed-mediated growth protocol [139] and the bare PGE simply immersed for 15 min in a water suspension of them at 75 °C.

3. Conclusions and future perspectives

Pencil mine electrodes paved the way to be considered as valuable alternative to other carbon-based electrodes as evidenced is this review. The thin dimensions and negligible cost enables uses as easily

polarizable and disposable electrodes. Moreover, the ability to offer renewed surface by simple cut, provides good reproducibility as well as implementation efficiency. Several factors may affect PGE performance and the analyst should take them in consideration in order to achieve the best analytical results. The electron transfer efficiency varies according to pencil lead hardness and even may vary according to the pencil manufacturer. Also, the pre-treatment given to the active surface of the electrode plays a crucial role in the outcome of the analysis. A suitable pre-treatment may eliminate background currents by removing impurities or create oxygen functionalities that may enhance the immobilization of the biological entity.

Regarding biosensors, a relevant part of published works refers to enzymes immobilization thus explaining the review organization but with a brief reference to different immobilized biological entities namely, nucleic acids, antibodies and whole microorganisms (bacteria) depending on the envisaged application. In the end of our bibliographic research we have accounted 37 enzymatic and 1 bacteria PGE biosensors applied to the analysis of glucose, xanthine, hydrogen peroxide, oxygen, ascorbic acid, cholesterol, ethanol, L-lactate, L-glutamate, uric acid, drugs, triglycerides, pesticides, bacterial survival, hormones and viral antigens. The enzyme glucose oxidase is the most used enzyme in PGE biosensors due to general commercial success of glucose biosensors and to the clinical significance of the glucose analyte. Studies on laccase activities towards oxygen were also important for the development of enzymatic biofuel cells and self-powered sensors. More recently, pencil leads have been used to draw electrodes and conductive circuits in paper-based sensors making these systems simpler, inexpensive and solvent-free. But as far we know, the application of pencil drawn electrode with enzymes is still limited or even non-existing, predicting a new window of opportunities in research.

Acknowledgements

Álvaro Torrinha acknowledges the scholarship conceded by FSE and FCT (PD/BD/109660/2015). This work received financial support from the European Union (FEDER funds POCI/01/0145/FEDER/007265) and National Funds (FCT/MEC, Fundação para a Ciência e Tecnologia and Ministério da Educação e Ciência) under the Partnership Agreement PT2020 UID/QUI/50006/2013.

References

[1] J. Mašek, J. Electroanal. Chem. 1 (1960) 416–421.
[2] W. Selig, Anal. Lett. 15 (1982) 309–329.
[3] K. Aoki, T. Okamoto, H. Kaneko, K. Nozaki, A. Negishi, J. Electroanal. Chem. 263 (1989) 323–331.
[4] S. Sujaritvanichpong, K. Aoki, Electroanalysis 1 (1989) 397–403.
[5] A.M. Bond, P.J. Mahon, J. Schiewe, V. Vicente-Beckett, Anal. Chim. Acta 345 (1997) 67–74.
[6] A. Bund, J. Dittmann, D. Lordkipanidze, G. Schwitzgebel, Fresenius J. Anal. Chem. 356 (1996) 27–30.
[7] C. Chen, E. Tamiya, K. Ishihara, Y. Kosugi, Y. Su, N. Nakabayashi, I. Karube, Appl. Biochem. Biotechnol. 36 (1992) 211–226.
[8] H. Hara, Y. Kondoh, O. Mitani, S. Okazaki, Anal. Chem. 62 (1990) 1139–1143.
[9] H. Hara, H. Ohkubo, K. Sawai, Analyst 118 (1993) 549–552.
[10] H. Kaneko, M. Yamada, A. Negishi, T. Kawakubo, Y. Suda, Carbon micro-sensor electrode and method for preparing it. US Patent 5281319, 1993.
[11] H. Kaneko, A. Negishi, K. Nozaki, Carbon sensor electrode and process for producing the same. US Patent 5503728, 1996.
[12] K. Miyazaki, G. Matsumoto, M. Yamada, S. Yasui, H. Kaneko, Electrochim. Acta 44 (1999) 3809–3820.
[13] M.V. Pishko, I. Katanis, S.-E. Lindquist, A. Heller, Y. Degani, Mol. Cryst. Liq. Cryst. 190 (1990) 221–249.
[14] N. Ishida, K. Saito, Pencil lead and manufacturing method of the same. US Patent No 4017451, 1977.
[15] M.P. Down, C.W. Foster, X. Ji, C.E. Banks, RSC Adv. 6 (2016) 81130–81141.
[16] R. Navratil, A. Kotzianova, V. Halouzka, T. Opletal, I. Triskova, L. Trnkova, J. Hrbac, J. Electroanal. Chem. 783 (2016) 152–160.
[17] P. Tavares, P. Barbeira, J. Appl. Electrochem. 38 (2008) 827–832.
[18] S.H. Lee, J.Y. Ban, C.-H. Oh, H.-k Park, S. Choi, Sci. Rep. 6 (2016) 28588.
[19] C.W. Foster, D.A.C. Brownso, A.P.R. Souza, E. Bernalte, J. Iniesta, M. Bertotti, C.E. Banks, Analyst 141 (2016) 4055–4064.
[20] J.K. Kariuki, J. Electrochem. Soc. 159 (2012) H747–H751.
[21] P. Masawat, S. Liawruangrath, Y. Vaneesorn, B. Liawruangrath, Talanta 58 (2002) 1221–1234.
[22] S. Buratti, M. Scampicchio, G. Giovanelli, S. Mannino, Talanta 75 (2008) 312–316.
[23] R.L. Mc Creery, Carbon electrodes: Structural effects on electron transfer kinetics, in: A.J. Bard (Ed.), Electroanalytical Chemistry, 17 Marcel Dekker, New York, 1991, pp. 221–374.
[24] R.L. Mc Creery, K.K. Cline, Carbon electrodes, in: P. Kissinger, W.R. Heineman (Eds.), Laboratory Techniques in Electroanalytical Chemistry, second ed, Marcel Dekker Inc, New York, 1996, pp. 293–332.
[25] N. Vishnu, A.S. Kumar, Anal. Methods 7 (2015) 1943–1950.
[26] S. Teepoo, P. Chumsaeng, P. Nethan, W. Prueprang, P. Tumsae, Int. J. Electrochem. Sci. 7 (2012) 4645–4656.
[27] J. Wang, A.-N. Kawde, Anal. Chim. Acta 431 (2001) 219–224.
[28] R. Akanda, M. Sohail, A. Aziz, A.-N. Kawde, Electroanalysis 28 (2016) 408–424.
[29] I.G. David, D.-E. Popa, M. Buleandra, J. Anal. Methods Chem. (2017) 2017.
[30] A.-N. Kawde, N. Baig, M. Sajid, RSC Adv. 6 (2016) 91325–91340.
[31] A. Erdem, P. Papakonstantinou, H. Murphy, Anal. Chem. 78 (2006) 6656–6659.
[32] J. Wang, A.-N. Kawde, E. Sahlin, Analyst 125 (2000) 5–7.
[33] Y. Yardım, E. Keskin, A. Levent, M. Özsöz, Z. Şentürk, Talanta 80 (2010) 1347–1355.
[34] D. Demetriades, A. Economou, A. Voulgaropoulos, Anal. Chim. Acta 519 (2004) 167–172.
[35] X. Cai, G. Rivas, P.A.M. Farias, H. Shiraishi, J. Wang, E. Palecek, Electroanalysis 8 (1996) 753–758.
[36] N. Mano, F. Mao, A. Heller, J. Am. Chem. Soc. 125 (2003) 6588–6594.
[37] M. Rasmussen, R.E. Ritzmann, I. Lee, A.J. Pollack, D. Scherson, J. Am. Chem. Soc. 134 (2012) 1458–1460.
[38] F.C.P.F. Sales, R.M. Lost, M.V.A. Martins, M.C. Almeida, F.N. Crespilho, Lab Chip 13 (2013) 468–474.
[39] R.C. Engstrom, V.A. Strasser, Anal. Chem. 56 (1984) 136–141.
[40] H. Karadeniz, A. Erdem, A. Caliskan, C.M. Pereira, E.M. Pereira, J.A. Ribeiro, Electrochem. Commun. 9 (2007) 2167–2173.
[41] T. Kilic, S.N. Topkaya, D.O. Ariksoysal, M. Özsöz, P. Ballar, Y. Erac, O. Gozen, Biosens. Bioelectron. 38 (2012) 195–201.
[42] S. Mathur, A. Erdem, C. Cavelius, S. Bartha, J. Altmayer, Sens. Actuators B 136 (2009) 432–437.
[43] P. Palaska, E. Aritzoglou, S. Girousi, Talanta 72 (2007) 1199–1206.
[44] M.H. Pournaghi-Azar, F. Ahour, M.S. Hejazi, Electroanalysis 21 (2009) 1822–1828.
[45] R.C. Engstrom, Anal. Chem. 54 (1982) 2310–2314.
[46] A. Özcan, Y. Şahin, Electroanalysis 21 (2009) 2363–2370.
[47] A.A. Ensafi, E. Heydari-Bafrooei, M. Amini, Biosens. Bioelectron. 31 (2012) 376–381.
[48] B. Rezaei, M.H. Esfahani, A.A. Ensafi, IEEE Sens. J. 16 (2016) 7037–7044.
[49] A. Özcan, S. İlkbaş, A.A. Özcan, Talanta 165 (2017) 489–495.
[50] S. Karakaya, Y. Dilgin, Electroanalysis 29 (2017) 1626–1634.
[51] N. Vishnu, M. Gandhi, D. Rajagopal, A.S. Kumar, Anal. Methods 9 (2017) 2265–2274.
[52] A. Özcan, Electroanalysis 26 (2014) 1631–1639.
[53] F. Kuralay, S. Tunç, F. Bozduman, L. Oksuz, A.U. Oksuz, Talanta 160 (2016) 325–331.
[54] M.R. Majidi, K. Asadpour-Zeynali, B. Hafezi, Microchim. Acta 169 (2010) 283–288.
[55] M. Vestergaard, K. Kerman, E. Tamiya, Anal. Chim. Acta 538 (2005) 273–281.
[56] M.R. Majidi, K. Asadpour-Zeynali, B. Hafezi, Electrochim. Acta 54 (2009) 1119–1126.
[57] E. Eksin, A. Erdem, Electroanalysis 26 (2014) 1945–1951.
[58] C.R. Lowe, Trends Biotechnol. 2 (1984) 59–65.
[59] V.M. Owen, Ann. N.Y. Acad. Sci. 501 (1987) 233–239.
[60] B. Dogan-Topal, B. Uslu, S.A. Ozkan, Biosens. Bioelectron. 24 (2009) 2358–2364.
[61] A.A. Ensafi, B. Rezaei, M. Amini, E. Heydari-Bafrooei, Talanta 88 (2012) 244–251.
[62] J.-M. Engasser, C. Horvath, Diffusion and kinetics with immobilized enzymes, in: Jr.L.B. Wingard, E. Katchalski-Katzir, L. Goldstein (Eds.), Applied Biochemistry and Bioengineering. Immobilized Enzyme Principles, Academic Press, New York, 1976, pp. 128–216.
[63] R.A. Kamin, G.S. Wilson, Anal. Chem. 52 (1980) 1198–1205.
[64] R. Wilson, A.P.F. Turner, Biosens. Bioelectron. 7 (1992) 165–185.
[65] S. Witt, G. Wohlfahrt, D. Schomburg, H.-J. Hecht, H.M. Kalisz, Biochem. J. 347 (2000) 553–559.
[66] K. Ichimura, J. Polym. Sci. Pol. Chem. 22 (1984) 2817–2828.
[67] S.A. Jaffari, J.C. Pickup, Biosens. Bioelectron. 11 (1996) 1167–1175.
[68] C. Cheng, K.-C. Chang, C.-S. Chen, D.G. Pijanowska, J. Chin. Chem. Soc. 58 (2011) 739–748.
[69] C. Cheng, K.-C. Chang, D.G. Pijanowska, J. Electroanal. Chem. 666 (2012) 32–41.
[70] M. Dervisevic, E. Çevik, M. Şenel, Enzym. Microb. Technol. 68 (2014) 69–76.
[71] M.Y. Elahi, A.A. Khodadadi, Y. Mortazavi, J. Electrochem. Soc. 161 (2014) B81–B87.
[72] A.A. Sehat, A.A. Khodadadi, F. Shemirani, Y. Mortazavi, Int. J. Electrochem. Sci. 10 (2015) 272–286.
[73] K. Vijayaraj, S.W. Hong, S.-H. Jin, S.-C. Chang, D.-S. Park, Anal. Methods 8 (2016) 6974–6981.
[74] S. Teanphonkrang, A. Schulte, Anal. Chem. 89 (2017) 5261–5269.
[75] Ö. Sağlam, B. Kızılkaya, H. Uysal, Y. Dilgin, Talanta 147 (2016) 315–321.
[76] B. Ertek, C. Akgül, Y. Dilgin, RSC Adv. 6 (2016) 20058–20066.
[77] A. Heller, B. Feldman, Chem. Rev. 108 (2008) 2482–2505.
[78] D.G. Dilgin, B. Ertek, Y. Dilgin, J. Iran. Chem. Soc. 15 (2018) 1355–1363.

[79] T. Kojima, T. Nishina, M. Kitamura, N. Kamatani, K. Nishioka, Clin. Chem. 32 (1986) 287–290.
[80] M. Kathiwala, A.O. Aïtum, J. Perry, Á. Brajter-Toth, Analyst 133 (2008) 810–816.
[81] A. McBurney, T. Gibson, Clin. Chim. Acta 102 (1980) 19–28.
[82] R. Devi, S. Yadav, R. Nehra, S. Yadav, C.S. Pundir, J. Food Eng. 115 (2013) 207–214.
[83] R. Devi, S. Yadav, R. Nehra, C.S. Pundir, Int. J. Biol. Macromol. 62 (2013) 629–635.
[84] M. Dervisevic, E. Custiuc, E. Çevik, M. Şenel, Food Chem. 181 (2015) 277–283.
[85] M. Dervisevic, E. Dervisevic, H. Azak, E. Çevik, M. Şenel, H.B. Yildiz, Sens. Actuators B 225 (2016) 181–187.
[86] C. Enroth, B.T. Eger, K. Okamoto, T. Nishino, T. Nishino, E.F. Pai, Proc. Natl. Acad. Sci. USA 97 (2000) 10723–10728.
[87] R. Hille, T. Nishino, FASEB J. 9 (1995) 995–1003.
[88] E.A. Veal, A.M. Day, B.A. Morgan, Mol. Cell 26 (2007) 1–14.
[89] M. Ushio-Fukai, Cardiovasc. Res. 71 (2006) 226–235.
[90] S. Chen, R. Yuan, Y. Chai, F. Hu, Microchim. Acta 180 (2013) 15–32.
[91] J.A. Imlay, Annu. Rev. Biochem. 77 (2008) 755–776.
[92] J.N. Rodríguez-López, D.J. Lowe, J. Hernández-Ruiz, A.N.P. Hiner, F. García-Cánovas, R.N.F. Thorneley, J. Am. Chem. Soc. 123 (2001) 11838–11847.
[93] N.C. Veitch, Phytochemistry 65 (2004) 249–259.
[94] M. Dervisevic, E. Çevik, Z. Durmuş, M. Şenel, Mater. Sci. Eng. 58 (2016) 790–798.
[95] I. Yamazaki, K. Yokota, R. Nakajima, Biochem. Biophys. Res. Commun. 21 (1965) 582–586.
[96] J. Narang, N. Malhotra, G. Singh, C.S. Pundir, Biosens. Bioelectron. 66 (2015) 332–337.
[97] J.A. Cracknell, K.A. Vincent, F.A. Armstrong, Chem. Rev. 108 (2008) 2439–2461.
[98] D. Kashyap, C. Kim, S.Y. Kim, Y.H. Kim, G.M. Kim, P.K. Dwivedi, A. Sharma, S. Goel, Int. J. Hydrog. Energy 40 (2015) 9515–9522.
[99] M. Bandapati, P.K. Dwivedi, B. Krishnamurthy, Y.H. Kim, G.M. Kim, S. Goel, Int. J. Hydrog. Energy 42 (2017) 27220–27229.
[100] Á. Torrinha, M.C.B.S.M. Montenegro, A.N. Araújo, Electroanalysis 29 (2017) 1–8.
[101] P.T. Gardner, T.A.C. White, D.B. McPhail, G.G. Duthie, Food Chem. 68 (2000) 471–474.
[102] A. Barberis, Y. Spissu, G. Bazzu, A. Fadda, E. Azara, D. Sanna, M. Schirra, P.A. Serra, Anal. Chem. 86 (2014) 8727–8734.
[103] A. Barberis, Y. Spissu, A. Fadda, E. Azara, G. Bazzu, S. Marceddu, A. Angioni, D. Sanna, M. Schirra, P.A. Serra, Biosens. Bioelectron. 67 (2015) 214–223.
[104] I. Tabas, J. Clin. Investig. 110 (2002) 583–590.
[105] N. Chauhan, J. Narang, C.S. Pundir, Am. J. Anal. Chem. 2 (2010) 41–46.
[106] M. Dervisevic, E. Çevik, M. Şenel, C. Nergiz, M.F. Abasiyanik, J. Electroanal. Chem. 776 (2016) 19–24.
[107] V. Narwal, C.S. Pundir, Enzym. Microb. Technol. 100 (2017) 11–16.
[108] J. Zhu, X.-Y. Wu, D. Shan, P.-X. Yuan, X.-J. Zhang, Talanta 130 (2014) 96–102.
[109] M. Adeva-Andany, M. López-Ojén, R. Funcasta-Calderón, E. Ameneiros-Rodríguez, C. Donapetry-García, M. Vila-Altesor, J. Rodríguez-Seijas, Mitochondrion 17 (2014) 76–100.
[110] J.T.M. Wouters, E.H.E. Ayad, J. Hugenholtz, G. Smit, Int. Dairy J. 12 (2002) 91–109.
[111] B. Batra, V. Narwal, C.S. Pundir, Eng. Life Sci. 16 (2016) 786–794.
[112] K. Dagar, C.S. Pundir, Enzym. Microb. Technolnol. 96 (2017) 177–186.
[113] O. Niwa, T. Horiuchi, K. Torimitsu, Biosens. Bioelectron. 12 (1997) 311–319.
[114] B. Batra, M. Yadav, C.S. Pundir, Biochem. Eng. J. 105 (2016) 428–436.
[115] W.-C. Tsai, S.-T. Wen, Anal. Lett. 39 (2006) 891–901.
[116] E. Wilkins, M. Carter, J. Voss, D. Ivnitski, Electrochem. Commun. 2 (2000) 786–790.
[117] D. Ivnitski, J. Rishpon, Biosens. Bioelectron. 11 (1996) 409–417.
[118] D. Ivnitski, T. Wolf, B. Solomon, G. Flemminger, J. Rishpon, Bioelectrochem. Bioenerg. 45 (1998) 27–32.
[119] J. Rishpon, D. Ivnitski, Biosens. Bioelectron. 12 (1997) 195–204.
[120] L. Fojt, L. Strašák, V. Vetterl, Bioelectrochemistry 70 (2007) 91–95.
[121] F. Moghtader, G. Congur, H.M. Zareie, A. Erdem, E. Piskin, RSC Adv. 6 (2016) 97832–97839.
[122] Y.T. Yaman, Ö. Akbal, G. Bolat, B. Bozdogan, E.B. Denkbas, S. Abaci, Biosens. Bioelectron. 104 (2018) 50–57.
[123] J.S. Mattick, I.V. Makunin, Hum. Mol. Genet. 15 (2006) R17–R29.
[124] B.D. Adams, C. Parsons, L. Walker, W.C. Zhang, F.J. Slack, J. Clin. Invest. 127 (2017) 761–771.
[125] D.P. Kalogianni, P.M. Kalligosfyri, I.K. Kyriakou, T.K. Christopoulos, Anal. Bioanal. Chem. 410 (2018) 695–713.
[126] J. Mandli, H. Mohammadi, A. Amine, Bioelectrochemistry 116 (2017) 17–23.
[127] J. Mandli, A. Amine, J. Solid State Electrochem. 22 (2018) 1007–1014.
[128] M. Kaplan, T. Kilic, G. Guler, J. Mandli, A. Amine, M. Ozsoz, Biosens. Bioelectron. 92 (2017) 770–778.
[129] R.E. Sabzi, B. Sehatnia, M.H. Pournaghi-Azar, M.S. Hejazi, J. Iran. Chem. Soc. 5 (2008) 476–483.
[130] M.I. Pividori, S. Alegret, DNA adsorption on carbonaceous materials, Immobilisation of DNA on Chips I. Topics in Current Chemistry, 260 Springer, Berlin, Heidelberg, 2005, pp. 1–36.
[131] J. Liu, Z. Cao, Y. Lu, Chem. Rev. 109 (2009) 1948–1998.
[132] R. Stoltenburg, C. Reinemann, B. Strehlitz, Biomol. Eng. 24 (2007) 381–403.
[133] I. Willner, M. Zayats, Angew. Chem. Int. Ed. 46 (2007) 6408–6418.
[134] G.K. Mishra, V. Sharma, R.K. Mishra, Biosensors 8 (2018) 28.
[135] A. Erdem, E. Eksin, M. Muti, Colloid Surf. B 115 (2014) 205–211.
[136] E. Eksin, A. Erdem, A.P. Kuruc, H. Kayi, A. Ögünç, Electroanalysis 27 (2015) 2864–2871.
[137] A.A. Ensafi, E. Khoddami, B. Rezaei, Colloid Surf. B 159 (2017) 47–53.
[138] R.P. Talemi, S.M. Mousavi, H. Afruzi, Mater. Sci. Eng. C 73 (2017) 700–708.
[139] M. Chirea, Catalysts 3 (2013) 288–309.

Appendix B – List of publications

Á. Torrinha, M.C.B.S.M. Montenegro, A.N. Araújo, Implementation of a Simple Nanostructured Bio-electrode with Immobilized Rhus Vernicifera Laccase for Oxygen Sensing Applications, Electroanalysis, 2017, 29, 1566-1572.

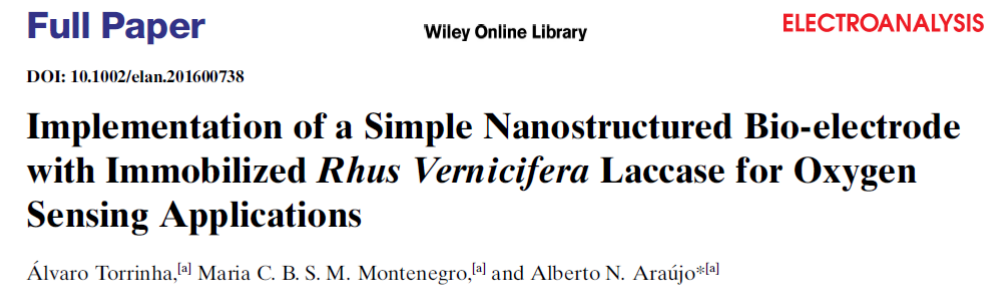

Full Paper Wiley Online Library ELECTROANALYSIS

DOI: 10.1002/elan.201600738

Implementation of a Simple Nanostructured Bio-electrode with Immobilized *Rhus Vernicifera* Laccase for Oxygen Sensing Applications

Álvaro Torrinha,[a] Maria C. B. S. M. Montenegro,[a] and Alberto N. Araújo*[a]

A. Torrinha, M.C.B.S.M. Montenegro, A.N. Araújo, Biosensing based on pencil graphite electrodes, Talanta, 2018, 190, 235-247.

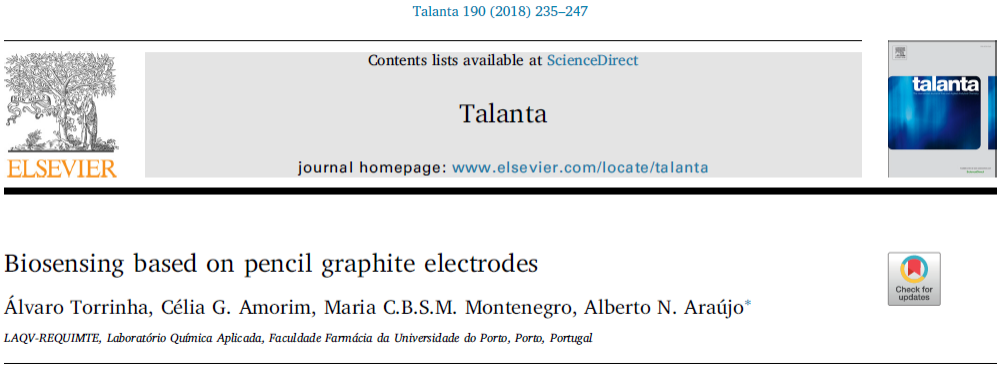

Talanta 190 (2018) 235–247

Contents lists available at ScienceDirect

Talanta

journal homepage: www.elsevier.com/locate/talanta

Biosensing based on pencil graphite electrodes

Álvaro Torrinha, Célia G. Amorim, Maria C.B.S.M. Montenegro, Alberto N. Araújo*

LAQV-REQUIMTE, Laboratório Química Aplicada, Faculdade Farmácia da Universidade do Porto, Porto, Portugal

A. Torrinha, M.C.B.S.M. Montenegro, A.N. Araújo, Microfluidic Platform with an Embedded Pencil Graphite Electrode Biosensor for the Detection of Glucose and Cadmium, Journal of the Electrochemical Society, 2019, 166,: B155-B160.

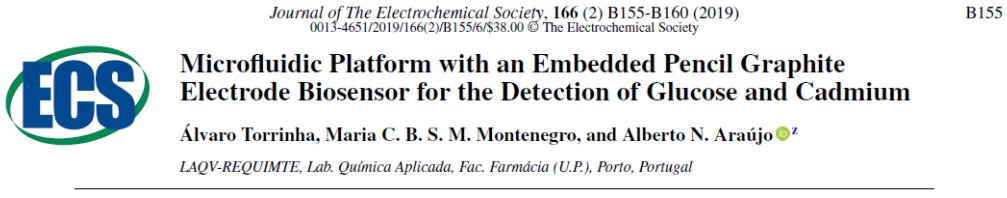

Journal of The Electrochemical Society, **166** (2) B155-B160 (2019) B155

0013-4651/2019/166(2)/B155/6/$38.00 © The Electrochemical Society

Microfluidic Platform with an Embedded Pencil Graphite Electrode Biosensor for the Detection of Glucose and Cadmium

Álvaro Torrinha, Maria C. B. S. M. Montenegro, and Alberto N. Araújo

LAQV-REQUIMTE, Lab. Química Aplicada, Fac. Farmácia (U.P.), Porto, Portugal

A. Torrinha, M.C.B.S.M. Montenegro, A.N. Araújo, Conjugation of a glucose oxidase and bilirubin oxidase bioelectrodes as biofuel cell in a finger-powered microfluidic platform, Electrochimica Acta, 2019, 318, 922-930.

Electrochimica Acta 318 (2019) 922–930

Contents lists available at ScienceDirect

Electrochimica Acta

journal homepage: www.elsevier.com/locate/electacta

Conjugation of glucose oxidase and bilirubin oxidase bioelectrodes as biofuel cell in a finger-powered microfluidic platform

Álvaro Torrinha, Maria C.B.S.M. Montenegro, Alberto N. Araújo*

LAQV-REQUIMTE, Laboratório Química Aplicada, Faculdade de Farmácia da Universidade do Porto, Porto, Portugal

Submitted:

Á. Torrinha, N. Jiyane, M. Sabela, K. Bisetty, M.C.B.S.M. Montenegro, A.N. Araújo, Bilirubin oxidase immobilized on pencil graphite electrodes for application as oxygen biosensors and biocathodes, Bioelectrochemistry, 2019 – In revision.

Lab-on-a-chip platforms embedding self-powered electrochemical sensors: a walkthrough approach for bio-analytical applications

Álvaro Miguel Carneiro Torrinha

Faculdade de Farmácia